Proceedings of the Fourteenth Annual Pacific Climate (PACLIM) Workshop

Asilomar, California - April 6-9, 1997

Edited by
Raymond Wilson and Vera L. Tharp

Technical Report 57
of the
Interagency Ecological Program
for the
Sacramento-San Joaquin Estuary

PACLIM

Climate Variability of the Eastern North Pacific and Western North America

Sponsors

The Fourteenth Annual Pacific Climate Workshop is sponsored by:

The Wrigley Institute for Environmental Studies (Anthony Michaels)

The U. S. Geological Survey Water Resources Division (Harry Lins)

The U. S. Geological Survey Geological Research Division (Richard Poore)

The American Geophysical Union (A. F. Spilhaus, Jr.)

The California Department of Water Resources (Randy Brown)

Publication of this proceedings has been sponsored by the

INTERAGENCY ECOLOGICAL PROGRAM

for the

SACRAMENTO-SAN JOAQUIN ESTUARY

A Cooperative Program of:

California Department of Water Resources
State Water Resources Control Board
U.S. Bureau of Reclamation
U.S. Geological Survey

California Department of Fish and Game
U.S. Fish and Wildlife Service
U.S. Army Corps of Engineers
U.S. Environmental Protection Agency
National Marine Fisheries Service

These proceedings were published by the Interagency Ecological Program for the Sacramento-San Joaquin Estuary (Interagency Program)
in a cooperative effort with the
United States Department of the Interior, Geological Survey, Menlo Park, California.
Information generated by the PACLIM Workshop provides the Interagency Program with a climatological perspective that cannot be obtained from its own studies.
Views and conclusions contained in this publication do not necessarily reflect the opinions of the Interagency Program or its member agencies.

Contents

Abstracts

Appendices

Authors

Jeff C. Babb
Canadian Grain Commission
303 Main Street
Winnipeg, Manitoba, Canada

Gregg M. Garfin
Laboratory of Tree-Ring Research
University of Arizona
Tucson, AZ 85721
520/626-3142
g@ltrr.arizona.edu

E. Ray Garnett
Canadian Wheat Board
423 Main Street
Winnipeg, Manitoba, Canada
ray_garnett@cwb.ca
204/983-3563

R. W. Higgins
Climate Prediction Center
NOAA/NWS/NCEP
Washington, DC

K.-U. Hinrichs
Woods Hole Oceanographic Institution
Marine Chemistry and Geochemistry Dept.
MS #4
Woods Hole, MA 02543
508/289-4471
richs@whoi.edu

Madhav L. Khandekar
52 Montrose Crescent
Unionville, Ontario, Canada L3R 7Z5
1 905 940 0105

Teh-Lung Ku
Department of Earth Sciences
University of Southern California
Los Angeles, CA 90089-0740
213/740-5826

Steven W. Leavitt
Laboratory of Tree-Ring Research
105 West Stadium
The University of Arizona
Tucson, AZ 85721
520/621-6468
leavitt@ltrr.arizona.edu

Hong-Chun Li
Department of Earth Sciences
University of Southern California
Los Angeles, CA 90089-0740
213/740-6733

Austin Long
Depts. of Geosciences and
Hydrology & Water Resources
The University of Arizona
Tucson, AZ 85721
520/621-8888
along@geo.arizona.edu

Mark Losleben
Mountain Research Station
University of Colorado
Nederland, CO 80466
303/492-8841
markl@culter.colorado.edu

K.C. Mo
Climate Prediction Center
NOAA/NWS/NCEP
Washington, DC

J. Rinna
Carl von Ossietzky Universität Oldenburg
Postfach 25 03
D-26111 Oldenburg, Deutschland
Telephone (49) 441-798-3415
rinna@ogc.icbm.uni-oldenburg.de

Maurice Roos
California Department of Water Resources
P.O. Box 942836
Sacramento, CA 94236-0001
916/574-2625

J. Rullkötter
Carl von Ossietzky Universität Oldenburg
Postfach 25 03
D-26111 Oldenburg, Deutschland
Telephone (49) 441-970-6359
j.rullkoetter@ogc.icbm.uni-oldenburg.de

Lowell D. Stott
Department of Earth Sciences
University of Southern California
Los Angeles, CA 90089-0740
213/740-5120

X. L. Wang
Research and Data Systems Corporation
Greenbelt, MD

G. James West
U.S. Bureau of Reclamation
2800 Cottage Way
Sacramento, CA 95825-1898

Wallace B. Woolfenden
Archaeologist
Lee Vining Ranger Station
P.O. Box 429
Lee Vining, CA 93541
760/647-3035

William E. Wright
Laboratory of Tree-Ring Research
105 West Stadium
The University of Arizona
Tucson, AZ 85721
520/621-9786
wwright@ltrr.arizona.edu

Y. Yao,
Research and Data Systems Corporation,
Greenbelt, MD

Acknowledgments

The PACLIM workshops are produced by an array of enthusiastic volunteers.

For 1997, thanks go to the following people and institutions: **USGS**: Caroline Isaacs and Don Gautier were co-chairmen for the workshop; Maria Castain dealt with invitations, gathering abstracts, handled registration, collected money and sold T-shirts. Lucenia Thomas also assisted with mailings. **Scripps**: Dan Cayan, assisted by Nicki Pyles, organized the agenda and assembled the abstracts; Larry Riddle operated the PACLIM website, designed the T-shirts, and obtained the easels and foam board for the poster session. The easels were lent by George Hemingway, California Cooperative Fisheries Investigations at Scripps. **WIES**: Special thanks to the Wrigley Institute for Environmental Studies and Tony Michaels for co-sponsoring and hosting the 1997 PACLIM workshop on Santa Catalina. The logistics of getting us all onto (and back off) the island were ably handled by Maureen Oudin and Gina Long, who arranged for ferry trips, luggage trucks, vans and water taxis and made us mainlanders feel welcome in this beautiful place.

Sponsorship and funding for the workshops come from a wide variety of sources. In addition to the agencies and programs responsible (listed separately), we also thank all those who helped in the funding process, including Tony Michaels, Harry Lins, Dick Poore, Fred Spilhaus, Paul Weiss, Lowell Stott, and Randy Brown.

For the scientific agenda of the workshop, we thank the indomitable Dan Cayan, with secretarial assistance from Nicki Pyles and logistic support from Larry Riddle. The meeting chairs and moderators are also gratefully acknowledged—Caroline Isaacs, Dan Cayan, Malcolm Hughes, Warren White, Ray Wilson, Lowell Stott, and Kelly Redmond. Finally, we thank all our speakers and poster presenters (listed in agenda) for their contributions and enthusiasm.

For the Proceedings volume, once again, enormous thanks go to Vera Tharp for her patience with diverse format types and her expertise with technical editing, graphics, tables, and highly skilled "pagemaking". Congratulations to Vera on her retirement this year. Special thanks also to Nancy Ullrey, Vera's able successor, who handled the final production details. Invaluable precedents for the 1996 volume were established by the previous editors of the PACLIM Proceedings—Dave Peterson (1984-1988) with the able assistance of Lucenia Thomas, Julio Betancourt and Ana MacKay (1989-1990), Kelly Redmond and Vera Tharp (1991-1993), and Caroline Isaacs and Vera Tharp (1994-1996).

The theme session for 1997, on teleconnections, was dedicated to the memory of Jerome Namias (1910-1997), a pioneer in climate research and extended range prediction, and an active PACLIM attendee throughout the first several years of the Workshop.

Ray Wilson
U.S. Geological Survey
Menlo Park, California

Statement of Purpose
Pacific Climate (PACLIM) Workshops

In 1984, a workshop was held on "Climatic Variability of the Eastern North Pacific and Western North America." From it has emerged an annual series of workshops held at the Asilomar Conference Center, Monterey Peninsula, California. These annual meetings, which involve 80-100 participants, have come to be known as PACLIM (Pacific Climate) Workshops, reflecting broad interests in the climatologies associated with the Pacific Ocean and western Americas in both the northern and southern hemispheres. Participants have included atmospheric scientists, hydrologists, glaciologists, oceanographers, limnologists, and both marine and terrestrial biologists. A major goal of PACLIM is to provide a forum for exploring the insights and perspectives of each of these many disciplines and for understanding the critical linkages between them.

PACLIM arose from growing concern about climate variability and its societal and ecological impacts. Storm frequency, snowpack, droughts and floods, agricultural production, water supply, glacial advances, stream chemistry, sea surface temperature, salmon catch, lake ecosystems, and wildlife habitat are among the many aspects of climate and climatic impacts addressed by PACLIM Workshops. Workshops also address broad concerns about the impact of possible climate change over the next century. From observed changes in the historical records, the conclusion is evident that climate change would have large societal impacts through effects on global ecology, hydrology, geology, and oceanography.

Our ability to predict climate, climate variability, and climate change critically depends on an understanding of global processes. Human impacts are primarily terrestrial in nature, but the major forcing processes are atmospheric and oceanic in origin and transferred through geologic and biologic systems. Our understanding of the global climate system and its relationship to ecosystems in the Eastern Pacific area arises from regional study of its components in the Pacific Ocean and western Americas, where ocean/atmosphere coupling is strongly expressed. Empirical evidence suggests that large-scale climatic fluctuations force large-scale ecosystem response in the California Current and in a very different system, the North Pacific central gyre. With such diverse meteorologic phenomena as the El Nino-Southern Oscillation and shifts in the Aleutian Low and North Pacific High, the Eastern Pacific has tremendous global influences and particularly strong effects on North America. In the western United States, where rainfall is primarily a cool-season phenomenon, year-to-year changes in the activity and

tracking of North Pacific winter storms have substantial influence on the hydrological balance. This region is rich in climatic records, both instrumental and proxy. Recent research efforts are beginning to focus on better paleoclimatic reconstructions that will put present-day climatic variability in context and allow better anticipation of future variations and changes.

The PACLIM Workshops address the problem of defining regional coupling of multifold elements, as organized by global phenomena. Because climate expresses itself throughout the natural system, our activity has been, from the beginning, multidisciplinary in scope. The specialized knowledge from different disciplines has brought together climatic records and process measurements to synthesize an understanding of the complete system. Our interdisciplinary group uses diverse time series, measured both directly and through proxy indicators, to study past climatic conditions and current processes in this region. Characterizing and linking the geosphere, biosphere, and hydrosphere in this region provides a scientific analogue and, hence, a basis for understanding similar linkages in other regions, as well as for anticipating the response to future climate variations. Our emphasis in PACLIM is to study the interrelationships among diverse data. To understand these interactive phenomena, we incorporate studies that consider a broad range of topics both physical and biological, time scales from months to millennia, and space scales from single sites to the entire globe.

Introduction

Raymond Wilson

The Fourteenth Annual PACLIM Workshop was held at the Wrigley Institute of Environmental Studies campus at Two Harbors, on Catalina Island, California. The island setting off the southern California coast was highly appropriate for a conference concerned with interactions between the atmosphere and ocean and their effects on terrestrial processes. Attended by about 81 registered participants (see Appendix C, Attendees), the workshop included 33 talks and 18 poster presentations. The talks consisted of a one-day theme session, Teleconnections, with ten featured (30-to-45-minute) talks (see Appendix A, Agenda). The theme session was dedicated to the memory of Jerome Namias (1910-1997). Throughout the remainder of the meeting were 22 shorter (20-minute) presentations. On Tuesday evening, Tony Michaels of WIES provided an entertaining, thought-provoking exploration of "Climate Science and Insurance Risk," complete with literary references to "The Tempest," wherein Shakespeare coined the phrase, "Brave New World." Poster presenters gave a short 1-2 minute introduction to their posters, which were displayed during the entire meeting (see Appendix B, Poster Presentations).

All presenters were invited to expand their abstracts into a manuscript for inclusion in the Proceedings volume, and nearly all presentations are included in manuscript or abstract form. In this Proceedings volume, nine papers are presented full-length, and two as extended abstracts. The abstracts submitted to the meeting are printed in a following section.

PACLIM, a Personal View

The Statement of Purpose briefly summarizes the history of the PACLIM workshops and ably summarizes our corporate goals: to understand the interaction of atmospheric and oceanic processes, their connection with terrestrial processes through geologic and biologic systems, the temporal and spatial climatic variations they produce, and the impact of these variations on society and the ecology on regional (eastern Pacific and Americas) and global scales. Over the past decade and a half, the PACLIM workshops have brought together a large "extended family" from a very broad range of disciplines—meteorology, hydrology, oceanography, glaciologists, paleontologists, limnologists, geomorphologists, and biologists, both marine and terrestrial. Particularly valuable, in my opinion, has been the mix of people representing the complete spectrum from "pure" academic research to the front lines of resource management.

My own view of PACLIM is that of a relative newcomer (1995, 1996, and 1997 meetings), with no formal credentials whatever in climate research—I am an engineering geologist and have spent two decades studying landslides. I stumbled into the climate business through research on the rainfall conditions that trigger debris-flows ("mudslides") in northern California. My USGS colleagues and I had embarked on this study after a catastrophic rain storm in the San Francisco Bay area in early January 1982 triggered thousands of debris flows and other landslides, killing 25 people and causing $66 million in property damages. The following year, a strong El Niño brought very wet conditions to northern California, producing more landslide damage, and a group of USGS researchers began a national program to reduce landslide hazards. Arising from the same climatic events, at least in part, the first PACLIM meeting was organized by Dave Peterson in 1984. It took over a decade, however, for me to broaden my interests beyond landslides toward the climatic processes that produce them.

Finally awakened to what PACLIM had been up to all these years, however, I have been warmly welcomed and delighted with the wealth of information and resources that suddenly surround me. The PACLIM workshops are useful both to climate specialists and to newcomers: the specialists exchange data and news of the latest developments within their fields (eg, Quaternary palynology, tree-ring studies, or ocean/continent teleconnections), just as in a technical session at the American Geophysical Union or American Meterological Society, only at PACLIM they have an audience that includes specialists in many other fields. For the newcomer, however, the smaller, informal PACLIM workshop presents an opportunity to not only hear lectures by the leading authorities, but to sit down and talk with them over dinner and to present their own ideas from a newcomer's perspective.

The biggest difference I see between PACLIM and the larger meetings of national organizations, however, is in the tone of the interchanges after the talks. PACLIM discussions usually take place in a spirit of cooperation and mutual exploration, rather than in competition for turf or priority. Younger investigators, and those wandering in from other fields, are encouraged to speak up and share ideas and perspectives. The field of climate studies, even when focused on the eastern Pacific and western Americas, is complex and covers vast scales in time and space, so that there is plenty of room for everyone to participate in its exploration. PACLIM, in that light, may be seen as a small trading post on the edge of a vast, rich frontier, and its annual meetings serve as its Rendezvous (the summer get-togethers of fur trappers in the early 1800's).

EL Niño 1998, a Prophecy Come to Pass

The year since the 1997 PACLIM has been a challenging and fascinating one for us all. We had barely returned to our offices when the rumors we had heard at the meeting became formal predictions of a new El Niño in the Pacific. Sea-surface temperatures were already rising, wind regimes shifting, and various other harbingers had already been noted around the dinner table by various meeting participants. So it has come to pass, a formidable El Niño, stronger even than 1982-83, with global consequences: drought and fires in Indonesia, floods in Peru (including mudslides covering part of the ancient "lines' across the Nazca Plain), disastrous ice storms in New England and the Maritimes, and as of this writing in early February 1998, floods and mudslides in northern California.

These events will doubtless provide some interesting presentations and conversations in PACLIM 1998. Maury Roos will have another exciting flood story to tell, although hopefully not quite as catastrophic as in the 1997 Water Year (Roos, this volume). The sea-surface temperature story should be very revealing. Vexing, but fascinating, questions have already arisen, such as, "Why is the Pacific Northwest so wet, and southern California so dry (as of the end of January 1998) relative to the pattern in previous El Niños of drier conditions in the Northwest and extremely wet conditions in southern California?"

Along with the climatological anomalies have come some social and political perturbations. The national media has had an insatiable interest in El Niño and its consequences. The whole subject, with teleconnections, sea-surface temperatures, sea-level variations, the Gilbert oscillation and all, has been lifted (fallen?) from the dusty shelves of academic journals into USA Today, CNN, and even situation comedies. There have been El Niño cartoons in the New Yorker, jokes on Letterman, and discussions ranging from earnest dissertations to conspiracy theories on innumerable Web pages.

What does all this mean to those of us involved with PACLIM? Well, we have a lot more of the public's attention now—however we decide to use it. Years of work that has seemed arcane and obscure is now in great demand. We live in "interesting times," with some of the sense of the old Taoist lament, but also a sense of new opportunities. I'm sure we will have much to tell each other at this year's meeting.

Influence of the North American Monsoon System on the United States Summer Precipitation Regime

R.W. Higgins, K.C. Mo, Y. Yao, and X.L. Wang

ABSTRACT: Key features of the United States summer precipitation regime are examined within the context of the evolving North American Monsoon System (NAMS). The focus is on the antecedent and subsequent atmospheric conditions over the conterminous United States relative to the onset of monsoon precipitation over the southwestern United States, which typically begins in early July. The onset of the monsoon in this region is determined using a precipitation index, based on daily observed precipitation for a 31-year period, 1963-1994. Lagged composites of the observed precipitation and various fields from the NCEP/NCAR Reanalysis for 1979-1994 provide a comprehensive picture of atmospheric conditions during the evolution of the United States warm-season precipitation regime. The summer precipitation regime is characterized by an out-of-phase relationship between precipitation over the Southwest and the Great Plains / Northern Tier and an in-phase relationship between precipitation over the Southwest and the East Coast. Changes in the upper-tropospheric wind and divergence fields (mean vertical motion) are broadly consistent with the evolution of this precipitation pattern. Enhanced upper-tropospheric divergence in the vicinity and south of the upper-tropospheric monsoon high coincides with enhanced upper-tropospheric easterlies and Mexican monsoon rainfall after onset. Over the Great Plains and along the Northern Tier, the middle and upper-tropospheric flow is more convergent, and rainfall diminishes after onset to the north and east of the monsoon high. There is increased upper-tropospheric divergence and precipitation after onset in the vicinity of an "induced" trough over the eastern United States. Consideration of the interannual variability of the monsoon precipitation over the Southwest reveals that wet (dry) monsoons are associated with an enhancement (suppression) of the upper-tropospheric monsoon anticyclone consistent with changes in the upper-tropospheric divergence, mid-tropospheric vertical motion, and precipitation patterns. The intensity of the monsoon anticyclone is a fundamental control on summertime precipitation over the Great Plains. Recent major drought (flood) episodes in the central United States, such as the 1988 Midwest drought and the 1993 Midwest flood, were associated with what may be broadly characterized as a strengthening (weakening) of the NAMS. Wet (dry) summer monsoons have tended to follow winters characterized by dry (wet) conditions in the Southwest and wet (dry) conditions in the Pacific Northwest. This association is attributed, in part, to the "memory" imparted to the atmosphere by the accompanying Pacific sea-surface temperature anomalies.

Introduction

A fundamental and necessary first step toward understanding warm-season precipitation variability over North America is the clear documentation of the major elements of the warm-season precipitation regime within the context of the evolving atmosphere-ocean-land annual cycle. Monsoon circulation systems, which develop over low latitude continental regions in response to thermal contrast between the continent and adjacent oceanic regions, are a major component of continental warm-season precipitation regimes. The North American warm season is characterized by such a monsoon system (hereafter referred to as the North American Monsoon System or NAMS). This system provides a useful framework for describing and diagnosing warm-season climate

In: R.C. Wilson and V.L. Tharp, Editors. 1998. *Proceedings of the Fourteenth Annual Pacific Climate (PACLIM) Workshop, April 6-9, 1997.* Interagency Ecological Program, Technical Report 57. California Department of Water Resources.

controls and the nature and causes of year-to-year variability. This system displays many similarities (as well as differences) with its Asian counterpart (e.g. Tang and Reiter 1984). While the NAMS is less impressive than its Asian sister, it still has a tremendous impact on local climate.

The life cycle and large-scale features of the NAMS can be described using terms typically reserved for the much larger Asian Monsoon system; that is, we can characterize the life cycle in terms of development, mature, and decay phases. A detailed discussion of the life cycle of the NAMS, including a literature review, is found in Higgins et al. (1997b). A schematic illustrating the key elements of the NAMS during the mature phase is shown in Figure 1. Attempts to describe and understand the major elements of the NAMS and their evolution have been hampered to a large extent by the lack of adequate *in situ* and satellite data. Over the last two decades, operational data-assimilation systems have provided global gridded atmospheric analyses necessary for climate studies of phenomena such as the monsoon. However, operationally mandated changes in the assimilation systems have introduced inhomogeneities in the data record that have led to difficulties in defining anomalies (e.g. Trenberth and Olson 1988). In addition, computer limitations have generally restricted the range of variables and the number of levels that

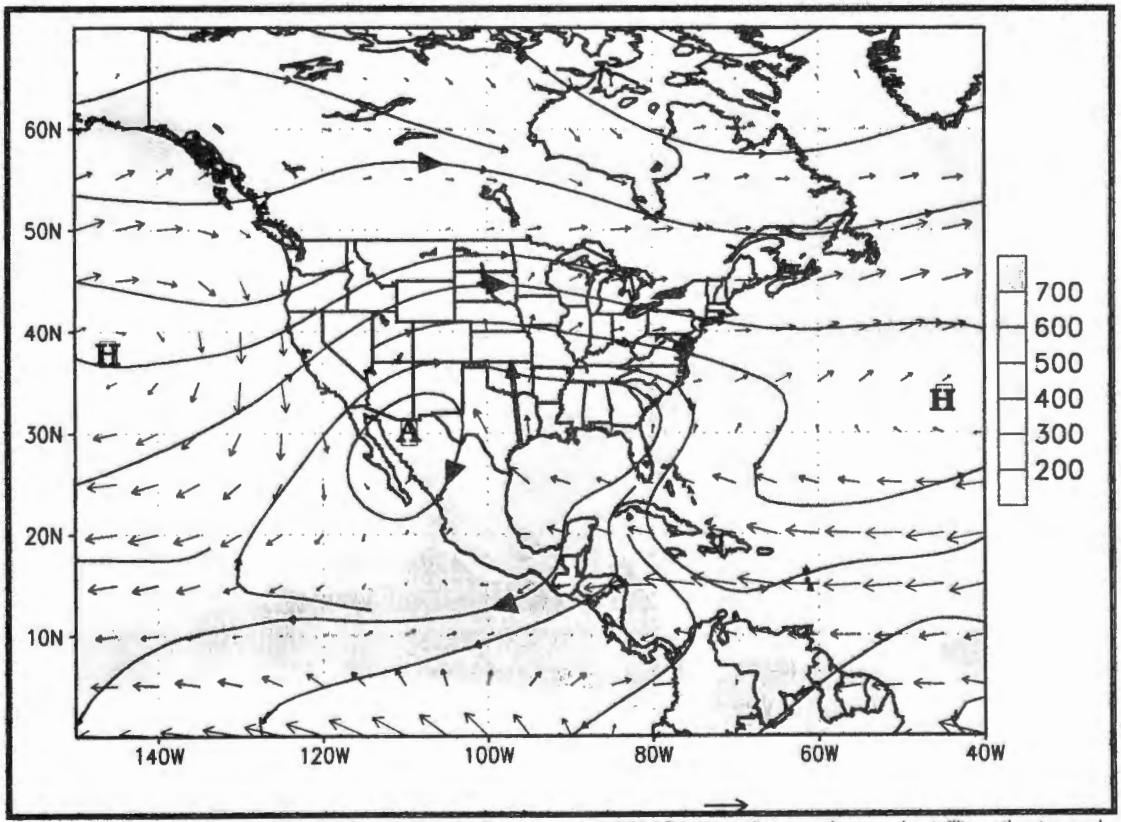

Figure 1. Mean (July-September 1979-1995) 925-hPa vector wind, 200-hPa streamlines, and merged satellite estimates and station observations of precipitation (shading). Circulation data are taken from the NCEP/NCAR Reanalysis archive. The position of the North American Monsoon Anticyclone is indicated by "A". The Bermuda and North Pacific subtropical high pressure centers are indicated by "H". Precipitation amounts are in mm. The characteristic vector length is 10 m s^{-1}. The approximate location of the Great-Plains low-level jet is indicated by the heavy solid arrow.

can be archived. Clearly, advances in describing, understanding, and modeling the warm-season precipitation regime over North America will require homogeneous data sets.

The NCEP/NCAR Reanalysis Project [currently underway at NCEP in cooperation with NCAR; Kalnay et al. 1996] will provide at least 40 years (1957-1996+) of global gridded fields produced with a fixed state-of-the-art analysis system and large input data base (including data available after the operational cutoff time). This data set provides many new opportunities for studies of the NAMS. A gridded hourly precipitation data base for the United States (1963-1995) developed by Higgins et al. (1996) provides the basis for daily (and hourly) precipitation analyses over regions influenced by the NAMS. In this study we exploit the Reanalysis data (for 1979-1994) and the observed precipitation data (for 1963-1994) to diagnose the large-scale features of the United States warm-season precipitation regime. The onset of monsoon rainfall over the southwestern United States is determined using a precipitation index, based on the daily observed precipitation for a 31-year (1963-1994) period and a threshold crossing procedure. The strategy is to use lagged composites of various atmospheric circulation fields relative to monsoon onset in the southwestern United States to identify major features of the United States summer precipitation regime. The mean seasonal evolution of the NAMS is considered in more detail in Higgins et al. (1997b); the interannual variability of the NAMS is discussed in Higgins et al. (1997c).

Data Analysis

To study the summer precipitation regime over the United States relative to the onset of monsoon rainfall over the southwestern United States, we use a monsoon index based on hourly, gridded precipitation analyses over the conterminous United States (Higgins et al. 1996) for the period January 1, 1963, through December 31, 1994. The analyses were gridded to a horizontal resolution of 2 degrees latitude by 2.5 degrees longitude. A precipitation index (PI) was obtained by averaging daily accumulations of observed precipitation at each grid point of the rectangular region (112.5°W - 107.5°W, 32°N - 36°N) over Arizona and western New Mexico. Histograms of the mean (1963-1994) daily rainfall (and the 5-day running mean) during summer at each grid point over the southwestern United States (not shown) reveal that all of the grid points used for the PI exhibit rapid increases in rainfall by early July. Monsoon onset dates were determined using the resulting time series and a threshold crossing procedure. The PI magnitude and duration criteria used were +0.5 mm day^{-1} and 3 days, respectively; the monsoon onset date for each year occurs when the selection criteria are first satisfied after June 1. Composite evolution fields for 1963-1994 (observed precipitation) and 1979-1994 (Reanalysis fields) were obtained by averaging over all of the

monsoons relative to the day when the PI first satisfies the threshold criteria; this day is designated as the onset day, or day 0. Note that by realigning the time series in this way, we are not performing a simple average based on calendar day. The onset date of the monsoon over the southwestern United States for 1963-1994 ranges from June 21 to August 3; the average date of the monsoon onset for the period is July 7.

The composite evolution of the PI (Figure 2) shows the onset of the southwestern rains. It is important to note that the compositing scheme based on the PI makes the monsoon onset appear to be abrupt, because it is keyed to synoptic as well as climate variability as evidenced by the pronounced overshoot. Composites of observed precipitation and various fields from the NCEP/NCAR Reanalysis (including heights, winds, and moisture) were constructed each day for the 90-day period from 45 days before onset (day -45) to 44 days after onset (day +44).

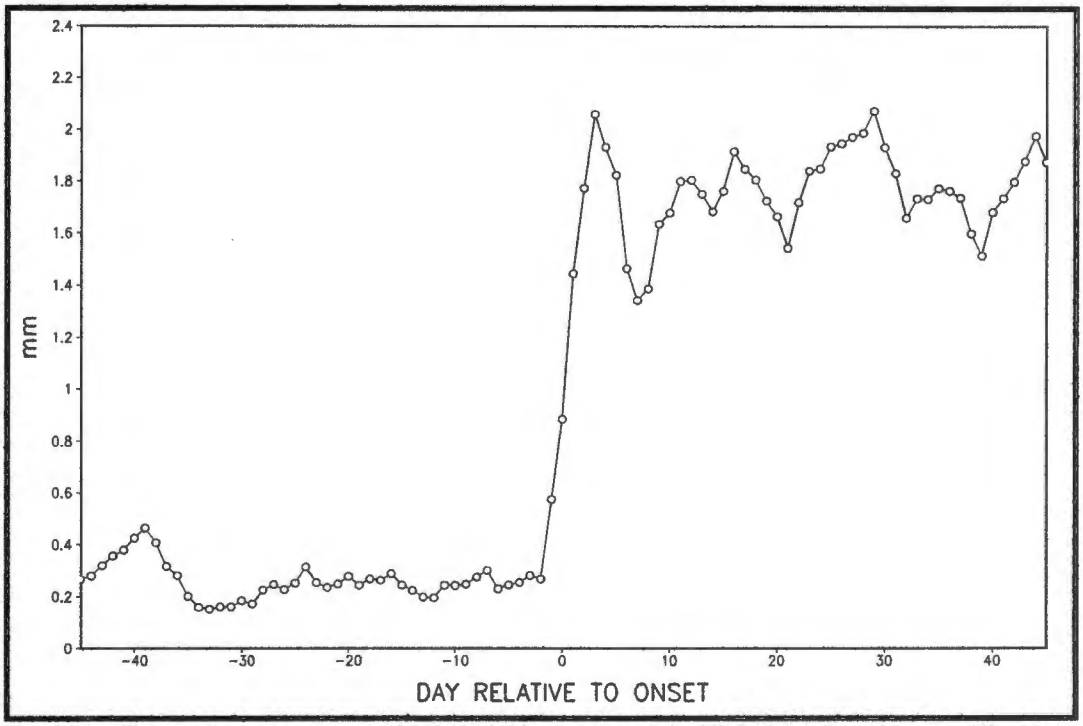

Figure 2. Evolution of the composite mean (1963-1994) daily precipitation index (PI) (Units: mm) over Arizona and New Mexico. The average date of monsoon onset is July 7 (defined as day 0 in the composite analysis).

Features of the United States Summer Precipitation Regime

During July-September, usually the three rainiest summer months, rainfall in excess of 70 mm is found from the Great Plains to the East Coast (Figure 3). New Mexico experiences slightly more rainfall than Arizona. The extension of the Mexican Monsoon rainfall into the southwestern United States is clearly evident in Figure 4, which shows the ratio (expressed in percent) of rain falling during July-September to the annual

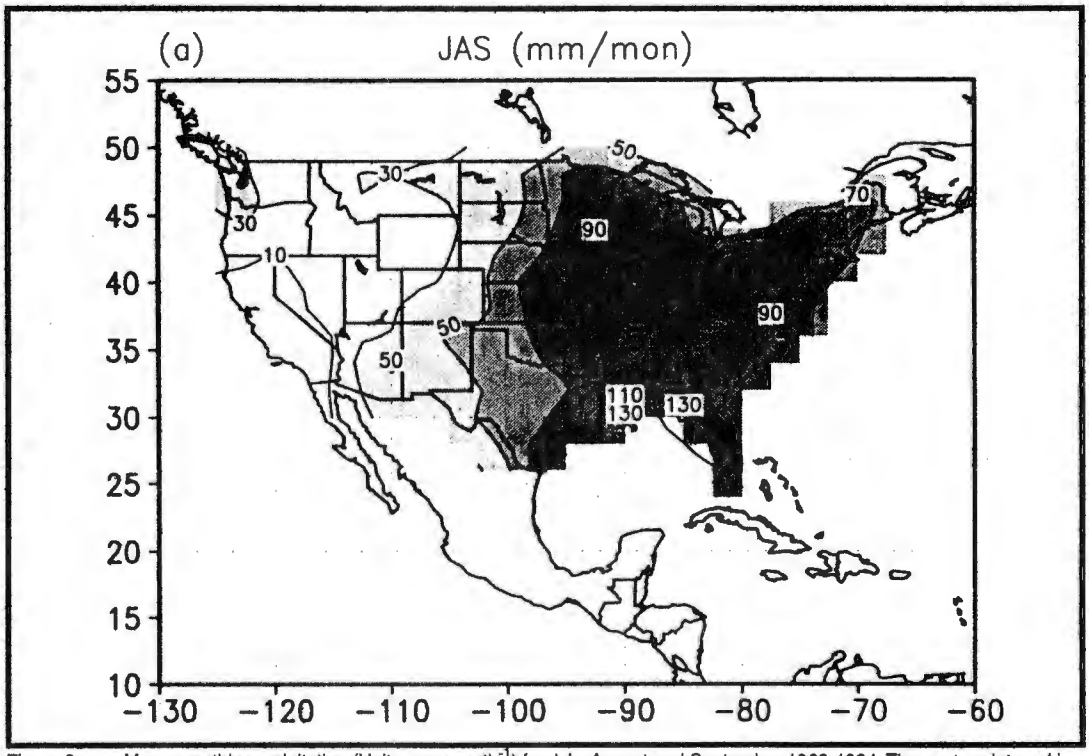

Figure 3. Mean monthly precipitation (Units: mm month^{-1}) for July, August and September 1963-1994. The contour interval is 20 mm month^{-1} and values greater than 30 mm month^{-1} are shaded.

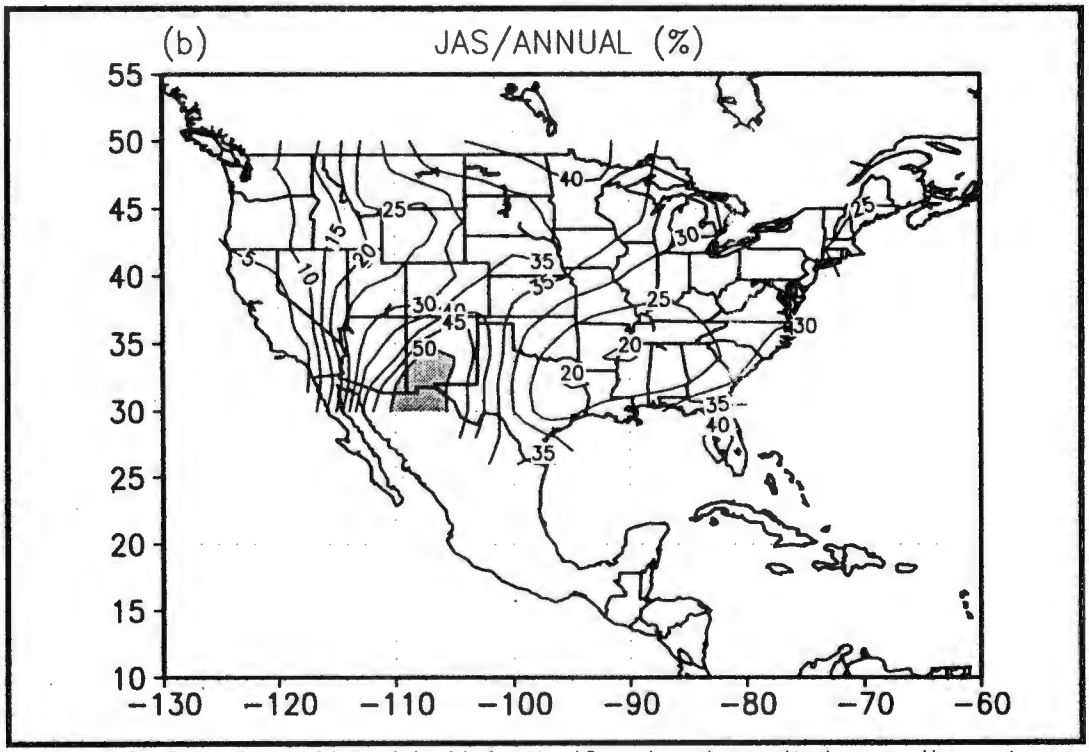

Figure 4. Contribution of the precipitation during July, August and September to the annual total, expressed in percent. The contour interval is 5% and values greater than 40% are shaded.

mean precipitation. The maximum values extend northeastward across New Mexico and into the high plains of southeastern Colorado and western Kansas. Climatological aspects of the onset of the summer rains over the southwestern United States and western Mexico can be viewed from maps of the mean rainfall difference between June and July (Figure 5), when the largest monthly variation in rainfall occurs for the southwestern United States. The most dramatic increases in rainfall over the continent occur along the west slopes of the SMO (not shown), where local increases greater than 160 mm are found. Over the southwestern United States there are increases exceeding 20 mm over much of Arizona and New Mexico (Figure 5); there is a rapid decrease in the rainfall change to the east and north of this region and an increase in rainfall along the east coast. Over the Great Plains and along the Northern Tier, the rainfall decreases between June and July by roughly the same amount as the rainfall increases in the southwestern United States. Along the eastern seaboard and portions of the Gulf Coast, there are rainfall increases between June and July. Previous studies have linked the onset of summer rains over northern Mexico and the southwestern United States to a decrease of rainfall over the Great Plains (e.g. Mock 1996; Tang and Reiter 1984; Douglas et al. 1993; Arthur Douglas, personal communication) and to an increase of rainfall along the East Coast (Tang and Reiter 1984).

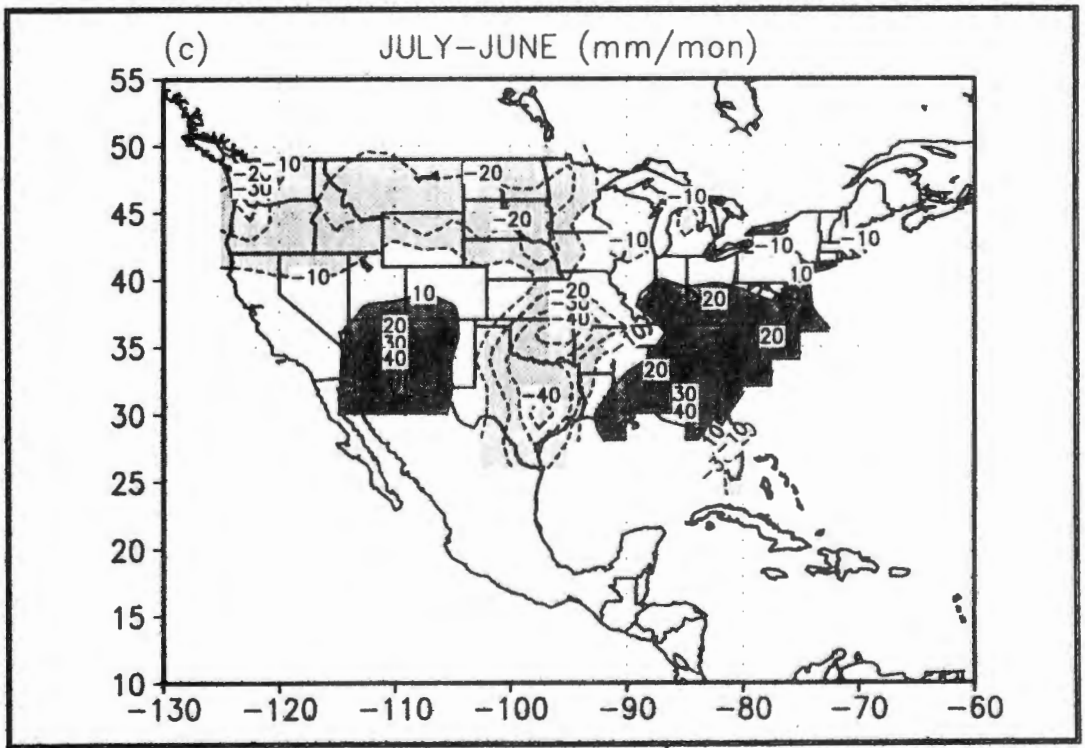

Figure 5. Analysis of mean July minus June precipitation (Units: mm month^{-1}) for 1963-1994. The contour interval is 10 mm month^{-1} and positive (negative) values are shaded dark (light).

The large-scale, low-level flow over the southern United States and Mexico is strongly influenced by the subtropical highs (Figure 6), with brisk southerlies over the southern Great Plains (reflecting the Great Plains low-level jet) and northwesterlies west of Baja California (reflecting the Baja jet). Weak evidence of the thermal low can be seen in the cyclonic winds over the Desert Southwest. The winds at 500-hPa (Figure 7) are characterized by easterlies over the Tropics, widespread westerlies poleward of roughly 35°N, and an anticyclonic circulation centered over the Rio Grande Valley. We note that at 500-hPa there is a strong southerly component in the winds around the west side of the monsoon high. The 500-hPa vertical velocity (Figure 8) indicates localized ascent over the Great Basin, the Southern Rockies, the SMO, and the southeastern United States. Descent is situated over the Plains states, extending from the Gulf Coast to the Canadian border, the Great Lakes, the East Pacific Ocean and the northern Gulf of California. The region of upward motion is consistent with monsoon precipitation. The distribution of specific humidity at the surface (Figure 6) strongly reflects the underlying terrain, with high values flanking the southern Rockies and the Mexican Plateau. Surface humidity increases eastward into the southeastern United States, and a moist tongue extends up the Gulf of California and along the western coast of Mexico. In the middle troposphere (Figure 7), a band of enhanced moisture extends from the eastern tropical Pacific into Mexico and then New Mexico. The precipitable water (Figure 9) indicates abundant moisture over the eastern tropical Pacific, southern Gulf of California and Baja California, western Mexico, and the eastern half of the United States.

Evolution of the United States Summer Precipitation Regime

A map of the change in composite mean observed precipitation represented as the difference between the 45-day period after onset (day 0 to day +44) and the 45-day period before onset (day -45 to day -1) (Figure 10) yields a pattern quite similar to the intermonthly (July minus June) precipitation map discussed earlier; this result is consistent with the fact that the southwestern rains typically appear near the beginning of July. After onset, the Great Plains and Northern Tier experience a drying trend as a result of the strengthened and expanded middle- and upper-tropospheric monsoon high, but mesoscale convective activity, occasional upper-level disturbances, localized mountain valley circulations, and nocturnal LLJ-related precipitation keep the region relatively wet compared to the drier winter months (Tang and Reiter 1984; Augustine and Caracena 1996, Higgins et al. 1997a).

A longitude-time diagram of composite mean observed precipitation anomalies (departures from the June-August 1963-1994 mean) averaged between 34°N and 38°N (Figure 11) shows that, prior to onset, negative

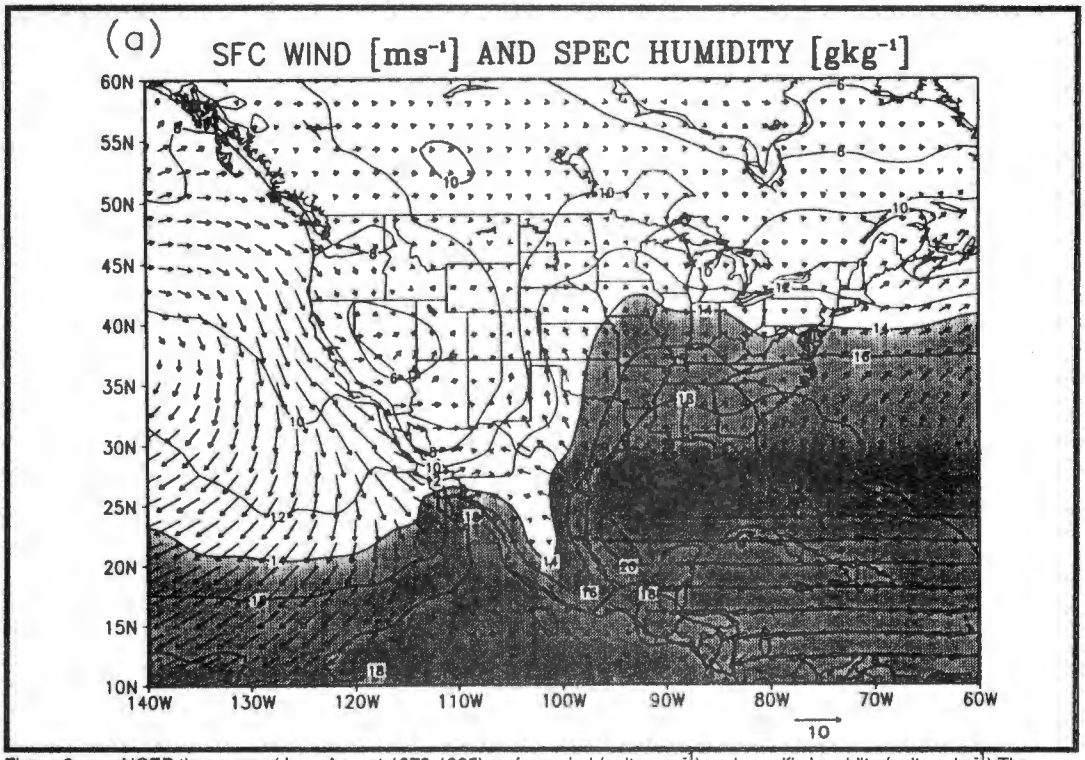

Figure 6. NCEP time-mean (June-August 1979-1995) surface wind (units: m s^{-1}) and specific humidity (units: g kg^{-1}) The standard vector length is 10 m s^{-1}. The contour interval is 2 g kg^{-1}. The shading denotes specific humidity greater than 14 g kg^{-1}.

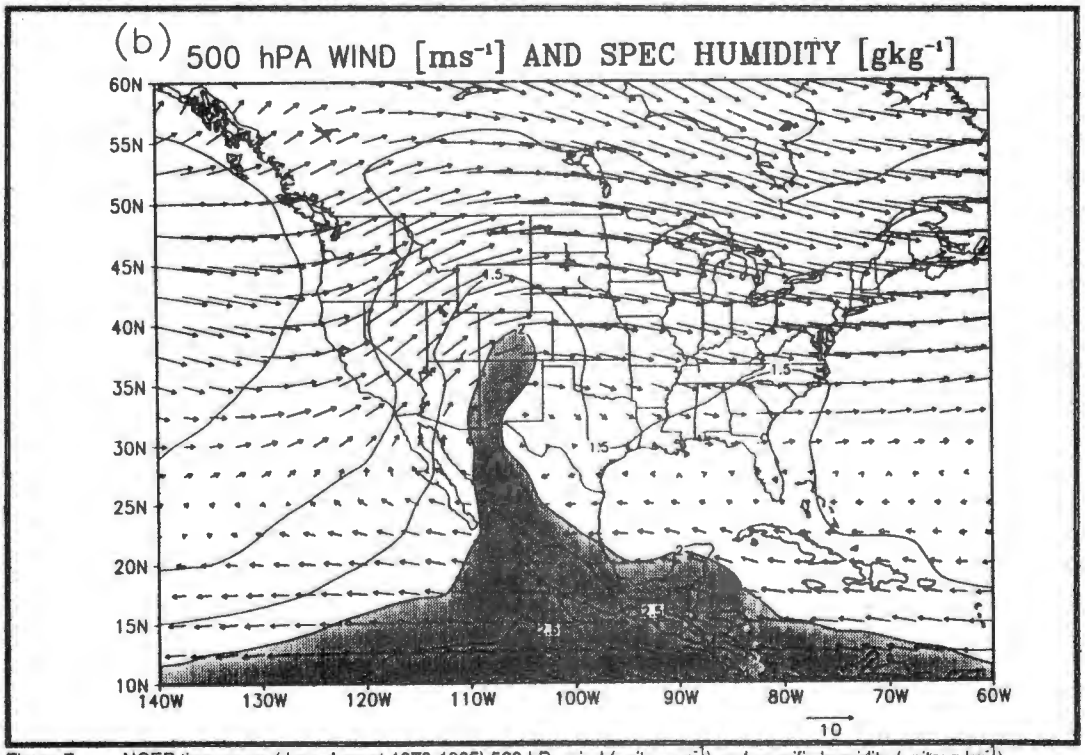

Figure 7 NCEP time-mean (June-August 1979-1995) 500-hPa wind (units: m s^{-1}) and specific humidity (units: g kg^{-1}) The standard vector length is 10 m s^{-1}. The contour interval is 0.5 g kg^{-1}. The shading denotes specific humidity greater than 2 g kg^{-1}.

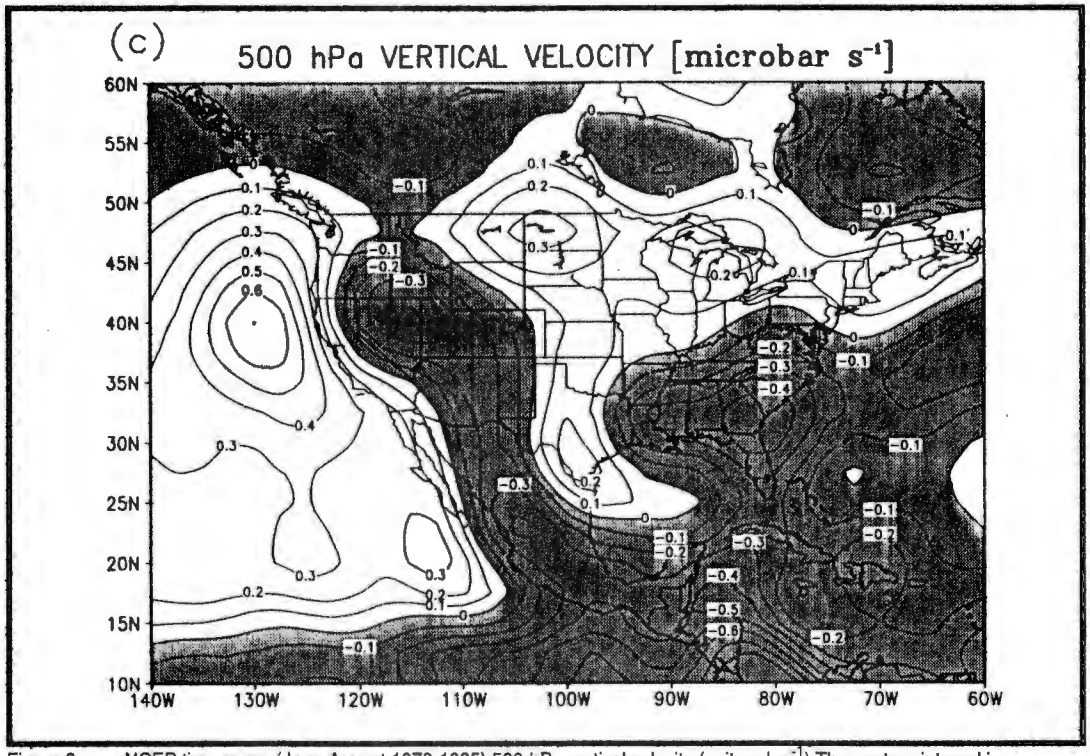

Figure 8. NCEP time-mean (June-August 1979-1995) 500-hPa vertical velocity (units: μb s^{-1}) The contour interval is 0.1 μb s^{-1}. The shading denotes upward motion.

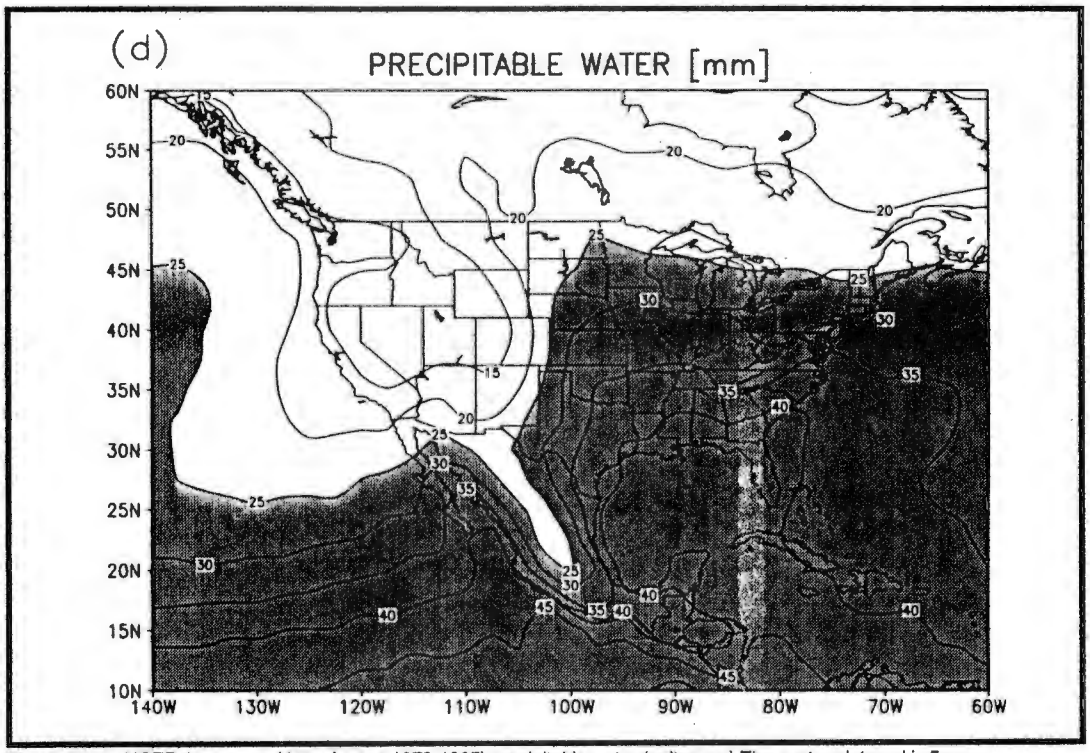

Figure 9. NCEP time-mean (June-August 1979-1995) precipitable water (units: mm) The contour interval is 5 mm. The shading denotes precipitable water greater than 25 mm.

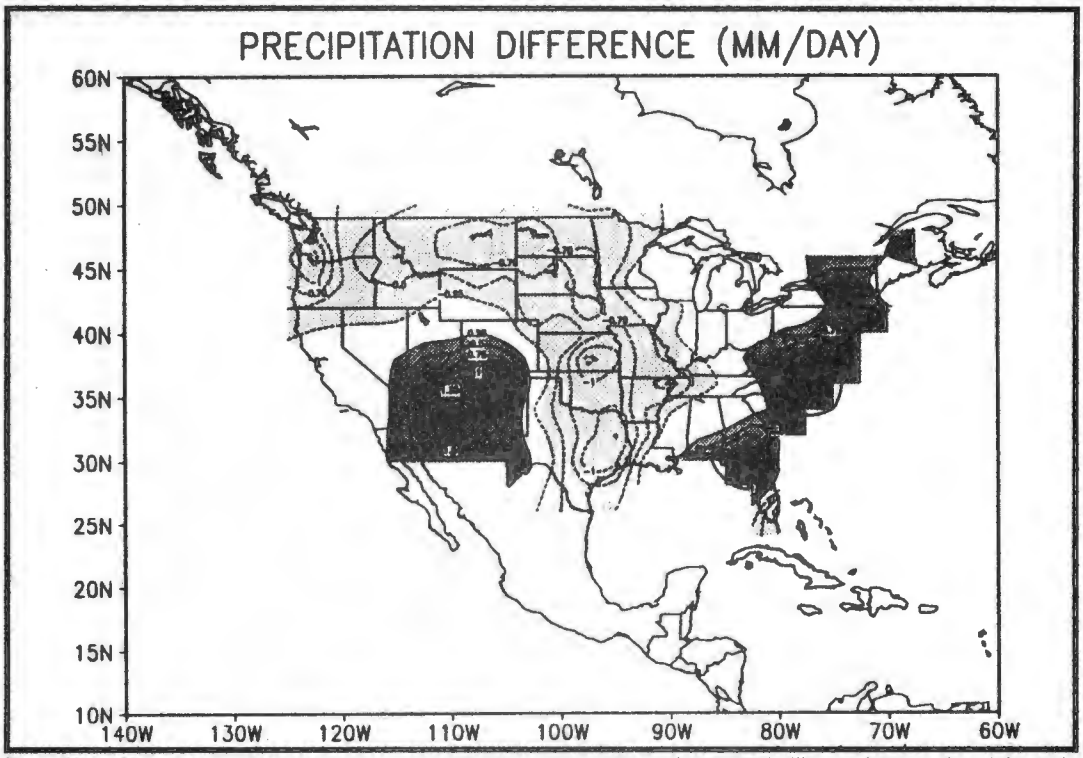

Figure 10. Map of observed precipitation represented as the composite mean (1963-1994) difference between the 45-day period after onset (day 0 to day +44) and the 45-day period before onset (day -45 to day -1). The contour interval is 0.25 mm day^{-1}, the zero contour is omitted for clarity and values greater than 0.25 mm day^{-1} (less than -0.25 mm day^{-1}) are shaded dark (light).

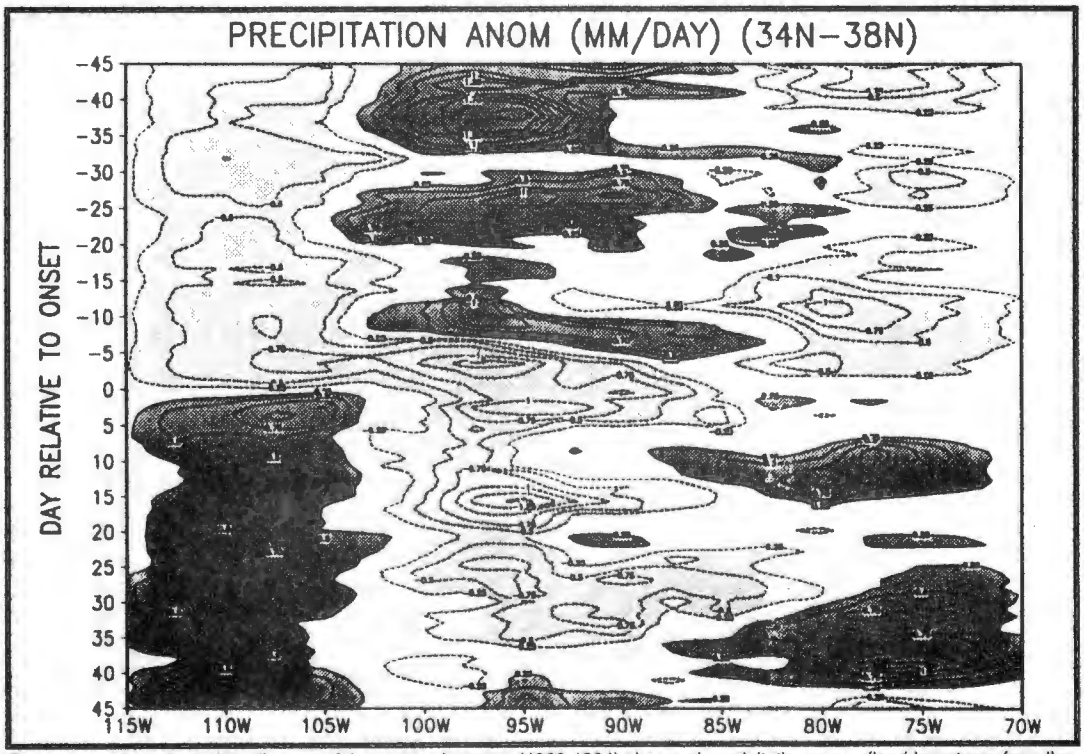

Figure 11. Longitude-time diagram of the composite mean (1963-1994) observed precipitation anomalies (departures from the June-August 1963-1994 time-mean) averaged between 34°N and 38°N. Results are shown for a 3-day running mean. The contour interval is 0.25 mm day^{-1}, the zero contour is omitted for clarity and values greater than 0.25 mm day^{-1} (less than -0.25 mm day^{-1}) are shaded dark (light).

anomalies over the southwest monsoon region are associated with positive anomalies over the Great Plains and negative anomalies along the East Coast; this phase of the precipitation pattern persists for several weeks prior to monsoon onset. After onset, the opposite phase of the pattern appears as indicated in Figure 11. The eastward spread of negative anomalies and the transition to the summer precipitation regime occurs very rapidly around the time of onset. Figure 11 also shows a decrease in rainfall over the central United States roughly 5 days before onset. It is evident that the summer rainfall over the central and particularly the eastern United States is much more episodic than that in the Southwest monsoon region.

Changes in the tropospheric circulation and divergence (mean vertical motion) fields during the evolution can be related to changes in the continental precipitation regime. A region of enhanced upper-tropospheric divergence in the vicinity and south of the monsoon high coincides with enhanced upper-tropospheric easterlies (or weaker westerlies) (Figure 12), enhanced mid-tropospheric vertical motion (Figure 13), and enhanced monsoon rainfall (Figure 10). In contrast, the flow is more convergent and rainfall diminishes to the north and east of the monsoon high (Figure 12), particularly over the Great Plains in the vicinity of strong mid-tropospheric subsidence (Figure 13); the monsoon high organizes the flow at middle and upper levels over the Great Plains, thereby acting as an effective control on LLJ-related rainfall (Higgins et al. 1997a). There is some evidence of increased upper-tropospheric divergence (Figure 12), vertical motion (Figure 13) and precipitation (Figure 10) near an "induced" trough over the eastern United States. Typically, enhanced rainfall appears along the east coast roughly 10 days after onset (Figure 11), which may be a characteristic lag time for development of the eastern trough.

In a study of the influence of the Great Plains low-level jet on summertime precipitation over the United States, Higgins et al. (1997a) found that enhanced LLJ-related rainfall over the Great Plains was associated with suppressed rainfall over the southwestern United States and along the East Coast. Their precipitation anomaly pattern (see Figure 14 in that study) is strikingly similar to the one shown in Figure 10. Recall from Figure 11, however, that there is a marked decrease in LLJ-related rainfall over the Great Plains after onset. To determine whether this decrease in rainfall after onset is due to some fundamental change in the LLJ, we examined the average frequency of occurrence of criterion 1 jets (Bonner 1968) during the nighttime hours for May, June, July, and August 1985-1989 using the NCEP/NCAR Reanalysis and the approach outlined in Higgins et al. 1997a. We find little intermonthly change in the LLJ frequency maxima over the Great Plains with a relatively small *increase* in LLJ frequency from June to July over the southern Plains (not shown, but see Figure 18 of Higgins et al. 1997b). Intermonthly changes

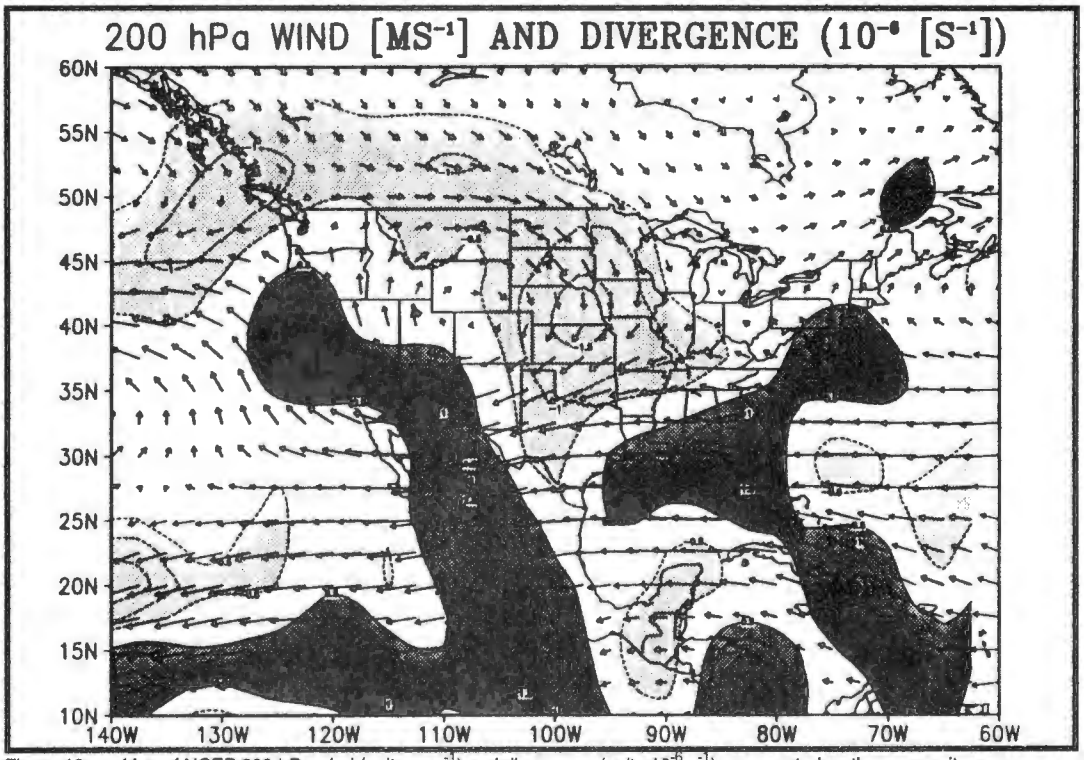

Figure 12. Map of NCEP 200-hPa wind (units: m s^{-1}) and divergence (units:10^{-6} s^{-1}) represented as the composite mean (1979-1994) difference between the 45-day period after onset and the 45-day period before onset. The contour interval is $0.5x10^{-6}$ s^{-1}.

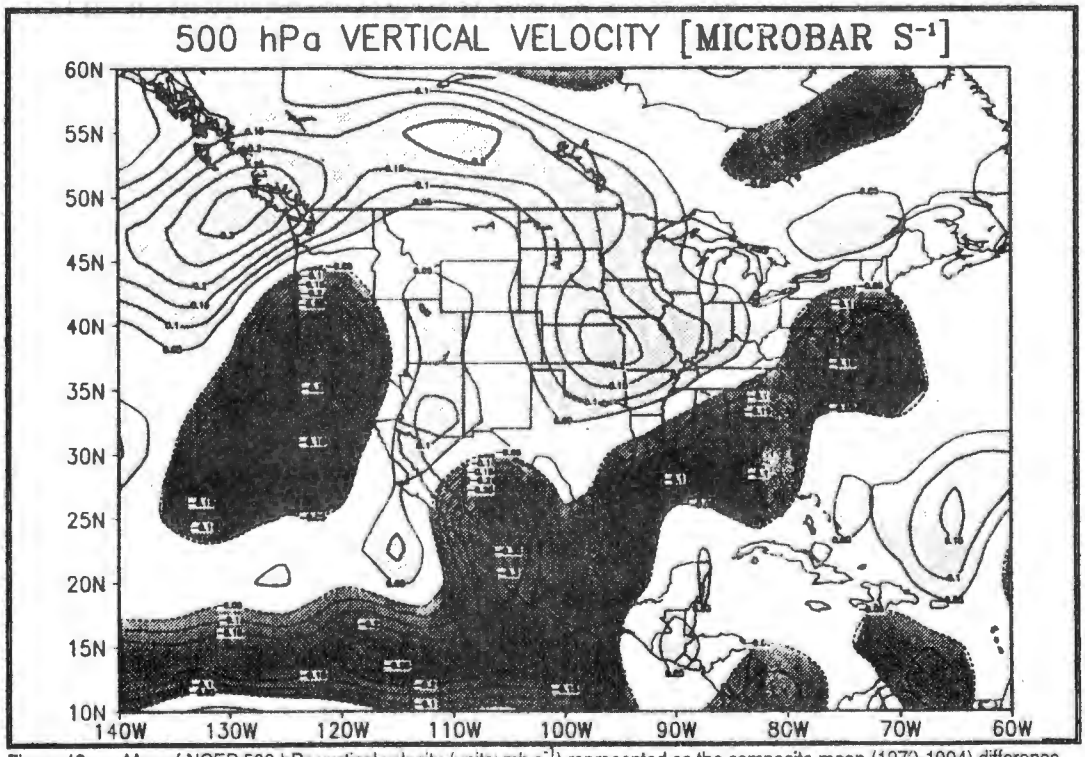

Figure 13. Map of NCEP 500-hPa vertical velocity (units: mb s^{-1}) represented as the composite mean (1979-1994) difference between the 45-day period after onset and the 45-day period before onset. The contour interval is 0.05 mb s^{-1}.

in moisture transport for criterion 1 jets show some evidence of the impact of the middle- and upper-tropospheric ridge over western North America, but there is little change in the moisture transport over the Great Plains. This implies that LLJ-related rainfall is controlled by changes in the large-scale flow related to the evolution of the North American Monsoon System. In particular, the northward migration of the upper-tropospheric monsoon high leads to upper-tropospheric convergence (Figure 12) and mid-tropospheric subsidence (Figure 11) over the Great Plains, thereby limiting LLJ-related rainfall after onset.

Interannual Variability of the United States Summer Precipitation Regime

The social and economic impacts of large-scale hydrologic anomalies, such as the 1993 Midwest flood and the 1988 Midwest drought, are considerable. These events remind us that year-to-year variability of warm season precipitation is large. In semiarid regions, such as Arizona and New Mexico, interannual variability tends to be even larger in relation to seasonal mean rainfall. Relationships between interannual variability of the United States summer precipitation regime and the intensification, weakening, or changes in position of the climatological-mean features that organize this regime are considered in detail in Higgins et al. (1997c).

The PI may be used to classify individual years as wet or dry for 1963-1994 by averaging daily precipitation for the 90-day period after monsoon onset (Figure 14). If we order the individual values on Figure 14 from largest to smallest and use the top (bottom) 25% to classify wet (dry) monsoons, then we find

Wet: 1967, 1972, 1977, 1983, 1984, 1986, 1988, 1990

Dry: 1965, 1969, 1973, 1974, 1978, 1979, 1980, 1993

The remaining 50% (16 years) are considered normal years. This classification gives a reasonable separation between wet and dry monsoons; mean values for the 90-day period after onset are 1.77 mm day^{-1} for wet, 0.98 mm day^{-1} for dry, and 1.37 mm day^{-1} for all monsoons. The average date of onset is July 1 for wet monsoons and July 11 for dry monsoons. Based on this classification, we note that the 1988 Midwest drought (1993 Midwest flood) occurred during a wet (dry) Southwest monsoon; this out-of-phase relationship between the Southwest and the Great Plains is a key aspect of the NAMS.

The composite evolution of the PI for wet and dry monsoons is shown in Figure 15. In both wet and dry years, the onset of the Southwest monsoon rains is clearly evident, just as it is in the composite based on all years. Wet monsoons are characterized by a much longer period of

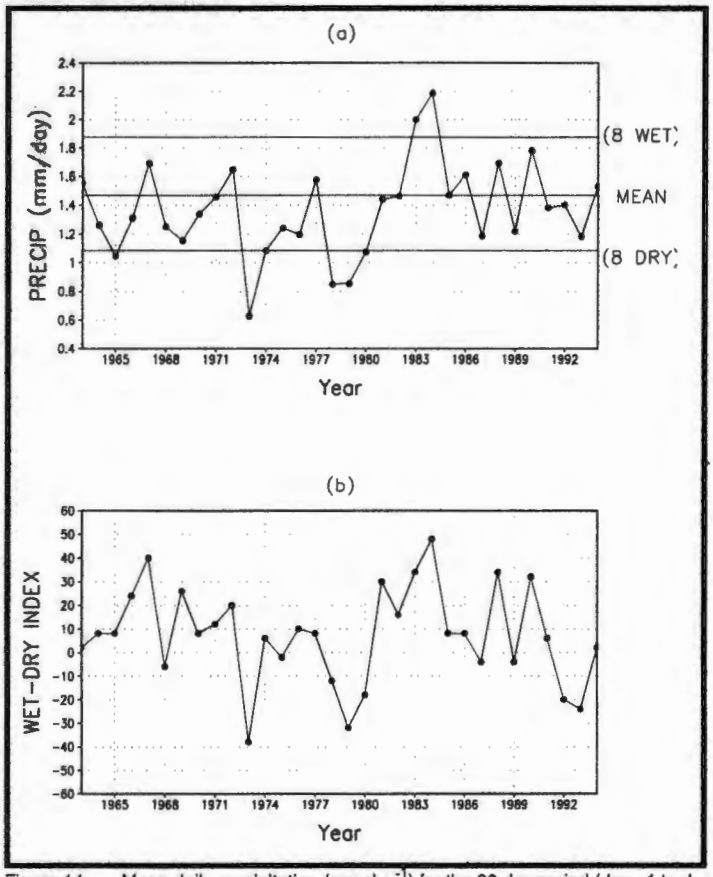

Figure 14. Mean daily precipitation (mm day^{-1}) for the 90 day period (day +1 to day +90) after monsoon onset based on the PI.

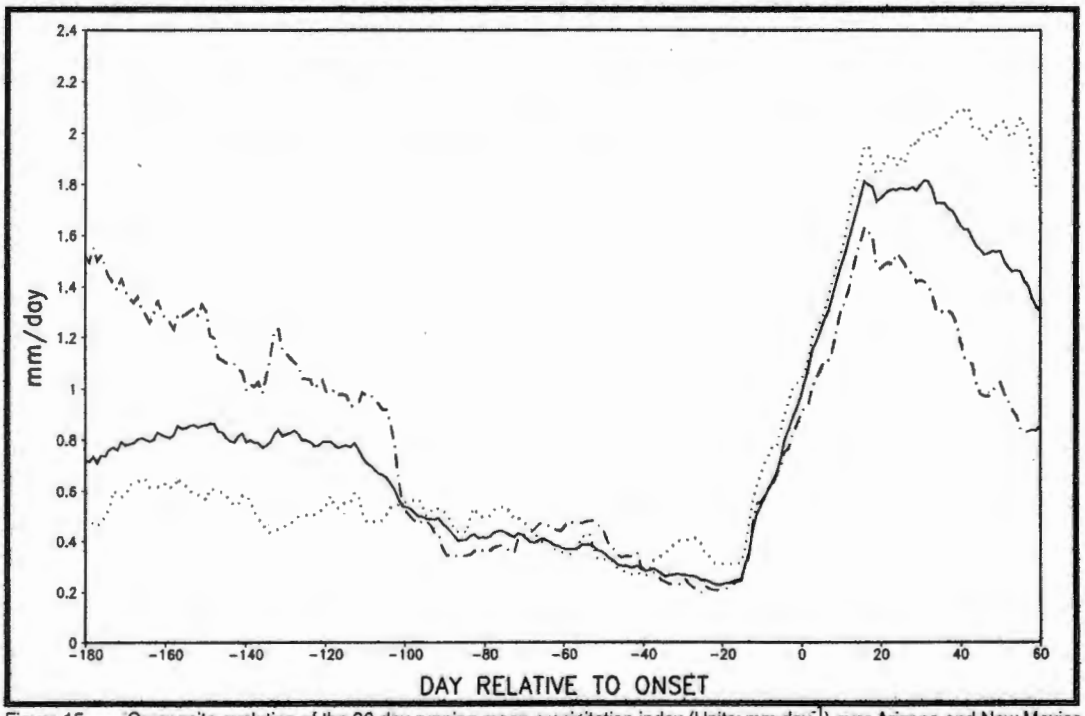

Figure 15. Composite evolution of the 30-day running mean precipitation index (Units: mm day^{-1}) over Arizona and New Mexico for wet monsoons (dotted line), dry monsoons (dot-dashed line) and all (1963-1994) monsoons (solid line). The average date of monsoon onset is July 1 for wet monsoons, July 11 for dry monsoons and July 7 for all monsoons (defined as day 0 in each case).

heavy rainfall after onset than dry ones. Interestingly, the composite evolution also shows that wet (dry) summer monsoons are preceded by relatively dry (wet) conditions during the preceding winter (roughly days -180 to -100).

The interannual variability of the continental-scale precipitation pattern closely mimics changes associated with development of the monsoon. Maps of the composite mean observed precipitation represented as the difference between the 45-day period after onset (day 0 to day +44) and the 45-day period before onset (day -45 to day -1) for wet, dry, and all monsoons (not shown) indicate that the continental-scale precipitation pattern is preserved in each case. In each composite, the Southwest is wetter after onset, but there is relatively more precipitation during wet monsoons. In each composite, the Great Plains and Northern Tier are drier after onset as a result of the strengthened and expanded middle and upper tropospheric monsoon high, but wet monsoons are associated with a relatively drier Great Plains. Over portions of the Upper Midwest, differences between wet and dry monsoons are even larger than in the Southwest, emphasizing the potential impact of monsoon variability on ground water and irrigation for these regions. Examination of the period after onset (day +1 to day +90; roughly July-September) clearly shows enhanced (suppressed) rainfall over the southwestern United States for wet (dry) monsoons. A difference map (not shown) shows that rainfall during wet monsoons exceeds that of dry monsoons by more than 0.7 mm day^{-1}, on average, over southeastern Arizona and southwestern New Mexico, where the composites are almost mirror images of each other. During wet monsoons much of the central Great Plains, lower Mississippi Valley, and East Coast is relatively dry, while the Great Lakes and southern Texas are relatively wet. During dry monsoons much of the Mississippi Valley, Ohio Valley, and mid-Atlantic is relatively wet.

Wet (dry) monsoons are also associated with a stronger (weaker) upper-tropospheric monsoon anticyclone over the western United States, consistent with changes in the upper tropospheric divergence, mid-tropospheric vertical motion, and precipitation patterns (see Higgins et al. 1997c for details). The intensity of the monsoon anticyclone appears to be one of the most fundamental controls on summertime precipitation downstream over the Great Plains. Recent major drought (flood) episodes in the central United States, such as the 1988 Midwest drought (1993 Midwest flood), were associated with what may be broadly characterized as a stronger (weaker) NAMS.

The interannual variability of the United States warm season precipitation regime is linked to the season-to-season "memory" of the coupled atmosphere-ocean system over the eastern tropical Pacific (see Higgins et al. 1997c for details). Composites of observed sea-surface temperature, subsurface ocean temperature, precipitation, and OLR during the

seasons preceding wet and dry monsoons reveal a number of coherent changes in the eastern Pacific ITCZ-cold tongue complex that clearly affect the warm season precipitation regime over the United States. In particular, SST anomalies in the eastern Pacific cold tongue and precipitation anomalies in the ITCZ, present during the winter and spring preceding the monsoon, are linked via an anomalous local Hadley circulation to the warm season precipitation regime over the United States and Mexico. Wet (dry) summer monsoons tend to follow winters characterized by dry (wet) conditions in the Southwest (Figure 14) and wet (dry) conditions in the Pacific Northwest. This association is attributed, in part, to the "memory" imparted to the atmosphere by the accompanying Pacific SST anomalies (Higgins et al. 1997c).

Acknowledgments

We wish to thank Jess Charba for the hourly precipitation data and the Environmental Modeling Center Reanalysis Team for the NCEP/NCAR Reanalysis data. The authors are also indebted to Chester Ropelewski, Eugene Rasmusson, Dan Cayan, John Janowiak, and Vernon Kousky for insightful discussions. This work was partially supported by the NOAA Office of Global Programs under the Pan American Climate Studies (PACS) project and the GEWEX Continental-Scale International Project (GCIP) and by Interagency Agreement No. S-41367-F under the authority of NASA/GSFC.

References

Augustine, J.A., and F. Caracena. 1996. Lower-tropospheric precursors to nocturnal MCS development over the central United States. *Wea. and For.* 9:116-135.

Bonner, W.D. 1968. Climatology of the low-level jet. *Mon. Wea. Rev.* 96:833-850.

Douglas, M.W., R.A. Maddox, K. Howard, and S. Reyes. 1993. The Mexican Monsoon. *J. Climate* 6:1665-1677.

Higgins, R.W., J.E. Janowiak, and Y. Yao. 1996. A gridded hourly precipitation data base for the United States (1963-1993). NCEP/Climate Prediction Center ATLAS No. 1, 47 pp. (Available from Climate Prediction Center/NCEP/NWS/NOAA, Camp Springs, MD).

Higgins, R.W., Y. Yao, E.S. Yarosh, J.E. Janowiak, and K.C. Mo. 1997a. Influence of the Great Plains low-level jet on summertime precipitation and moisture transport over the central United States. *J. Climate.* 10:481-507.

Higgins, R.W., Y. Yao, and X. Wang. 1997b. Influence of the North American Monsoon System on the United States summer precipitation regime. *J. Climate* (Nov 1997).

Higgins, R.W., K.C. Mo, and Y. Yao. 1997c. Interannual variability of the United States summer precipitation regime. (Submitted to *J. Climate*).

Kalnay, E., and co-authors. 1996. The NCEP/NCAR Reanalysis Project. *Bull. Amer. Meteor. Soc.* 77:437-471.

Mock, C.J. 1996. Climatic controls and spatial variations of precipitation in the western United States. *J. Climate* 9:1111-1125.

Tang, M., and E.R. Reiter. 1984. Plateau monsoons of the Northern Hemisphere: A comparison between North America and Tibet. *Mon. Wea. Rev.* 112:617-637.

Trenberth, K.E., and J.G. Olson. 1988. An evaluation and intercomparison of global analyses from the National Meteorological Center and the European Center for Medium-Range Weather Forecasts. *Bull. Amer. Meteor. Soc.* 69:1047-1057.

A Late Glacial Age Pollen Biozone for Central California

G. James West

ABSTRACT: Pollen biozones are analytic units characterized by their pollen spectra or assemblages. A late glacial age pollen biozone from Sacramento (American River sediments) is characterized by high pine (*Pinus*) and fir (*Abies*) pollen values. Equivalent age central California biozones from Laguna de las Trancas and Clear Lake with similar pollen spectra indicate a regional chronostratigraphic unit with climatic implications. Such pollen values imply significantly cooler and, perhaps, wetter conditions than today. This interpretation is in contrast to late glacial age pollen spectra from the east side of the Sierra Nevada that suggest cold and dry conditions. Like today, a steep climatic gradient during the last full glacial is inferred.

Introduction

Pollen analysis of sediments below the new Federal Courthouse in Sacramento suggests that significant changes in vegetation and climate have occurred since the last full glacial. It is argued here that these changes have regional importance for the dating and interpretation of late glacial environments in central California. The sampling locality, Sutter Lake (also known as China Lake), has been completely altered over the last 100 years and is now covered with asphalt and concrete (Figure 1).

Before 1769, four plant communities were of paramount importance in the Sacramento area: Riparian Gallery Forest, Oak Woodland, Valley Grassland, and Freshwater Marsh (Figure 1). The only true forest in the area was the Riparian Gallery Forest, which lined portions of the Sacramento and American rivers (Jepson 1893; Thompson 1961; Stebbins and Taylor 1973). Located on the alluvial fan and floodplain soils of the river levees, these forests formed a dense multistoried vegetation community with a greater niche diversity than any other native ecosystem. Mature stands were typified by a dense crown cover and thick understory; these forests could be subdivided further based on elevation in relation to the river, the amount of seasonal flooding, and substrate. Tall cottonwood (*Populus fremontii*), valley oak (*Quercus lobata*), walnut (*Juglans hindsii*), California sycamore (*Platanus racemosa*), and Oregon ash (*Fraxinus latifolia*) formed the deciduous canopy, with white alder (*Alnus rhombifolia*), box elder (*Acer negundo*), and elderberry (*Sambucus mexicana*) dominating the subcanopy. The understory was a dense tangle of willows (*Salix* spp.), lianas, grapevines (*Vitis californica*), and numerous tall herbaceous plants.

In: R.C. Wilson and V.L. Tharp, Editors. 1998. *Proceedings of the Fourteenth Annual Pacific Climate (PACLIM) Workshop, April 6-9, 1997.* Interagency Ecological Program, Technical Report 57. California Department of Water Resources.

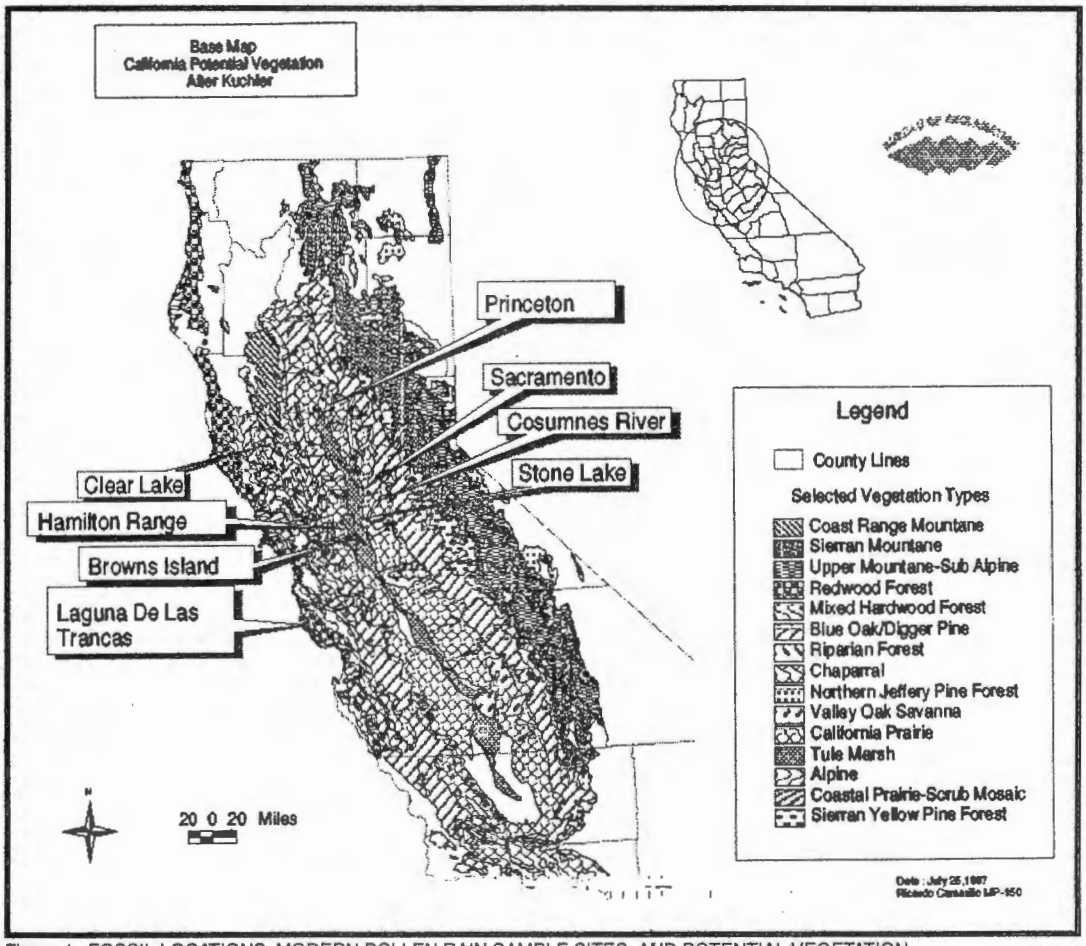

Figure 1. FOSSIL LOCATIONS, MODERN POLLEN RAIN SAMPLE SITES, AND POTENTIAL VEGETATION

The riparian Oak Woodland community, usually associated with alluvial mineral soils formed on overbank deposits, paralleled the Riparian Gallery Forest and also occurred as discontinuous stands on the better drained soils (Tugel 1993). The dominant arboreal form was the valley oak, although box elder and Oregon ash also were common. The Oak Woodland was characterized by a sparse understory, consisting of poison-oak (*Rhus diversiloba*), elderberry, buckeye (*Aesculus californicus*), wild rose (*Rosa californica*), and a few other woody shrubs. The herbaceous layer of the understory was similar in composition to the Valley Grassland, but with increased abundance of wild rye (*Elymus triticoides*), one of the few rhizomatous grasses common to the pristine Central Valley (Stebbins and Taylor 1973). It is thought that this grass formed a sod in some Oak Woodlands (Clements and Shelford 1939). The open and parklike appearance of this community probably was accentuated by aboriginal burning practices.

The Valley Grassland or Central Valley Prairie was restricted to alluvial mineral soils with poorer drainage that flanked the Oak Woodland and extended into the lower foothills before giving way to the Blue Oak Woodland. Perennial bunch grasses such as needle grass (*Stipa* spp.),

blue grass (*Poa* spp.), and three-awn (*Aristida* spp.) were the dominant species (Barry 1972). This community was regularly burnt by aboriginals to enhance reproduction of specific taxa, gather edible insects and control others, and drive game.

Freshwater Marsh, which formerly covered large areas of low-lying ground in the area, flooded periodically and retained standing water throughout most of the year (Mason 1969). Soils associated with the marshlands were clay loams to peats (McElhiney 1992;Tugel 1993). Although dominated by tules (*Scirpus* spp.), this community also contained cattails (*Typha* spp.), reeds (*Phragmites communis*), and other marsh plants. Aquatic species, common in places that had deeper permanent water, included pondweed (*Potamogeton* spp.), yellow pond lily (*Nuphar polysepalum*), and knotweed (*Polygonum* spp.).

Beginning with the European settlement from 1769 to 1848, the vegetation of the lower Sacramento Valley changed radically. Many alien species, mainly derived from southern Eurasia, were introduced and began to displace native taxa. Agriculture and uncontrolled livestock grazing drastically affected the native vegetation. These changing land use patterns, in turn, altered the subsistence system of the native peoples and thus their effect on the vegetation. Co-occurring with these events was the rapid and devastating decline in the native population due to introduced diseases, particularly smallpox and malaria (Cook 1943).

The large influx of people with the gold rush amplified both the direct and indirect changes in the vegetation. As a result, remnants of native vegetation in Sacramento were almost totally eliminated. The floods of 1850, 1852, and 1853 created a demand for levees and the filling of low-lying areas (Brienes 1979). These activities destroyed the vegetation and changed the habitats to such an extent that the former vegetation could not re-establish itself. Sutter Lake, which had supported freshwater marsh flora during the early gold rush, was affected. It became, like several other low-lying areas, a dump for the waste created by the rapidly growing city. Prior to 1905 the lower reach of the American River was altered and shunted to the north (Dillinger 1991). By 1910, Sutter Lake was completely filled to enlarge the railyards.

Methods

Nine samples collected by Jack Meyer (Sonoma State University) from borings at the new Federal Courthouse were provided for analysis. The boring for the samples was made at the HI56 Block of Sacramento, some 400 feet north of I Street. A push tube was used to sample the sediments. Standard palynological techniques were used to process the samples. Prior to chemical treatment, the samples were swirled to concentrate the pollen size fraction of the sediments by the method outlined in Mehringer

(1967). Four tablets with exotic *Lycopodium* spores were added to each sample to monitor processing and determine pollen concentration values (Stockmarr 1971). A Nikon Labophot microscope with phase contrast was used to scan the samples. Pollen identifications are based on herbarium specimens obtained from the Jepson Herbarium, U.C. Berkeley, and the Tucker Herbarium, U.C. Davis, as well as standard texts. Vials of the remaining processed samples, as well as a fraction of the original samples, are stored at the Department of Anthropology, U.C. Davis.

Results

The core profile and sample location is presented in Figure 2. Three main units were identified by Meyer — an upper historic-age brown silt and sand (0-24 feet), a dark clay (24-27.5 feet), and a lower unit of gray sand, silt and clay (>27.5 feet). An additional unit, a gray sandy gravel (>60 feet), was observed in boreholes B1 and D2. No samples were provided from the upper unit. Six of the nine samples examined contained pollen: 3(27-27.5 feet), 4(33-33.5 feet), 6(37.5-38 feet), 7(49-49.5 feet), 8 (50.5-51 feet), and 9(52-53 feet). Pollen is sparse and with little exception poorly preserved in sample 3, a black clay. Pollen preservation in the remaining samples from the gray sandy silt ranges from fair to good, but in all

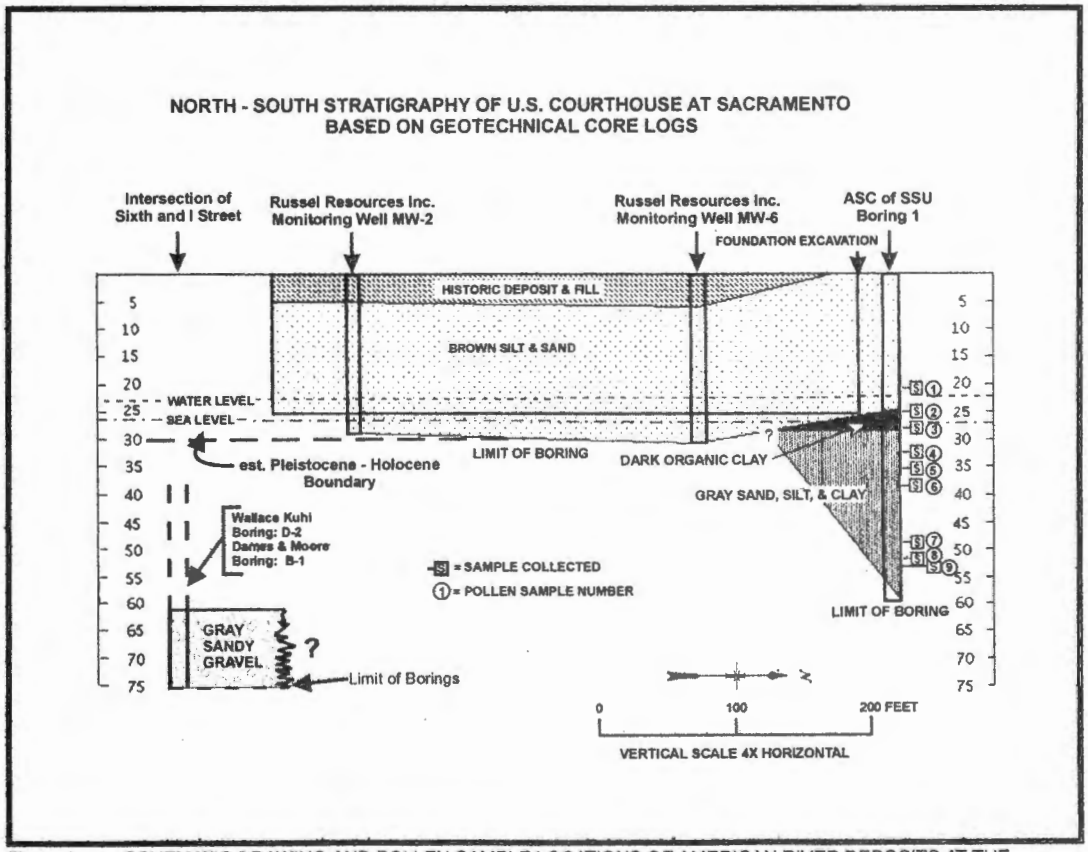

Figure 2. SCHEMATIC DRAWING AND POLLEN SAMPLE LOCATIONS OF AMERICAN RIVER DEPOSITS AT THE FEDERAL COURTHOUSE, SACRAMENTO, CALIFORNIA (ASC of SSU: Anthropolotical Studies Center of Sonoma State University)

instances pollen concentration is low. All the samples contained charcoal. Sample 2(25 feet), also a black clay, had no pollen grains but charcoal was abundant. Counts were made for five samples (3,4,6,7,8).

Thirty-five pollen types were recognized: 11 arboreal forms, 20 non-arboreal, and 4 aquatic-emergent types (Table 1). Arboreal types dominated the counts, with pine (*Pinus*) being the most common taxa. Unknown and undifferentiated grains ranged from about 10 percent to over 31 percent. Many of the unknown grains were small tricolpate and tricolporate grains that were most likely derived from non-arboreal species. No pollen grains from alien taxa were observed.

Radiocarbon Age Determination

A single sample of wood from sample 8 at 50.1-51 feet was submitted for AMS radiocarbon age determination and returned an age of 1110±50 BP (Beta 103621). The calibrated results (2 sigma, 95% probability) give an age range of about AD 855 to 1020 and the intercept of the radiocarbon age with the calibration curve is AD 970. The sample was associated with well preserved unoxidized woody debris, bark, and, most significantly, a red fir (*Abies magnifica*) needle. The age determination is not compatible with the assumed age of the deposit, and the sample may have been moved down the bore hole during drilling or be from a tree root.

Modern Day Pollen Samples

Modern pollen rain from freshwater marsh, riparian, grassland, and oak woodland of the Sacramento-San Joaquin drainage is presented in Table 2. Pine pollen values range from 3.7 to 23.6 percent. The highest pine pollen value is from an open water area (Stone Lake) reflecting a relative drop-off in the pollen from local plants. Fir pollen grains were noted in 4 of the 6 modern samples and are represented as <1 percent of the pollen rain. Other important types in the modern samples are oak, alder, members of the sunflower (Asteraceae) family, grass (Poaceae) family, goosefoot (Chenopodiaceae) family, and sedge (Cyperaceae) family.

Discussion

Sample Site and Pollen Spectra

The edge of Sutter Lake was roughly 50 feet north of I Street and it is assumed that the 60-foot-deep boring penetrated the middle of the lake. The samples examined and discussed here came from the dark clay and gray sand, silt, and clay units. It is thought that the dark clay is representative of Sutter Lake, a former oxbow lake of the American River.

Table 1
POLLEN COUNTS FOR SACRAMENTO/AMERICAN RIVER SEDIMENTS

Sample:	3		4		6		7		8		Mean
Depth:	*27'*		*33'*		*37.5'*		*49'*		*50.5'*		n=4
Pinus	4		130	*51.0%*	79	*40.1%*	62	*32.6%*	76	*29.6%*	38.3
Abies	0		13	*5.1%*	13	*6.6%*	5	*2.6%*	12	*4.6%*	4.7
TCT	1		12	*4.7%*	10	*5.1%*	18	*9.5%*	30	*11.7%*	7.7
Quercus	3		24	*9.4%*	12	*6.1%*	22	*11.6%*	7	*2.7%*	7.4
Alnus	0		26	*10.2%*	16	*8.1%*	20	*10.5%*	24	*9.3%*	9.5
Fraxinus	1		1		0		0		1		
Pseudotsuga	0		3	*1.2%*	1		2		0		
Tsuga mert	0		0		0		1		0		
Populus	0		0		0		0		2		
Acer	0		1		0		0		0		
Corylaceae	0		1		0		1		2		
Platanaceae	1		0		0		1		0		
Rhus	0		2		2		1		1		
Rhamnaceae	3		3		5	*2.5%*	3	*1.6%*	0		
Rosaceae	4		7	*2.7%*	14	*7.1%*	10	*5.3%*	5	*1.9%*	
Artemisia	1		4	*1.6%*	1		3	*1.6%*	9	*3.5%*	
Asteraceae hi	3		4	*1.6%*	5	*2.5%*	8	*4.2%*	9	*3.5%*	
Asteraceae lo	0		3		10	*5.1%*	1		3	*1.2%*	
Liguliflorae	0		3		0		0		3	*1.2%*	
Poaceae	0		6	*2.4%*	4	*2.0%*	6	*3.2%*	5	*1.9%*	
Chenopod	1		2		1		5	*2.6%*	3	*1.2%*	
Polygonaceae	0		3		5	*2.5%*	0		2		
Eriogonium	0		0		0		3	*1.6%*	1		
Rumex	0		1		0		1		0		
Polemonaceae	0		0		0		0		1		
Gilia	0		0		0		1		0		
Onagraceae	0		0		1		0		0		
Apiaceae	0		2		2		1		0		
Malvaceae	0		0		1		0		0		
Ranunuc.	1		1		1		0		0		
Ericaceae	0		0		1		0		0		
Cruciferae	0		0		0		1		0		
Arceuthobium	0		0		0		1		0		
Linaceae	0		0		1		0		0		
Cyperaceae	0		2		6	*3.0%*	8	*4.2%*	2		
Salix	0		0		5	*2.5%*	5	*2.6%*	6	*2.3%*	
Isotes	0		1		1		1		2		
Utricularia	1		0		0		0		0		
Total:	24		255		197		191		206		
Unkn/Undiff	11	*31.4%*	28	*9.9%*	47	*19.3%*	30	*13.6%*	51	*19.8%*	
Grand total:	35		283		244		220		257		
Lycopodium	350		288		365		>325		348		

Table 2
MODERN SURFACE POLLEN RAIN SAMPLES OF THE
LOWER SACRAMENTO-SAN JOAQUIN DRAINAGE VEGETATION COMMUNITIES, MAJOR POLLEN TYPES BY PERCENT
(From West 1977)
* Present less than 1%.

Locality: Vegetation:	Browns Island Freshwater Marsh	Princeton Riparian	Stone Lake #1 Freshwater Marsh	Stone Lake #2 Freshwater Marsh	Hamilton Range Grassland	Cosumnes River Oak Woodland
Pinus	9.7	14.6	3.7	23.6	5.8	10.6
Abies	*	*	0	*	0	*
TCT	0.9	*	0	1.3	*	0.8
Quercus	8.8	7.4	6.2	5	3.2	29.9
Populus	0	6	*	0	0	0
Juglans	*	3.3	0	*	*	*
Platanus	0	1.1	0	0	0	0
Fraxinus	*	1.1	0	0	0.9	4.1
Alnus	2.9	4.6	0.7	1	1.6	4.7
Salix	2	4.4	20	*	0	2.3
Aster. Hi	12.9	2.7	2.4	3.3	27.7	*
Aster. Lo	3.6	9	3.9	2	29	1.5
Poaceae	8.8	7.9	3.27	14.5	12	32.5
Chenopod.	4.5	3	4.7	4.3	2.9	1.9
Polygonaceae	2.4	1.1	1.9	3.7	0	*
Cyperaceae	28.3	3	36	18.5	*	*

If this assignment is correct, then the reduced gray sand, silt and clay underlying Sutter Lake is prehistoric. The sand and silt grains from this unit have angular edges with little or no weathering. At the time the boring was made, the top of the water table was about 22 feet below the surface and probably protected the pollen grains from oxidation. Present-day sea level is about 26 feet below the surface, just above the gray sand, silt, and clay unit.

There is insufficient pollen in Sample 3, the dark clay Sutter Lake sediments, on which to comment. Bladderwort (*Uticularia*) pollen suggests that this aquatic was growing in the lake. No pollen grains from other aquatic-emergent plants are present, suggesting either differential preservation or that these plants had already been extirpated from the lake. The increased biological activity brought on by dumping may also have contributed to the poor pollen preservation, but specific proof is lacking.

The samples from the gray sand, silt, and clay unit have high pine pollen values of 33 to 51 percent. As many as ten species may be contributors to the *Pinus* category. The values are far greater than modern surface samples from the Sacramento-San Joaquin River drainage (Table 2), where the highest values observed are almost 15 percent for a Riparian Forest along the Sacramento River and 23.6 percent for one of the open water samples at Stone Lake, a Fresh Water Marsh near the Sacramento and Cosumnes rivers. Historic-age samples from Sacramento IJ site did

not exceed 18 percent (West 1989). The highest pine value observed in Holocene age sediments from the Sacramento-San Joaquin Delta, dated between 2850 and 3940 YBP, is 32 percent for a single sample below a widespread silty clay layer (West 1977) that may be Neoglacial in age. Pine values comparable to samples 4 and 6 are found today above 3000-3500 feet in the Sierra Nevada (Adam 1967; Anderson and Davis 1988). Anderson and Davis noted that, for the Sierra, pine was not present with values below 24 percent. Even taking into consideration the effects of long-distance transport, it would appear that pines were growing in the area of the lower American River at the time the gray sand, silt, and clay unit was deposited.

Also striking are the relatively high values for fir (*Abies*) in samples 4 (5.1), 6 (6.6) and 8 (4.6). Two species most likely are represented — white (*A. concolor*) and red (*A. magnifica*) fir. A single red fir needle was found in sample 8 (50.5-51 feet). Today, white fir is found above 3000 feet and red fir above 5000 feet in the Sierra. Fir trees are absent in the Sierra when fir pollen percentages are less than 2-4 percent (Anderson and Davis 1988). Fir has a large, relatively heavy pollen grain that, while resembling pine, has a smaller dispersal range. It is unlikely that fir values this high can be explained solely by long-distance transport. Although fir pollen is present in four of the modern surface samples of the Sacramento-San Joaquin drainage, in no instance does it reach 1 percent of the pollen spectrum (Table 2). Like pine, fir must have been growing in the vicinity of the lower American River.

Alder (*Alnus* spp.) pollen, most likely derived from white alder (*A. rhombifolia*) (although mountain alder (*A. tenuifolia*) could also be a contributor), ranges in value from 8 to 10 percent, reflecting its importance as a riparian tree. Highest values for alder are found in the Sierra between 1500 and 3000 feet. In addition to alder, sample 6 pollen values indicate that sedges and willows were present, possibly growing on the margins of a nearby water course or pond.

Oak (*Quercus* spp.) is present in samples 4 and 6 (9.4 and 6.1 percent), sample 7 (11.6 percent) and sample 8 (2.7) but does not approach values found in the Cosumnes River Oak Woodland (30 percent) (Table 2), and in the Sierra Oak Woodland and chaparral communities today (between 35 and 58 percent) (Anderson and Davis 1988). Five of the six Sierran species are arboreal and most abundant below 3000 feet but also are found above 6000 feet. Thus, while oaks were present during the time of deposition of samples 4, 6, 7 and 8, they were far less prominent than today and may have been derived from higher elevation species.

Age and Environment of Gray Sand, Silt, and Clay Unit

Minimally, if this unit was deposited during late glacial times, sea level was more than 150 feet lower than today (Atwater et al. 1977) and the American River fan extended farther westward of Sacramento (Shlemon 1972). Post-glacial sea level rise slowed significantly after 8000 years ago and essentially reached modern levels by about 6000 years ago (Atwater et al. 1977). The top of the bore hole is about 26 feet above sea level, and the samples with high pine and fir values are some 9-26 feet below sea level. The present-day river surface is about 5 feet above mean low water level, and channel depth ranges from 4 to 10 feet. Based on this line of reasoning, and assuming that tectonic subsidence has been minimal, the upper part of the unit should date to the late Pleistocene or early Holocene (late Modesto age). The sediments fill a channel that was entrenched during the last major Sierran glacial advance and covered with fine-grained outwash during deglaciation (Shlemon 1972). Shlemon recognized two distinct fills of Modesto age in the lower American River area. The oldest is a basal gravel fill that has been traced in numerous bridge boring and well logs some 50 feet below sea level at the Sacramento River confluence. This would be 10-15 feet below sample 8 and can be observed in boreholes B1 and D2. The younger Modesto age fill, described by Shlemon (1972) as "primarily coarse- to medium-grained granitic sand" underlies a terrace on the south side of the modern river. These younger sediments merge downstream into Holocene flood plain and natural levee deposits of the Sacramento River.

There is no evidence of Holocene tectonism that could account for the below sea level elevation of the unit (Shlemon and Begg 1972). However, the radiocarbon age determination of 1110 BP on a piece of wood recovered from sample 8 (50.5-51 feet) does not provide support for a late glacial age. The radiocarbon sample could possibly be a root or material that moved down the hole during drilling. Another explanation is that the sedimentary unit was deposited during a catastrophic event when flows were sufficient to scour and move relatively intact packets of sediments from upland areas. The composition and condition of the sedimentary unit samples and low pollen concentration values suggest rapid deposition with little alteration after deposition. This alternative explanation is not supported by other fossil data downstream in the Sacramento-San Joaquin Delta (West 1977) but cannot be completely rejected. A date from the red fir needle might clarify this conflict and will be obtained when funds become available.

Regional Comparison

Comparable pollen spectra with high pine and fir values from non-glaciated low elevation sites occur at Clear Lake (Adam 1988) (also in samples below 20 meters in Clear Lake core CL-73-5 dated to 24,080±1000

(W-3220), (Table 3)) and Laguna de las Trancas (Adam et al. 1981). At Clear Lake, grand fir (*A. grandis*) needles have been found in full glacial age sediments from cores CL-73-1 and core 4 (Adam 1988). Grand fir is presently restricted to the coast as far south as the Russian River, where it grows in lower elevation (generally <2000 feet), more temperate habitats than stands of white fir (Griffen and Critchfield 1972). Its presence at Clear Lake would suggest more mesic, cooler, less seasonal conditions than today. Full glacial temperatures have been estimated to be 6-8°C cooler than today at Clear Lake (Adam and West 1983), although more recent estimates suggest 5-7°C cooler (West nd). Although undated, Adam, Byrne and Luther (1981) assign the Laguna de las Trancas pine-fir pollen zone to the coolest part of the last full glacial cycle of about 12,000 to 24,000 years ago. Adam et al. (1981) consider that grand fir was present at Laguna de las Trancas and conclude 2-3°C cooler temperatures for the last full glacial.

The pollen spectra of the Sacramento samples appear to be comparable with these other sites. A significant climatic factor in the American River drainage would have been cold air drainage, which could have allowed more cold-tolerant taxa to expand down slope. Most likely pine and fir trees extended down the American River canyon to elevations of less than a 1000 feet. Summers were probably shorter and cooler. Because of cold air drainage, winters in the Sacramento region may have had periods of very cold temperatures when high atmospheric pressures occurred.

Table 3
CLEAR LAKE CORE CL-73-5, POLLEN PERCENTAGES OF SELECTED SAMPLES AND MAJOR TAXA
(West, unpublished data)
(Radiocarbon age determination: Sample 2373, 21.75 meters, *24,080±1,000* (W-3220))

Sample:	2134	2136	2138	2033	2035	2036	2042	2045	Mean
Depth (meters):	20.1	20.3	20.5	21.75	21.95	22.05	23	23.3	n=8
Pinus	66	54	72	65	58	60	66	68	63.5%
Abies	10	5	4	9	10	3	6	5	6.6%
TCT	13	21	13	11	19	31	4	16	15.9%
Quercus	0	3	0.4	0.5	0.8	6	2	0.7	1.7%
Alnus	2	1	2	0.5	0.8	3	0	0.3	1.1%
Pollen Sum	221	219	225	177	228	281	127	258	

Conclusions

Although poor pollen preservation precluded examination of the transition of vegetation from the prehistoric period to the historic, the prehistoric samples provide important new information on the age of the sedimentary unit and local late Pleistocene environments. Based on comparative pollen data, the unit is late Pleistocene in age, specifically the last full glacial (about 12,000-24,000 years ago). Composition of the vegetation was significantly different than today, with the elevational ranges of some taxa occurring as much as 3000 feet lower than present. Within the lower American River drainage, pine and fir trees were common, alder was the dominant riparian tree, and oaks were restricted to protected areas where they could survive the colder temperatures. A steep climatic gradient for the west slope of the Sierra is inferred for the last full glacial. Relatively high pine and fir values for central California suggest that a late glacial pollen biozone may have utility for regional age and climatic determinations.

Acknowledgments

I would like to acknowledge the constructive comments from Roy J. Shlemon and editorial help from Katherine L. Keysor West. Samples were provided by Jack Meyer, Sonoma State University. Owen K. Davis confirmed the identification of the red fir needle. Partial funding for this work was provided by the Anthropological Studies Center, Sonoma State University. I am responsible for any shortcomings and errors.

References

Adam, D.P. 1967. Late Pleistocene and Recent Palynology in the Central Sierra Nevada, California. Pages 275-301 in *Quaternary Paleoecology*. E.J. Cushing and H.E. Wright, Jr., editors. Yale University Press, New Haven.

Adam, D.P. 1988 Palynology of Two Upper Quaternary Cores from Clear Lake, Lake County, California. *U.S. Geological Survey Professional Paper 1363*, Washington, D.C. 86 pp.

Adam, D.P., R. Byrne, and E. Luther. 1981. A Late Pleistocene and Holocene Pollen Record from Laguna de Las Trancas, Northern Coastal Santa Cruz County, California. *MadroZo* 28(4):255-272.

Adam, D.P., and G.J. West. 1983. Temperature and precipitation estimates through the last Glacial Cycle from Clear Lake, California, Pollen Data. *Science* 219:168-170.

Anderson, R.S., and O.K. Davis. 1988. Contemporary Pollen Rain Across the Central Sierra Nevada, California, U.S.A.: Relationship to Modern Vegetation Types. *Arctic and Alpine Research* 20(4):448-460.

Atwater, B.F., C.W. Hedel, and E.J. Helley. 1977. Late Quaternary Depositional History, Holocene Sea-Level Changes, and Vertical Crustal Movement, Southern San Francisco Bay, California. *U. S. Geological Survey Professional Paper 1014.* Washington, D.C. 15 pp.

Barry, W.J. 1972. *The Central Valley Prairie.* Volume 1. State of California, The Resources Agency, Department of Parks and Recreation, Sacramento. 82 pp.

Brienes, M. 1979. Sacramento Defies the Rivers, 1850-1878. *California History* Vol. LVIII, No. 1:2-19.

Clements, F.B. and V.E. Shelford. 1939. *Bio-ecology.* John Wiley & Sons, New York. 425 pp.

Cook, S.F. 1943. The Conflict between the California Indian and the White Civilization: I. *Ibero-Americana:21*, University of California, Berkeley.

Dillinger, W.C. 1991. *A History of the Lower American River.* Natural History Association, Sacramento. 165 pp.

Griffen, J.R., and W.B. Critchfield. 1972. The distribution of forest trees in California. Berkeley, California Pacific SW. Forest and Range Experiment Station. pp. 114. (*USDA Forest Service Research Paper PSW-82*) (Reprinted with Supplement, 1976).

Jepson, W.L. 1893. The Riparian Botany of the Lower Sacramento. *Erythea* 1:238-246.

Küchler, A.W. 1977. Map of natural vegetation of California, in M.G. Barbor and J. Major, editors, *Terrrestrial vegetation of California,* New York, John Wiley & Sons .

Mason, H.L. 1969. *A Flora of the Marshes of California.* University of California Press, Berkeley. 878 pp.

McElhiney, M.A. 1992. *Soil Survey of San Joaquin County, California.* USDA Soil Conservation Service. 480 pp.

Mehringer, P.J. Jr. 1967. Pollen Analysis of the Tule Springs Area, Nevada. In Pleistocene Studies in Southern Nevada. H.M. Wormington and D. Ellis, Editors, *Nevada State Museum Anthropological Papers* 13:129-200.

Shlemon, R.J. 1972. The Lower American River Area, California: A Model of Pleistocene Landscape Evolution. *Yearbook of Association of Pacific Coast Geographers* 34:61-86.

Shlemon, R.J., and E. Begg. 1972. A Holocene Soil Landscape Chronology, Southwestern Sacramento Valley, California. In International Geography. W.P. Adams and F.M. Helleiner, Editors, University of Toronto Press, Montreal, p. 277-279.

Stebbins, G.G., and D. Taylor. 1973. A Survey of the Natural History of the South Pacific Border Region, California. *Institute of Ecology Publication: 4.* University of California, Davis. 495 pp.

Stockmarr, J. 1971.Tablets with Spores used in Absolute Pollen Analysis. *Pollen et Spores* Vol. XIII, No. 4:615-621.

Thompson, K. 1961. Riparian Forests of the Sacramento Valley, California. *Association of American Geographers Annuals* 51(3):294-315.

Thompson, T.H., and A.A. West. 1880. *History of Sacramento County.* Thompson and West, Oakland.

Tugel, A. 1993. *Soil Survey of Sacramento County, California.* USDA Soil Conservation Service. 399 pp.

West, G.J. 1977. *Late Holocene Vegetation History of the Sacramento-San Joaquin Delta, California.* Report Prepared by Cultural Heritage Section, California Department of Parks and Recreation for California Department of Water Resources, Interagency Agreement B-50173. Sacramento. 60 pp.

West G.J. 1989. *Pollen Analysis of Cultural Deposits from the IJ89 Site, Sacramento, California.* Report prepared for Anthropological Studies Center, Sonoma State University, Rohnert Park. 10 p.

West G.J. No date. Clear Lake Pleistocene-Holocene temperature estimates revisited. Ms. in preparation.

ENSO Signal in $\delta^{13}C$ of Pre- and Post-False Latewood of Ponderosa Pine Tree Rings in Southeastern Arizona

Steven W. Leavitt, William E. Wright, and Austin Long

ABSTRACT: The summer monsoonal precipitation in Arizona is preceded by a pronounced dry period (foresummer drought), which frequently exerts sufficient water stress on *Pinus ponderosa* trees that they cease growth until monsoonal rains reinvigorate cambial activity. A "false latewood" band within a tree ring commonly results from these events, serving as a time marker to which we employ $\delta^{13}C$ to examine plant-water conditions during the periods before and after the band. We sampled tree rings from several trees (four cores per tree) from the Santa Catalina Mountains in southeastern Arizona. $\delta^{13}C$ was analyzed on the holocellulose fraction of pre- and post-false latewood of each tree back to the mid-1980s. In most years, the pre-false latewood portion of the ring has higher $\delta^{13}C$ (^{13}C enrichment), indicating greater water stress. However, when the pre-false portion was divided into two parts, the first typically had low $\delta^{13}C$ (^{13}C-depletion) compatible with abundant winter-spring moisture, and the second had high $\delta^{13}C$, consistent with the foresummer drought stress. Despite typical intra-site $\delta^{13}C$ variability of 1-3‰ among trees, the pre- to post-false $\delta^{13}C$ patterns are coherent among trees. The isotopic chronology over the period 1985-1995 showed low $\delta^{13}C$ in 1992 and 1993 (El Niño) and high $\delta^{13}C$ in 1989 (La Niña). Excess moisture and reduced water stress are consistent with a previously observed teleconnection between high El Niño-associated rainfall in the Southwest and large tree rings. This method may, therefore, have utility in reconstructing seasonal water stress and the ecophysiological "relief" provided by El Niño for the past several hundred years.

Introduction

Tree rings in the southwestern United States frequently contain a "time marker" that facilitates comparison between environmental conditions early and late in the growing season. The bimodal precipitation distribution in the Southwest (Figure 1) regularly induces a "false" latewood band (false ring) in response to the May-June foresummer drought, after which tree-ring development resumes with the onset of summer monsoon rains. The pre-false-latewood portion of the ring should then be dominated by environmental effects from winter/spring (*ie*, just prior to growth and during initial ring formation) and the post-false latewood portion of the ring should reflect environmental effects in summer (onset of summer monsoon is early July) and fall.

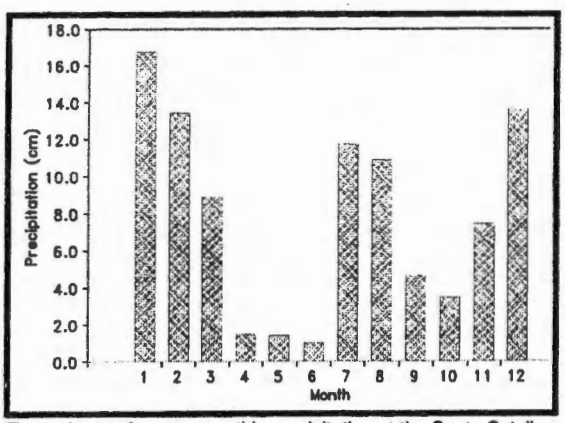

Figure 1. Average monthly precipitation at the Santa Catalina Mountains Palisades Ranger Station during 1990-1996. (1=January....12=December)

We examined environmental differences in these periods within and among years by means of stable-carbon isotope ratios ($\delta^{13}C$ [in ‰]= [$^{13}C/^{12}C_{sample}$) $^{13}C/^{12}C_{PDB\ standard}$ -1] x1000) of the tree-ring sub-

In: R.C. Wilson and V.L. Tharp, Editors. 1998. *Proceedings of the Fourteenth Annual Pacific Climate (PACLIM) Workshop, April 6-9, 1997.* Interagency Ecological Program, Technical Report 57. California Department of Water Resources.

divisions. The stable-carbon isotope fractionation model of Farquhar *et al* (1982) outlines the types of parameters that influence plant $\delta^{13}C$:

$$\delta^{13}C_{plant} = \delta^{13}C_{air} - a - (b - a)C_i/C_a$$

where $\delta^{13}C_{plant}$ is a function of $\delta^{13}C$ of the atmospheric CO_2 ($\delta^{13}C_{air}$) and C_i/C_a, the ratio of intercellular CO_2 concentration (C_i) to atmospheric CO_2 concentration (C_a). The term *a* represents the fractionation during CO_2 diffusion through stomata (–4.4‰) and *b* represents fractionation by ribulose bisphosphate (RuBP) carboxylase (–27 ‰). In principle, C_i/C_a may be influenced by many environmental factors (summaries in O'Leary 1981; Farquhar *et al* 1982; Francey and Farquhar 1982) including light, relative humidity, nutrient availability and soil moisture, all of which can affect rates of stomatal conductance and carbon fixation. Tree-ring studies have found various empirical relationships of $\delta^{13}C$ to relative humidity (Saurer and Siegenthaler 1989), to humidity and cloud cover (Ramesh *et al* 1986), to light (Francey and Farquhar 1982), to drought and moisture stress (Leavitt and Long 1989; Dupouey *et al* 1993; Leavitt 1993; Livingston and Spittlehouse 1993; Saurer *et al* 1995; Livingston and Spittlehouse 1996), and to pollution such as ozone and sulfur dioxide (Martin *et al* 1988; Martin and Sutherland 1990). In the southwestern United States, $\delta^{13}C$ seems to be a particularly good indicator of moisture stress and drought, perhaps because of the correlation among many environmental parameters; *eg*, low humidity, low precipitation, high sunlight during drought periods — all conditions that would favor higher plant $\delta^{13}C$ (^{13}C enrichment).

This paper presents intra-ring results from several ponderosa pine (*Pinus ponderosa*) trees at a site in southern Arizona, and examines the relationship of stable-carbon isotopic composition to drought and ENSO over the last decade.

Methods

We collected 4.5-mm-diameter exploratory tree-ring cores from 11 *Pinus ponderosa* trees at seven sites in the Santa Catalina Mountains of southeastern Arizona in May 1995, in order to identify a site suitable for intensive investigation. Thirteen trees were then sampled on June 21, 1995, by coring from four orthogonal radial directions of each tree using a 12-mm-diameter borer at a site (field designation "Heli") near the Palisades Ranger Station (elevation 2300 meters). Multiple samples per tree and multiple trees helped to ensure accurate representation of the site (Leavitt and Long 1984). The trees from this site tended to have false latewood bands and large rings in most years from 1980 to present. Large rings are especially useful for the ultimate analysis of carbon, oxygen, and hydrogen isotopic composition. Additional trees were sampled with

12-mm cores from this site on July 8, 1995 (3 trees), and August 16, 1995 (3 trees).

Core samples from all trees were sanded, dated, and carefully inspected for ring size and false ring presence. A subset of trees in the age range of about 60-80 years was selected for additional processing and isotopic analysis. Pre- and post-false latewood ring widths were measured. Prior to the destructive processing for isotopic analysis, photographic and electronic images of each of the rings back to 1980 were taken and archived.

Initially, tree rings from several trees were separated into pre- and post-false latewood subdivisions, but early results suggested a third subdivision would be useful to interpretation, and subsequent trees were subdivided into pre-1, pre-2, and post-false latewood bands. In both subdivision schemes, the false-latewood band itself was contained in either the "pre-" or "pre-2" subdivision, but never in the post-false subdivision. Samples were ground, extracted first with toluene/ethanol and then ethanol alone, and delignified to holocellulose in an acidified Na-chlorite solution (Leavitt and Danzer 1993). Holocellulose was combusted to CO_2 in the presence of excess oxygen in a recirculating microcombustion system. The CO_2 was measured mass-spectrometrically with results expressed as $\delta^{13}C$ with respect to the international PDB standard (Craig 1957; Coplen 1996). Repeated combustion and analysis of two different holocellulose lab standards during the period of isotopic measurement gave standard deviations of 0.15‰ (n=15) and 0.25‰ (n=9).

Results

Although wood from all trees was analyzed separately, representative examples of variability of $\delta^{13}C$ among trees at a site are captured in Figure 2 for 1990, 1991, and 1992. Data for any given subdivision range 1.5-2.5‰ among the seven trees, which is consistent with other findings for pine trees in the western United States (Leavitt and Long 1982, 1984). Despite the range of absolute values, the intra-annual patterns are generally consistent among trees at the site. Among slight exceptions, the oldest tree (#4) shows the least pre- to post- variability, and the tree closest to a small streambed near the foot of the hillside (#12) did not have a false latewood band in 1990 and 1992. Overall, the intra-annual patterns are similar in 1990 and 1991 but quite different in 1992.

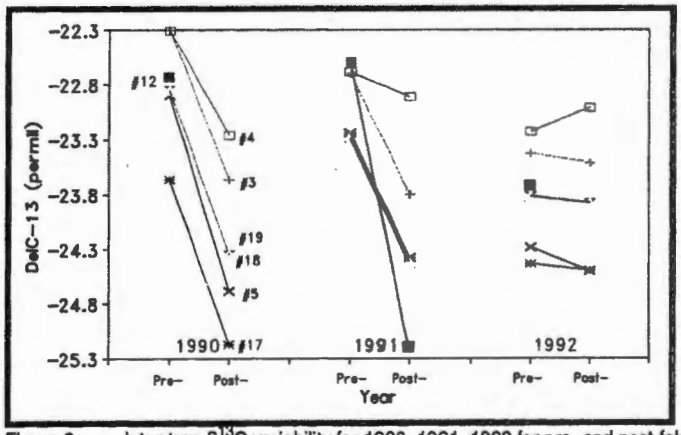

Figure 2. Inter-tree $\delta^{13}C$ variability for 1990, 1991, 1992 for pre- and post-false latewood subdivisions for seven *Pinus ponderosa* trees at the Santa Catalina Mountains "Heli" site.

These two modes of intra-annual variation are seen again in Figure 3 where the average pre- and post-false latewood $\delta^{13}C$ values of all trees are plotted for 1985-1995. Years 1992, 1993, and 1995 show relatively little intra-annual $\delta^{13}C$ change compared to the large downward shift in all other years. This pattern of $\delta^{13}C$ of the pre-false latewood band being frequently much heavier (^{13}C-enriched) isotopically relative to the post-false latewood band is somewhat surprising. Given the relationship of high $\delta^{13}C$ associated with water stress established by Leavitt and Long (1989) for southwestern piñon pine (*Pinus edulis*), these results suggest that the onset of summer monsoonal rains results in a less water-stressed condition than that before the false latewood band. This seems unusual, because abundant soil moisture is normally expected at the beginning of the growing season as water derived from winter precipitation recharges the soil. Yet, the pre-false portion of the ring actually contains wood formed during the fore-summer drought when water stress should be very high, which may be dominating the pre-false isotopic composition.

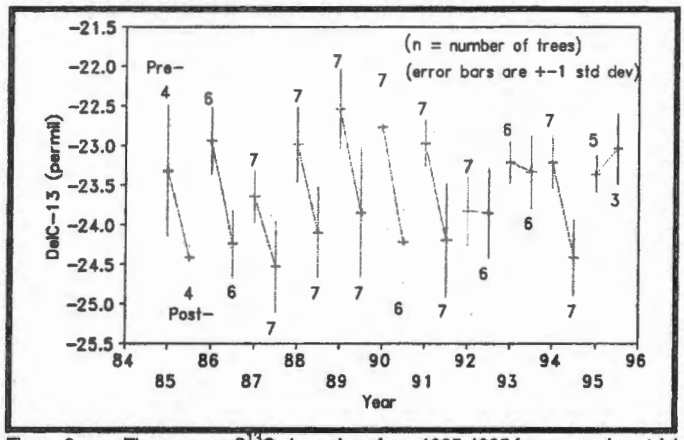

Figure 3. The average $\delta^{13}C$ chronology from 1985-1995 for pre- and post-false latewood subdivisions. Error bars are ±1s, and the integers signify the number of *P. ponderosa* trees in the average.

The response expected *a priori* is confirmed in the average patterns of three trees for which three intra-annual subdivisions were made (Figure 4). Generally the pre-2 portion of the ring containing the false latewood band indeed tends to be the heaviest isotopically, with either the pre-1 or the post-false subdivisions being isotopically most ^{13}C-depleted (most negative).

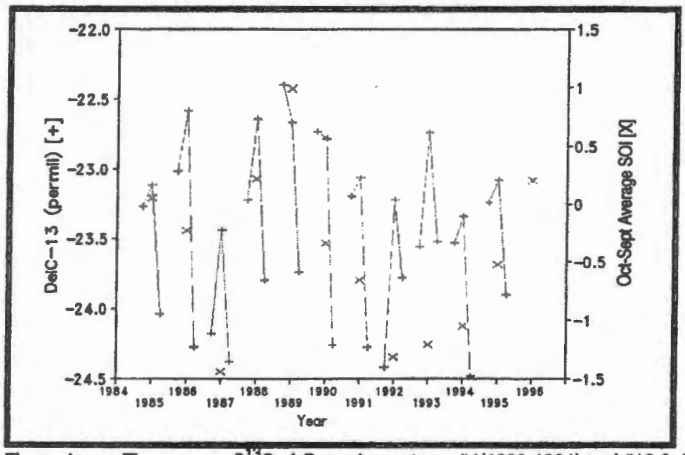

Figure 4. The average $\delta^{13}C$ of *P. ponderosa* trees #4(1989-1991) and #18 & 19 (1985-1995) divided into three subdivisions (pre-1, pre-2 and post-false latewood). The 12-month average (October through September) Southern Oscillation Index (SOI) is also plotted on the second y-axis.

Given the previous relationships found between southwestern piñon pine and drought (Leavitt and Long 1989), Palmer Drought Severity Indices (PDSI) were compared with average $\delta^{13}C$. Figure 5 shows the strongest relationship (inverse) of April-June average PDSI with the $\delta^{13}C$ of the pre-false latewood subdivision. The correlation coefficient is -0.67, which is significant at $P<0.05$. The correlation might be stronger if PDSI were available locally rather than regionally.

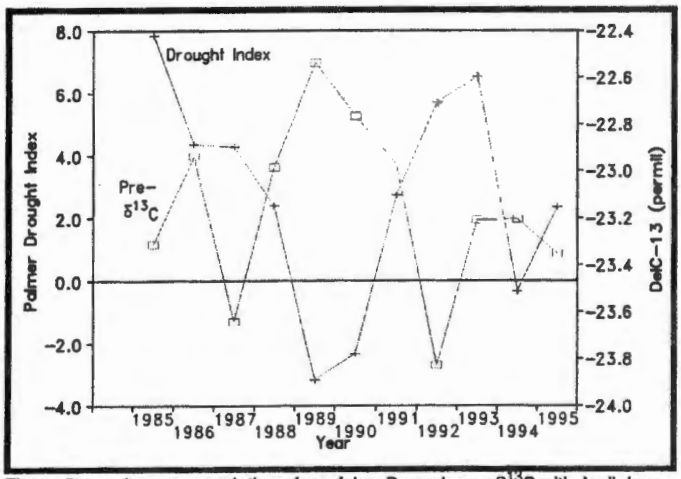

Figure 5. Inverse correlation of pre-false *P. ponderosa* $\delta^{13}C$ with April-June average PDSI from the southern Arizona Climate subdivision (r^2=0.45).

El Niño has been shown to have an effect on climate in the Southwest, producing wetter-than-average conditions, especially in winter (Andrade and Sellers 1988; Ropelewski 1992). October-September annual averages of Southern Oscillation Index (SOI) are plotted in Figure 4, showing a positive relationship with the tree-ring $\delta^{13}C$. The r^2 values for SOI versus pre-1, pre-2, and the unweighted average whole-ring $\delta^{13}C$ were 0.70 ($P<0.01$), 0.42 ($P<0.05$), and 0.66 ($P<0.01$), respectively. Correlation with post-false $\delta^{13}C$ was not significant (r^2=0.05). Among average SOI for groups of months, the January-April SOI average was particularly strongly correlated with $\delta^{13}C$, with r^2 equal to 0.70 ($P<0.01$), 0.25 (ns), 0.01 (ns) and 0.51 ($P<0.05$) for pre-1, pre-2, post- and whole-year average $\delta^{13}C$, respectively. This relationship is consistent with previous correlations of low southwestern wildfire with ENSO events (Swetnam and Betancourt 1990).

Finally, because isotopic analysis tends to be fairly expensive and time-consuming compared to standard dendrochronological methods using ring widths, we tested whether pooling of rings of trees before analysis would produce isotopic results any different than analyzing the trees separately and taking unweighted averages, as done in this investigation. We took ring-subdivision widths from each tree as the parameter with which to weight their separate $\delta^{13}C$ values and derive an effective $\delta^{13}C$ of the site had the trees been pooled before analysis. The comparison of separate $\delta^{13}C$ values of each tree averaged together with the simulated $\delta^{13}C$ value had we pooled all trees before analysis is shown in Figure 6. With the exception of 1993 and 1995, the differences are ≤0.1‰, which is well within the limits of our analytical error. The largest difference in 1995 is only 0.4‰. Actual mass rather than width would be a more representative weighting factor for these isotopic calculations.

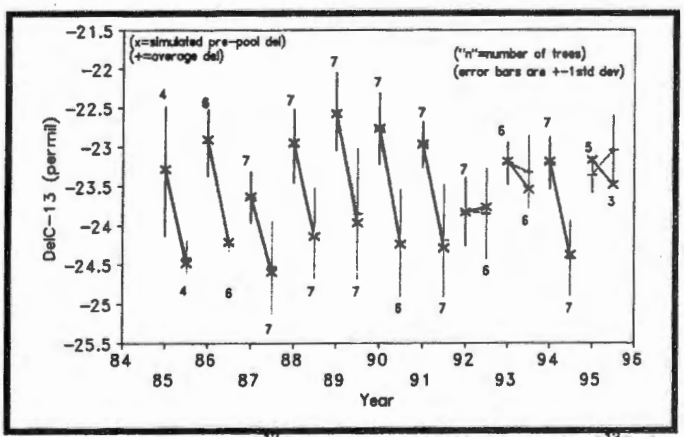

Figure 6. Comparison of $\delta^{13}C$ chronology derived from averaging $\delta^{13}C$ of trees analyzed separately (+'s; same curve as Figure 3), and a chronology (x's) derived from weighting each tree by its ring size for each year to calculate the bulk isotopic composition of cellulose from all trees; *ie*, simulating the $\delta^{13}C$ chronology we would obtain if rings were pooled prior to chemical preparation and isotopic analysis.

Conclusions

Ponderosa pine tree rings show intra-annual $\delta^{13}C$ changes that appear to be consistent with eco-physiological response to water stress. The greatest water stress appears in the "pre-2" portion of the ring associated with the foresummer drought and formation of the false latewood band. These seasonal $\delta^{13}C$ patterns among trees are highly coherent, suggesting a common climatic driving mechanism. The same site isotopic chronology can be obtained by physically pooling tree rings before analysis as would be derived by analyzing trees separately and averaging isotopic results. Well-mixed pooled samples can thus substantially reduce the time and expense of preparation and isotopic analysis.

Response to water stress is seen in the inter-annual shifts in $\delta^{13}C$, such that in the 1989 drought year, the $\delta^{13}C$ tends to be less negative (^{13}C enriched). The $\delta^{13}C$ values of pre-false rings correlate significantly with late-spring Palmer Drought Indices (negative), and also with full-year and winter/early-spring average Southern Oscillation Index (positive).

Work continues to add new ponderosa $\delta^{13}C$ chronologies from other southwestern United States mountain ranges and to examine details of differences of $\delta^{13}C$ (and $\delta^{18}O$) among sites to assess onset and strength of the summer monsoon.

Acknowledgments

We thank K. Kuehn and T. Stier for valuable field and laboratory assistance, and B. McCaleb for help in mass spectrometer analysis. This research was supported by NSF Grant #ATM-9421041.

References

Andrade, E.R., and W.D. Sellers. 1988. El Niño and its effect on precipitation in Arizona. *J. Climatol.* 8:211-219.

Coplen, T.B. 1996. New guidelines for reporting stable hydrogen, carbon and oxygen isotope-ratio data. *Geochimica et Cosmochimica Acta* 602:3359-3360.

Craig, H. 1957. Isotopic standards for carbon and oxygen and correction factors for mass spectrometric analysis of carbon dioxide. *Geochimica et Cosmochimica Acta* 12:133-149.

Dupouey, J.-L., S. Leavitt, E. Choisnel, and S. Jourdain. 1993. Modelling carbon isotope fractionation in tree rings based on effective evapotranspiration and soil water status. *Plant, Cell and Environment* 16:939-947.

Farquhar, G.D., M.H. O'Leary, and J.A. Berry. 1982. On the relationship between carbon isotope discrimination and the intercellular carbon dioxide concentration in leaves. *Aust. J. Plant Physiol.* 9:121-137.

Francey R.J., and G.D. Farquhar. 1982. An explanation of C-13/C-12 variations in tree rings. *Nature* 297:28-31.

Leavitt, S.W., and S.R. Danzer. 1993. Method for batch processing small wood samples to holocellulose for stable-carbon isotope analysis. *Anal. Chem.* 65:87-89.

Leavitt, S.W., and A. Long. 1982. Evidence for $^{13}C/^{12}C$ fractionation between tree leaves and wood. *Nature* 298:742-744.

Leavitt, S.W., and A. Long. 1984. Sampling strategy for stable carbon isotope analysis of tree rings in pine. *Nature* 311:145-147.

Leavitt, S.W., and A. Long. 1986. Stable-carbon isotope variability in tree foliage and wood. *Ecology* 67:1002-1010.

Leavitt, S.W., and A. Long. 1989. Drought indicated in carbon-13/carbon-12 ratios of southwestern tree rings. *Water Resources Bull.* 25:341-347

Leavitt, S.W., and A. Long. 1991. Seasonal stable-carbon isotope variability in tree rings: possible paleoenvironmental signals. *Chem. Geol. (Isot. Geos. Sec.)* 87:59-70.

Leavitt, S.W. 1993. Seasonal $^{13}C/^{12}C$ changes in tree rings: species and site coherence, and a possible drought influence. *Can. J. For. Res.* 23:210-218.

Livingston, N.J., and D.L. Spittlehouse. 1993. Carbon isotope fractionation in tree rings in relation to the growing season water balance. Pages 141-152 in *Stable Isotopes and Plant Carbon-Water Relations.* J.R. Ehleringer, A.E. Hall, and G.D. Farquhar, eds., Academic Press, San Diego.

Livingston, N.J., and D.L. Spittlehouse. 1996. Carbon isotope fractionation in tree ring early and late wood in relation to intra-growing season water balance. *Plant, Cell and Environment* 19:768-774.

Martin, B., A. Bytnerowicz, and Y.R. Thorstenson. 1988. Effects of air pollutant on the composition of stable carbon isotopes, $\delta^{13}C$, of leaves and wood, and on leaf injury. *Plant Physiol.* 88:218-223.

Martin, B., and E.K. Sutherland. 1990. Air pollution in the past recorded in width and stable carbon isotope composition of annual growth rings of Douglas-fir. *Plant, Cell and Environment* 13:839-844.

O'Leary, M.H. 1981. Carbon isotope fractionation in plants. *Phytochemistry* 20:553-567.

Ramesh, R., S.K. Bhattacharya, and K. Gopalan. 1986. Climatic correlations in the stable isotope records of silver fir (*Abies pindrow*) trees from Kashmir, India. *Earth Planet. Sci. Lett.* 79:66-74.

Ropelewski, C.F., 1992. Predicting El Niño events. *Nature* 356:476-477.

Saurer, M., and U. Siegenthaler. 1989. $^{13}C/^{12}C$ ratios in trees are sensitive to relative humidity. *Dendrochronologia* 7:9-13.

Saurer, M., U. Siegenthaler, and F. Schweingruber. 1995. The climate-carbon isotope relationship in the tree rings and the significance of site conditions. *Tellus* 47B:320-330.

Swetnam, T.W., and J.L. Betancourt. 1990. Fire-Southern Oscillation relations in the southwestern United States. *Science* 249:1017-1020.

Decadal Climatic Reconstruction from Stable Isotope Records of Speleothem in Shihua Cave, China: A Summer Monsoon Domain

Teh-Lung Ku, Hong-Chun Li, and Lowell D. Stott

ABSTRACT: Precipitation around Beijing, China, at 40°N and 116°E is dominantly supplied by the summer monsoons. To reconstruct the paleomonsoon variability, we have analyzed $\delta^{18}O$ and $\delta^{13}C$ of a stalagmite collected from Shihua Cave on the outskirts of Beijing. The stalagmite has been dated by ^{210}Pb, ^{14}C, and growth-lamina counting, showing a mean growth rate of 0.044 mm/year. A total of 133 samples were analyzed for the uppermost 2 centimeters of the specimen, providing isotopic records at resolutions of about 3 years over the last 490 years. A comparison of the $\delta^{18}O$ record with the recorded precipitation in Beijing and Tianjin (about 130 kilometers southeast of Beijing) back to 1840 AD shows that high precipitation correlates with negative $\delta^{18}O$ peaks. The long-term $\delta^{18}O$ trend records temperature changes. Between 1620 and 1900 AD (covering the major part of the Little Ice Age in Europe), the temperature was cooler than the 490-year mean. Temperatures warmer than the average prevailed during 1520-1620 and 1900-present. Superimposed on the long-term trend were about 14 $\delta^{18}O$ cycles of 30-40 year periodicity, with wet periods centered around 1985, 1955, 1910, 1880, 1840, 1800, 1760, 1730, 1690, 1660, 1630, 1600, 1560, and 1530 AD. The periodicity may well reflect changes in the strength of summer monsoons in eastern China. The $\delta^{13}C$ record exhibits cyclic variations similar to the $\delta^{18}O$ record, with high rainfall periods registering lighter $\delta^{13}C$ signals. These signals may ride on a longer $\delta^{13}C$ variation trend of the soil CO_2, a trend that reflects climate-induced changes in the local C_3 vs. C_4 plant population. The $\delta^{13}C$ data for the last 50 years further record the effect of enhanced fossil fuel CO_2 in the atmosphere on the $\delta^{13}C$ of soil CO_2.

Introduction

Precipitation in much of the eastern China is dominated by the summer monsoons. In winter, the region is under the influence of the Siberian High, which produces outflow of cold, dry continental air off the Asian continent. With the onset of summer, warm, moist and unstable air moves inland from the subtropical anticyclones of the western Pacific (Figure 1). These maritime air masses associated with the summer monsoons may bring more than 75% of the year's precipitation into the eastern part of China (Figure 2). Variations in the strength and timing of the monsoons have caused regional drought or flood conditions at times, and it would be important to recognize any patterns of such variations. Indeed, historical records in Beijing, Tianjin, and Shanghai appear to show a 30- to 40-year cyclic pattern of rainfall (seen later in Figure 5). To look into such a cyclicity over times longer than a mere century, we have studied the $\delta^{18}O$ record of a stalagmite grown in Shihua Cave, located about 50 kilometers southwest of Beijing, China.

In: R.C. Wilson and V.L. Tharp, Editors. 1998. *Proceedings of the Fourteenth Annual Pacific Climate (PACLIM) Workshop, April 6-9, 1997.* Interagency Ecological Program, Technical Report 57. California Department of Water Resources.

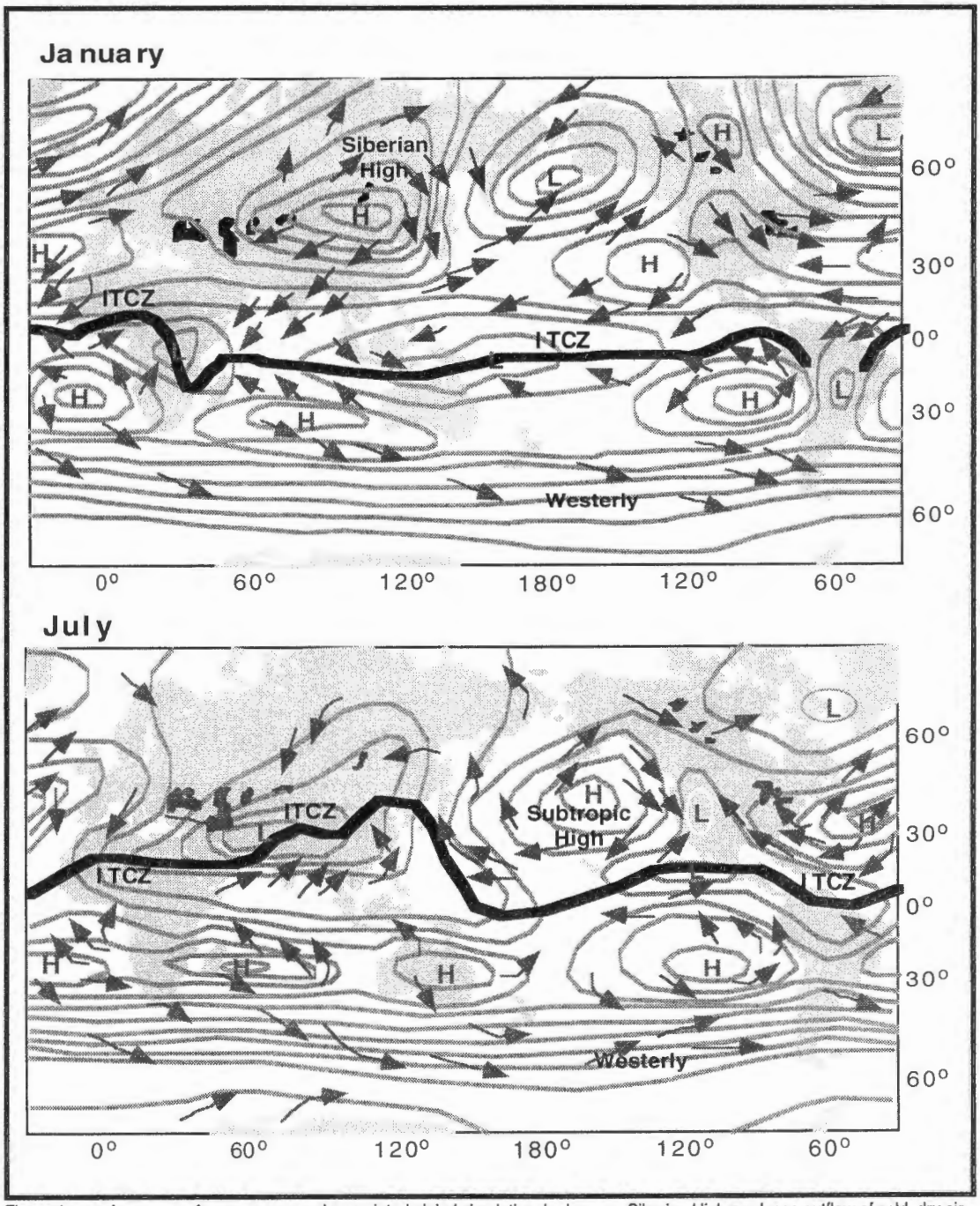

Figure 1. Average surface pressure and associated global circulation. In January, Siberian High produces outflow of cold, dry air off the Asian continent. In July, the low pressure system over Tibetan region and the high pressure systems over the oceans drive the summer monsoon. Warm, moist, and unstable air masses move inland from the western Pacific, bringing with them >75% of the rainfall in eastern China.

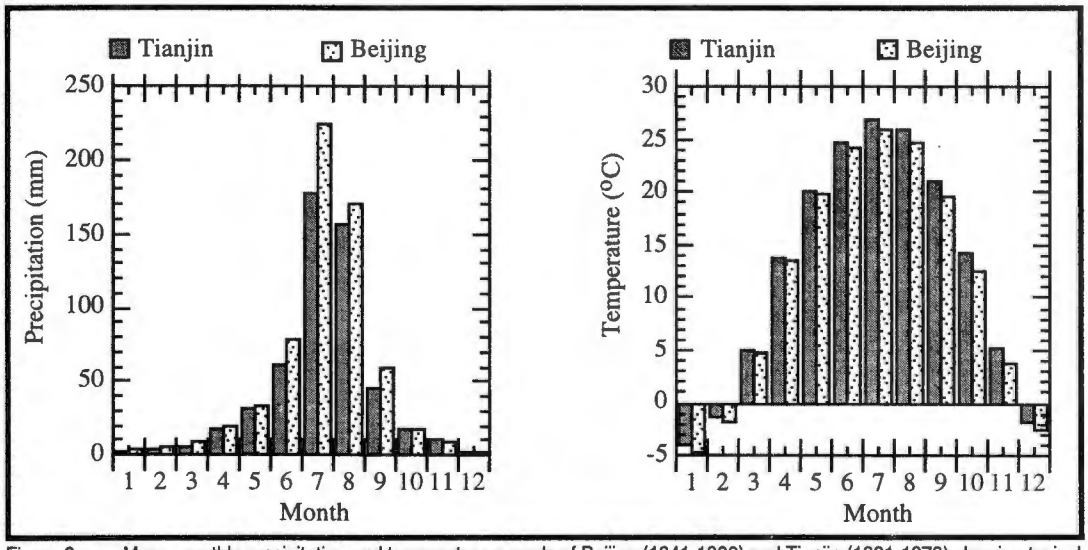

Figure 2. Mean monthly precipitation and temperature records of Beijing (1841-1990) and Tianjin (1891-1979) showing typical monsoonal climates with wet, hot summers and dry, cold winters.

The $\delta^{18}O$ of a stalagmite is generally in equilibrium with those of the cave drip water and regional surface water (Yonge *et al* 1985; Schwarcz 1986; Dorale *et al* 1992; Gascoyne 1992; Bar-Matthews *et al* 1996; Lauritzen 1996; Li *et al* 1997). As precipitation increases and air temperature decreases, the $\delta^{18}O$ of precipitation ($\delta^{18}O_p$) becomes more negative. As a result of the Rayleigh distillation process, maritime air masses after long-distance transit often have more negative $\delta^{18}O$ values than those of local air masses. The inverse relationship between $\delta^{18}O_p$ and the amount of precipitation, to a large degree also reflecting the Rayleigh process, has been well documented by observation made in tropical and mid-latitude regions (Dansgaard 1964; Rozanski *et al* 1993). Measurements of modern precipitation show that $d\delta^{18}O_p/dT$ ranges from 0.5 to 0.7‰/°C (Dansgaard 1964; Rozanski *et al* 1993). This temperature effect on $\delta^{18}O_p$ often overrides the temperature coefficient of –0.23‰/°C (O'Neil *et al* 1969) for the calcite-water isotopic fractionation. Cave temperatures are close to the mean annual surface temperatures, which for a given location hardly vary more than ±2°C over time spans of 1000 years or less. Therefore, on decadal time scales, the climatic influence on $\delta^{18}O_p$ is primarily due to a change in precipitation rather than in temperature. We may thus read the high-resolution record of the Shihua Cave stalagmite by taking a decrease of $\delta^{18}O$ to mean an increase of rainfall resulting from strengthening of the East Asian summer monsoons. Conversely, a more positive $\delta^{18}O$ signal reflects a decrease of precipitation and weakening of the summer monsoon.

Material, Analysis, and Result

Shihua Cave, formed in carbonate rocks of mid-Ordovician age, is at an elevation of 200 meters and lies 30-130 meters below the present land surface (Figure 3). At the present, the cave water dripping rate responds to changes in surface precipitation within about a week. Tritium measurements indicate that the replacement time of water above the cave is about 3 years (Table 1, Li *et al* 1996a). Li *et al* (1996a) have shown that surface waters in the area and cave water have similar $\delta^{18}O$ values: –9.4±0.3‰ (SMOW) and –9.2‰, indicating that ground water and cave water have undergone minimal evaporation. Temperatures inside the cave remain close to the annual mean surface temperature of about 13°C. At this temperature, the $\delta^{18}O$ (PDB) of calcites precipitating from drip water under isotopic equilibrium should be about –8.25‰ (Epstein *et al* 1953; O'Neil *et al* 1969). This value is close to the post-1985 values of –8.19 to –8.39‰ found in stalagmite sample S312 collected in November 1995 from Shihua Cave.

Table 1
δD, $\delta^{18}O$, AND TRITIUM VALUES OF WATER SAMPLES IN THE SHIHUA CAVE AREA

The similarity of δD, $\delta^{18}O$ and ^{3}H among surface, ground, and cave waters indicates that the water has not experienced much evaporation, and surface water penetrates into the cave in relatively short time.

Sample	Type	δD (‰)	$\delta^{18}O$ (‰)	^{3}H (TU)
	Rain		-10.0	~35
S301	Ground Water	-69	-9.8	25.4±0.9
S302	River Water	-66	-9.6	34.1±1.1
S303	Ground Water	-67	-9.6	32.3±1.1
S304	Ground Water	-65	-9.3	30.4±1.0
S305	Drip Water	-66	-9.4	25.3±0.9
S306	Drip Water	-68	-9.0	33.1±1.1
S307	Pool Water	-60	-9.4	27.6±1.0
S308	Pool Water	-61	-9.2	38.0±1.2
Average		-65.4±3.0	-9.4±0.3	30.8±4.5

At the time of collection, sample S312 (Figure 4), a stalagmite about 20 centimeters high, was in growth position; its uppermost tip was receiving drip water from the cave ceiling and containing >15 dpm/g of ^{210}Pb activities. From the exponential decrease of ^{210}Pb (to a depth of about 1.5 centimeters, ^{14}C dating and lamination counting, Li *et al* (1996b) showed that the top 13 centimeters of S312 had grown continuously, with an average rate of 0.044 mm/year. We sampled the uppermost 2 centimeters of the specimen along the central growth-axis using a computer-aided triaxial sampler (Quinn *et al* 1996) to a resolution of about 3 years. A total of 133 compositions using a V.G. Prism II mass spectrometer, to which was attached an Autocarb device for reaction of powdered carbonate with 100% H3PO4 at 90 °C. During the computer-controlled automated

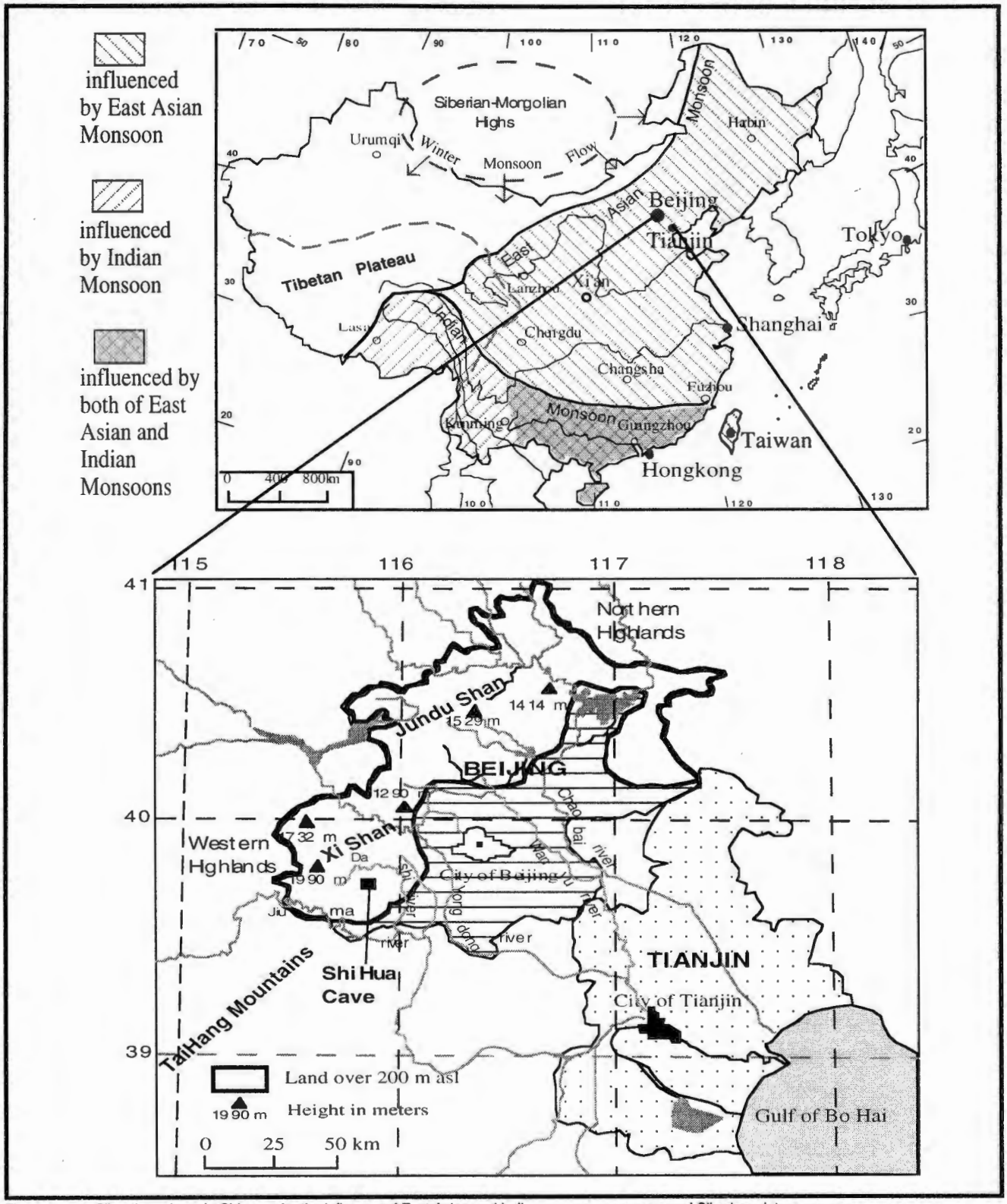

Figure 3. Climatic regimes in China under the influence of East Asian and Indian summer monsoons and Siberian winter monsoon. Also shown is the location of Shihua Cave near Beijing.

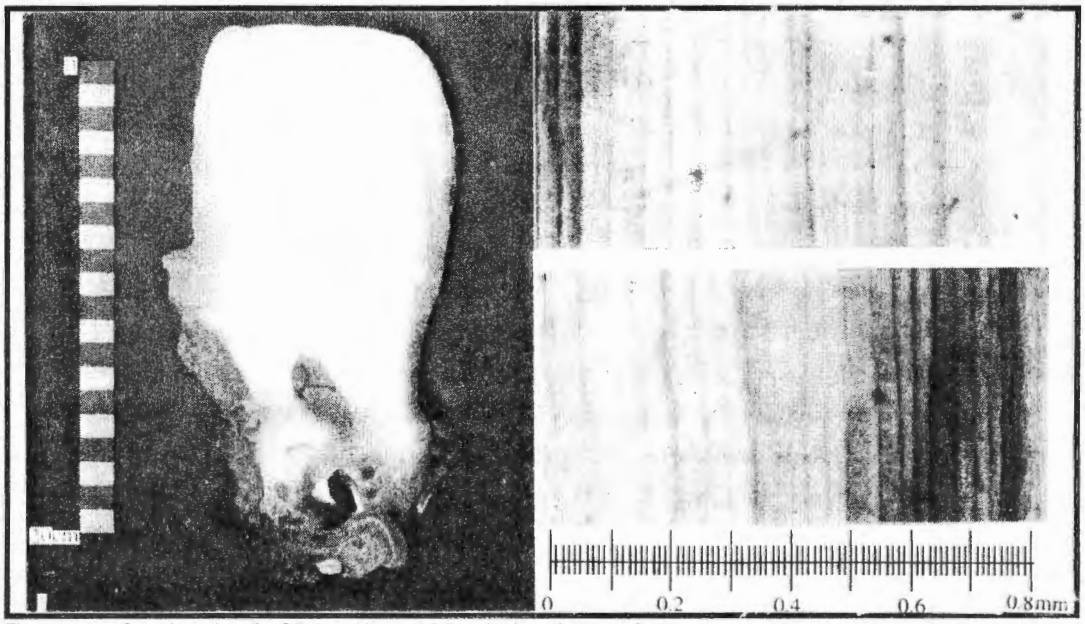

Figure 4. Sample stalagmite S312 and its growth bands viewed under microscope.

operations, for every five sample runs there was a standard (USC Paleo-2) run. Results of the analysis are reported in the conventional delta notation with respect to the PDB standard. The estimated one-sigma measurement errors were ±0.15‰ for $\delta^{18}O$ and ±0.1‰ for $\delta^{13}C$, based on reproducibility of the standard runs.

The $\delta^{18}O$ and $\delta^{13}C$ results are plotted in Figure 5 against age. The age assignment, based on the mean growth rate of 0.044 mm/year and assuming the topmost sample to have an age of 1994 AD, has an overall uncertainty of about ±10% (Li *et al* 1996b). The $\delta^{18}O$ values vary from –7.86‰ to –9.49‰, averaging –8.90‰, and the $\delta^{13}C$ values vary from –6.38‰ to –8.27‰, averaging –7.36‰. Their variations over the past 500 years show a distinct periodicity of 30-40 years. hese variations are best explained as reflecting changes in precipitation, with maximum wetness marked by the short arrows shown in the figure.

$\delta^{18}O$ and $\delta^{13}C$ as Precipitation Proxy

Precipitation in eastern China depends on the strength of the summer monsoons. Stronger monsoons would push the maritime air masses farther inland, and precipitation occurs mostly at the frontal zone. In a typical year, movement of this frontal zone follows a rough schedule of arriving in southern China in spring, moving toward the Yangtze drainage basins during early summer, and reaching northern China and Inner Mongolia during July and August. The warm, wet summer climate of the Beijing-Tianjin area, particularly in June to August, is well illustrated by the data displayed in Figure 2, showing monthly precipitation and temperature averaged over many years. The record extends from 1841 to

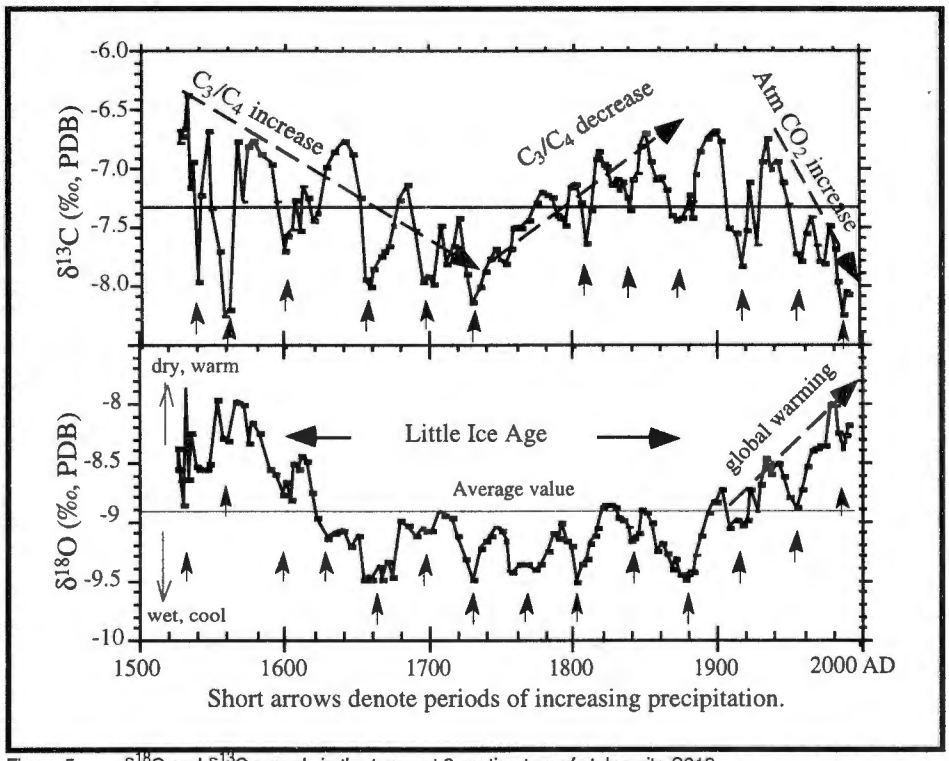

Figure 5. $\delta^{18}O$ and $\delta^{13}C$ records in the topmost 2 centimeters of stalagmite S312. Short arrows marking the $\delta^{18}O$ and $\delta^{13}C$ minima denote precipitation maxima. Horizontal lines represent average values of the two records.

1990 for Beijing and from 1891 to 1979 for Tianjin. Shifts in the position, strength, and persistence of the monsoons occasionally may lead to yearly contrasting conditions of southern drought/northern flood (and vice versa) in China. In this regard, recognition of any discernible variation patterns in the monsoon strength over time, as we see in the isotopic record of S312 would be of great value and interest.

The cyclic patterns shown in Figure 5 may well be a manifestation of the fluctuations in the strength of the Asian summer monsoons. To validate this speleothem $\delta^{18}O$-climate connection, we compare in Figure 6 the $\delta^{18}O$ record with the precipitation and temperature records of Beijing, Tianjin, and Shanghai (31°N, 121°E). In view of the 3-year resolution of the speleothem record and a possible time lag between surface and cave waters, 5-year running averages of the time-series precipitation data are taken for the comparison. Although the pre-1890 data in Beijing are far from complete, precipitation in both Beijing and Tianjin displays 30- to 40-year cyclic variations similar to those of the S312 record. This cyclicity is also shown by the 1872-1990 data collected from Shanghai where the climate has an even stronger monsoonal influence than Beijing and Tianjin. Note that the highest precipitation in Beijing and Tianjin occurred during times of relatively low mean annual temperatures (Figure 6b), a reflection of a prolonged rainy season during summer. Thus

the meteorological records indicate alternations of wet-cool and dry-warm climates during the last century or so in northern China, with a periodicity of 30-40 years. This pattern matches the Shihua Cave $\delta^{18}O$ curve reasonably well considering the uncertainties in dating of the stalagmite (Figure 5). The post-1840 match shows a good correspondence between light $\delta^{18}O$ record with the historical records shows a correspondence between light $\delta^{18}O$ and high precipitation, which is consistent with the theoretical considerations stated earlier.

Similar to the $\delta^{18}O$ record, $\delta^{13}C$ also exhibits 30- to 40-year cyclic variation (Figure 5). In principle, the carbon isotopic composition of carbonate stalagmite reflects the $\delta^{13}C$ of soil CO_2 above the cave, which varies as a function of the relative proportion of C_3-photosynthesizing plants to and C_4-photosynthesizing plants grow at a locality (Cerling 1984; Cerling *et al* 1989; Quade *et al* 1989). The growth of C_3 plants, which include trees, most shrubs and herbs, and cool season grasses and have $\delta^{13}C$ values between –25‰ and –32‰ (Cerling *et al* 1989), are favored under wet and cool climatic conditions. Plants of the C_4 photosynthesizing pathway, which include maize, sorghum, subtropic prairie grasses, and savanna grasses of Africa and South America and have $\delta^{13}C$ values ranging from –10‰ to –14‰ (Cerling *et al* 1989), grow best under conditions of higher minimum summer temperature and low soil moisture. At a given locality, the C_3/C_4 plant ratio is modulated by changes in climate, and the variation of this ratio can be recorded by the $\delta^{13}C$ in speleothems, on time scales greater than decades.

On decadal or shorter scales, however, the $\delta^{13}C$ record of a speleothem may also mark the variability of precipitation, with high rainfall periods register lighter $\delta^{13}C$ signals. When precipitation increases, the $\delta^{13}C$ of stalagmites will decrease for the following reasons:

- Shortening the residence time of seepage water in the overlying limestone, leading to a reduced amount of dissolved bedrock $CaCO_3$;
- Reduced P_{co2} in seepage water resulting in less $CaCO_3$ dissolution;
- Increase of cave water drip rate, causing less CO_2-degassing from the water.

Hence, the general coincidence between $\delta^{18}O$ and $\delta^{13}C$ (perhaps with the exceptions around 1630 and 1760 AD) in showing the 30- to 40-year cycles can be explained as resulting from the cyclic variations in precipitation. During the past 490 years, there are about fourteen cycles of 30- to 40-year duration, with wet periods centered around 1985, 1955, 1910, 1880, 1840, 1800, 1760, 1730, 1690, 1660, 1630, 1600, 1560, and 1530 AD (Figure 5).

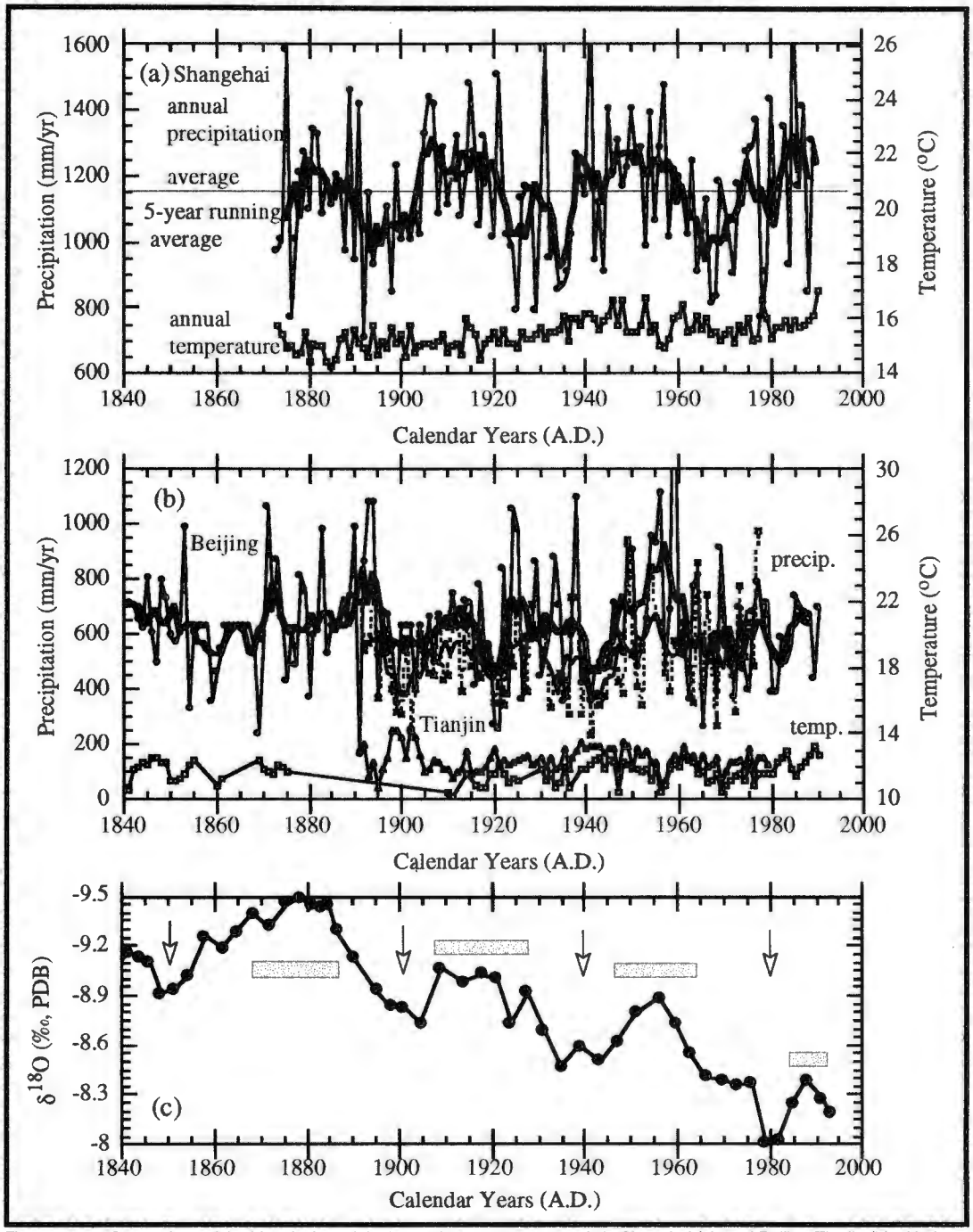

Figure 6. Comparison of the historical precipitation and temperature records in Shanghai (a), and Beijing-Tianjin (b) with the $\delta^{18}O$ record in S312 (c). The precipitation records appear to exhibit 30-40 year cycles; high precipitation corresponds to low temperature. In (c), light $\delta^{18}O$ is seen to match high precipitation (indicated by horizontal bars).

Extending farther back in time, a comparison can be made of the $\delta^{18}O$ record of S312 with the tree-ring data at Mt. Huashan in Shaanxi Province (Hughes *et al* 1994). Located in a climatic regime similar to Shihua Cave, Mt. Huashan also receives most of its precipitation in the summer and fluctuates about the mean of 415 mm/year back to 1600 AD. The comparison shows a passing resemblance of the two patterns between 1600 and 1920 (Figures 7a and 7b).

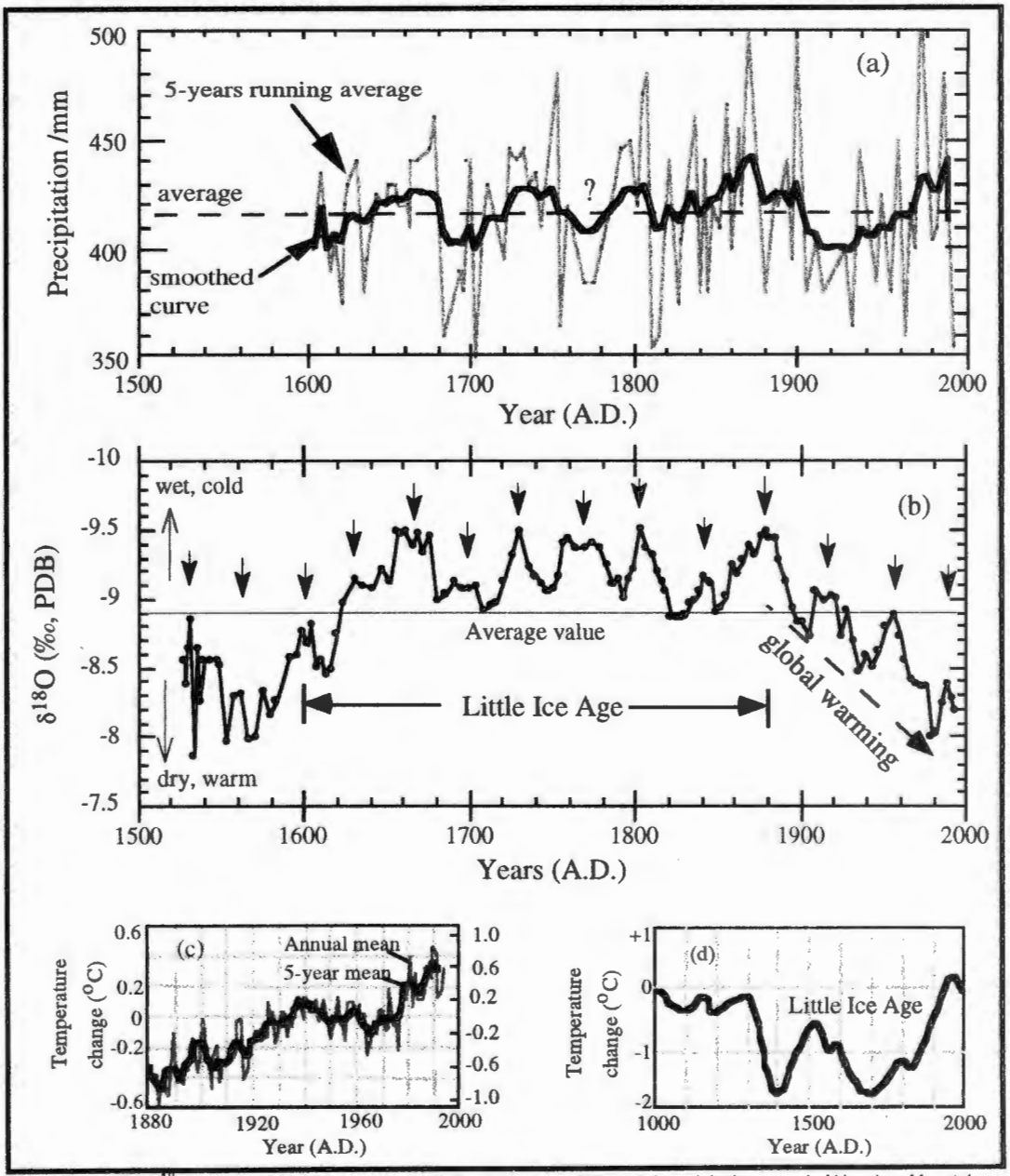

Figure 7. The $\delta^{18}O$ record in S312 (b) compared with the tree-ring reconstructed precipitation record of Huashan Mountain, Shaanxi (a) and with the global temperature changes recorded instrumentally (c) and from tree-ring studies (d). Data sources in (a), (c), and (d): Hughes *et al* 1994; Strahler and Strahler 1997; Lutgens and Tarbuck 1995.

Long-Term $\delta^{18}O$ Change as an Indicator of Temperature Change

The precipitation cycles revealed by the $\delta^{18}O$ record of S312 appear to ride on a larger variation trend. On time scales of longer than about 50 years, the trend since 1880 AD has been toward heavy $\delta^{18}O$, a trend in concert with the warming trend of global temperature (Figures 7b and 7c), manifesting the positive correlation between $\delta^{18}O_p$ and temperature. If we take the mean $\delta^{18}O$ over the last 500 years as a gauge of the average temperature for the period, then temperatures lower than the average prevailed in Beijing between 1620 and 1900 AD (Figure 7b), a period corresponding to a good latter part of the Little Ice Age in Europe (Figure 7d). Figure 7b also shows that 1520-1620 and 1900-1994 were warmer than the average and that a cooling trend occurred between 1570 and 1660, as opposed to a warming trend since 1880. Whether this latest warming trend is a consequence of the greenhouse effect or represents a part of natural variations remains to be seen. The speleothem record indicates that a warming trend comparable to the present one had also occurred before 1555 AD, leading to temperatures during 1555-1570 close to present levels.

$\delta^{13}C$ Records Post-1920 CO_2 Increase

The $\delta^{13}C$ in S312 gradually decreased from 1540 to 1700 AD, paralleling the long-term $\delta^{18}O$ trend (Figure 5). This may indicate that the C_3/C_4 plant ratio in the region increased as temperature decreased. Between 1700 and 1880 AD, the $\delta^{13}C$ has an increasing trend, even though temperature remained below the 500-year mean as shown by the $\delta^{18}O$ record. We hypothesize that the $\delta^{13}C$ change reflects a reduced C_3/C_4 plant ratio due to the increase of agricultural C_4 plants, such as maize and sorghum, resulting from the large population increase during that period.

The most interesting feature of the $\delta^{13}C$ change is that its trend is opposite to that of $\delta^{18}O$ during the last 50 years or so (Figure 5). This $\delta^{13}C$ decreasing trend cannot be explained by temperature change or the variation of the C_3/C_4 plant ratio. Instead, it could have recorded the effect of enhanced fossil fuel CO_2 in the atmosphere on the $\delta^{13}C$ of soil CO_2. Friedli *et al* (1986) measured the $\delta^{13}C$ in CO_2 extracted from Antarctic ice and found a value of –6.5‰ between 1750 and 1920 AD. This value decreased to –7.8‰ until 1983. Marino and McElroy (1991) analyzed the $\delta^{13}C$ of carbon in C_4 plant cellulose and reconstructed the $\delta^{13}C$ of atmospheric CO_2. Their data show that $\delta^{13}C$ decreased from –6.5‰ in 1948 to –8.2‰ in 1984. Keeling *et al* (1989) directly monitored CO_2 concentration and CO_2 in the atmosphere and concluded that the $\delta^{13}C$ of atmospheric CO_2 declined with the increasing CO_2 concentration between 1956 and 1989. The drop rate of the $\delta^{13}C$ is about 0.034‰/year.

All these results indicate that enhanced fossil fuel CO_2 concentrations in the atmosphere cause a decrease of $\delta^{13}C$ in atmospheric CO_2. This effect is recorded in the $\delta^{13}C$ of stalagmite S312. Figure 5 shows that the $\delta^{13}C$ of the stalagmite has decreased from –6.7‰ to –8.1‰ since 1940, with a rate of –0.028‰/year, in excellent agreement with previous studies (Friedli *et al* 1986; Marino and McElroy 1991; Keeling *et al* 1989; Baskaran and Kishnamurthy 1993).

Summary

Isotopic records in speleothems offer valuable proxy information on high-resolution paleoclimatic variability. On decadal or shorter scales, $\delta^{18}O$ variations reflect changes in precipitation, with lighter $\delta^{18}O$ corresponding to increased rainfall. Long-term (>50 years) $\delta^{18}O$ variations primarily record variations in temperature, with lighter $\delta^{18}O$ corresponding to colder temperatures. The observed $\delta^{18}O$ variations in stalagmite S312 (Figure 5) show climate changes during the past 500 years in northeastern China, as follows. Compared to the 500-year mean, the temperature in Beijing and Tianjin was lower between 1620 and 1900 AD and higher during 1520-1620 and since 1900. Superimposed on this long-term temperature trend are fourteen cycles (30-40 year duration) of precipitation changes, with wet periods centered around 1985, 1955, 1910, 1880, 1840, 1800, 1760, 1730, 1690, 1660, 1630, 1600, 1560, and 1530 AD. They are likely a manifestation of fluctuations in the strength of the East Asian summer monsoons. The $\delta^{13}C$ record of the stalagmite on decadal or shorter scales confirms the cyclic variations in precipitationdeciphered by the $\delta^{18}O$ record, with high rainfall being registered by lighter $\delta^{13}C$ signals. The $\delta^{13}C$ data for the last 50 years further record the enhanced fossil fuel CO_2 in the atmosphere.

References

Bar-Matthews, M., A. Ayalon, A. Matthews, E. Sass, and L. Halicz. 1996. Carbon and Oxygen isotope study of the active water-carbonate system in a karstic Mediterranean cave: Implications for paleoclimate research in semiarid regions. *Geochim. Cosmochim. Acta*, 60:337-347.

Baskaran, M., and R.V. Kishnamurthy. 1993. Speleothems as proxy for the carbon isotope composition of atmospheric CO_2. *Geophys. Res. Lett.*, 20:2905-2908.

Cerling, T.E. 1984. The stable isotopic composition of soil carbonate and its relationship to climate. *Earth Planet. Sci. Lett.*, 71:229-240.

Cerling, T.E., J. Quade, Y. Wang, and J.R. Bowman. 1989. Carbon isotopes in soil carbonates. In: Swart, P.K. *et al* (eds.), Climate change in continental isotopic records. *Amer. Geophys. Union, Monograph*, 78:217-231.

Dansgaard, W. 1964. Stable isotopes in precipitation. *Tellus XVI* (4)436-468.

Dorale, J.A., L.A. Gonzalez, M.K. Reagan, D.A. Pickett, M.T. Murrell, and R.G. Baker. 1992. A high-resolution record of Holocene climate change in speleothem calcite from Cold Water Cave, Northeast Iowa. *Science*, 258:1626-1630.

Epstein, S., R. Buchsbaum, H.A. Lowenstam, and H.C. Urey. 1953. Revised carbonate-water isotopic temperature scale. *Bull .Geol .Soc. Amer.*, 64:1315-1326.

Friedli, H., H. Lotscher, H. Oeschger, U. Siegenthaler, and B. Stauffer. 1986. Ice core record of the $^{13}C/^{12}C$ ratio of atmospheric CO_2 in the past two centuries. *Nature*, 324:237-238.

Gascoyne, M. 1992. Paleoclimate determination from cave deposits. *Quatern. Sci. Rev.*, 11:609-632.

Hughes, M.K., X.D. Wu, X.M. Shao,and G.M. Garfin. 1994. A preliminary reconstruction of rainfall in North-Central China since AD 1600 from tree-ring density and width. *Quatern. Res.*, 42:88-99.

Keeling, C.D., R.B. Bacastow, A.F. Carter, S.C. Piper, W.P. Timothy, M. Heimann, W.G. Mook, and H. Roeloffzen. 1989. A three dimensional model of atmospheric CO_2 transport based on observed winds: 1. Analysis of observational data. *Am. Geophys. Union, Monogr.*, No. 55:165-236.

Lauritzen, S.-E. 1996. Climate change: The karst record. *Karst Waters Institute Special Publication 2*: Extended abstracts of a Conference held at University of Bergen, Norway, August 1-4th 1996.

Li, H.-C., T.-L. Ku, S.-S. Zhao, T.S. Liu, W.-J. Jiao, J.-H. Yin, T.-Y. Li, and J.-B. Lu. 1996a. Isotope studies of ShiHua cave-I: δD, $\delta^{18}O$ and tritium activity of ShiHua cave, Beijing. *Seismology and Geology*, 18:325-328. (In Chinese)

Li, H.-C., T.-L. Ku, W.-J. Chen, W.-Q. Jiao, S.-S. Zhao, T.-M. Chen, and T.-Y. Li. 1996b. Isotope studies of Shihua Cave, Beijing -II: Radiocarbon dating and age correction of stalagmite. *Seismology and Geology*, 18:329-338.

Li, H.-C., T.-L. Ku, W.-J. Chen, and T.-Y. Li. 1997. Isotope studies of ShiHua cave-III: Reconstruction of paleoclimate and paleoenvironment of Beijing during the last 3,000 years from $\delta^{13}C$ and $\delta^{18}O$ records in stalagmite. *Seismology and Geology*, 19:77-86. (In Chinese)

Lutgens, F.K., and E.J. Tarbuck. 1995. *The Atmosphere: An Introduction to Meteorology*. A Simon & Schuster Co., Englewood Cliffs, NJ, 462 pp.

Marino, B.D., and M.B. McElroy. 1991. Isotopic composition of atmospheric CO_2 inferred from carbon in C_4 plant cellulose. *Nature*, 349:127-131.

O'Neil, J.R., R.N. Clayton, and T.K. Mayeda. 1969. Oxygen isotope fractionation in divalent metal carbonates. *J. Chem. Phys.*, 51:5547-5558.

Quade, J., T.E. Cerling, and J.R. Bowman. 1989. Systematic variations in carbon and oxygen isotopic composition of pedogenic carbonate along elevational transects in the southern Great Basin, United States. *Geol. Soc. Am. Bull.*, 101:464-475.

Quinn, T.M., F.W. Taylor, T.J. Crowley, and S.M. Link. 1996. Evaluation of sampling resolution in coral stable isotope records: A case study using records from New Caledonia and Tarawa. *Paleoceanography*, 11:529-542.

Rozanski, K., L. Arzguas-Araguas, and R. Gonfiantini. 1993. Isotopic patterns in modern global precipitation. Pages 1-36 in *Climate Change in Continental Isotopic Records*. P.K. Swart *et al*, editors. Amer. Geophys. Union, Monograph 78.

Schwarcz, H.P. 1986. Geochronology and isotopic geochemistry of speleothem. Pages 271-303 in *Handbook of Environmental Isotope Geochemistry*, Vol. 2. P. Fritz and J. Ch. Fontes, editors. Elsevier.

Strahler, A.H., and A.N. Strahler. 1997. *Physical Geography: Science and Systems of the Human Environment*. John Wiley & Sons, Inc., 637 pp.

Yonge, C.J., D.C. Ford, and J. Gray. 1985. Stable isotope studies of cave seepage water. *Chem. Geol.*, 58:97-105.

The Response of Desert Vegetation to Climate Change during the Past 150,000 Years in the Southern Owens Valley Region, California

Wallace B. Woolfenden

Analysis of the pollen preserved in the upper 90-meter section of a mostly continuous 323-meter core (OL-92) from Owens Lake, southeastern California, has produced a climatically sensitive record of the terrestrial vegetation dating from the penultimate glaciation (151 ka) to the early Holocene (9 ka) (Woolfenden 1996). The entire core, retrieved by the U.S. Geological Survey in the summer of 1992, has produced a paleoclimatic record for the past about 800 ka (Smith and Bischoff 1997).

The pollen time series shows long-term trends in abundance of pine, fir, juniper, saltbush, sagebrush, greasewood, *Ambrosia*-type (mostly white bursage), and other, less frequent, pollen taxa. High percentages of juniper pollen with low percentages of desertscrub pollen during the intervals of about 150-120 ka and 73-20 ka alternate with low percentages of juniper pollen and relatively high percentages of desertscrub and oak pollen during the intervals of about 118-103 ka and 18-10 ka and into the Holocene. Sagebrush pollen varies with juniper pollen but has a tendency to lead it in time. Pine and fir pollen varies inversely with juniper over the long term. These trends are interpreted as vegetation change in response to glacial-interglacial cycles. During cold-wet glacial and stadial climates, there was a downslope expansion of juniper woodland and sagebrush scrub, contraction of Sierra Nevada montane forest, and displacement of warm desertscrub. Such vegetation changes allow for estimated departures from modern average values of -2°C to -6°C for temperature and +100 mm to +350 mm for precipitation. Conversely, under warmer and drier interglacials and interstadials, warm desert shrubs expanded their range in the lowlands, juniper and sagebrush retreated upslope, and Sierran forests expanded. Estimated departures from modern average values were -0.5° to +3.7°C for temperature and +13 mm to -26 mm for precipitation. The postulated decrease in Sierra Nevada montane conifers during periods of glacial maxima can be partly attributed to the occupation of montane forest habitat by an expanded ice cap, just as variations in saltbush and greasewood pollen may partly reflect the changing extent of valley habitat due to lake-level fluctuations of Pleistocene Owens Lake.

In: R.C. Wilson and V.L. Tharp, Editors. 1998. *Proceedings of the Fourteenth Annual Pacific Climate (PACLIM) Workshop, April 6-9, 1997.* Interagency Ecological Program, Technical Report 57. California Department of Water Resources.

The reconstructed vegetation history is in general accord with the chronologies of glacial advances in the Sierra Nevada and lake-level fluctuations of Pleistocene Owens Lake, demonstrating a regional climatic correlation. Comparison of the pollen spectra spanning the penultimate (oxygen isotope stage [OIS] 6) and ultimate (OIS 2) glacial maxima shows the former to have been longer and more intense, as also indicated by the topographic relationships of the Sierra Nevada glacial moraines. Similarly, the higher abundance of *Ambrosia* pollen during the last interglaciation (OIS 5e), compared to the Holocene, indicates warmer temperatures in the former. The presence of high oak percentages also during the last interglaciation suggest an expansion of the summer monsoon. At a larger scale, the match of the juniper pollen time series with the marine oxygen isotope chronostratigraphy (Figure 1) suggests a link between vegetation change in the southern Owens Valley and global climate change.

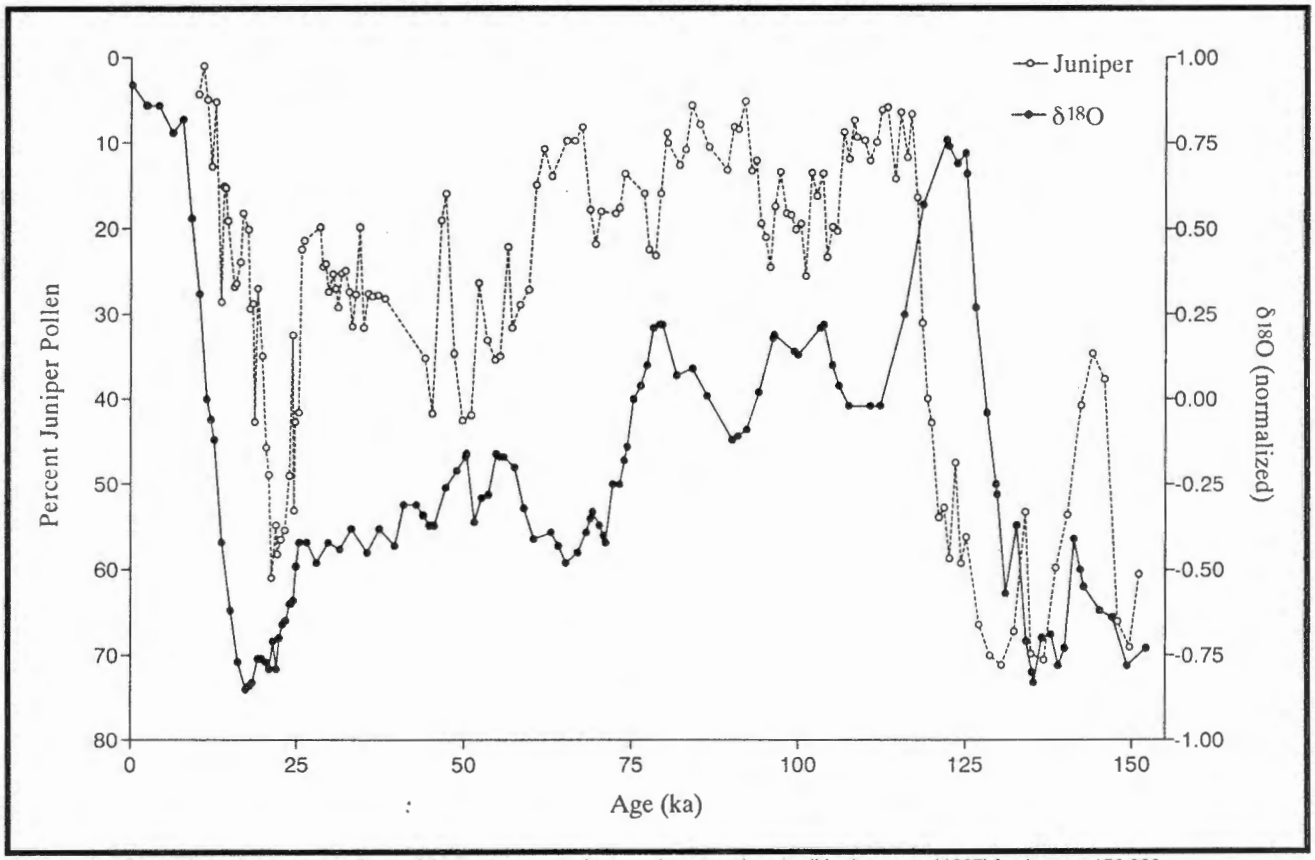

Figure 1. Comparison of *Juniperus* pollen and the marine oxygen isotope chronostratigraphy (Martinson *et al* 1987) for the past 150,000 years. Since both curves express similar climatic trends, the y axis for the Juniperus pollen percentages is inverted to show the correspondence in direction between the curves.

References

Martinson, D.G., N.G. Pisias, J.D. Hays, J. Imbrie, T.C. Moore, and N.J. Shackleton. 1987. Age dating and the orbital theory of the Ice Ages: Development of a high-resolution 0 to 3,000,000-year chronostratigraphy. *Quaternary Research* 27:1-29.

Smith, G.I., and J.L. Bischoff (editors). 1997. *An 800,000-Year Paleoclimatic Record from Core OL-92, Owens Lake, Southeast California.* Geological Society of America Special Paper 317. Boulder, CO. 165 pp.

Woolfenden, W.B. 1996. *Late Quaternary Vegetation History of the Southern Owens Valley Region, Inyo County, California.* Unpublished Ph.D. Dissertation, The University of Arizona, Tucson, Arizona, 347 pp.

Relationship of High Elevation Surface Temperatures of the Central Rocky Mountain Region to Atmospheric Turbidity and the North Pacific Pattern

Mark Losleben

Temperature records show a non-linear relationship between annual temperature variations at high and low elevations in the Rocky Mountain region of northern Colorado and southern Wyoming for the 1951-1995 period. This non-linearity is reflected by a changing lapse rate, which implies changes in climatically important factors such as water vapor content, atmospheric stability, and cloud cover, all of which contribute to feedback processes involving precipitation, snowpack, and temperature. This study has found a significant statistical relationship between high elevation temperature in this region with atmospheric turbidity, and also during a period of anomalous cold, with the North Pacific pattern.

Atmospheric turbidity varies with time and place and is a measure of aerosols, including water vapor, haze, and dust. Turbidity measurements are often used as an indicator of volcanic activity. However, since they are also indicative of other climatically important constituents, they may also be used as an index of changing climatic factors, such as shifts in atmospheric circulation patterns. The Linke atmospheric turbidity index at Tucson, Arizona, is one of the longest mid-latitude indices in the western United States and has a correlation of -0.65 for 1957-1995, with the longest high elevation temperature record of the study region, which is at D1, Niwot Ridge, Colorado.

The North Pacific pattern is an area weighted sea level pressure index for the region 30N-65N, 160E-140W, for the 1951-1995 (Trenberth and Hurrell 1994). The correlation with high elevation temperatures of the study region with this index is very poor overall (r=0.005) but very strong for May 1981-October 1986 (r=0.65) May 1981 through October 1986 was anomalously cold at — and only at — the high elevations of this region (two to three standard deviations below the long-term, 1951-1995, average). In addition to the North Pacific relationship, 700-mb pressure height anomaly maps for January show higher pressure over the north Pacific Ocean and western United States and lower pressure over the eastern United States during this anomalous cold period, compared to the long-term average, suggesting changes in atmospheric circulation patterns.

In: R.C. Wilson and V.L. Tharp, Editors. 1998. *Proceedings of the Fourteenth Annual Pacific Climate (PACLIM) Workshop, April 6-9, 1997.* Interagency Ecological Program, Technical Report 57. California Department of Water Resources.

In summary, there is a rather good statistical relationship between temperature at high elevations of this central Rocky Mountain region and the Linke atmospheric turbidity index from Tucson for the past 40 years. However, during May 1981 to October 1986, a significant cooling occurred above 3000 meters in this region, and for this cool period there is a significant correlation with the North Pacific pattern. This correlation combined with the 700-mb pressure anomalies suggests that a change in circulation patterns during this period may have contributed to cooler temperatures at high elevations in northern Colorado and southern Wyoming.

The following data sources were used in this study:

- The annual regional high elevation temperature record is an average of standardized temperatures from six stations at elevations in excess of 3000 meters AMSL. The stations are: D1 and C1 on Niwot Ridge (1951-1995); Berthoud Pass, Colorado (1964-1984); and Mill Pond (1976-1987), Little Brooklyn (1976-1987), and Telephone Lakes, Wyoming (1976-1988).
- The low elevation annual temperature record was constructed in the same way from seven stations at elevations lower than 3000 meters. These stations are: Denver (1951-1994), Boulder (1951-1987), Longmont (1951-1989), Estes Park (1951-1993), Grand Lake (1951-1993), and Steamboat Springs, Colorado (1951-1991), and Centennial, Wyoming (1976-1986).
- The Linke turbidity index was obtained from William Sellers, University of Arizona, Tucson, and is an atmospheric measure of the clear sky burden of water vapor and aerosols, for the period 1957-1995.
- The North Pacific pattern is from Trenberth and Hurrell (1994, *Climate Dynamics* 9:303-319.) and is an area-weighted sea level pressure over the region 30N-65N, 160E-140W, for the period 1951-1995.

Addendum II: Paleoclimate and the Solar Insolation/Tidal Resonance Model

Thor Karlstrom

Previous PACLIM papers (Karlstrom 1995, 1996, 1997) analyze numerous independently dated paleoclimatic records that evidently provide substantial empirical support for the Solar Insolation/Tidal Resonance Climate Model. This model was first referred to as the Milankovitch/Pettersson Climate Theory (Karlstrom 1961 cf). The records presented in this paper also support the model and include unpublished time-frequency diagrams, long records published in *Science* and *Quaternary Research* after completion of my last paper, as well as records whose indices have been kindly provided by colleagues of the 1997 Santa Catalina PACLIM workshop.

Direct Empirical Test of the Solar Insolation/Tidal Resonance Climate Model

The Solar Insolation/Tidal Resonance Model differs from the prevailing standard climate model of the Quaternary (Martinson *et al* 1987) in requiring:

- Different ice-age histories for the Northern and Southern Hemispheres as these are modulated by opposing solar-insolation trends across the equator, rather than global synchronism in response to Northern Hemisphere continental glaciations modulated in turn solely by higher northern latitude summer solar-insolation trends; and
- That the secondary paleoclimatic oscillations (those from a few years to several thousands of years in duration) in sensitive paleoclimatic records include a series of superposed harmonically related climatic cycles. These appear to be globally synchronous, and apparently are in response to changing circulation patterns modulated in some fashion by tidal-force resonances in the atmosphere.

Thus, given accurately enough dated paleoclimatic records and sufficient global coverage, the prevailing standard climate model and the Solar Insolation/Tidal Resonance Model are amenable to direct testing since both propose specific but different timescales for climatic phasing. The procedures for testing the validity of the models are, therefore, direct and

In: R.C. Wilson and V.L. Tharp, Editors. 1998. *Proceedings of the Fourteenth Annual Pacific Climate (PACLIM) Workshop, April 6-9, 1997.* Interagency Ecological Program, Technical Report 57. California Department of Water Resources.

straightforward. Either independently dated terrestrial records from different latitudes show different primary trends that broadly parallel the local insolation trends in support of the Insolation/Tidal model, or they all, no matter what the latitude or hemisphere, broadly parallel the "standard" marine record that is specifically fine-tuned to N60º Latitude insolation (see Figure 24).

The test for higher frequency oscillations is equally straightforward since the model proposes a series of temporally fixed subharmonic cycles, including an average 556-year cycle specifically referenced to Pettersson's (1914) last period of maximum tidal forces (AD 1433 or 517 BP). Correlation between empirically-derived and dated natural climatic oscillations and theoretical cycle turning points is accepted as significant if series-matching is 70 percent or better for the cycle identified by wave length in years within the accompanying parentheses [*eg*, R=0.80 (556); R=0.72 (278)]

Analytical Procedure

My analyses of time series generally follow conventional procedures of dating, plotting, and smoothing. All records analyzed are independently dated and their timescales are accepted as published. These records are replotted on timescales common to the model and consistently oriented according to the paleoclimatic equation of inferred Cool/Wet (up) versus inferred Warm/Dry (down). All temperature and correlative records are, therefore, inverted relative to moisture and correlative records. Similarly, presentation of bioclimatic records follows the conventions of Hevly and Karlstrom (1974) whereby in percent frequency diagrams, components of inferred dry or warm are subtracted from components of inferred wet or cold to maintain parallelism between negatively and positively correlated components. To facilitate comparison of records with different amplitudes of oscillation, many are normalized by use of Z scores (standard deviation units). The amplitudes of secondary oscillations are further amplified in some records by differencing (viz. derivatives). Different levels of smoothing (or filtering) prove useful in clarifying cycle patterns and their phasings. Half-cycle smoothing positioned on turning points of theoretical cycles (Karlstrom 1996) prove particularly useful in defining the phasing of secondary oscillations in highest resolution paleoclimatic records such as tree ring, varve series, archaeology, or historical accounts. Stacking of multi- or single-component records is a common procedure that should enhance their signal/noise ratios. Time-frequency analyses of dated basal contacts (Point Boundaries) of discontinuous stratigraphic sections (such as glacial or alluvial deposits with partial exposures and numerous disconformities) provide a statistical means for suggesting regional patterns and correlations of depositional histories. All of these procedures are exemplified in one or more of the figures below.

Additional Supporting Paleoclimatic Records

Figures 1-4
Time-Frequency Diagrams of Basal-Contact Dates from Chronostratigraphic Sections in Western North America

By clustering in restricted time intervals, the datasets suggest regional correlations among Glacial, Alluvial, Lacustrine, Eolean and Colluvial depositional events that are, in turn, strongly in phase with the 556-year Phase Cycle and with lesser, but still significant, tendencies for phasing with the 278-year Subphase Cycle. Results of these analyses, since they relate to radiocarbon descriptions published through 1972, can be readily and incisively tested against datasets similarly selected from the thousands of basal-contact dates published since then.

Figure 1 shows radiocarbon dates selected from alpine glacial deposits in North America, South America, and Europe by Porter and Denton (1964) in deriving their twofold Neoglacial classification. The dates generally cluster around the turning points of the higher frequency cycles inferred from south-central Alaska and collated chronostratigraphy (Karlstrom 1961 cf), The dataset is consistent with the interpretation of common glacial histories modulated by the Phase and Subphase Cycles.

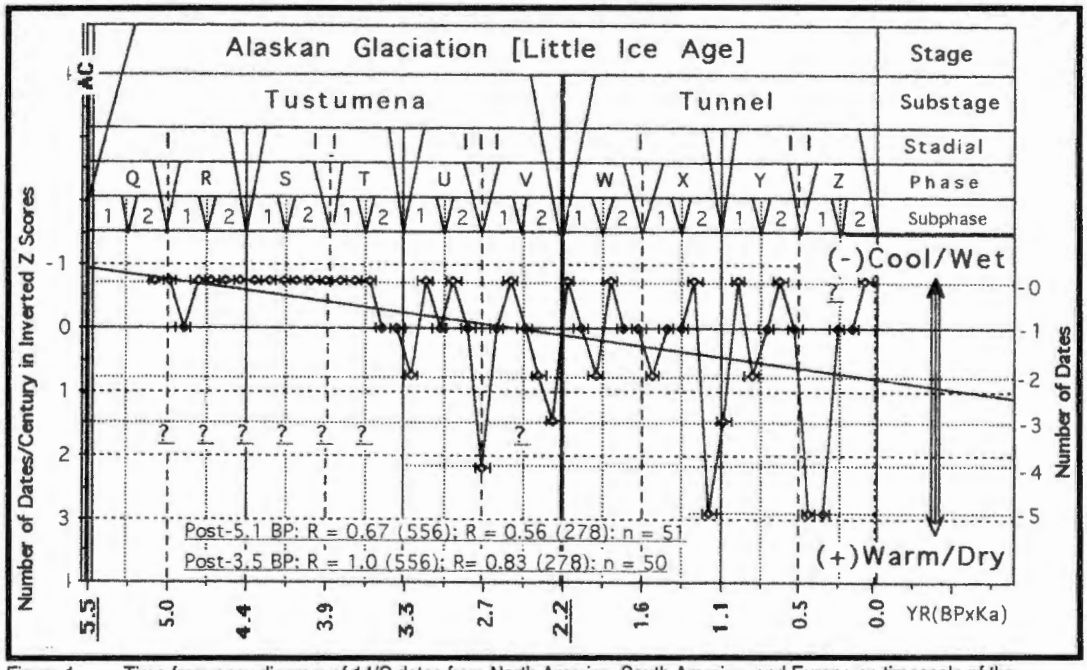

Figure 1 Time-frequency diagram of 14/C dates from North America, South America, and Europe on timescale of the 556-year Phase Cycle and its 2/1 (278-year) Subphase Resonance. Radiocarbon dates listed by Porter and Denton (1967) in deriving their Neoglacial chronology of two main intervals of glaciation post-3300-years BP in age. Note that in this time interval, their selected dates strongly cluster on cyclical boundaries of the Cook Inlet, Alaska, glacial and Southwest Alluvial classifications (top 5 rows), suggesting high-frequency depositional histories common with those of south-central Alaska and the Southwest. Diagram from Figure 5, Column 7, in Karlstrom (1975).

Figure 2 shows radiocarbon dates selected from alpine glacial deposits in Alaska and Yukon Territory by Denton and Karlen (1972) in deriving a revised Neoglacial classification. The dates again generally cluster around the turning points of the higher frequency cycles inferred from south-central Alaska and collated chronostratigraphic data, and again suggest modulation by the Phase and Subphase Cycles.

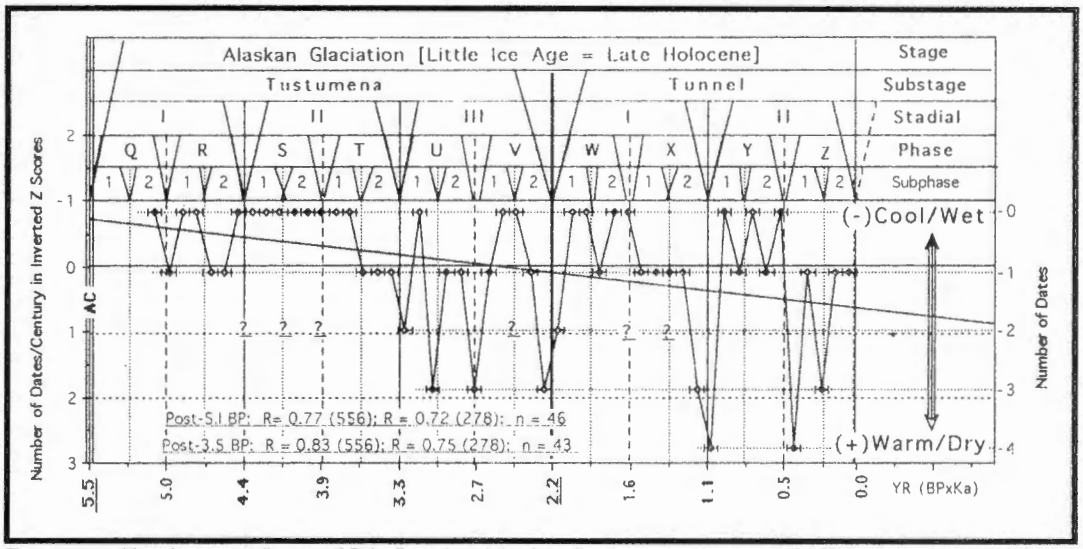

Figure 2 Time-frequency diagram of Point Boundary dates from Southeastern Alaska and Yukon Territory on timescale of the 556-year Phase Cycle and its 2/1 (278-year) Subphase Resonance. From dates selected by Denton and Karlen (1973) in deriving their revised Neoglacial classification. Note that this second set of dates again strongly clusters near the Phase and Subphase boundaries of the Cook Inlet glacial and Southwest Alluvial classifications (Karlstrom 1961, 1988, 1995). The statistical correlation is particularly compelling for the post-3.5 BP interval with the greatest density of dates in suggesting parallel, higher frequency depositional and climatic histories throughout this part of the Northwest — as also apparently confirmed by the expanded dataset shown in Figure 3. Diagram from Figure 5, Column 4, in Karlstrom (1975).

Figure 3 shows radiocarbon dates from basal-contacts of Glacial, Alluvial, Lacustrine, Eolean and Colluvial (GALEC) deposits. Samples selected by the author from the radiocarbon literature through 1972 (Karlstrom 1975) using the following criteria: (1) description in the literature sufficiently precise to identify the sample as associated with basal contacts of the above types of deposits; (2) only dates accepted by the collector as uncontaminated and stratigraphically defined; (3) only dates derived from organic carbon, charcoal, and wood (dates based solely on bone, carbonate and humic components were not included because of their greater potential for contamination by both younger or older carbon); and (4) no dates accepted with unusually large sigmas of counting error. The expanded database fortifies the impression of common Neoglacial depositional histories throughout western North America. The GALEC data also suggest correlative events in different depositional environments according to the following paleoclimatic equations: Glacial advance = valley-bottom aggradation accompanying rising water tables (providing a repeatedly renewed supply of exposed sediment for wind transportation and marginal deposition of loess and dune sand) = rising lake levels = slope instability and enhanced colluviation = Cooler and

Wetter climate; conversely, glacial retreat = stream-channel dissection accompanying lowering water tables, valley-bottom vegetation and soil formation (which drastically reduces available sediment supply for wind transportation) = lowering lake levels = slope stability and less colluviation = Warmer and Drier climate. For a more detailed analysis of these interacting geologic processes see Karlstrom (1988)

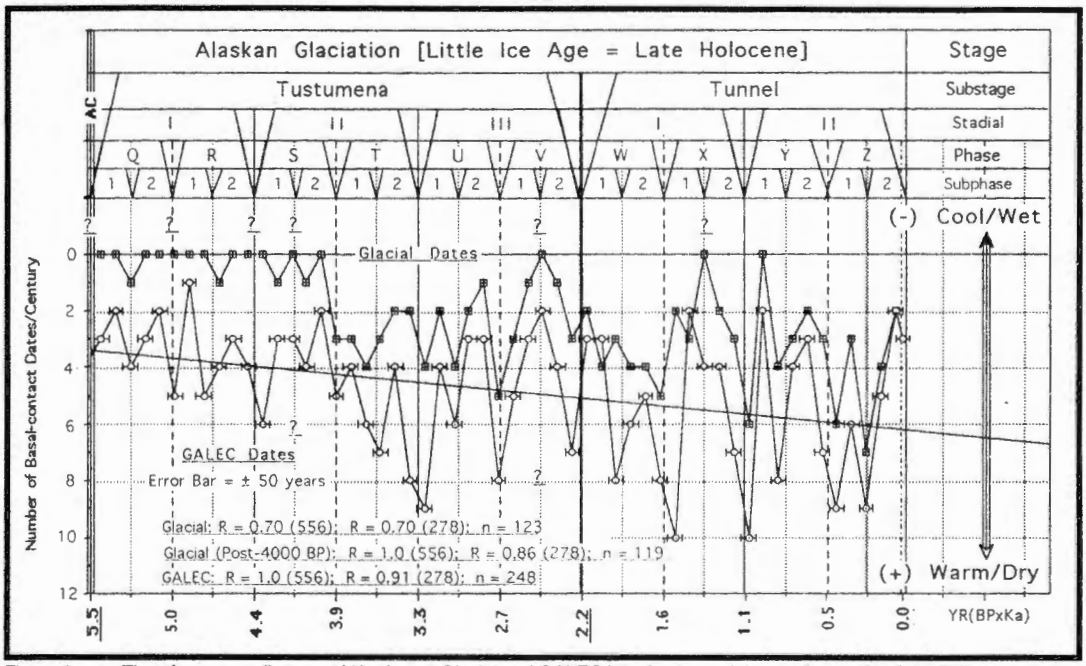

Figure 3 Time-frequency diagram of Northwest Glacial and GALEC basal-contact dates on timescale of the 556-year Phase Cycle and its 2/1 (278-year) Subphase Resonance. Basal-contact dates selected from the radiocarbon literature, mainly from Radiocarbon 1-15, for Oregon, Washington, British Columbia, Alaska, Yukon Territory, and Alberta (Karlstrom 1975). Glacial dates are those under Glacial till and outwash. GALEC dates are those under Glacial deposits plus those under Alluvial, Lacustrine, Eolean, and Colluvial deposits. Note that the expanded statistical database amplifies the cluster pattern shown by the glacial record and extends it back to 5500 years BP. This suggests generally parallel depositional histories in differing depositional environments according to the following paleoclimatic equation: Cool/Wet climate = glacial deposition contemporaneous with valley-bottom aggradation (providing a ready sediment supply for wind transportation and loess/dune deposition), with rising lakes and lacustrine deposition, and with increased colluviation resulting from water-saturated slope materials under accelerated freeze and thaw activity. Conversely, basal contacts as marked by soil, diastem, and associated vegetation = generally nondepositional environments with lower water table, drainage entrenchment (gullying), and bottom-land soil formation during preceding Warmer/Drier intervals. For similar statistical correlation of Southwest Alluvial, Eolean, and Colluvial chronostratigraphy, see Karlstrom (1988).

Figure 4 is a summary of time-frequency analyses of radiocarbon dates from western North America. The figure includes the time-frequency diagrams of Figures 1-3, along with time-frequency diagrams of selected basal-contact (Point Boundary) dates from the Midwest and Southwest. The expanded database from an extended region and its strong correlation with smaller datasets, including sets independently selected by other researchers, strongly suggests that the data-selection criteria are objective and valid. The general replication of cluster patterns essentially requires that most of the selected basal-contact dates fall in the 100-year intervals designated by their mean conventional radiocarbon ages. These statistical correlations with the Phase and Subphase Cycles are further replicated by other types of high-resolution proxy records as dated historically, by tree-rings, as well as by radiocarbon (examples are

provided in Figures 6, 7, 17, 18, 19, and 20). Note that because of dating uncertainties, radiocarbon analysis is not taken below 100-year class intervals, which in effect filters out all cycles less than 200-years in duration. Analysis of shorter cycles therefore requires the use of more precisely dated records such as may be provided by tree rings, varves, and historical accounts (for examples see Figures 5, 6, 7, 17, and 18). The North American Stratigraphic Code (NASC) in 1983 formalized the use of dated basal contacts in chronostratigraphic analyses by defining them as Point Boundaries.

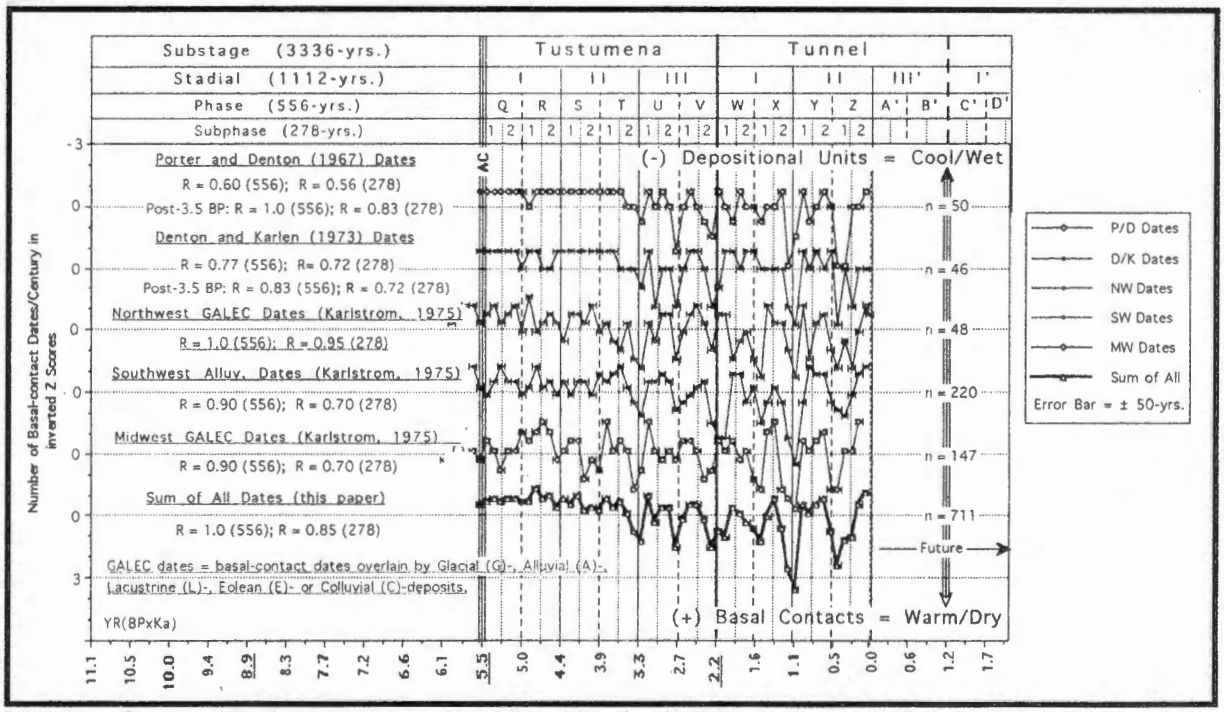

Figure 4 Summary of time-frequency analyses of basal-contact dates from North America plotted per century on timescale of the 556-year Phase Cycle and its 2/1 (278-year) resonance. Data selected mainly from Radiocarbon 1-15 according to the following criteria. Dates on wood or organic carbon associated with buried soils and diastems as described and accepted as valid by the contributing researchers. Many of the published dates are excluded because of too vague stratigraphic description or because of dating on materials (carbonates, bone, and humic components) more likely to be contaminated by older or younger carbon. Finally, no dates were included with unusually large sigmas of counting error. Beyond strengthening the statistical correlation between depositional histories and the Tidal-Resonance Model throughout much of western North America, the replication of cluster patterns essentially requires that most of the selected dates fall in the 100-year intervals designated by their mean conventional radiocarbon ages. The North American Stratigraphic Code (NASC 1983) formalized the use of basal-contact dates in chronostratigraphic analyses by defining them as Point Boundaries.

Figures 5 and 6
Volcanism, Aerosols, Climate, and Tidal Resonances

At high frequencies, volcanism correlates positively with aerosols and with high-frequency tidal resonances but negatively with transitory cooler temperatures. At lower frequencies, however, increased volcanism evidently correlates with generally warmer/drier climate on turning points of the Phase and Subphase Cycles. These correlations strongly suggest that increased tidal stresses on the lithosphere can trigger volcanic process close to endogenetic thresholds as well as steer atmospheric processes toward milder climates.

Figure 5 is a time-frequency diagram of historically recorded major volcanic eruptions, which positively correlates with the Aerosol record as well as with high-frequency tidal resonances, but which negatively correlates with the global temperature record. This weak negative correlation is compatible with other evidence suggesting transitory cooling during, and a few years following, major volcanic eruptions.

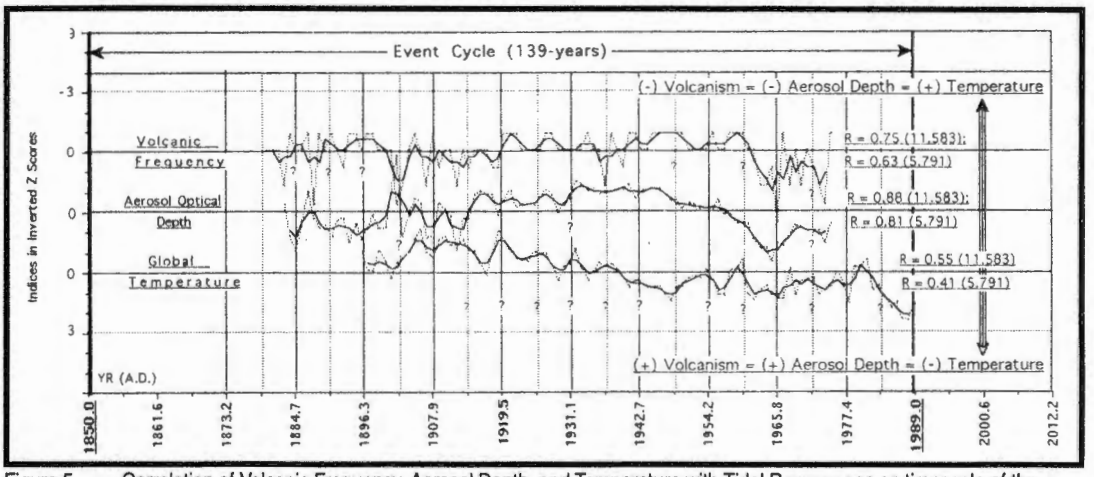

Figure 5 Correlation of Volcanic Frequency, Aerosol Depth, and Temperature with Tidal Resonances on timescale of the 11.583-year Cycle and its 2/1 (5.791-year) resonance. Temperature indices are from James and Wigley (1990); volcanic frequency and werosol depth indices are from Bryson and Goodman (1980). Smoothing is by 3-year running means. Note the weak to strong tendencies of the volcanic frequency and aerosol depth records to phase with tidal resonances, whereas the temperature record shows a tendency for cooler temperatures during volcanic intervals. This negative correlation, although weak, appears compatible with other evidence for transitory cooling by ejecta and aerosol loading of the atmosphere during and 1 or 2 years following major volcanic eruptions.

Figure 6, consisting of time-frequency diagrams of radiocarbon-dated volcanic deposits (lava and pyroclastic), shows a strong tendency to cluster during the Warm/Dry epicycles of the Phase and Subphase cycles. Compare with Figures 1-4 and 17-20. The statistical correlation with turning points of tidal resonances strongly suggests that increased tidal stress acts as a triggering mechanism affecting timing of volcanic events nearing endogenetic eruptive thresholds. However, because of the statistical nature of the correlation and the presumed mechanism of triggering variable endogenetic conditions, predictions of the timing and magnitude of specific volcanic events by changing tidal forces remains uncertain. The same uncertainty applies equally to tidal-stress predictions of individual earthquakes, but, as with the common practice of probability weather predictions, such predictions may prove useful in broadly estimating intervals of increased or decreased probability of occurrence in a given area.

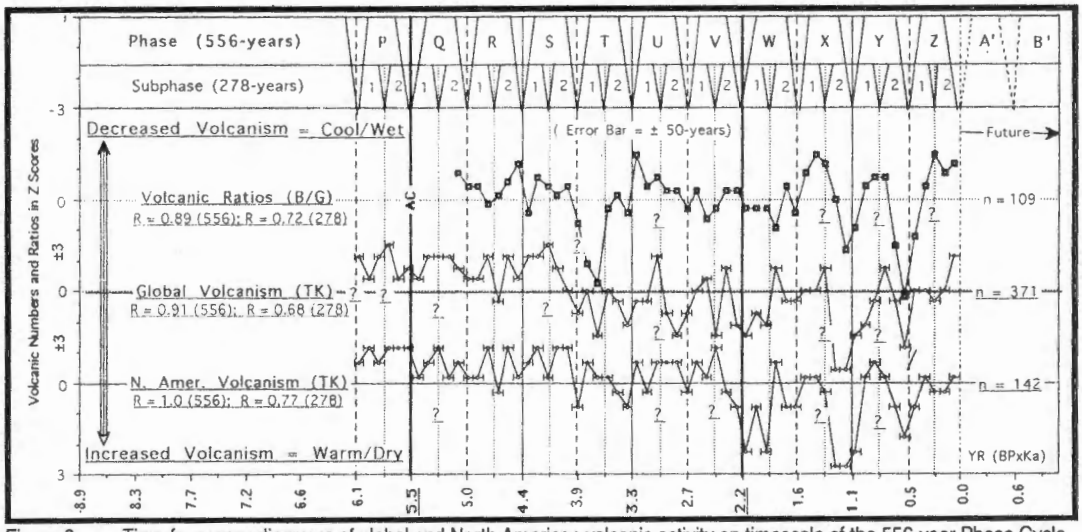

Figure 6 Time-frequency diagrams of global and North American volcanic activity on timescale of the 556-year Phase Cycle and its 2/1 (278-year) resonance. Volcanic ratio indices are from Bryson and Goodman (1980); number indices are from Karlstrom (1975). One-hundred-year class intervals centered in centuries act as low-pass filter restricting analyses to cycles with wavelengths of more than 200 years. Note strong tendency for clustering during the warm/dry epicycles of the Phase Cycle and the lesser, but still positive, tendencies during those of the Subphase Cycle. The similarity of results from independently selected datasets strongly suggests that tidal resonances play a significant role in triggering volcanic activity. Further, the positive correlation suggesting increased volcanism during warm/dry epicycles minimizes the importance of transitory cooling (and local warming) of the atmosphere by volcanic ejecta as a causal factor in these longer-term climatic changes (contrast with the higher frequency correlations in Figure 5). To predict local volcanic events solely by tidal intensity, however, is highly uncertain because of the statistical nature of the correlation and because of the presumed triggering mechanism that requires endogenetic threshold conditions that can vary appreciably among volcanic centers. The figure combines the datasets shown in Figures 27 and 28 of Karlstrom (1997).

Figure 7
Isotope-Temperature and Precipitation Record of Northern China

Isotope temperature and precipitation since AD1500 inferred by Ku *et al* (1998) from 18/O indices of a stalagmite in Shihua Cave of northern China. Dated isotope indices were kindly supplied by Ku (written communication 1997). The record is consistent in climatic sign with instrumental records and with the historically recorded flood- and frost-frequency records of China (indices from Bradley 1982). Particularly impressive is the correlation of the ~35-year precipitation cycle with a high frequency component (34.75-years: 4/1 of the 139-year Event Cycle) of the Tidal Resonance Model. This cycle is evidently also expressed in the Chinese decadal record of historical frosts (Karlstrom 1997) and is referred to as the Bruckner Cycle because of Bruchner's earlier identification of a similar-length cycle in lake-level and precipitation records (de Boer 1967)

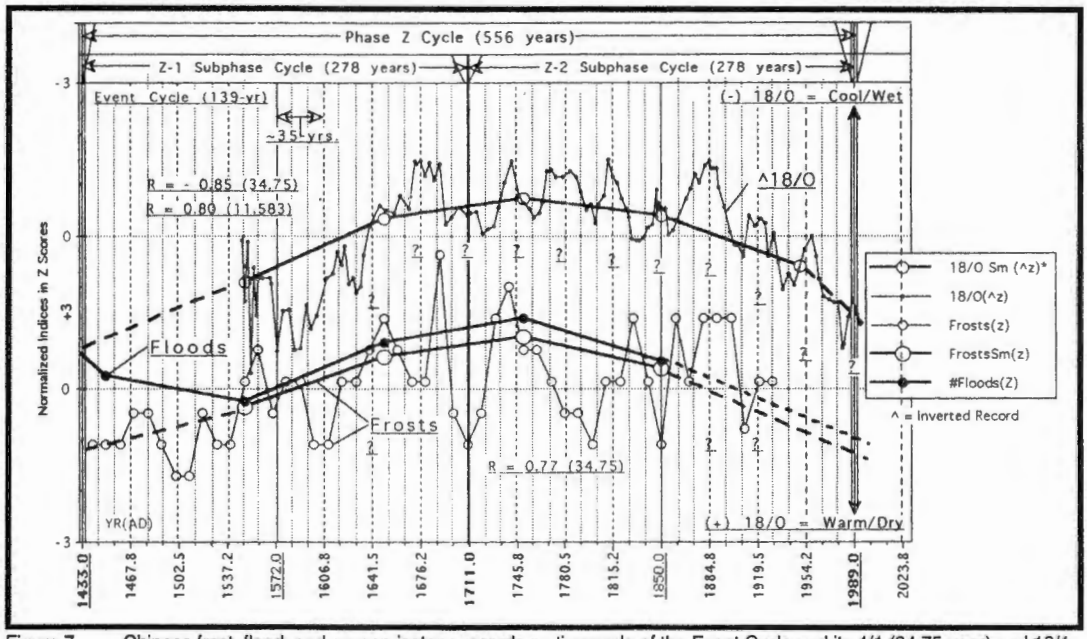

Figure 7 Chinese frost, flood, and oxygen-isotope records on timescale of the Event Cycle and its 4/1 (34.75-year) and 12/1 (11.583-year) resonances. Isotope indices of lamination-counting and radiocarbon-dated stalagmite of Shihua Cave, Beijing, China from Ku et al (1998). Historically dated Chinese flood and frost indices are from Bradley (1982. Ku *et al* (1998) interpret the primary trends of their isotope record as primarily reflecting temperature, the secondary decadal trends as primarily reflecting precipitation, and with decreasing temperature and increasing precipitation correlating with decreasing isotope values. Note the climatic compatibility of this isotope record with that of the flood (precipitation) and frost (temperature) records and with harmonic elements of the Tidal Resonance Model. Particularly note the strong tendency for in-phase relationships of the frost and isotope records with the 4/1 (34.75-year) resonance, suggesting that an increase of frosts corresponds to a decrease in $\delta^{18}O$ caused by precipitation increase and temperature decrease during intervals of minimal tidal forces. Intensified monsoonal precipitation could cause the long-term decline of temperature. the ~35-year cycle is defined as the Bruckner Cycle because at the beginning of the century, Bruckner defined a similar length cycle from precipitation and lake-level records. That this cycle is real and not an artifact of analyses is supported by the presented proxy records and by its phasing with a subharmonic element of the Tidal Resonance Model.

Figures 8-12
Paleoclimatic Records from Middle to Lower Latitudes in the Northern Hemisphere and Correlation with Similar Latitude Solar Insolation Trends

Primary trends of numerous paleoclimatic records in North America strikingly parallel, with appropriate but variable lags, the local solar insolation trends that largely reflect precessional controls between 35° and 45° north latitudes. These correlations strongly suggest modulation of terrestrial climate directly by local solar insolation rather than by in-phase responses to Northern Hemisphere continental glaciations modulated by higher northern latitude summer solar-insolation trends.

Figure 8 shows multicomponent paleoclimatic record from Owens Lake Basin, California. Component indices dated between 55,000- and 10,000-years BP from Benson *et al* (1996). Main trends of record parallel those of the local (N35° latitude) solar insolation curve and with higher lakes and glacial advances correlating with insolation minima. As reconstructed in the figure, high lakes and glaciations occurred during

intervals of both cooler and wetter climate. This differs from the interpretation of Benson *et al* (1996) of glaciations and pluvials as occurring during cooler and drier climates. In this they agree with Gallaway's (1970) and Brackenridge's (1978) interpretation of Pleistocene climates, but not with those of Wells (1979), Street and Grove (1979), Woolfenden (1997: see Fig. 11), Menking (1977), and others who also consider that Southwest pluvials and glaciations occurred concurrently under generally wetter and cooler climatic conditions.

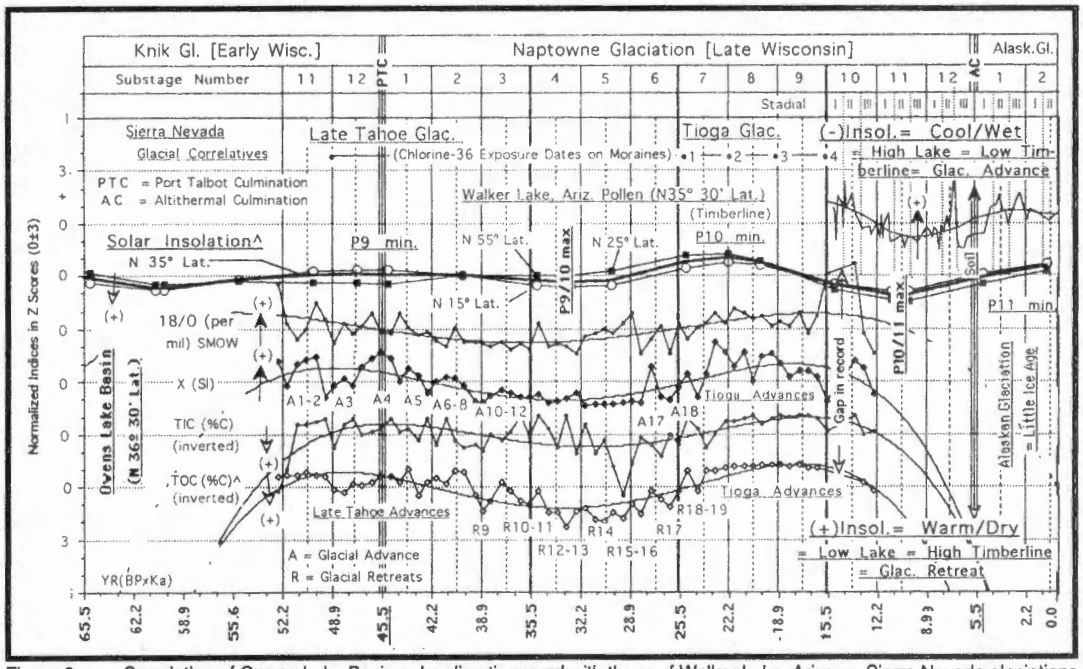

Figure 8 Correlation of Owens Lake Basin paleoclimatic record with those of Walker Lake, Arizona, Sierra Nevada glaciations, and with comparable latitude Precessional Solar Insolation on timescale of the 3336-year Substage Cycle and its 2/1 (1668-year) and 3/1 (1112-year) resonances. Radiocarbon-dated Owens Lake Basin isotope (18/O), magnetic intensity (X), total inorganic carbon (TIC), and total organic carbon (TOC) indices of Benson *et al* (1996) replotted at 613-year intervals. Radiocarbon-calibrated, chlorine-36 exposure ages of Sierra Nevada moraines are from Phillips *et al* (1996). Radiocarbon-dated Walker Lake pollen indices are from Hevly (1988 in Karlstrom 1997). Note that the primary trends of these records strikingly parallel, and appropriately lag, the mid-latitude Precessional Insolation trends (Milankovitch 1941), strongly suggesting cause-and-effect relationships. As reconstructed, (–) Solar Insolation = Wet/Cool climate = Glacial Advance = High Lake = Low Timberline = (+) Magnetic Intensity and 18/O, but (–) TOC and TIC resulting from organic concentration during low closed drainage phases, and organic dilution by mineral sedimentation (increasing magnetic intensity) and overflow during higher outlet phases. These paleoclimatic inferences differ from those of Benson *et al* (1996), who argue for lower lakes during cooler and drier periods of glacial advance but are similar to those of Woolfenden (1997) and Menking *et al* (1997), who provide the most recent interpretations of Owens Lake core data. Numbering of Precessional Minima from Figure 25.

Figure 9 shows correlation of the Owens Lake record with other Southwest pluvial records. The primary trends of the Owens Lake record strikingly parallel those of Street and Grove's (1979) time-frequency diagram of dated regional lake phases and of Currey and Oviat's (1988) detailed reconstruction of the Lake Bonneville record. This parallelism of lake-level oscillations in large and small lake basins and general phasing with local insolation trends is striking and suggests modulation by summer solar insolation as well as common response to changing regional ground water levels. Street and Grove's and Currey and Oviat's pluvial records also show weak to strong tendencies of secondary oscillations to phase with subharmonic elements of the Tidal Resonance

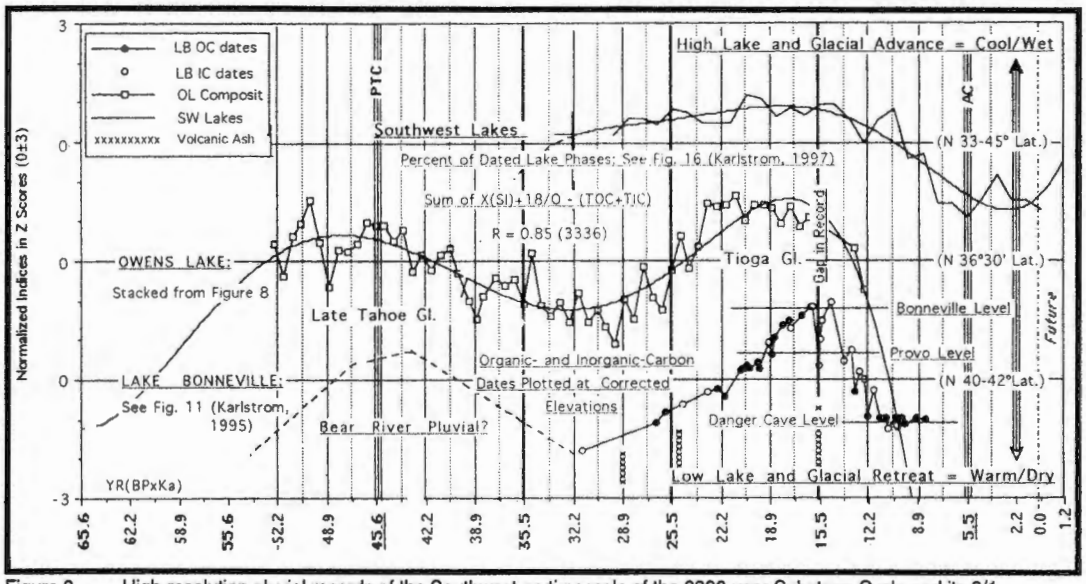

Figure 9 High-resolution pluvial records of the Southwest on timescale of the 3336-year Substage Cycle and its 2/1 (1668-year) resonance. Southwest lake-phase indices are from Street and Grove (1979); Owens Lake pluvial and glacial indices from Benson *et al* (1996) and Phillips *et al* (1996); and Lake Bonneville indices are from Currey and Oviat (1985). The Owens Lake glaciopluvial record as reconstructed strikingly parallels the other two pluvial records and positions the 16,000- to 13,000-year gap concurrent with both the abrupt lake lowering about 15,500 years BP and the following abrupt rise above the Red Pass threshold about 14,000 years BP in the Bonneville record. Correlation with the Owens Lake record indicates that the undated Bear River Pluvial may have been contemporaneous with the Lake Tahoe glaciopluvial and thus date about 45,000 years BP.

Model as discussed in Karlstrom (1997). As shown in Figure 14 below, the stacked Owens Lake record also suggests similar higher frequency tendencies.

Figure 10 shows correlation of Southwest pluvial records of Figure 9 with other high resolution North America paleoclimatic records located between latitudes 35° and 45°. The added records (glaciations inferred from Ionium/Uranium-dated hot springs deposits in Yellowstone National Park; precipitation from radiocarbon-dated Midwest pollen record; isotope-temperature from Ionium/Uranium-dated cave carbonate of Iowa; and changing timberlines from radiocarbon-dated pollen records of Idaho and Arizona) also appear to be similarly modulated by the local insolation trends.

Figure 11 shows the bioclimatic (pollen) record of Owens Lake, which provides paleoclimatic evidence back to 155,000 years BP. Dating by radiocarbon, tephrochronology and magnetic reversals (Biskof *et al* 1997). Dated pollen indices were kindly provided by Wallace Woolfenden (written communication 1997). As interpreted by Woolfenden (1977) and as reconstructed in the figure, the pollen data apparently record lowering timberline and rising lake levels during cooler and wetter climatic conditions. Although there is a strong tendency for the record to phase with the local solar insolation curve, this tendency appears in part to be obscured by a stronger tendency to phase with elements of the Tidal-Resonance Model.

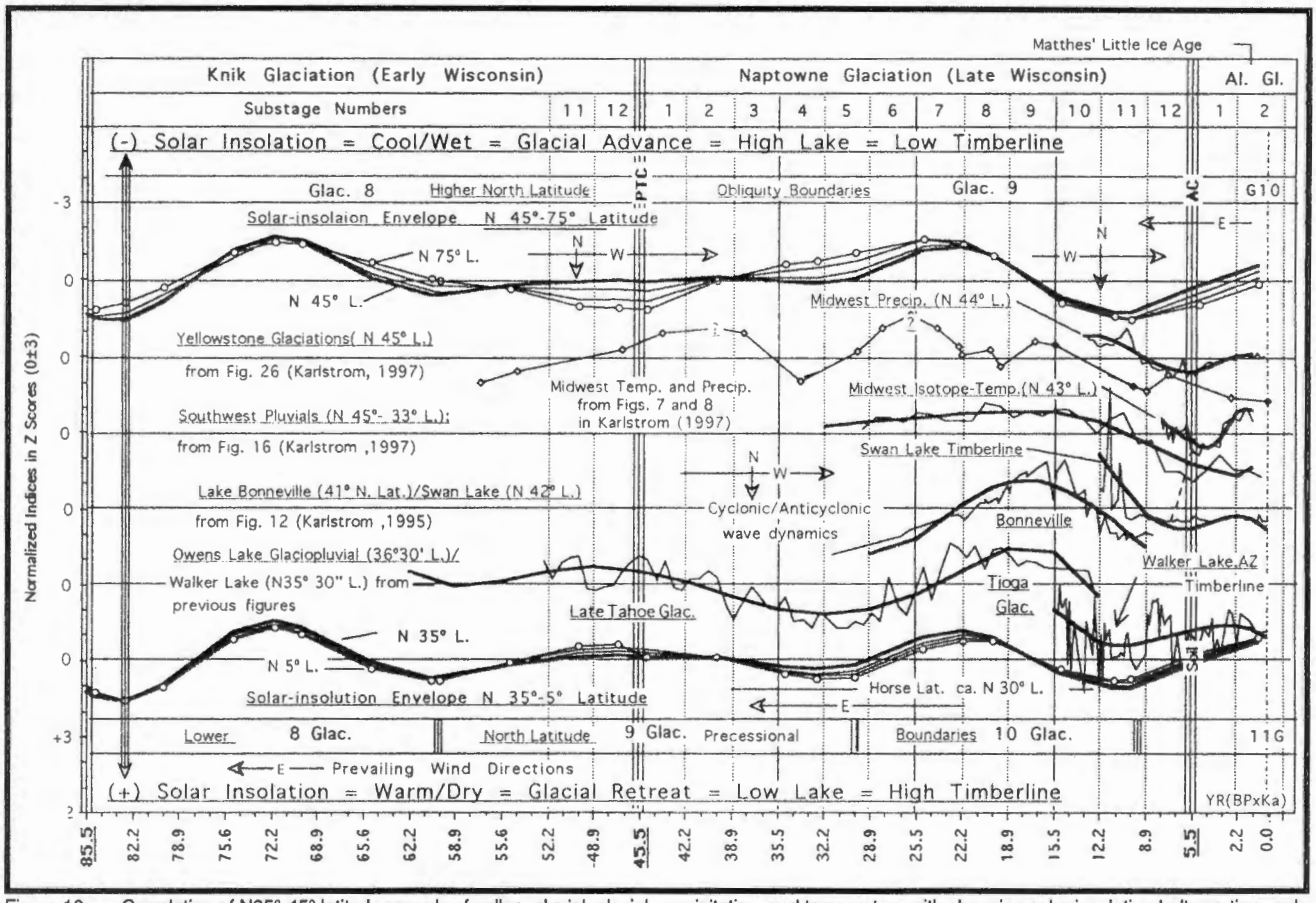

Figure 10 Correlation of N35°-45° latitude records of pollen, pluvial, glacial, precipitation, and temperature with changing solar insolation belts on timescale of the 3336-year Substage Cycle. Paleoclimatic indices are from indicated sources; Solar Insolation indices are from Milankovitch (1941). Note the progressive shift in timing of Insolation maxima from higher latitude Obliquity troughs to the shorter wavelength lower latitude Precessional troughs plus the strong tendency for corresponding shifts in paleoclimatic trends depending on latitude.

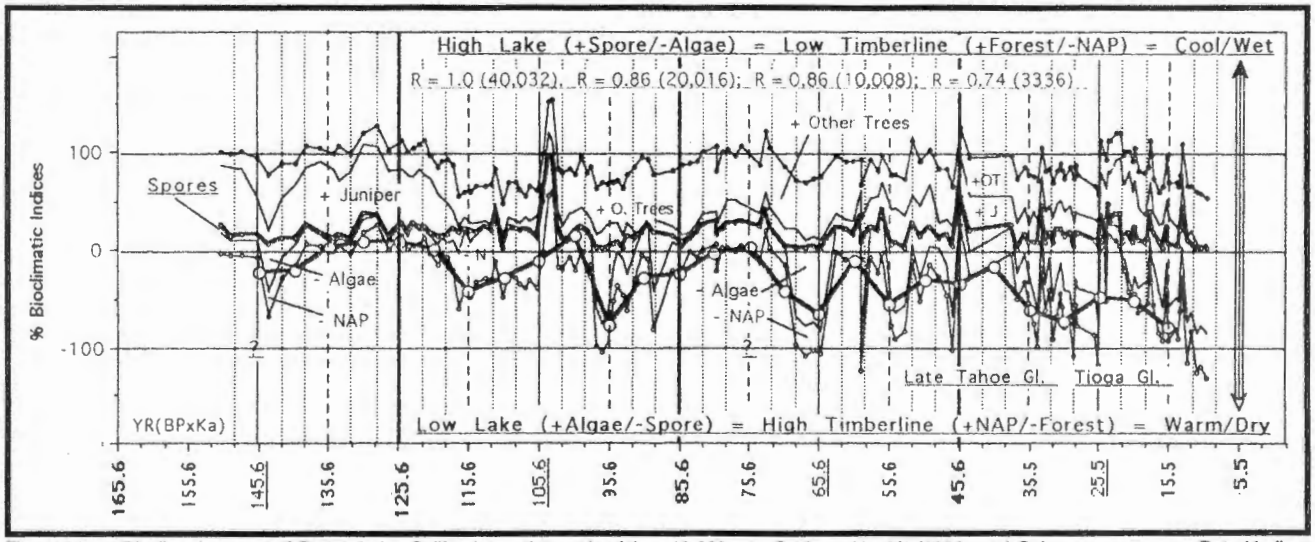

Figure 11 Bioclimatic record of Owens Lake, California, on timescale of the ~10,000-year Cycle and its 3/1 (3336-year) Substage resonance. Dated indices are from Woolfenden (1997 and written communication 1997), who notes the general correlation between higher lake levels and glacial advances during climatic changes from warm/dry to cooler and wetter conditions. As reconstructed above, higher lake levels coincide with lower timberlines, glacial advances and with generally cooler and wetter climates. Note also the weak to strong tendencies for the primary and secondary trends to phase with the timing of harmonic elements of the Tidal Resonance Model, along with some tendency for troughs to deepen concurrent with precessional maxima about 30,000, 65,000, 85,000, 105,000, 125,000?, and 145,000 years BP (see Figure 25).

Figure 12 is a bioclimatic record of Lake Biwa, Japan, and correlation with similar-latitude (N35° latitude) solar insolation. Numerical indices of Biogenic Silica Content (BSC) and Eolian Quartz Content (EQC) from Xiao *et al* (1997a, b); their dating by regional tephrochronology. The authors correlate the Lake Biwa record with the "standard" marine record of Martinson *et al* (1987) as this is fine-tuned to the N60° latitude solar insolation curve (see Figures 23 and 25). With an apparent lag of about 6000 years, the pluvial record better parallels the N35° latitude solar insolation curve. This is again consistent with the concept of terrestrial climate modulation by local (but latitudinally changing) solar insolation, instead of the conventional concept of synchronous global trends dominated by Northern Hemisphere continental glaciations modulated by higher northern latitude summer insolation.

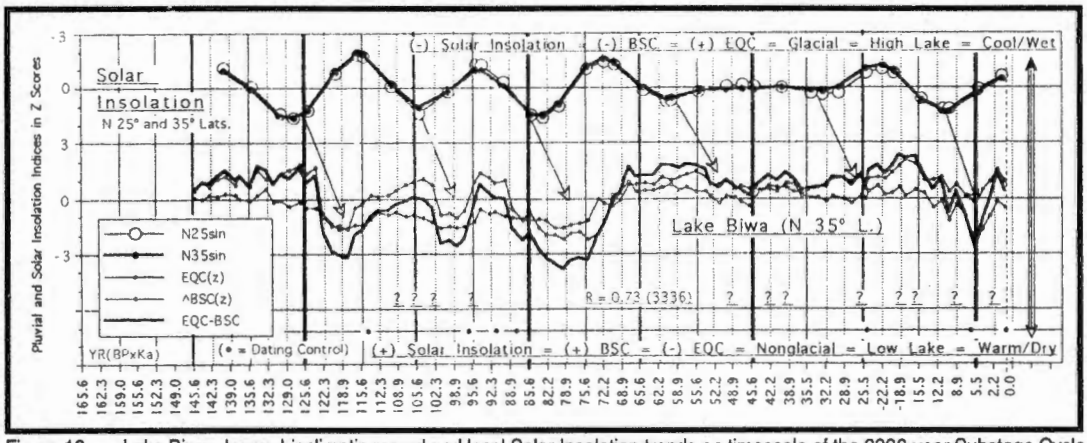

Figure 12 Lake Biwa, Japan, bioclimatic record and local Solar Insolation trends on timescale of the 3336-year Substage Cycle. Lake Biwa indices of Biogenic Silica Content (BSC) are from appendix in Xiao *et al* (1997a), of Eolean Quartz Content (EQC) from Table 2 in Xio *et al* (1997b); dating by correlation to regional volcanic ash series. Note: (1) the lagged parallelism of the primary bioclimatic trends with those of the local, primarily precessional, Solar Insolation; and (2) the weak, but evidently significant, tendency of the secondary bioclimatic trends to phase with turning points of the 3336-year Substage Cycle. Xiao *et al* correlate the Biwa record with Martinson's "standard" marine chronology (see Figure 23). As shown above, a somewhat better correlation is apparent with the local insolation record. Essentially similar results obtained with their Biogenic Silicate Flux (BSF) and Eolean Quartz Flux (EQF) indices.

Figure 13
Paleoclimatic Record from Upper Northern Hemisphere Latitude and Correlation with Similar Latitude Solar Insolation Trends

The Greenland GISP2 ice-core record (N70° latitude) of isotope temperature (18/O) and methane is shown as dated and correlated by Brooks *et al* (1997) with the N60° latitude solar insolation trends. Not surprising because of common correlations, their record strikingly parallels my ~N60° latitude glacial record of Cook Inlet, Alaska. (Karlstrom 1961, 1964). Both increased isotope temperature and increased methane content correlate with solar insolation maxima, strongly suggesting the importance of natural (nonanthropogenic) climatic processes in determining varying amounts of greenhouse gases in the atmosphere. Similar correlations between solar insolation, glaciation, temperature, and

greenhouse gas CO2 is recorded in the Antarctic Vostok ice core (see Figure 25). The historical increase in atmospheric CO2 and temperature, since it occurs during a natural cyclical trend toward warming (see Figure 17 for one example), can in large part result from natural processes instead of solely from pollution of the atmosphere since the beginning of the Industrial Revolution.

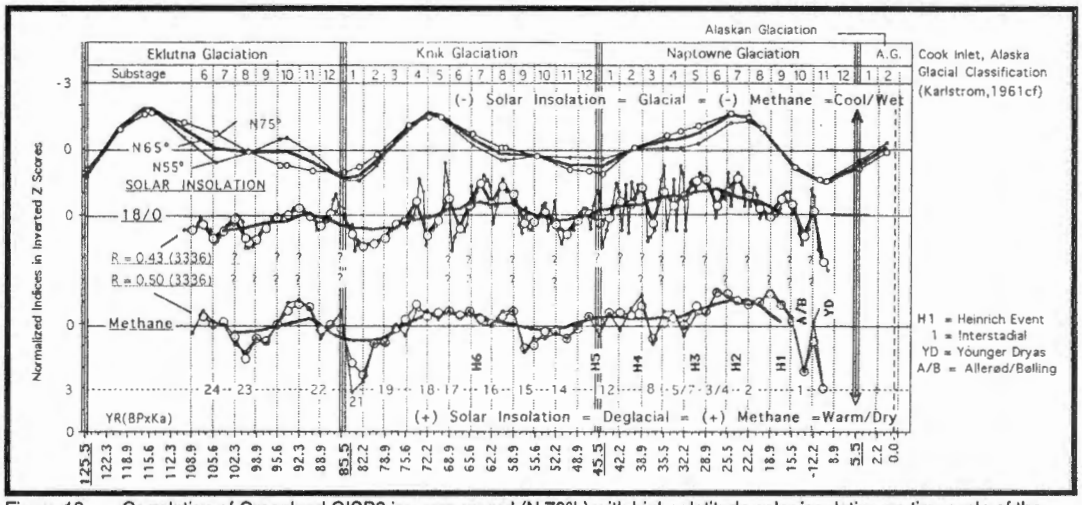

Figure 13 Correlation of Greenland GISP2 ice-core record (N 70°L) with higher latitude solar insolation on timescale of the 3336-year Substage Cycle and its x12 (40,032-year) superharmonic. Isotope and methane indices and dating of marine Heinrich (cold) events and terrestrial Bølling/Allerød (warm) and Younger Dryas (cold) events by correlation with the CISP2 timescale from Brooks *et al* (1996). Their ice-core indices are replotted at centered 500-year intervals filtering out secondary cycles of less than 1000 years and further smoothed to emphasize longer-term trends. Brooks *et al* correlate their GISP2 record with the N60° latitude solar insolation curve, which is dominated by the Obliquity Cycle as slightly modified by precessional trends that predominate at lower latitudes (see Figure 25). Note: (1) the striking parallelism with the comparable latitude Cook Inlet glacial record; (2) the generally positive correlation between glacial climate and the "greenhouse" methane gas, which emphasizes the important role of past climatic (nonanthropogenic) changes in governing the gaseous content of the atmosphere (also see Karlstrom 1995); and (3) the lack of correlation between GISP2 secondary oscillations and the Substage Cycle, which may result largely from remaining uncertainties in the GISP2 timescale. The degree of age discrepancy resulting from correlations to the radiocarbon timescale or to the GISP2 timescale is analyzed in Figure 14.

Figure 14
Marine Heinrich and Terrestrial Dryas Events and the Lake Owens and GISP2 Chronologies

In considering correlation with marine Heinrich events dated by the Greenland GISP2 ice-core record, Benson *et al* (1996) note anomalous phasing between secondary oscillations in different components of their Lake Owens record, as well as unresolved uncertainties in ice-core dating. They conclude, therefore, that though both paleoclimate records apparently demonstrate a series of real secondary cold/warm oscillations, specific correlations of Owens Lake events with Heinrich events are currently untenable. Brooks *et al* (1996), on the other hand, through pattern matching with the GISP2 record provide dates for the secondary Heinrich and Dryas events that differ dramatically (2000 to 8000 years older) from their radiocarbon ages. Two main uncertainties apply to correlations with the GISP2 timescale:

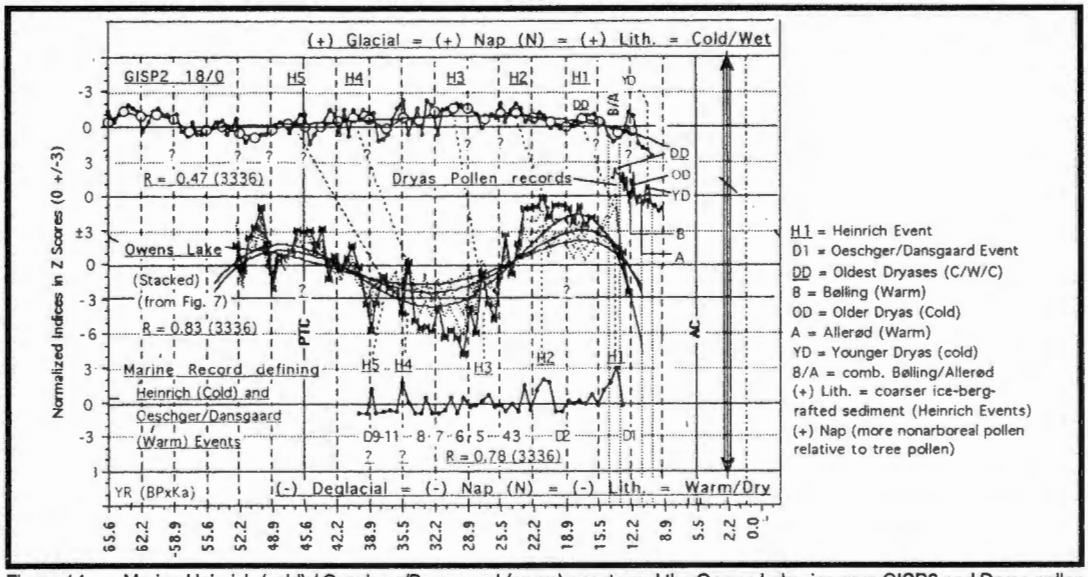

Figure 14 Marine Heinrich (cold) / Oeschger/Dansgaard (warm) events and the Owens Lake, ice core GISP2 and Dryas pollen records on timescale of the 3336-year Substage Cycle and its 3/1 (1112-year) resonance. Owens Lake indices and Heinrich/Oeschger marine indices are from Benson *et al* (1996), replotted at 613-year intervals; GISP2 ice core indices are from Brooks *et al* (1996), replotted at 500-year intervals; and indices of two records of the classic Dryas pollen series from Switzerland and Denmark (see Figure 20). Note: (1) the parallelism between the two Dryas seauences; (2) the generally positive correlation of the radiocarbon-dated pollen, lake and marine records among themselves and in phasing with the Substage Cycle; and (3) the dramatic differences (2000-8000) years in dating of the Heinrich and Dryas events resulting from pattern matching to the GISP2 curve. Two main uncertainties are involved: (1) pattern matching, which is particularly uncertain between records with differing response functions, sample spacing, smoothing, primary trends, and distribution of distorting noise; and (2) unresolved discrepancies in timescales obtained from different ice cores.

- The use of pattern matching, which is particularly uncertain when applied to proxy records from different environments and with differing response functions, irregular sample spacing, different levels of smoothing, and variable noise/signal ratios; and
- The remaining discrepancies in timescales obtained from different ice-cores.

As shown in the figure, stacking of the component parts of the Owens Lake record provides a record of secondary oscillations, many of which phase with the Heinrich and Dryas events and with turning points of the 3336-year Substage Cycle. No such correlation with the secondary oscillations of the GISP2 record is evident. Stacking is a procedure that should cancel out chance trends and, thus, enhance the signal/noise ratio in multiple component records.

Figures 15 and 16
Paleoclimatic Record from Southern Hemisphere Latitude 55° and Correlation with Similar Latitude Solar Insolation Trends, the Precessional Elements of which are 180 Degrees Out of Phase with their Northern Hemisphere Counterparts

Figure 15 is a bioclimatic record of Harberton Bog, Tierra del Fuego between 14,000 years BP and the present, and correlation with the S60° latitude solar insolation curve. Dated indices kindly supplied by Markgraf (written communication 1997). The primary trends of the record parallel those of the local solar insolation but with an apparent lag of about 4000 years. The record is thus out of phase with records from counterpart Northern Hemisphere latitudes (also see Figures 24 and 25). On the other hand, the secondary oscillations of the record evidently phase strongly with both the Stadial and Phase Cycles or generally synchronous with Northern Hemisphere counterparts.

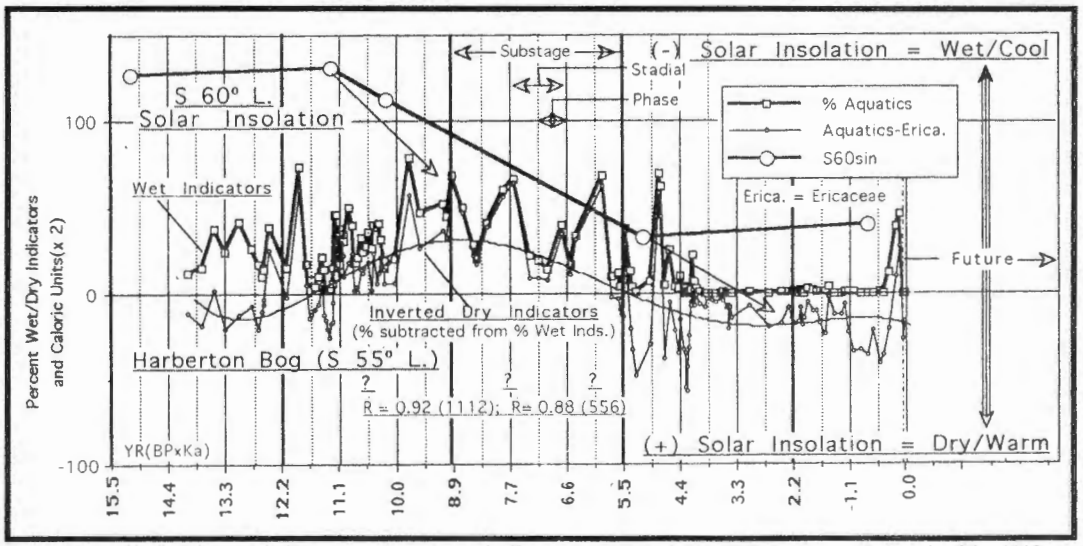

Figure 15 Bioclimatic record of Harberton Bog, Tierra del Fuego, and local solar insolation trends on timescale of the 1112-year Stadial Cycle and its 2/1 (556-year) resonance. Numerical indices of Harberton Bog provided by Markgraf (written communication 1997). Summer half-year solar insolation indices are from Melankovitch (1941). Note: (1) the broad parallelism and appropriate response lag of the primary moisture trends with the local solar insolation record, which at these and higher latitudes reflect more and more the Obliquity Cycle over that of the Precessional Cycle (see Figure 25); and (2) the strong tendency of the secondary moisture trends to phase with turning points of the 1112-year Stadial Cycle and its 2/1 (556-year) resonance. Figure 16 shows that the isotope-temperatures of the Harberton Bog sequency are negatively correlated with the moisture record or consistent with the paleoclimatic equation of cool/wet versus warm/dry.

Figure 16 shows the moisture and isotope-temperature record of Harberton Bog, Tierra del Fuego. Indices dated between 13,500 and 10,500 years BP from Markgraf and Kenny (1997), who note the general negative correlation between effective moisture and derived temperatures, or consistent with the paleoclimatic equation of cooler and wetter versus warmer and drier. The temperature record evidently phases strongly with the Stadial and Phase Cycles and less so, but still significantly, with the Subphase Cycle.

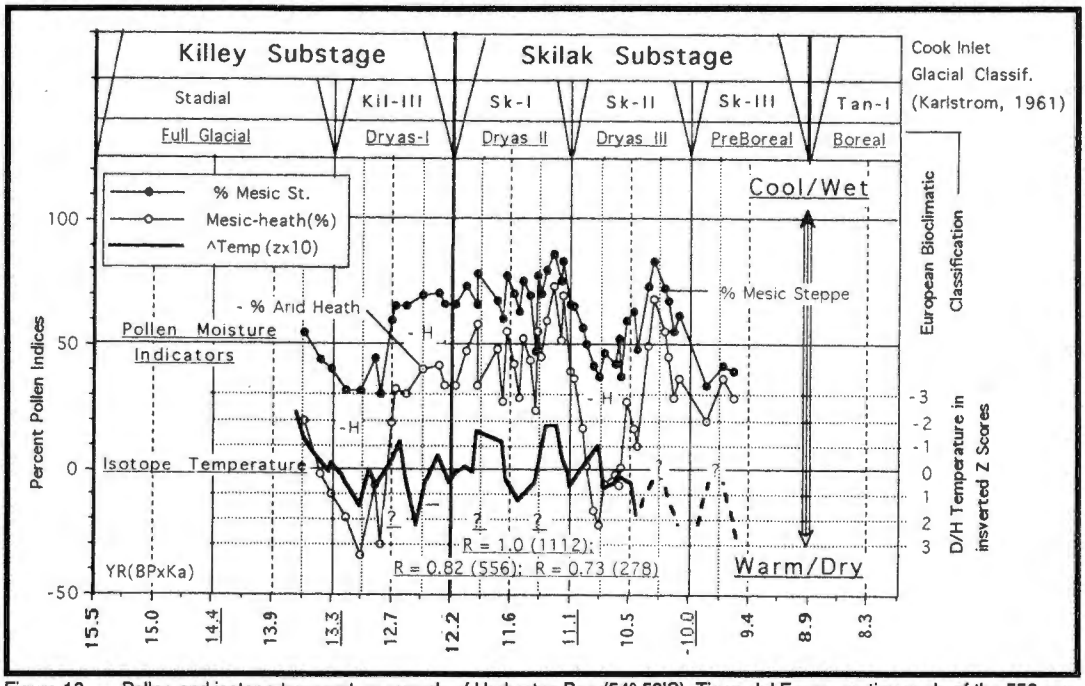

Figure 16 Pollen and isotope-temperature records of Harberton Bog (54° 53'S), Tierra del Fuego, on timescale of the 556-year Phase Cycle and its 2/1 (278-year) resonance. Radiocarbon-dated indices from Markgraf and Kenny (1997), who identify mesic steppe components as wetter indices and the negatively correlated heath as drier indicators Note the broad parallelism of these wet/dry indicators with the inverted sign of the isotope-temperature record. Also note the very strong tendency for the temperature record to phase with the 1112-year Stadial Cycle and the lesser but still significant tendencies with its 2/1 (556-year) and 4/1 (278-year) resonances.

Figures 17-25
Selected Paleoclimate Records Discussed in Previous Papers that Best Illustrate Elements of the Solar Insolation/Tidal Resonance Climate Model

These figures are included for convenient reference and comparison with the new records analyzed in this paper. Figure 17 shows North American Southwest tree rings, the 139-year Event Cycle, and phasing with the 278-year Subphase Cycle. Figure 18 shows the California marine record, collated Japanese tree rings, and the 278-year Subphase Cycle. Figure 19 shows the Alaska bioclimate, the 556-year Phase Cycle, and its 2/1 (278-year) resonance. Figure 20 shows European paleoclimatic records, the 1112-year Stadial Cycle, and its 2/1 (556-year) and 4/1 (278-year) resonances. Figure 21 presents the equatorial Pacific marine record and the 1112-year Stadial Cycle since 18,000 years BP. Figure 22 shows the Yukon Territory bioclimate, the 3336-year Substage Cycle, and its 3/1 (1112-year) resonance since 30,000 years BP. Figure 23 shows two "standard" glacial meltwater marine records fine-tuned to N60° latitude solar insolation. Figure 24 presents Northern and Southern Hemisphere glacial records and apparent correlation to hemispherically opposing solar-insolation trends. Figure 25 shows records illustrating latitudinal solar-insolation control on terrestrial climates.

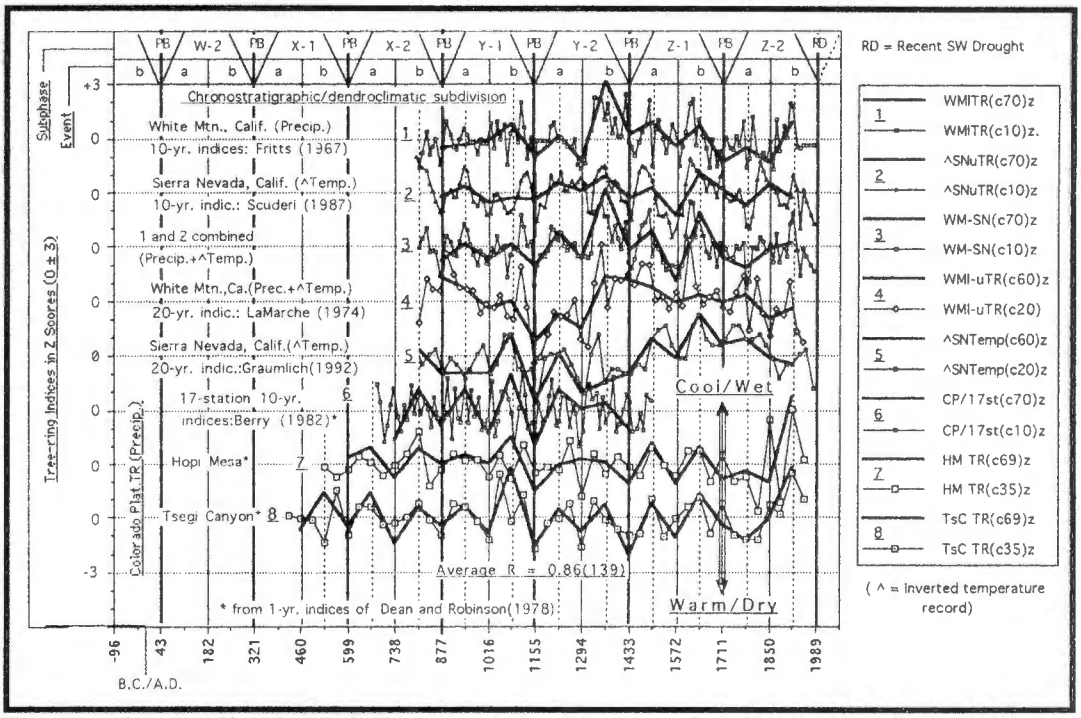

Figure 17 Summary evidence for a dendroclimatic cycle in phase with the 139-year Event Cycle. Half-cycle smoothing positioned on cycle turning points. Trend correlations, temperature as well as precipitation, range from 0.75 to >0.90, or within the upper range of tree-ring/climate calibrations. This suggests that the cycle is real, regionally robust, and related to changing atmospheric dynamics and circulation patterns. Similar half-cycle analyses of other records may define differing regional patterns and responses, advancing understanding of climatic/biologic process. Modified from Figure 10 in Karlstrom (1995). PB = Point Boundary (clustering of Southwest alluvial basal-contact dates) from Karlstrom (1988).

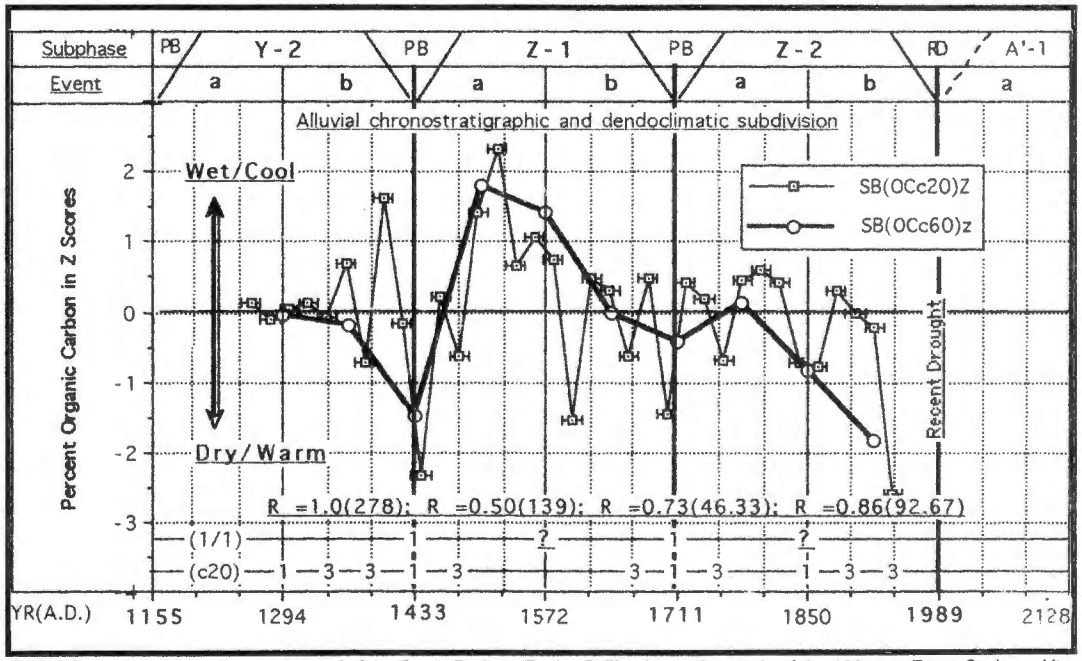

Figure 18 Varve-dated marine record of the Santa Barbara Basin, California, on timescale of the 139-year Event Cycle and its 3/1 (46.33-year) resonance. Indices from Pandolfi *et al* (1980) replotted at 20-year intervals. Original indices collated with a Japanese tree-ring record that reflects cycles of 273±20 years (Uranium) and 271±11 years (D/H). The Santa Barbara core record demonstrates a similar-length marine cycle that is in phase with the 278-year Subphase Cycle. These correlations suggest that more organic carbon was supplied during major Southwest wet (depositional) intervals than during major dry intervals. The record also shows a strong tendency to phase with the ~46-year resonance and a stronger tendency with its double (93-year) Gleisberg Cycle. Analysis by half-cycle smoothing positioned on turning points of the 139-year Event Cycle. From Figures 12 and 15 in Karlstrom (1995).

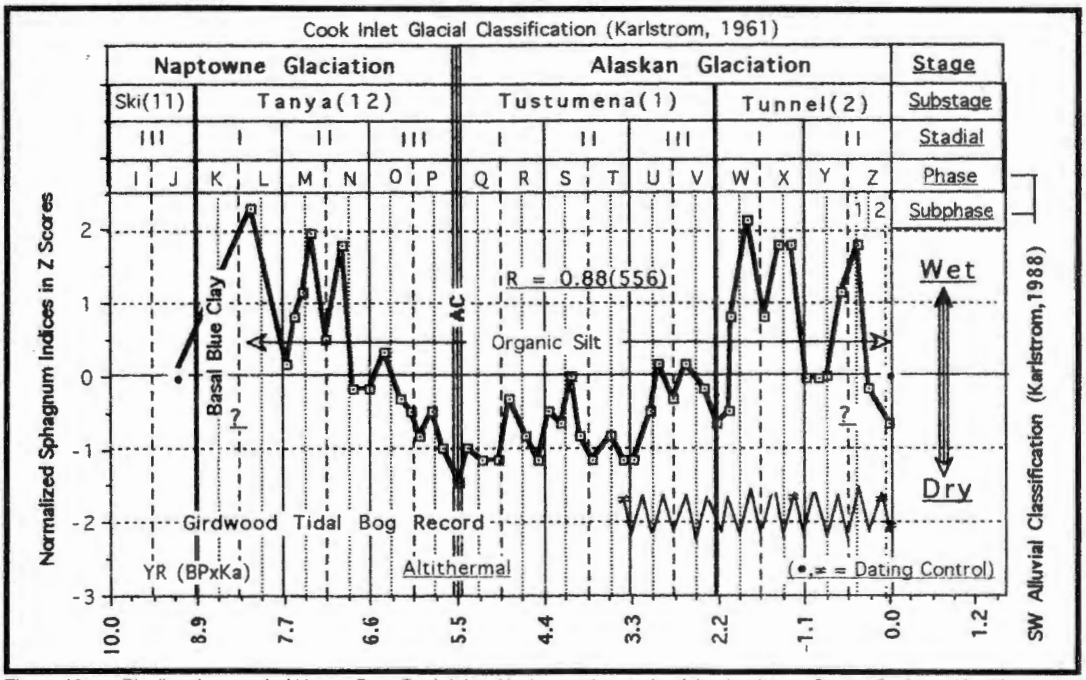

Figure 19 Bioclimatic record of Homer Bog, Cook Inlet, Alaska, on timescale of the 1112-year Stadial Cycle and its 2/1 (556-year) Phase Resonance and 4/1 (278-year) Subphase Resonance. Pollen indices from Heuser (1965) time-calibrated by basal date listed in Karlstrom (1964). The higher frequency Girdwood Bog record is schematically plotted as interpreted climatically in Karlstrom (1961). Because of lesser sensitivity and wider sampling intervals, Homer Bog shows the strongest tendency to oscilate in phase with the 556-year Phase Cycle and positions the driest Postglacial interval contemporaneous with that in the Southwest Altithermal (AC) and in the late Atlantic of northern Europe (see Figure 20). Modified from Figure 18 in Karlstrom (1995).

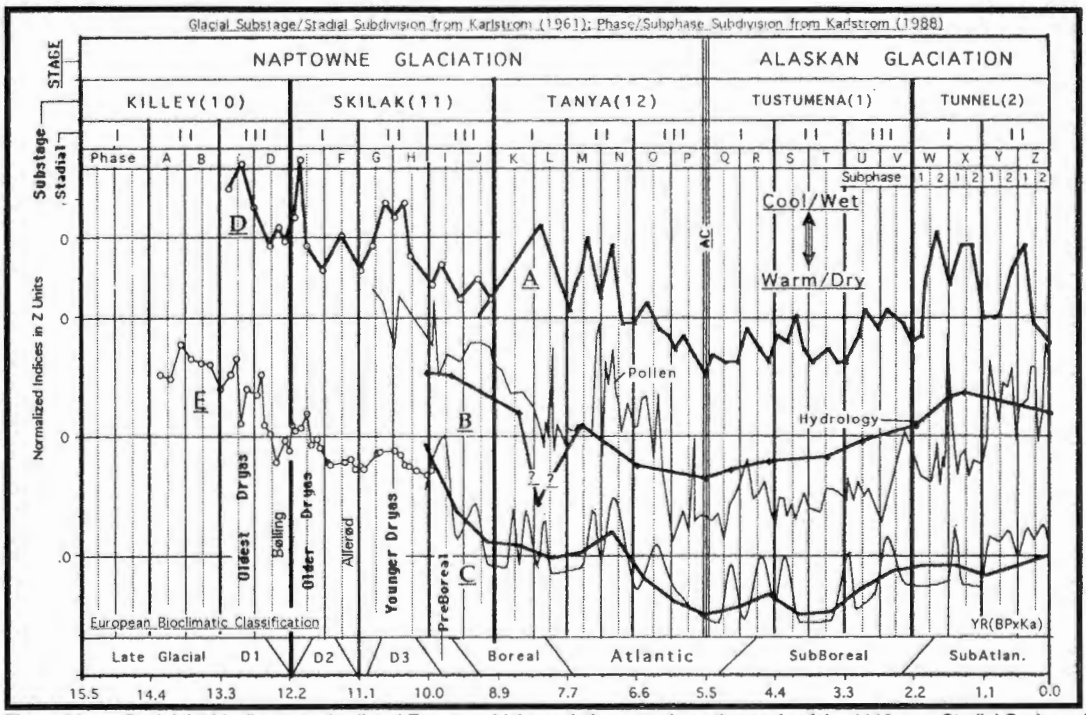

Figure 20 Cook Inlet bioclimate and collated European high-resolution records on timescale of the 1112-year Stadial Cycle and its 2/1 (556-year) and 4/1 (278-year) resonances. (A) Cook Inlet Homer Bog. (B) Agarode Bog/hydrology of Sweden (Nilsson 1964). (C) Alps timberline fluctuations (Beug 1982). (D) Danish Bølling Bog (in Karlstrom 1961). (E) Swiss Wachseldorn Bog (Oeschger et al 1980), which though sampled at shorter intervals replicates with some fidelity the classic Late Glacial Dryas sequence of Denmark in (D). Data from Figures 2 and 3 in Karlstrom (1996).

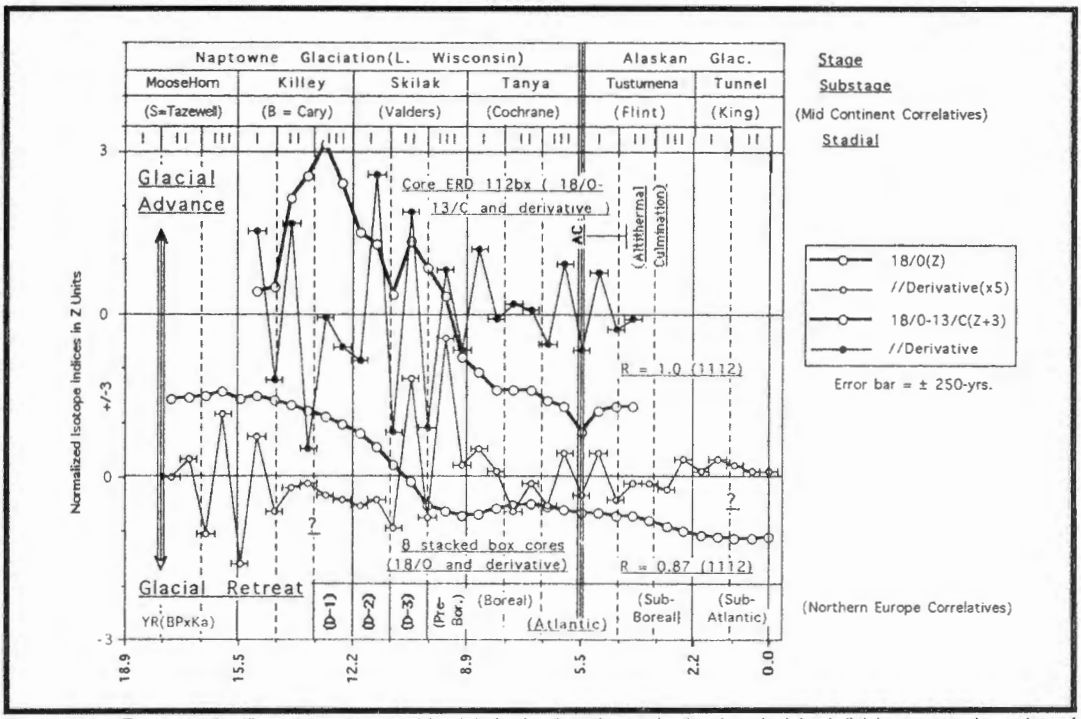

Figure 21 Equatorial Pacific ocean-core record (and derivatives) on timescale showing glacial subdivisions on turning points of the 3336-year Substage Cycle and its 3/1 Stadial (1112-year) Resonance. Centered 500-year isotope indices from Berger *et al* (1987); dating by fine-tuning to Solar Insolation curve. Alaska glacial chronology and correlatives from Karlstrom (1961, 1976b). Lower row = classic bioclimatic (pollen) subdivision of Late Glacial and Postglacial time as radiocarbon dated in Sweeden, Denmark, and Switzerland (compare with terrestrial records in Figure 20). The derivatives suggest that secondary trends of glacial melting (18/O) and surface water temperature ($\delta^{13}C$) were strongly in phase with the Stadial Cycle during the last 18,000 years. Note also that the classic European Dryas sequence and North American glacial events are evidently clearly recorded by contemporaneous meltwater and surface water temperature oscillations in these ocean records.

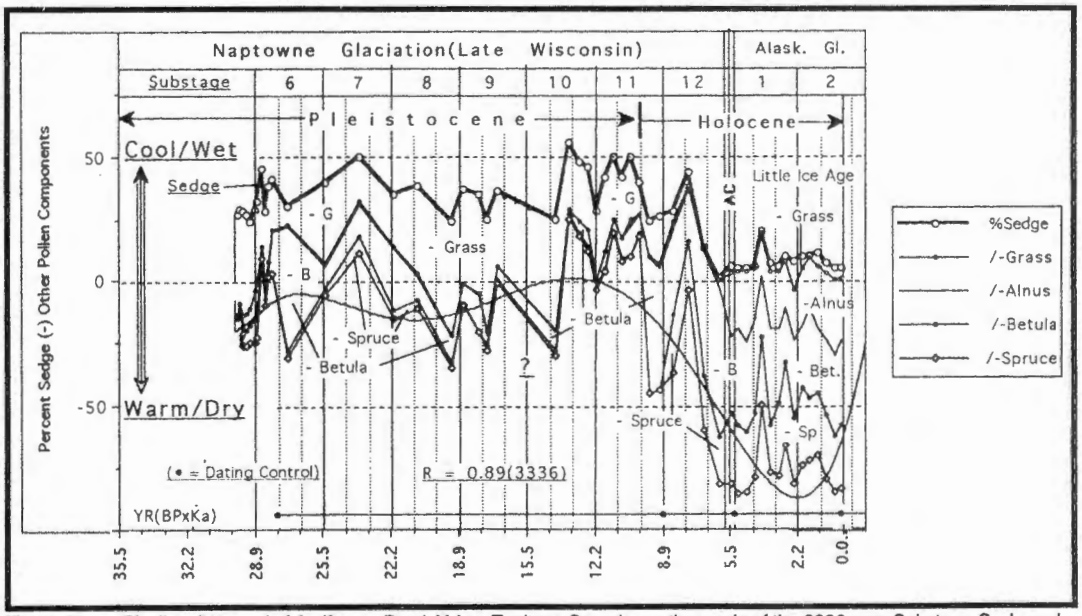

Figure 22 Bioclimatic record of Antifreeze Pond, Yukon Territory, Canada, on timescale of the 3336-year Substage Cycle and its 3/1 (1112-year) Stadial Resonance. Pollen indices from Rampton (1970). Alaska glacial classification and cyclical subdivision from Karlstrom (1961). Trend analysis suggests a strong response to the Substage Cycle and, where the sampling interval is sufficiently close, to the Stadial Cycle. Modified from Figure 24 in Karlstrom (1995).

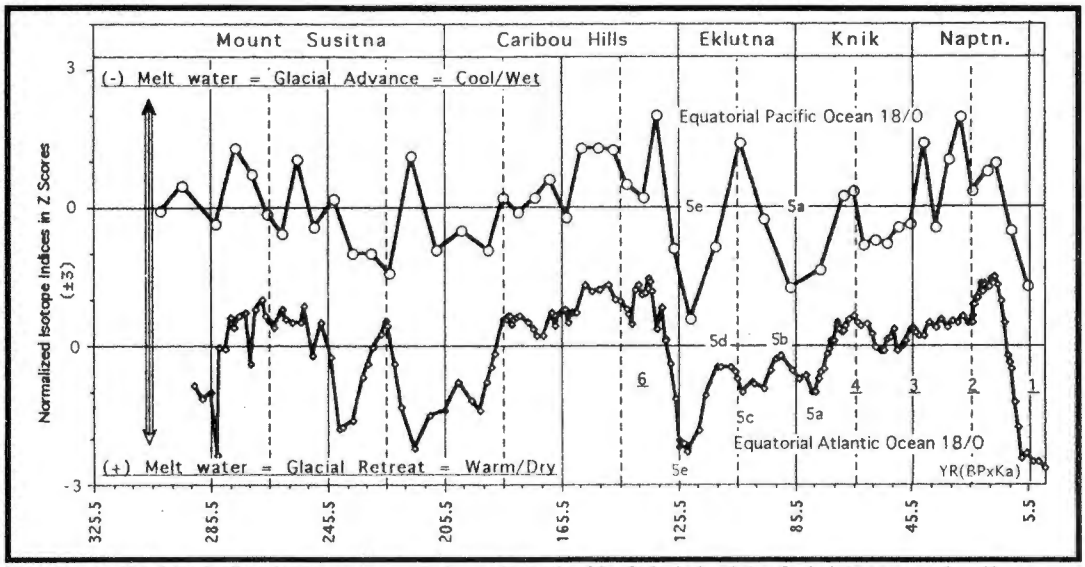

Figure 23 Two "standard" marine Ice Age chronologies on timescale of the Obliquity Insolation Cycle (~40,000 years) and its 2/1 (~20,000 years) resonance assuming a response lag of about 4,500 years (Karlstrom 1961). Isotope indices of an equatorial Pacific Ocean core are from Chuey *et al* (1987); the equatorial Atlantic record is from Martinson *et al* (1987). Both chronologies are fine-tuned to the Milankovitch N60° latitude Climatic Model assuming corresponding response lags. The two records differ mainly in (1) out-of-phase relationships about 225,000 years BP, and (2) relative glacial amplitudes of the last 125,000 years. These differences suggest either heterogenieties in the global record or remaining difficulties with dating procedures and sample mixing. Note the tendency for near in-phase oscillations with the Obliquity 2/1 (~20,000-year) resonance. Most Quaternary researchers continue to correlate their terrestrial paleoclimatic records with Martinson *et al* isotope record on the assumption that it provides a global climatic signal. Scores of chronostratigraphic records presented in this and previous papers appear to contradict this assumption and to support the Solar Insolation/Tidal Resonance Model, which requires opposing longer-term climatic trends in the two hemispheres but globally synchronous secondary climatic oscillations. From Figure 28 in Karlstrom (1995).

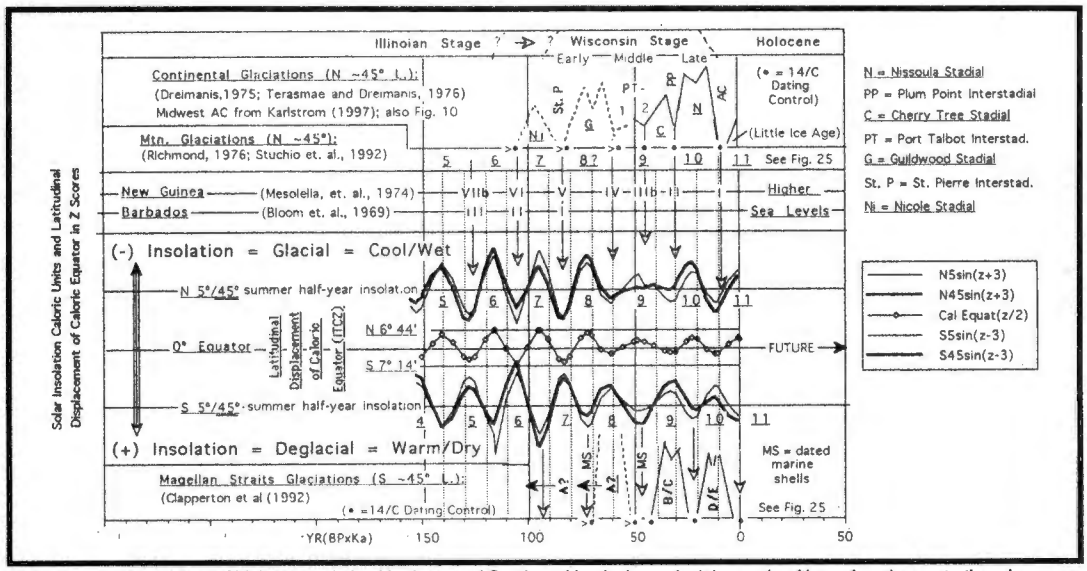

Figure 24 Correlation of highest-resolution Northern and Southern Hemisphere glacial records with marine chronostratigraphy (glaceoeustatic sea levels) and, in turn, with opposing hemispheric processional trends and latitudinal displacements of the Caloric Equator (presumably also of the Intertropical Convergence Zone). Both Richmond (1976) and Terasmae and Dreimanis (1976) see a remarkable coincidence between their dated Northern Hemisphere glacial records and the dated sea level records. These correlations support the concept of glacioeustacy but not necessarily that of interhemispheric climatic synchrony. This is because the much greater volume of glacial ice in the Northern Hemisphere could mask opposing meltwater trends in the interconnected oceans of the Southern Hemisphere (Karlstrom 1966). Glapperton *et al* (1996) see no clear correlation of their Southern Hemisphere glacial record with that of the Northern Hemisphere. Moreover, their B/C and D/C morainal complexes as broadly dated between 45,000, 25,000 years BP and the present more closely parallel the local Southern Hemisphere precessional trends as these are displaced 10,000 years from their Northern Hemisphere counterparts and correlative glacial events. Insolation curves from Milankovitch (1941). From Figure 21 in Karlstrom (1997).

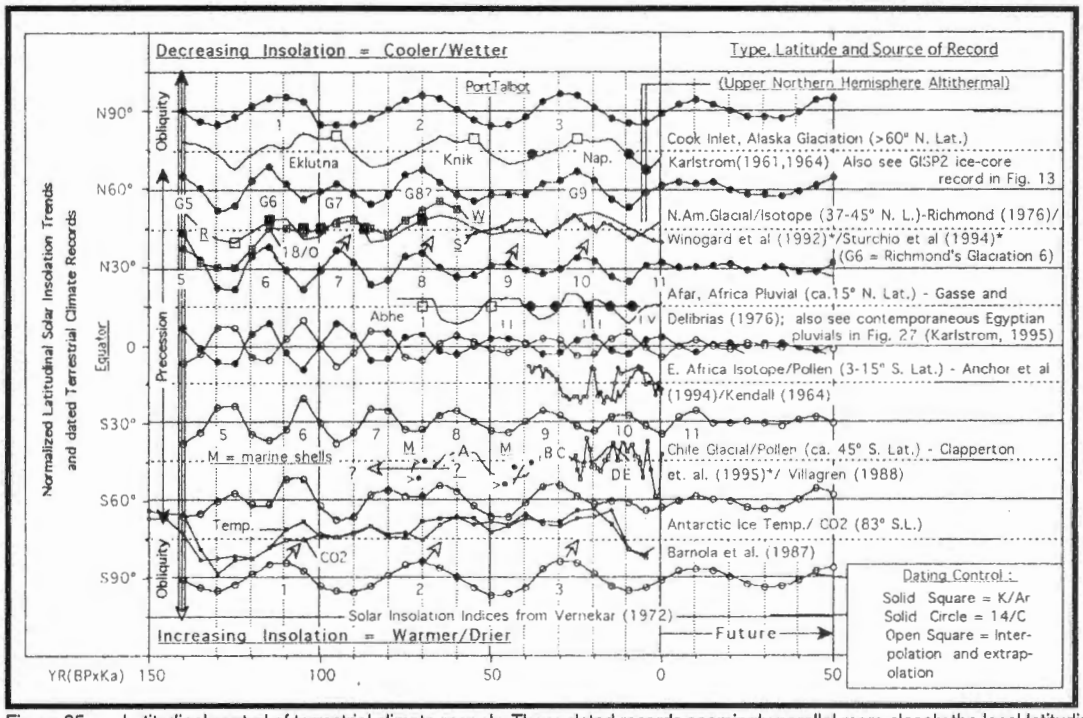

Figure 25 Latitudinal control of terrestrial climate records. These dated records seemingly parallel more closely the local latitudinal insolation trends than the dated records of other latitudes. If these climate records are representative of their respective latitudinal belts, the conventional concept of interhemispheric climatic synchrony dominated by high-latitude Northern Hemisphere insolation must be reassessed as a basis for Ice age correlations and global paleoclimatic reconstructions (Karlstrom 1961). Modified from Figure 26 in Karlstrom (1997). Records discussed in this paper (Figures 8-16, 24) substantially strengthen the case for latitudinal insolation controls and for opposite phasing of longer-term climatic trends across the Equator. Modified from Figure 29 in Karlstrom (1995).

Summary

Insofar as the presented new data generally fortify previous interpretations and correlations with the Solar-Insolation/Tidal-Resonance Climate Model, my conclusions remain the same as those presented in previous papers. Similar qualifications, however, are also in order. In the absence of a generally accepted climatic theory and fuller understanding of the physical linkages involved in changing climates, the indicated empirical correlations must be assumed to represent cause-and-effect relationships. Enough records from different latitudes are assumed to satisfy the important question of latitudinal representativeness. The published datings of the presented records (by Potassium/Argon, Ionium/Uranium, fission-track, magnetism, radiocarbon, archaeology, tree rings and historical accounts) are assumed to be sufficiently accurate for valid cross-correlation with the theoretical timings of the Solar-Insolation/Tidal-Resonance climate Model. It is important to note that similar qualifications relate to the prevailing climate model.

With these caveats in mind, I again conclude:

- Longer-term "Ice Age" changes were out of phase across the Equator and evidently modulated by precessional-insolation trends, which in the Northern Hemisphere are 180° degrees out of phase with those in the Southern Hemisphere. The supporting data run counter to the conventional assumption of inter-hemispheric synchrony and parallel glacial records and suggest that major revisions are required in the derived concepts of global atmospheric circulation dynamics and patterns. Theoretically, there appears to be no reason why, if the Northern Hemisphere glaciers responded directly to summer half-year insolation (the Milankovitch mechanism), the glaciers and associated hydrologic processes in the Southern Hemisphere were not similarly controlled by the opposing summer-insolation trends there. Interconnected ocean bodies explain why the greater volumes of continental ice in the Northern Hemisphere generally dominated the marine meltwater and glacioeustatic records of both hemispheres. In contrast, the terrestrial climatic records suggest that the current (nominal) atmospheric circulation barrier between hemispheric air masses created by the oscillating Intertropical Confluence Zone persisted throughout the time of record.
- In contrast to the above longer-term climatic trends, superposed secondary oscillations (those less than several thousands of years in duration) were synchronous across the Equator, and evidently modulated by tidal resonances that were generated essentially simultaneously throughout the global atmosphere.
- The correlation of increased global volcanic activity with warmer/drier epicycles of the Tidal-Resonance Model strongly suggests that tidal stressing of the lithosphere played a triggering role in volcanic eruptions and minimizes the importance of transitory cooling (and local warming) by volcanic ejecta as a causal factor in longer-term climate changes. To predict local volcanic events solely by tidal intensity, however, is highly uncertain because of the statistical nature of the correlation and because of the presumed triggering mechanism that requires endogenetic processes near threshold conditions.
- The Solar-Insolation/Tidal-Resonance Model appears to satisfy temporal and spatial similarities and differences in paleoclimatic records not explained by other climate models. For example, based on their dating of the Devils Hole speleothem record, Wingard *et al* (1992) question the validity of the Milankovitch orbital mechanism (as conventionally defined by Martinson *et al* 1987) as a modulator of global Ice Age climate. However, as shown in Figure 25, the apparent temporal discrepancy between their chronology and theory disappears when correlated, not with upper latitude insolation, but with that of the local mid-latitude insolation record. Researchers have

questioned or supported the validity of the Uranium/Thorium ages used in the Devils Hole chronology (Shackleton 1994; Ludwig *et al* 1993), the use of marine terminator ages for correlations with the terrestrial record (Emiliani 1993), and most recently, in keeping with the Solar-Insolation/Tidal Resonance Climate Model, have suggested resolution of the discrepancy by precessional solar-insolation controls that temporally vary with latitude (Crowley 1994; Shaffer *et al* 1996)

- The Solar-Isolation/Tidal Resonance Model is a viable scientific hypothesis in that it remains empirically testable by continued cyclical analyses of scores of other high-resolution paleoclimatic records available in the extensive international literature. Further testing should concentrate on the distribution of records improving uniformity of global coverage — particularly in upper latitudes to satisfy dominant Obliquity controls and along the Equator to satisfy past displacements of the Caloric Equator and associated Intertropical Convergence Zone. These longer-term Equatorial displacements, along with changing insolation gradients (Figures 10 and 24), are potentially important mechanisms for driving or modulating seasonal atmospheric circulation patterns in the two hemispheres.
- When sufficient supporting data are accumulated, it will be possible to significantly improve (within limits of sampling interval and dating resolution) the dating and correlation of secondary cycles by fine-tuning to the theoretical tidal-resonance model. This model is primarily built on the celestial-mechanics calculations of Pettersson (1914) as cyclically extended by Stacey (1963, 1967) and continues to provide a best fit for the paleoclimatic records presented in this and previous papers. However, other researchers have calculated somewhat different timings for maximum tidal forces, and additional celestial mechanics analyses of tidal force change are required to satisfy the general validity of current calculations, and to define the higher frequency components of planetary perturbations.

Acknowledgments

I acknowledge the stimulation of conversations with numerous attendees at the past five PACLIM workshops as well as the interchange of research data with some. The recent generous release for my analyses of time-series indices by Vera Markgraf, Wallace Woolfenden, and Teh-Lung Ku is particularly appreciated, as are comments by Eric Karlstrom, Vera Markgraf, Teh-Lung Ku, and Wallace Woolfenden on an early draft. All errors in this paper remain my own. I also acknowledge the contribution of my wife, Carol Ann, who insists that I should write so that she can understand.

In my 1997 acknowledgments, Kritiof Fryxell should read Fritiof Fryxell (an outstanding college professor and friend who was responsible for directing me and scores of other students into the field of geology).

Bibliography

Ancour, A-M, C. Hillaire-Marchel, and R. Bonnefille. 1994. Late Quaternary biomass changes from 13C measurements in a highland peat bog from Equatorial Africa (Barundi), *Quat. Research* 41:225-233.

Benson, L.V., J.W. Burdett, M. Kashgarian, S. P. Lund, F.M Phillips, and R.O. Rye. 1996. Climatic and Hydrologic Oscillations in the Owens Lake Basin and Adjacent Sierra Nevada, California. *Science* 374:746-749.

Barnola, J.M., D. Raymond, Y.S. Korotkevich, and C. Lorius.1987. Vostock ice core provides 160,000 year record of atmospheric CO2 *Nature* 329:410.

Bischof, J.L., T.W. Jr. Stafford, and M. Rubin. 1997. A time-depth scale for Owens Lake sediments of core OL-92: Radiocarbon dates and constant mass accumulation rate. *Geological Society of America Special Paper* 317:89-112.

Bloom, A.L., *et al.* 1974. Quaternary sea level fluctuations on a tectonic coast: New 230Th/234U dates from the Huon peninsula, New Guinea. *Quat. Research* 4:185-205.

Bradley, R.S. 1985. *Quaternary Paleoclimatology:* Allen and Unwin, Boston.

Brackenridge, G.R. 1978. Evidence for a cold, dry full-glacial climate in the American Southwest. *Quat. Research* 9:22-40.

Bright, R.C. 1968. Pollen and seed stratigraphy of Swan Lake, southeastern Idaho: Its relationship to regional vegetation history. *Jour. Idaho State Univ. Mus. Tebiwa,* 9.

Brooks, E.J., T. Sowers, and J. Orchardo. 1996. Rapid variations in atmospheric methane concentration during the past 110,000 years. *Science* 275:1067-1090.

Bryson, R. A., and Goodman. 1980. Volcanic Activity and Climatic Changes. *Science* 207:1041-1044

Chuey, J.M., D.K Rea, and N.G. Pisias. 1987. Late Pleistocene paleoclimatology of the central Equatorial Pacific: A quantitative record of Eolian and carbonate deposition. *Quat. Research* 38:323-33.

Clapperton, C.M., D.E. Sudgen, D.S. Kaufman, and R.D. McCulloch, 1995. The Last Glaciation in Central Magellan Strait, Southernmost Chile. *Quat. Research* 44:133-148.

Crowley, T.J. 1994. Potential reconciliation of Devils Hole and deep-sea Pleistocene chronologies. *Paleocoeanography* 9:1-5.

Currey, D.R., and C.G. Oviat. 1985. Durations, average rates and probable causes of Lake Bonneville expansions, stillstands, and contractions during the last deep-lake cycle, 32,000 to 10,0000 years ago. Pages 9-24 in P.A. Kay and H.F. Diaz, Eds. *Problems of and Prospects for Predicting Great Salt Lake Levels*, Papers from a conference held in Salt Lake City, March 24 -25, 1985.

Dean, J.S., and Robinson, W.J. 1978. Expanded tree-ring chronologies for the Southwest United States. *Chronology Series III, Laboratory of Tree-ring Research.* Univ. of Arizona, Tucson, 58 pp.

de Boer, H.J., 1967. Meteorological Cycles, Pages 564-571 in Rhodes Fairbridge, Editor, *The Encyclopedia of Atmospheric Sciences and Astrogeology.* Reinhold Publishing Corp. New York.

Denton, G.H., and W. Karlen. 1973. Holocene Climatic Variations — their pattern and possible causes. *Quat. Research* 3:155-205.

Dorale, J.A. 1992. A High Resolution Record of Holocene Climate Change in Speleothem Calcite from Cold Water Cave, Northeast Iowa, *Science*, 258:1626-1630

Emiliani, C. 1993. Milankovitch theory verified. *Nature* 364:583-584.

Gallaway, R.W. 1970. The full-glacial climate in the southwestern United States. *Annals of the Association of American Geographers* 60:245-256.

Gasse, F. and G. Delibrious. 1976. Les Lacs de L'afar Centrol (Ethiopie et F. T. A. I.). Pages 529-575, Shoji Horie, Ed. *Paleoclimatology of Lake Biwa and the Japanese Pleistocene* 4.

Graumlisch, L.J. 1992. A 1000-year record of climatic variability in the Sierra Nevada, California: Handout. Am. Quat. Assoc. 12th Biennial Meeting, August 24-26. Univ. of Calif., Davis.

Hevly, R.H. 1989. Post-15,500 BP Pollen of Walker Lake Arizona. (Preliminary manuscript).

Hevly, R.H., and T.N.V. Karlstrom. 1974. Southwest paleoclimate and continental correlations. Pages 257-295 in *Geology of Northern Arizona and notes on archaeology and paleoclimate.* Thor N.V. Karlstrom, Gordon Swann. and Raymond L. Eastwood, editors. Geol. Soc. of America Field Guide 1. Rocky Mountain Meeting, Flagstaff, Arizona.

Heusser, C.J. 1965. A Pleistocene phytogeographic sketch of the Pacific Northwest and Alaska, Pages 469-483 in *The Quaternary of the United States.* H.E. Wright and B.G. Frey, editors. Princeton Univ. Press, Princeton, NJ.

Mesolella, K.J. 1969. The astronomical theory of climatic change, Barbados data. *Jour. Geology* 2:250-274.

Karlstrom, T.N.V. 1961. The glacial history of Alaska: Its bearing on paleoclimatic theory. *Annals New York Academy of Science* 95, Article 1: 290-340.

_____. 1964. Quaternary geology of the Kenai Lowland and glacial history of the Cook Inlet Region, Alaska. *U. S. Geological Survey Professional Paper* 443. 69 pp.

_____. 1966. Quaternary Glacial Record of the North Pacific Region and Worldwide Climatic Change, pp.. 153-182, in *Pleistocene and Post-Pleistocene climatic variations in the Pacific Area* . D.J. Blumenstock, editor. Bishop Museum Press, Honolulu.

_____. 1975. Cenozoic Time-stratigraphy of Colorado Plateaus, Continental Correlations and some Paleoclimatic Implications. Handout, Symposium on Quaternary Stratigraphy, York University, Toronto, May 1975.

_____ 1976a. Stratigraphy and paleoclimate of the Black Mesa Basin. *U. S. Geological Survey Circular* 778:18-22.

_____. 1976b. Quaternary and upper Tertiary time-stratigraphy of the Colorado Plateaus, continental correlations and some paleoclimatic implications. Pages 275-282 in *Quaternary Stratigraphy of North America.* W. C. Mahany, editor. Bowden, Hutchinson and Ross Inc., Stroudsburg, PA.

_____. 1988. Alluvial chronology and hydrologic change of Black Mesa and nearby regions. Pages 45-91 in *The Anasazi in a Changing Environment.* George J. Gumerman, editor. School of American Research Advance Seminar Book, Cambridge Univ. Press, London

_____. 1995. A 139-year dendroclimatic cycle, cultural/environmental history, sunspots and longer-term cycles. Pages 137-159 in *Proceedings of the Eleventh Annual Pacific Climate (PACLIM) Workshop.* C.M. Isaacs and V.L. Tharp, editors. April 19-22, 1994, Interagency Ecological Program. Technical Report 40, California Department of Water Resources.

_____. 1996. The QBO, El Niño, and Tidal Resonance Model. Pages 241-253 in *Proceedings of the Twelfth Annual Pacific Climate {PACLIM} Workshop, May 2-5, 1995.* C.M. Isaacs and V.L. Tharp, editors. Interagency Ecological Program, Technical Report 46. California Department of Water Resources.

_____. 1997. Addendum 1: Paleoclimate and the Solar Insolation/Tidal Resonance Climate Model. Pages 201-224 in *Proceedings of the Thirteenth Annual Pacific Climate (PACLIM) Workshop, April 14-17, 1996.* C.M. Isaacs and V.L. Tharp, editors. Interagency Ecological Program, Technical Report 53. California Department of Water Resources.

Karlstrom, T.N.V., G.J. Gumerman, and R.C. Euler. 1976. Paleoenvironmental and cultural correlates in the Black Mesa region. Pages 149-161 in *Papers on the Archaeology of Black Mesa, Arizona,*. G.J. Gumerman and E.C. Euler, editors. Southern Illinois University Press, Carbondale.

Kendall, R.L. 1969. An ecological history of the Lake Victoria Basin. *Ecological Monographs* 39:121-176.

Ku, T.L., H.C. Li, and L.D. Stoot. 1998. Decadal climatic reconstruction from stable isotope records of speleothem in Shihua Cave, China: A summer monsoon domain. *Proceedings of the Fourteenth Annual Pacific Climate (PACLIM) Workshop.* This volume.

Markgraf, V., and R. Kenny. 1997. Character of rapid vegetation and climate change during the late-glacial in southernmost South America. in Briant Huntley *et al*, editors. *Past and Future Rapid Environmental Changes: The Spatial and Evolutionary Responses of Terrestrial Biota.* NATO ASI Series, Springer-Verlag, Berlin Heidelberg.

Martinson, D.G., N.G. Pisias, J.D. Hays, J. Imbrie, T.C. Moore Jr., and N.J. Shackleton. 1987. Age dating and the Orbital Theory of the Ice Ages: Development of a high-resolution 0 to 300,000-year chronostratigraphy. *Quat. Research* 27:1-29.

Mesolella, K.J. 1969. The astronomical theory of climatic change, Barbados data. *Jour. Geology* 2:250-274.

Menking, K.M., J.L. Biskof, J.A. Fitzpatrick, J.W. Burdette, and R.O. Rye. 1997. Climatic/ Hydrologic Oscillations since 155,000 years BP at Owens Lake, California, Reflected in Abundance and Stable Isotope Composition of Sediment Carbonate. *Quat. Research* 48:58-68.

Milankovitch, M. 1941. *Canon of Insolation and the Ice-age Problem.* Translated from German by Israel Program for Scientific Translation, Jerusalem. Available from U.S. Department of Commerce, Springfield, Virginia.

North American Stratigraphic Code. 1983. North American Commission of Stratigraphic Nomenclature. *American Association of Petroleum Geologists Bulletin* 67:841-875.

Pettersson, O. 1914. Climatic variations in historic and prehistoric time. *Svenska hydrogr. Biol. Komm. Skriftern* 5.

Phillips, F.M., M. G. Zreda, L.V. Benson, M.A. Plummer, D. Elmore, and P. Sharma. 1996. Chronology for Fluctuations in Late Pleistocene Sierra Nevada Glaciers and Lakes, *Science* 2174:749-751.

Phillips, F.M., M.G. Zreda, S.S. Smith, D. Elmore, P.W. Kubik, and P. Sharma. 1990. Cosmogenic Chlorine-36 Chronology for Glacial Deposits at Bloody Canyon, Eastern Sierra Nevada. *Science* 248:1529-1532.

Porter, S.C, and G.H. Denton. 1967. Chronology of Neoglacial in the North American Cordillera: *Amer. Jour. of Science* 165:177-210.

Richmond, G.M. 1976. Pleistocene stratigraphy and chronology in the mountains of western Wyoming. Pages 353-379 in *Quaternary Stratigraphy of North America.* W.C. Mahany, editor. Dowden, Hutchinson and Ross Inc., Stroudsburg, PA.

Shackleton, N.J. 1993. Last Interglacial in Devils Hole. *Nature* 362:596.

Shaffer, J.A., R.S. Cerveny, and R.I. Dorn. 1996. Radiocarbon windows as indicators of an astronomical influence on the Devils Hole chronology. *Geology* 24:1017-1020.

Stacey, C. 1963. Cyclical measures: Some tidal aspects concerning equinoctial years. *Annals New York Academy of Science* 105, Article 2: 421-460.

_____. 1967. Earth motions and time and astronomic cycles. Pages 335-340 and 999-1003 in *The Encyclopedia of Atmospheric Sciences and Astrogeology..* Rhodes Fairbridge, editor. Reinhold Publishing Corp. NY.

Street, F.A., and A.T. Grove. 1979. Global Maps of Lake-Level Fluctuations Since 30,000 yr BP. *Quat. Research* 12:83-118.

Sturchio, N.C., K.L. Pierce, M.T. Murrell, and M.L Sorey. 1994. Uranium- series Ages of Travertine and timing of the Last Glaciation in the Northern Yellowstone Area, Wyoming-Montana, *Quat. Research*, 42:265-277.

Terasmae J., and A. Dreimanis. 1976. Quaternary Stratigraphy of Southern Ontario. Pages 51-63 in *Quaternary Stratigraphy of North America.* W.C. Mahany, editor. Dowden, Hutchinson and Ross Inc., Stroudsberg, PA.

Vernekar, A.D. 1972. Long period global variations of incoming solar radiation, *Meteorological Monographs* 12 Whole monograph: 19 pages + 170 unnumbered pages.

Villagren, C. 1988. Late Quaternary vegetation of southern Isla Grande de Chloe, Chile: *Quat. Research* 29:294-306

Webb III, T., and R.A. Bryson. 1972. Late- and Postglacial Change in the Northern Midwest, USA: Estimates Derived from Fossil Pollen Spectra by Multivariate Statistical Analysis. *Quat. Research* 2:70-115.

Wells, P.V. 1979. An Equable Glaciopluvial in the West: Pleniglacial Evidence of Increased Precipitation on a Gradient from the Great Basin to the Sonoran and Chihuahuan Deserts. Quat. Research 12:311-325.

Wingard, I., J. Tyler, B. Coplen, J.M. Landwehr, A.C. Riggs, K.B. Ludwig, B.J. Szabo, P.T. Kolegar, and K.M. Revesz. 1992. Continuous 500,000-year climate record from vein calcite in Devils Hole, Nevada. *Science* 258:255-260.

Woolfenden, W. 1997. The response of Desert Vegetation to Climate Change during the Past 159,000 Years in the Southern Owens Valley Region, California. Abstract, PACLIM Workshop, Santa Catalina Island, California, April 1997.

Xiao, J., Y. Inouchi, H. Kumai, S. Yashikawa, Y. Kondo, T. Liu, and Z. An. 1997a. Biogenic Silica Record in Lake Biwa of Central Japan over the past 145,000 years. *Quat Research* 47:277-283.

_____. 1997b. Eolian Quartz Flux in Lake Biwa, Central Japan, over the Past 145,000 Years. *Quat. Research* 48:48-57.

Winter Atmospheric Circulation and Tree Growth in the Sierra Nevada

Gregg M. Garfin

ABSTRACT: Tree-ring data from mid-elevation (~2000 meters) giant sequoia and high-elevation (~3500 meters) pines were used to select extreme growth years from which temperature, precipitation, and large-scale winter 500 mb circulation patterns associated with the extreme tree growth anomalies were examined. Winters preceding extreme high growth in both giant sequoia and pines are warm and wet and are characterized by anomalous low pressure in the northeastern Pacific Ocean and a tendency for southwesterly flow and advection of warm maritime air into California. For the pines, such winters exhibit a PNA-like pattern of anomalous low pressure in the northern Pacific, anomalous high pressure over northwestern Canada, and anomalous low pressure across the southeastern United States. Circulation is more meridional circulation during the warm and dry winters preceding extreme low growth in giant sequoia. During winters associated with extreme low growth in the pines, maximum westerlies are north of their mean position and there is a tendency for enhanced ridging in the northeastern Pacific, which advects cool, dry air into the Sierra Nevada. The rich combinations of anomaly patterns suggest the possibility of reconstructing circulation patterns associated with extremes in Sierra Nevada climate.

Introduction

The recent prolonged drought of the late 1980s and early 1990s had profound effects on agricultural, industrial, and domestic water use in California. California experiences a sharp winter precipitation maximum, but demand for water is greatest during the summer — a situation similar to constraints on water use by Sierra Nevada trees. Although long records of climatic conditions in this region have been reconstructed, few dendrochronologists have examined relationships between tree growth, influenced by proximate climate factors such as temperature and precipitation, and atmospheric circulation (LaMarche 1974; Blasing and Fritts 1976; Hirschboeck *et al* 1996). Hirschboeck *et al* (1996) suggest that the direct process-based connection between large-scale circulation and local ring-width variation can be provided by synoptic climatological companion analyses to standard dendroclimatic reconstructions, such as the study presented below.

Dendroclimatic studies in the Sierra Nevada and adjacent ranges are abundant. Those focusing on upper atmospheric circulation are few, due to the lack of long records of upper air data. Some of the pertinent results of these studies are summarized as follows. LaMarche (1974) examined growth anomalies of long-lived bristlecone pine (*Pinus longaeva*) from upper and lower treeline sites in the White Mountains (immediately to the east of the Sierra). He inferred the following scenarios: during wet/cold season months, migratory depressions from the northern Pacific moved

In: R.C. Wilson and V.L. Tharp, Editors. 1998. *Proceedings of the Fourteenth Annual Pacific Climate (PACLIM) Workshop, April 6-9, 1997.* Interagency Ecological Program, Technical Report 57. California Department of Water Resources.

well south of the normal storm track and brought heavy precipitation to the White Mountains, whereas during dry months an upper level ridge persisted over western North America. LaMarche and Hirschboeck (1984) found that frost damage in bristlecone from California's White Mountains can be directly related to short-term outbreaks of polar air during the growing season. A deep mid-tropospheric trough over the western United States, often associated with blocking activity in the large-scale circulation, is the synoptic pattern they relate to frost damage. Hughes and Brown (1992) examined winter (December-February) sea level pressure anomaly patterns for four extreme 20th century low-growth years in drought-sensitive giant sequoia (*Sequoiadendron giganteum*) and noted that such winters are characterized by positive SLP anomalies over much of the western United States. They inferred that snow-bearing winter storms are diverted from the central and southern Sierra Nevada during these winters.

The main objective of this study is to establish the patterns of upper atmospheric circulation associated with extreme growth years in both mid- and high-elevation Sierra Nevada conifers. The approach used is inferential and builds upon the results of previous dendroclimatological research from the Sierra Nevada (Hughes and Brown 1992; Graumlich 1993). Relationships between tree growth and winter upper atmospheric circulation are examined using composites of temperature, precipitation and 500-mb height. The results presented here have broad implications for dendroclimatic reconstructions using the multimillennial tree-ring records from the region.

Data

Twenty ring-width chronologies of giant sequoia, foxtail pine (*Pinus balfouriana*) and whitebark pine (*Pinus albicaulis*) from elevations of about 2000-3500 meters (Brown *et al* 1992; Graumlich 1993; Hughes *et al* 1996; Lloyd 1996) were used in this study (Figure 1, Table 1). Chronologies used in this study were dated, measured, and standardized using standard dendrochronological techniques as described in Brown *et al* (1992), Graumlich (1993), and Lloyd (1996). Ring-width series for each core sample were standardized into dimensionless indices to remove growth trends related primarily to age, bole geometry, or disturbance in the case of sequoia. The resulting series were then autoregressively modeled to remove the effects of non-climatic persistence from the detrended ring-width series (Cook 1985; Cook and Holmes 1986). Residual chronologies were used to emphasize year-to-year variation.

Monthly precipitation and temperature data for the central Sierra Nevada were provided by the Climate Research Division at Scripps Institution of Oceanography, University of California, San Diego. These are regional averages for six relatively high elevation stations, and construction of

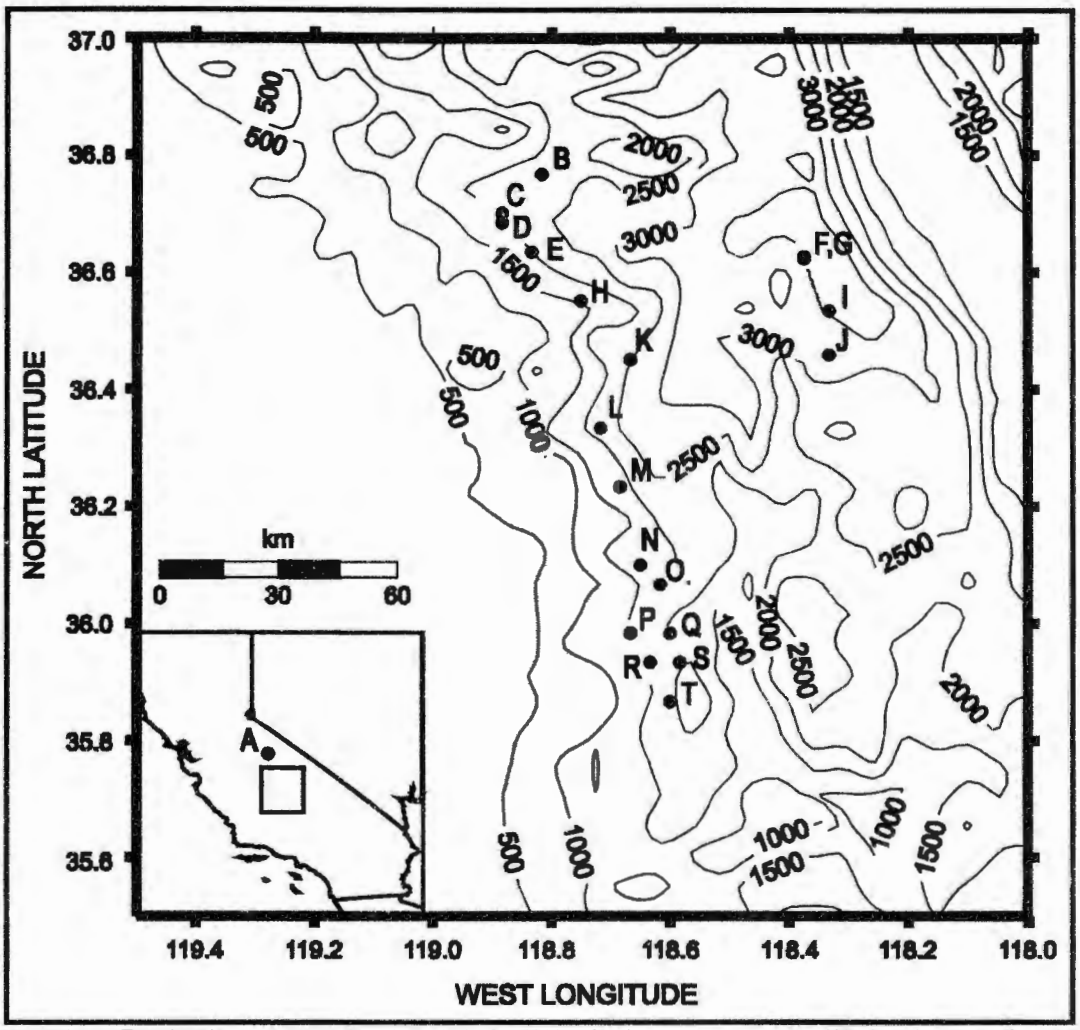

Figure 1 Tree-ring chronologies used in this analysis. See Table 1 for site names and species. Altitude estimates are from the U.S. Defense Mapping Agency's United States 30-Second DEM and are expressed in meters (Row *et al* 1995).

these series is detailed in Aguado *et al* (1992). The atmospheric circulation is represented by monthly analyses of Northern Hemisphere 500-mb height anomalies from a 1951-1980 reference period, gridded onto a 5° latitude-longitude grid, beginning in 1946 (Bradley *et al* 1994). Previous studies indicate that trees from the Sierra Nevada respond to winter precipitation (Hughes and Brown 1992; Graumlich 1993; Graybill and Funkhouser 1997). November-March precipitation and atmospheric circulation are examined below.

Table 1
SIERRA NEVADA TREE-RING SITES

Map Designation	Site	Species	Citation
A	Kuna Crest	PIAL	J. King: Unpublished
B	Camp Six	SEGI	Brown et al. 1992
C	Buena Vista	SEGI	Hughes et al. 1996
D	Big Baldy	SEGI	Hughes et al. 1996
E	Muir	SEGI	Hughes et al. 1996
F	Upper Wright Lakes	PIBA	Lloyd 1996
G	Bighorn Plateau	PIBA	Graumlich:Unpublished
H	Giant Forest	SEGI	Brown et al. 1992
I	Crabtree	PIBA	Graumlich 1993
J	Boreal Forest	PIBA	Lloyd 1996
K	East Fork	SEGI	Hughes et al. 1996
L	Garfield	SEGI	Hughes et al. 1996
M	Mountain Home	SEGI	Brown et al. 1992
N	Black Mountain	SEGI	Hughes et al. 1996
O	Red Hill	SEGI	Hughes et al. 1996
P	Parker Peak	SEGI	Hughes et al. 1996
Q	Long Meadow	SEGI	R. Touchan: Unpublished
R	Packsaddle	SEGI	M. Hughes: Unpublished
S	Starvation Creek	SEGI	M. Hughes: Unpublished
T	Deer Creek	SEGI	M. Hughes: Unpublished

PIAL = *Pinus albicaulis*
PIBA = *Pinus balfouriana*
SEGI = *Sequoiadendron giganteum*

Methodology

Extreme tree growth anomaly years for each of the two elevation classes (mid-elevation giant sequoia; high-elevation upper forest border pine) were selected on the basis of unrotated principal components analyses of the highly intercorrelated tree-ring chronologies for 1899-1987. Two separate PCAs were performed, one on the giant sequoia chronologies and one on the pine chronologies. Time series of scores from the first component of each individual analysis were selected as weighted averages of the chronology assemblages. From these time series, the highest and lowest deciles from 1947-1987 were selected as extreme growth years. The resulting extreme years for sequoia and pine chronologies are presented in Table 2.

Table 2
EXTREME GROWTH YEARS

S+	P+	S–	P–
1954	1969	1959	1949
1958	1977	1961	1960
1969	1980	1977	1972
1986	1984	1987	1987

Winter temperature and precipitation data were averaged for each of the four sets of growth anomaly years (sequoia positive [S+], sequoia negative [S–], pine positive [P+], pine negative [P–]) to analyze extreme growth response to climate. Similarly, composites of 500-mb height data were constructed for each of the four sets of growth anomaly years. Analyses of these composites are presented in the following section.

Extreme Growth Composite Anomaly Patterns

Extreme positive growth anomaly years in giant sequoia are characterized by wet winters with temperatures near the mean (Figure 2). The most important features of the 500-mb height composite for S+ decile years, a region of negative height anomalies in the mid-latitude northeastern Pacific and the region of positive height anomalies to its southeast, combine to produce southwesterly flow into California (Figure 3). This pattern of anomalies resembles 700-mb height patterns for

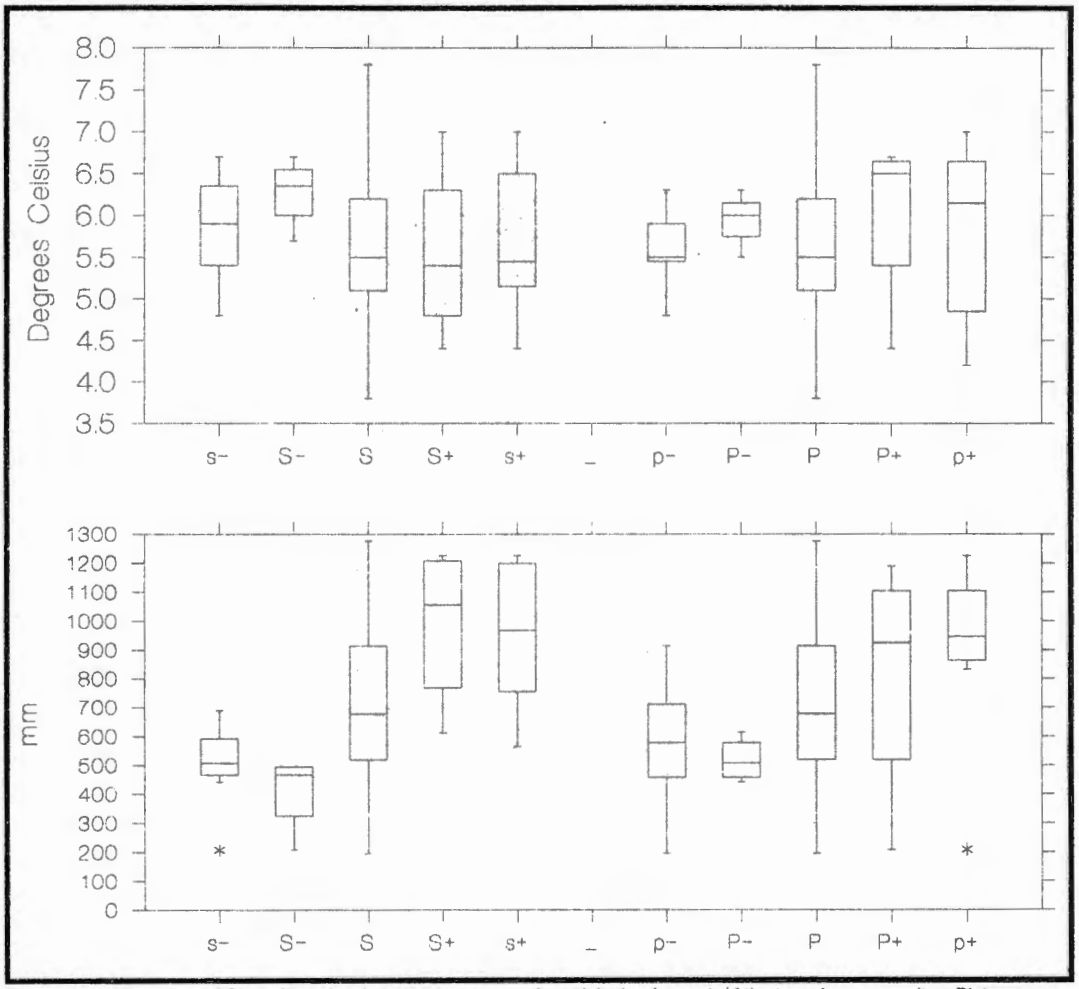

Figure 2 Box-plots of Sierra Nevada winter temperature and precipitation for each of the tree-ring composites. Plots are coded as follows: s– = sequoia lowest quintile of growth, S– = sequoia lowest decile of growth, S = sequoia mean 1946-1987, S+ = sequoia highest decile of growth, s+ = sequoia highest quintile of growth; p– = pine lowest quintile of growth, P– = pine lowest decile of growth, P = pine mean 1946-1987, P+ = pine highest decile of growth, p+ = pine highest quintile of growth. For details of box-plot calculations see SYSTAT, Inc. 1992.

wet and snowy winters presented by Cayan (1996) and McCabe and Legates (1995). Most of the individual composite years (not shown) display an alternating pattern of negative-positive-negative anomaly centers over the eastern Pacific, southern Canada/central United States, and eastern United States. This pattern is strikingly exhibited during the El Niño winters of 1958 and 1969 (Klein 1958; Wagner 1969). Monthly weather summaries for individual S+ winters show that these years exhibit the following general characteristics: strong westerlies displaced to the south of their mean position, strong southwesterly onshore flow, strong near-surface advection of maritime air from low latitudes, a low index longwave pattern, and a deepened east Pacific trough (O'Connor 1958; Klein 1958; Wagner 1969).

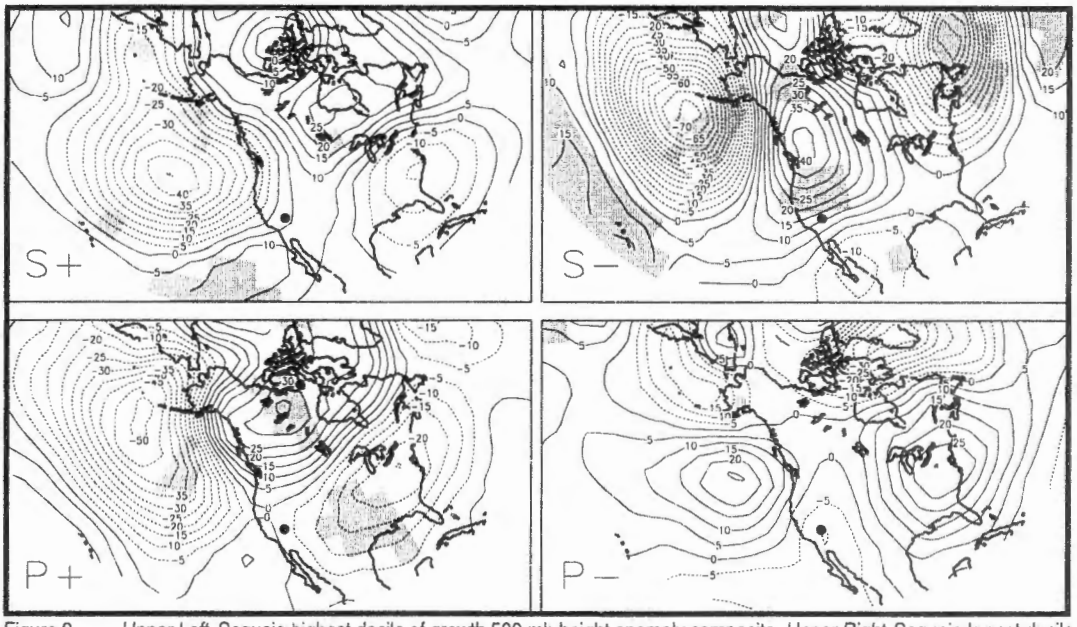

Figure 3 *Upper Left.* Sequoia highest decile of growth 500-mb height anomaly composite. *Upper Right.* Sequoia lowest decile of growth 500-mb height anomaly composite. *Lower Left.* Pine highest decile of growth 500-mb height anomaly composite. *Lower Right.* Pine lowest decile of growth 500-mb height anomaly composite. Solid contours indicate positive 500-mb height anomalies; dashed contours indicate negative 500-mb height anomalies. Grid boxes exhibiting significant anomalies ($\alpha = 0.05$) are shaded. The contour interval is 10 meters.

Extreme negative growth anomaly years in giant sequoia are characterized by warm, dry winters (Figure 2). The 500-mb composite for S– decile years is characterized by vigorous meridional circulation (Figure 3), in which an enhanced ridge over western North America inhibits mid-latitude zonal flow (Taubensee 1977). This pattern is similar to the winter SLP anomaly pattern reported by Hughes and Brown (1992) for years during which the August Palmer Drought Severity Index for California Division 5 (San Joaquin drainage) was especially negative. This circulation pattern also resembles the 700-mb circulation patterns for dry winters displayed in synoptic studies of western United States snowpack (Cayan 1996; McCabe and Legates 1995).

Monthly weather summaries for individual S– winters suggest vigorous meridional flow, exceptional persistence and amplification of this circulation pattern from month to month (Stark 1959, 1961; Wagner 1977; Namias *et al* 1988), and storm tracks deflected to the north of California or into the Gulf of Alaska (Green 1958; Dunn 1959; Stark 1961; Andrews 1961; Dickson 1977). Three of four S– Januarys (1959, 1961, 1987) were characterized by Namias *et al* (1988) as high persistence Januarys. These winters also exhibited stronger than normal westerlies over the subtropics and weaker than normal westerlies in temperate latitudes. It is interesting to note that the S– pattern is not merely the inverse of the S+ pattern. This effect, however, might reflect the fact that trees respond more directly to a climatic factor when it is limiting to growth, *eg*, low winter precipitation leading to summer water stress (S–), than to a situation in which a climatic factor is abundant and no longer limiting to growth (S+). Another interpretation is that dinnerences in these patterns reflect nonlinear modes of atmospheric circulation (c.f. Hoerling *et al* 1997).

Extreme positive growth anomaly years in the pines are characterized by warm, wet winters (Figure 2). The 500-mb height composite for P+ decile years is characterized by a chain of alternating anomaly centers, with negative anomalies over the north-central Pacific, positive anomalies over northern Canada, and negative anomalies over the southern and eastern United States (Figure 3). Monthly weather summaries for individual P+ winters suggest the following characteristics: strong zonal flow into the western United States or strong southward displaced westerlies, southwesterly flow into California, a weak West Coast ridge, and a tendency for blocking over western Canada or northern Alaska (Wagner 1969, 1980; Dickson 1980). The spatial structure of 500-mb height anomalies resembles the PNA anomaly pattern. Intriguingly, P+ years coincide with strong PNA winters only after 1976, possibly due to the well documented decade-long shift in North Pacific atmospheric circulation (Trenberth 1990; Trenberth and Hurrell 1994; Cayan *et al* 1995). Atmospheric circulation during the shift exhibited a deeper than normal Aleutian low pressure system during the winter half-year and other characteristics similar to P+ winters (see above).

Extreme negative growth anomaly years in the pines are characterized by mild, dry winters (Figure 2). The 500-mb height composite for P– decile winters displays significant negative height anomalies over the Bering Sea, positive anomalies over the northeast Pacific, positive anomalies over eastern North America and weak negative anomalies over the southwestern United States (Figure 3). This is the least robust of the 500-mb anomaly patterns presented. The positive height anomalies over the eastern Pacific indicate enhanced ridging over this region (and probably deflection of storms to the north of California), but the lack of statistical significance might indicate shifting of the main locus of a ridge

in this vicinity. Monthly weather summaries for individual P– winters suggest the following characteristics: frequent occurrence of a ridge in the eastern Pacific, Gulf of Alaska, or western North America; high frequency of anticyclones and strong subsidence over California; and location of the mean 700-mb jet to the north or south of California.

Conclusions

The most important findings of this paper are as follows.

- When both sequoia and pine exhibit extreme low growth anomalies in the same year, winter conditions are warm and dry, with enhanced ridging over the western United States and eastern Pacific and more meridional circulation.
- When both sequoia and pine exhibit extreme high growth anomalies in the same year, winter conditions are warm and wet, with enhanced low pressure over the north-central Pacific, maximum westerlies south of their mean position, and south-westerly flow toward the California coast.

Giant sequoia and high-elevation pine species grow in notably different environments and have different seasonal windows of growth. Consequently, they respond somewhat differently to climate. If combinations of extreme tree growth anomalies at mid- and high elevations were both consistent and relatively rare, then it might be possible to exploit these combinations to infer or specify the past extremes in Sierra Nevada climate and atmospheric circulation with confidence (cf. LaMarche 1974). Although past atmospheric circulation was not reconstructed in this study, modes of atmospheric circulation associated with extreme growth "events" were clearly delineated. Agreement with instrumental climate studies of Sierra Nevada precipitation, temperature, and atmospheric circulation (Cayan and Riddle 1992; Cayan 1996) demonstrates that this approach can be used to provide plausible circulation mechanisms linked to climate parameters influencing tree growth. In addition, this method is particularly well suited to examination of complacent tree species (*eg*, giant sequoia) that exhibit extremes in growth quite clearly against a background of low growth variability (Kelly *et al* 1989; Hughes and Brown 1992). Future work will examine the rich combinations of anomaly patterns (*eg*, S– P+) that might be explored using the longer record of SLP and the possibility of reconstructing circulation patterns associated with extreme growth years.

Acknowledgments

Gridded 500-mb height data (original source: NCAR) were kindly provided by Bob Lofgren, Laboratory of Tree-Ring Research, University of Arizona, and the Climate Lab, Department of Geosciences, University of Massachusetts, Amherst. Tree-ring chronologies were kindly provided by Malcolm Hughes, Lisa Graumlich, Ramzi Touchan, John King, and Andrea Lloyd. The original source of the United States 30-second DEM data used in Figure 1 is the U.S. Defense Mapping Agency Topographic Center and National Telecommunications Information Agency.

This work was supported by Cooperative Agreement CA 8033-1-0002 with the National Park Service (Malcolm Hughes, P.I.) and NOAA Grant NA66GP0311 (Malcolm Hughes, P.I.).

References

Aguado, E., D. Cayan, L. Riddle, and M. Roos. 1992. Climatic fluctuations and the timing of west coast streamflow. *Journal of Climate* 5:1468-1483.

Andrews, J.F. 1961. The weather and circulation of March 1961: another mild month in the United States. *Monthly Weather Review* 89:205-210.

Blasing, T.J., and H.C. Fritts. 1976. Reconstructing past climatic anomalies in the North Pacific and Western North America from tree-ring data. *Quaternary Research* 6:563-579.

Bradley, R. S., L.G. Ahern, and F.T. Keimig. 1994. A Computer-based atlas of global instrumental climate data. *Bulletin of the American Meteorological Society* 75:35-41.

Brown, P.M., M.K. Hughes, C.H. Baisan, T.W. Swetnam, and A.C. Caprio. 1992. Giant sequoia ring width chronologies from the central Sierra Nevada, California. *Tree-Ring Bulletin* 52:1-14.

Cayan, D.R. 1996. Interannual climate variability and snowpack in the western United States. *Journal of Climate* 9:928-948.

Cayan, D.R., A.J. Miller, T.P. Barnett, N.E. Graham, J.N. Ritchie, and J.M. Oberhuber. 1995. Seasonal-interannual fluctuations in surface temperature over the Pacific: effects of monthly winds and heat fluxes. In *Climate Variability on Decade to Century Time Scales.* National Academy of Sciences Press.

Cayan, D., and L. Riddle. 1992. Atmospheric circulation and precipitation in the Sierra Nevada. Pages 711-719 in *Managing Water Resources During Global Change.* American Water Resources Association.

Cook, E.R. 1985. *A Time Series Analysis Approach to Tree-Ring Standardization.* Ph.D. Dissertation, University of Arizona, Tucson.

Cook, E.R., and R.H. Holmes. 1986. Users manual for program ARSTAN. Pages 50-56 in *Tree-ring chronologies of western North America: California, eastern Oregon and northern Great Basin.* R.L. Holmes, R.K. Adams, and H.C. Fritts, editors. Laboratory of Tree-Ring Research, University of Arizona, Chronology Series 6.

Dickson, R.R. 1977. Weather and circulation of February 1977: widespread drought. *Monthly Weather Review* 105:684-689.

Dickson, R.R. 1980. Weather and circulation of February 1980: California floods. *Monthly Weather Review* 108:679-684.

Dunn, C.R. 1959. The weather and circulation of March 1959: record cold in Alaska but mild temperatures in the remainder of the United States. *Monthly Weather Review* 87:111-118.

Graumlich, L.J. 1993. A 1000-year record of temperature and precipitation in the Sierra Nevada. *Quaternary Research* 39:249-255.

Graybill, D.A. and G.S. Funkhouser. 1997 (in press), Dendroclimatic reconstructions during the past millennium in the Southern Sierra Nevada and Owens Valley, California, in Lavenberg, R. (ed.) Southern California Climate: Trends and Extremes During the Past 2000 Years, Contributions in Science, Natural History Museum of Los Angeles County, Los Angeles, California.

Green, R.A. 1958. The weather and circulation of December 1958. *Monthly Weather Review* 86:487-492.

Hirschboeck, K.K., F. Ni, M.L. Wood, and C.A. Woodhouse. 1996. Synoptic dendroclimatology: overview and outlook. Pages 205-223 in *Tree-Rings, Environment, and Humanity, Proceedings of the International Conference, Tucson, Arizona, 17-21 May 1994.* J.S. Dean, D.M. Meko, and T.W. Swetnam, editors.

Hoerling, M.P., A. Kumar, and M. Zhong. 1997. El Nino, La Nina, and the nonlinearity of their teleconnections. *Journal of Climate* 10:1769-1784.

Hughes, M.K. and P.M. Brown. 1992. Drought frequency in central California since 101 B.C. recorded in giant sequoia tree rings. *Climate Dynamics* 6:161-167.

Hughes, M.K., R. Touchan, and P.M. Brown. 1996. A multimillennial network of giant sequoia chronologies for dendroclimatology. Pages 225-234 in *Tree-Rings, Environment, and Humanity, Proceedings of the International Conference, Tucson, Arizona, 17-21 May 1994.* J.S. Dean, D.M. Meko, and T.W. Swetnam, editors.

Kelly, P.M., M.A.R. Munro, M.K. Hughes, and C.M. Goodess. 1989. Climate and signature years in west European oaks. *Nature* 340:57-60.

Klein, W.H. 1958. The weather and circulation of February 1958: a month with an expanded circumpolar vortex of record intensity. *Monthly Weather Review* 86:60-70.

LaMarche, Jr., V.C. 1974. Paleoclimatic inferences from long tree-ring records. *Science* 183: 1043-1048.

LaMarche, Jr., V.C., and K.K. Hirschboeck. 1984. Frost rings in trees as records of major volcanic eruptions. *Nature* 307:121-128.

Lloyd, A. 1996. *Patterns and Processes of Treeline Forest Response to Late Holocene Climate Change in the Sierra Nevada, California.* Ph.D. Dissertation, University of Arizona, Tucson.

McCabe, G.J. and D.R. Legates. 1995. Relationships between 700 hPa height anomalies and 1April snowpack accumulations in the western USA. *International Journal of Climatology* 15:517-530.

Namias, J., X. Yuan, and D.R. Cayan. 1988. Persistence of north Pacific sea surface temperature and atmospheric flow patterns. *Journal of Climate* 1:682-703.

O'Connor, J.F. 1958. The weather and circulation of January 1958, low index with record cold in southeastern United States. *Monthly Weather Review* 86:11-18.

Row, L.W. III, D.A. Hastings, and P.K. Dunbar. 1995. *TerrainBase: Worldwide Digital Terrain Data, Documentation Manual.* CD-ROM Release 1.0. Boulder, National Oceanic and Atmospheric Administration.

Stark, L.P. 1959. The weather and circulation of January 1959: a month of exceptional persistence from the preceding December. *Monthly Weather Review* 87:33-39.

Stark, L.P. 1961. The weather and circulation of February 1961: an example of attenuation in the long-wave pattern. *Monthly Weather Review* 89:178-184.

SYSTAT, Inc. 1992. *SYSTAT for Windows: Graphics, Version 5 Edition.* Evanston, SYSTAT, Inc., 636 p.

Taubensee, R.E. 1977. Weather and circulation of March 1977: record and near-record precipitation eases drought in parts of the Great Plains and Midwest. *Monthly Weather Review* 105:793-799.

Trenberth, K.E. 1990. Recent observed interdecadal climate changes in the Northern Hemisphere. *Bulletin of the American Meteorological Society* 71:988-993.

Trenberth, K.E., and J.W. Hurrell. 1994. Decadal atmosphere-ocean variations in the Pacific. *Climate Dynamics* 9:303-319.

Wagner, A.J. 1969. The weather and circulation of January 1969: continued strong high-latitude blocking and flood-producing rains in California. *Monthly Weather Review* 97:351-358.

Wagner, A.J. 1977. Weather and circulation of January 1977: the coldest month on record in the Ohio Valley. *Monthly Weather Review* 105:553-560.

Wagner, A.J. 1980. Weather and circulation of January 1980: commencement of a major index cycle. *Monthly Weather Review* 108:531-538.

The Great New Year's Flood of 1997 in Northern California

Maurice Roos

The New Year's flood of 1997 was probably the largest in the 90-year Northern California record, which begins in 1906. It was notable in intensity, volume of flood water, and the areal extent from the Oregon border to the southern end of the Sierra Nevada (Figure 1). Many new flood records were set.

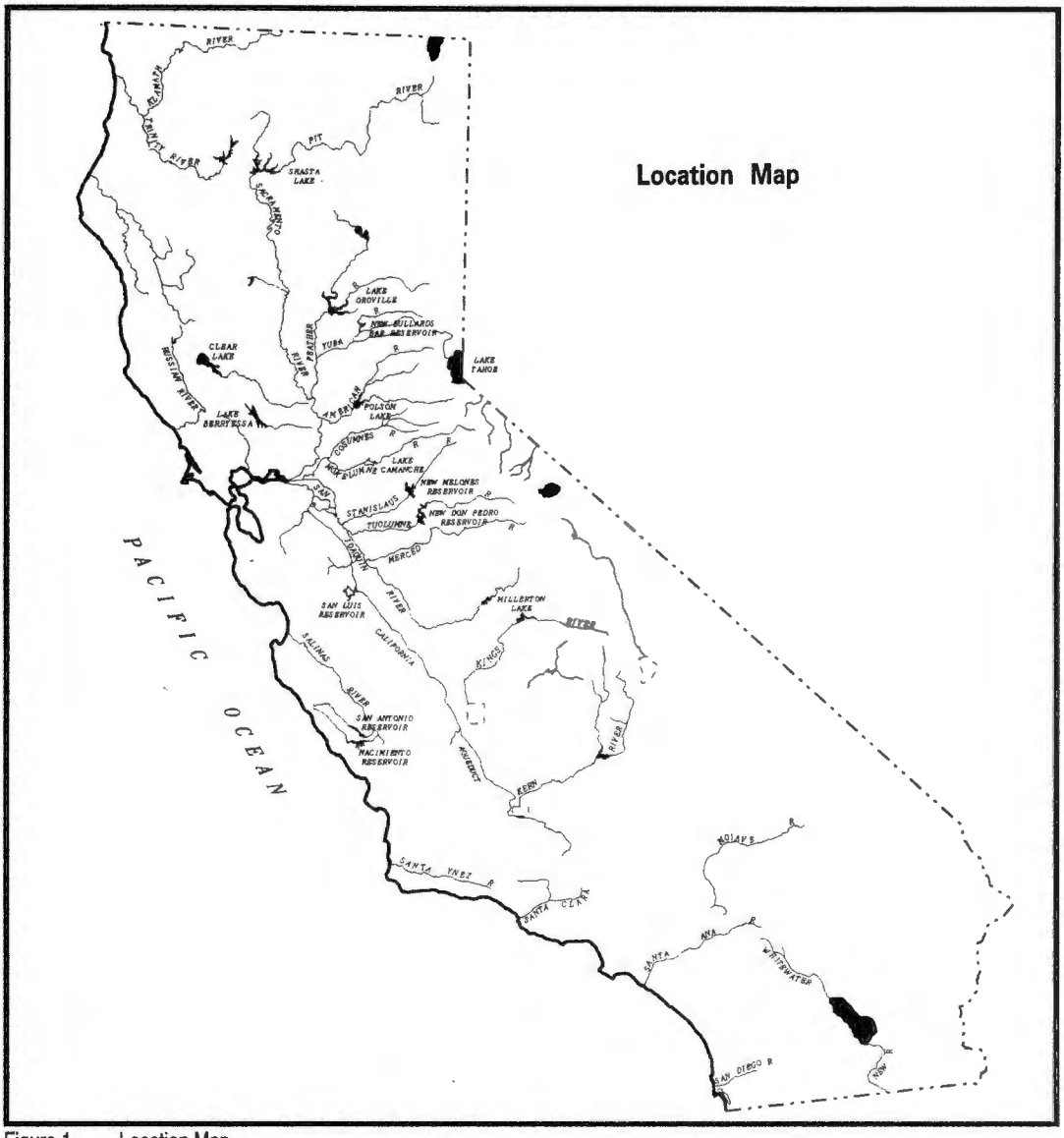

Figure 1 Location Map

In: R.C. Wilson and V.L. Tharp, Editors. 1998. *Proceedings of the Fourteenth Annual Pacific Climate (PACLIM) Workshop, April 6-9, 1997.* Interagency Ecological Program, Technical Report 57. California Department of Water Resources.

This was a classic orographic event, with warm, moist winds from the southwest blowing over the Sierra Nevada and dumping amazing amounts of rain at the middle and high elevations, especially over a 3-day period centered on New Year's Day. The sheer volume of runoff exceeded the flood control capacity of Don Pedro Dam on the Tuolumne River and Millerton Reservoir on the upper San Joaquin River with large spills of excess water. Most of the other large dams in Northern California were full or nearly full at the end of the storm.

Amounts of rain at lower elevations were not unusual. For example, downtown Sacramento, in the middle of the Central Valley, had 3.7 inches during the week from December 26 through January 2. But Blue Canyon, at the 1-mile elevation between Sacramento and Reno, had more than 30 inches, an orographic ratio of over 8, far more than the usual 3 to 4 for most storms. Many Central Valley folks could not understand that there was a problem, because they were not seeing a lot of rain. Meanwhile, the entire northern Sierra was seeing 20 inches, some 40 percent of average annual precipitation.

Floods were produced on the Coast Ranges as well, but not to record levels. The Russian, Napa, and Pajaro rivers did not rise as high as during the severe floods of 1995. Farther north, the Eel, Klamath, and Smith rivers rose higher than in 1995 but did not set records.

Antecedent conditions were conducive to high runoff. Heavy storms during the first half of December had saturated the ground.

The big storm was preceded by a very cold storm that produced heavy snow to low elevations a few days before Christmas. The lower-elevation snow melted during the New Year's storm (for example, at the mile high Blue Canyon station, 30+ inches of rain melted the 5 inches of water content in the snowpack), but the middle and high elevation snowpack remained, with the rain percolating through the pack. Not much loss was observed on the snow sensors higher than 6,000 feet, in spite of rain at elevations as high as 9,000 feet at times. Figure 2 shows accumulated precipitation on snow water content at the Alpha snow sensor at 7,600 feet near Echo Summit on Highway 50.

This contrasts with the popular impression that the melting snow caused the floods. Snowmelt, mostly from lower elevations, added perhaps 15 percent to the runoff, but the bulk of the runoff was simply from too much rainfall.

The total amount of precipitation at Blue Canyon for December and January was a record 75 inches, about 43 inches during December and 32 inches in January. The annual total at this station averages about 63 inches. The December amount was second wettest, after 1955, also a flood year.

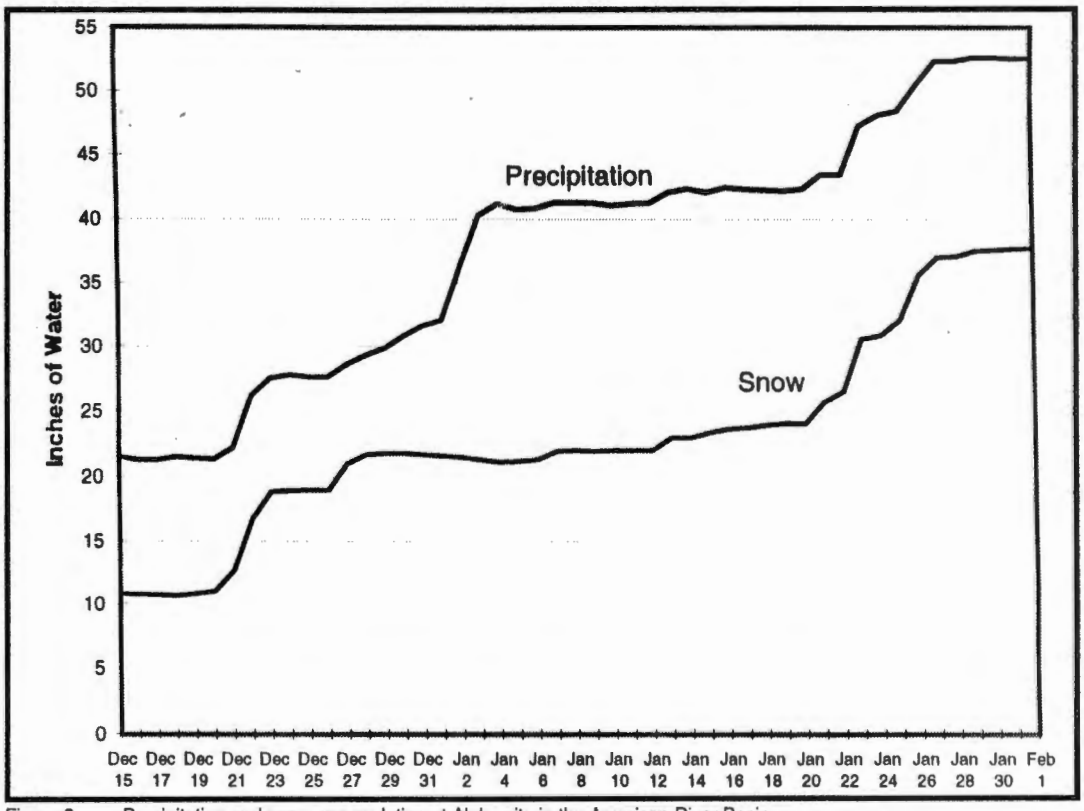

Figure 2 Precipitation and snow accumulation at Alpha site in the American River Basin

The overall Sacramento River regional flood control system performed well, greatly reducing peak flows on that system. Even so, at the latitude of Sacramento total flow in the river and in Yolo Bypass was estimated at 600,000 cubic feet per second, which is nearly half that of the combined flow of the Missouri and Mississippi rivers of 1.3 million cfs at St. Louis in the great flood of 1993. There were two serious levee breaks in the Sacramento Valley, one on the Feather River south of Marysville, the other on Sutter Bypass west of Yuba City (Figure 3). Major flooding occurred along the uncontrolled Cosumnes River southeast of Sacramento, on the Tuolumne River near Modesto, and on the San Joaquin River near Fresno. The volume of flood water overwhelmed dikes and produced massive flooding along the lower San Joaquin River from near the mouth of the Tuolumne River to the Sacramento-San Joaquin Delta near Manteca.

Rainfall was light after January 3, allowing the flood control system to drain and restoring reservoir flood control space. After January 20, another siege of heavy rain occurred. This was not as heavy as the year-end storms (about two-thirds as much and perhaps half as much at Shasta Dam) and, although warmer than normal, had snow levels about 2,000 feet lower, which helped hold more water on the mountains as snow. But even so, runoffs were large, with higher peaks on a few streams.

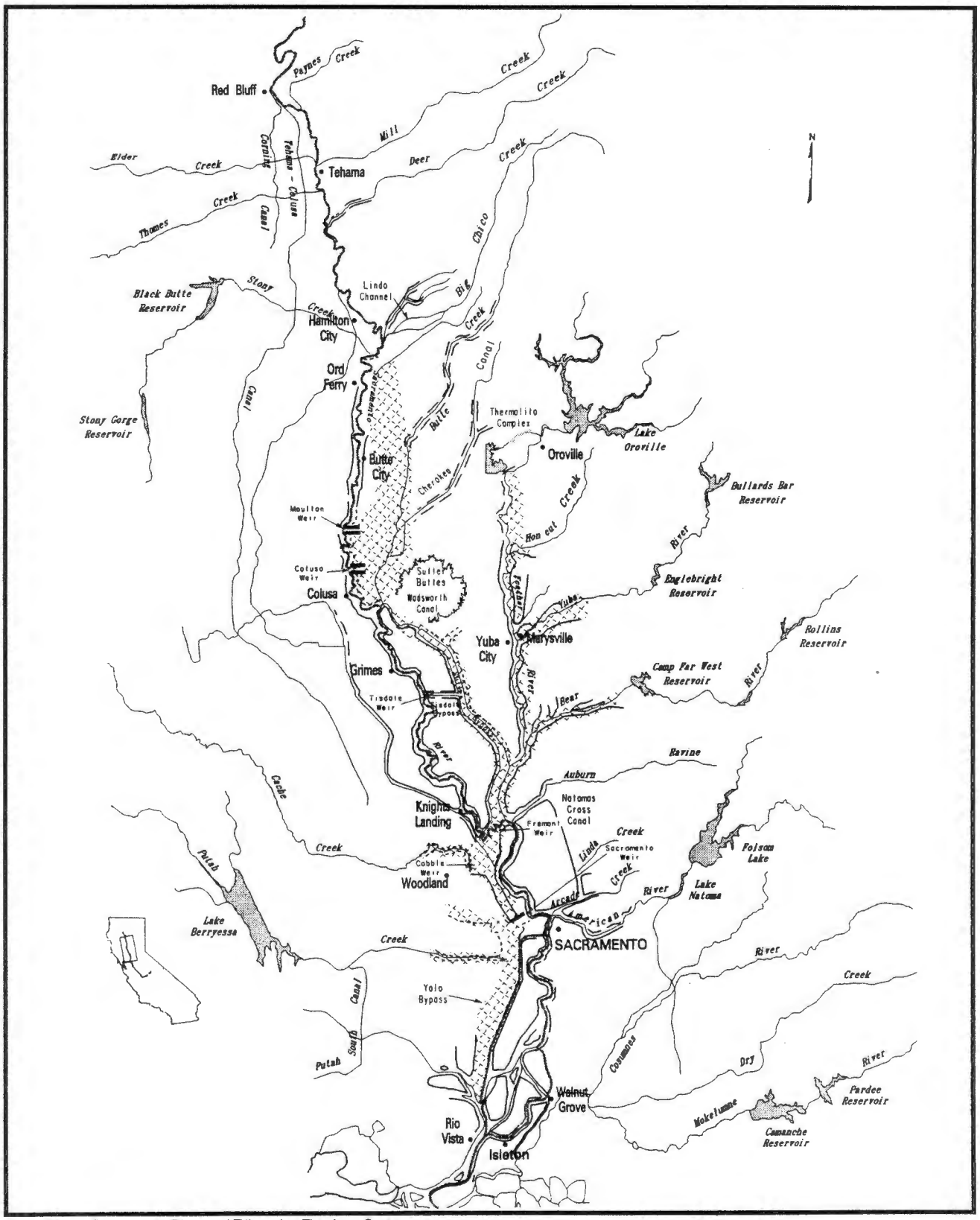

Figure 3 Sacramento River and Tributaries Floodway System

Sacramento River region reservoir flood control storage had been pretty well restored before the second storm, and it was handled quite easily, even restraining normal flood releases to avoid overtopping the partly completed levee break repairs on Sutter Bypass and along the Feather River south of Marysville. This time, low-elevation stations also caught heavy rain, with some local creek flooding.

In the San Joaquin River region (Figure 4), there had not been enough time to restore full flood control space. The channel capacity of the rivers is much more constricted than in the Sacramento Valley, limiting downstream releases. Rainfall amounts were quite heavy, with over 11 inches estimated in the Stanislaus and San Joaquin (above Friant) basins during a 7-day period. At one point, on January 24, in view of the weather forecasts, it appeared that a number of the foothill reservoirs would fill and spill and the California Office of Emergency Services and others were alerted. Happily, the next two days of rain were less than forecast and releases were controlled to channel capacity downstream. The subsequent peak at Newman gage on the San Joaquin River was 61.1 feet, exceeding the old record by 0.2 foot. Peak flow there was around 31,000 cfs. The sustained high flow continued to put strain on the levees, but no other significant breaks occurred.

Oroville Reservoir

Oroville Reservoir is a 3.5 million acre-foot reservoir on the Feather River of Northern California. It has 750,000 acre-feet of flood space, designed to control the standard project flood, a roughly 1/200 event. The standard project flood has a peak flow of 440,000 cubic feet per second and a 72-hour volume of 1.52 million acre-feet. This flood would be controlled to a release of 170,000 cfs — within channel design capacity downstream.

Initial estimates of peak inflow at Oroville were just over 300,000 cfs, reduced perhaps 30,000 cfs from unimpaired runoff by upstream storage. The estimated 3-day unimpaired volume seems to have been about 1.4 million acre-feet, about 92 percent of standard project flood. The peak is strange, looking almost truncated for about 12 hours (Figure 5).

In volume, this flood exceeded the previous record of the 1986 flood by quite a margin, perhaps 25 percent. At one point, on January 1, we thought the inflow would be so much that Lake Oroville would fill and spill — perhaps 250,000 cfs worth. People were evacuated from the city of Oroville downstream, but the rain eased a little sooner than expected, and the dam contained the runoff.

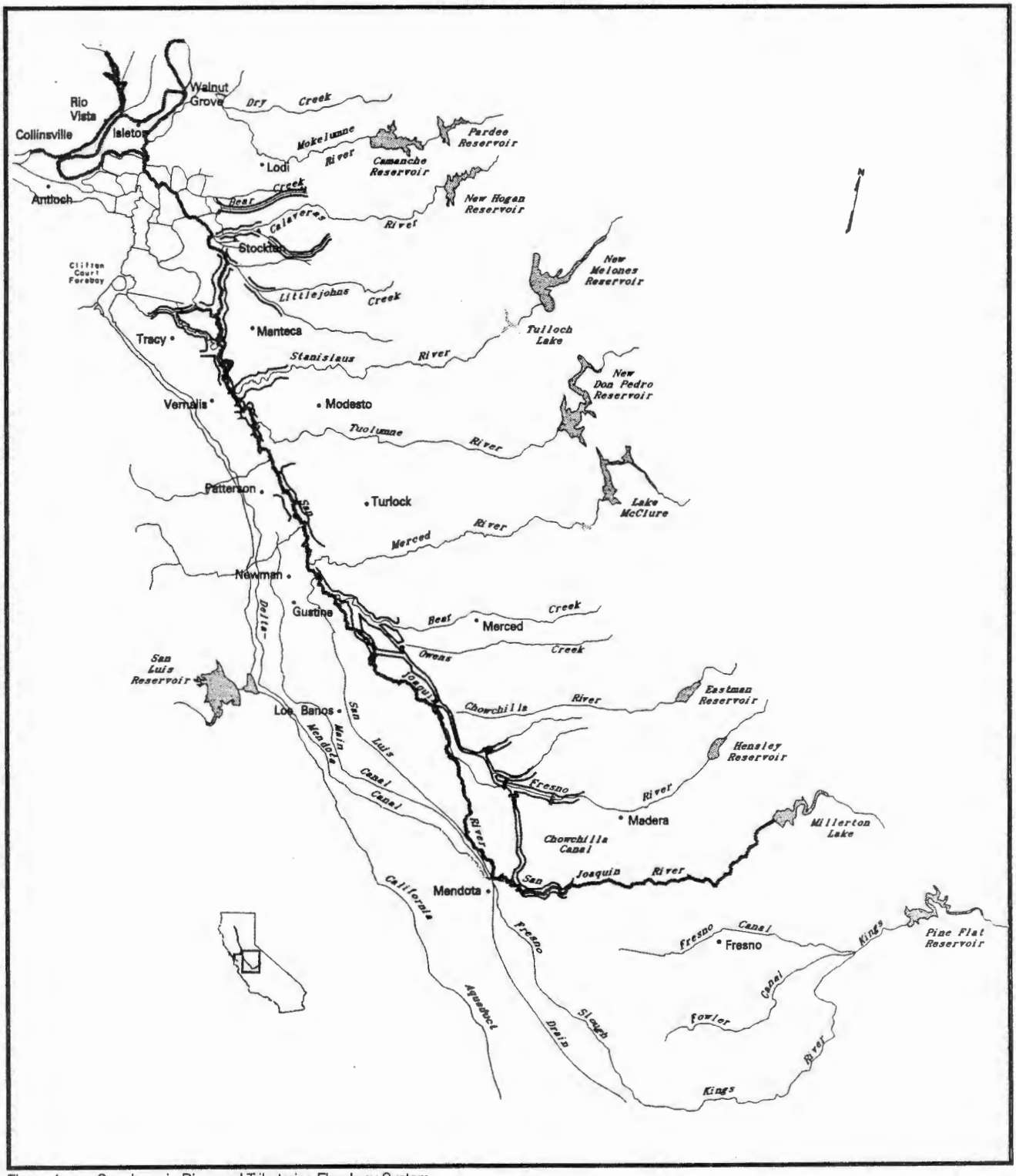

Figure 4 San Joaquin River and Tributaries Floodway System

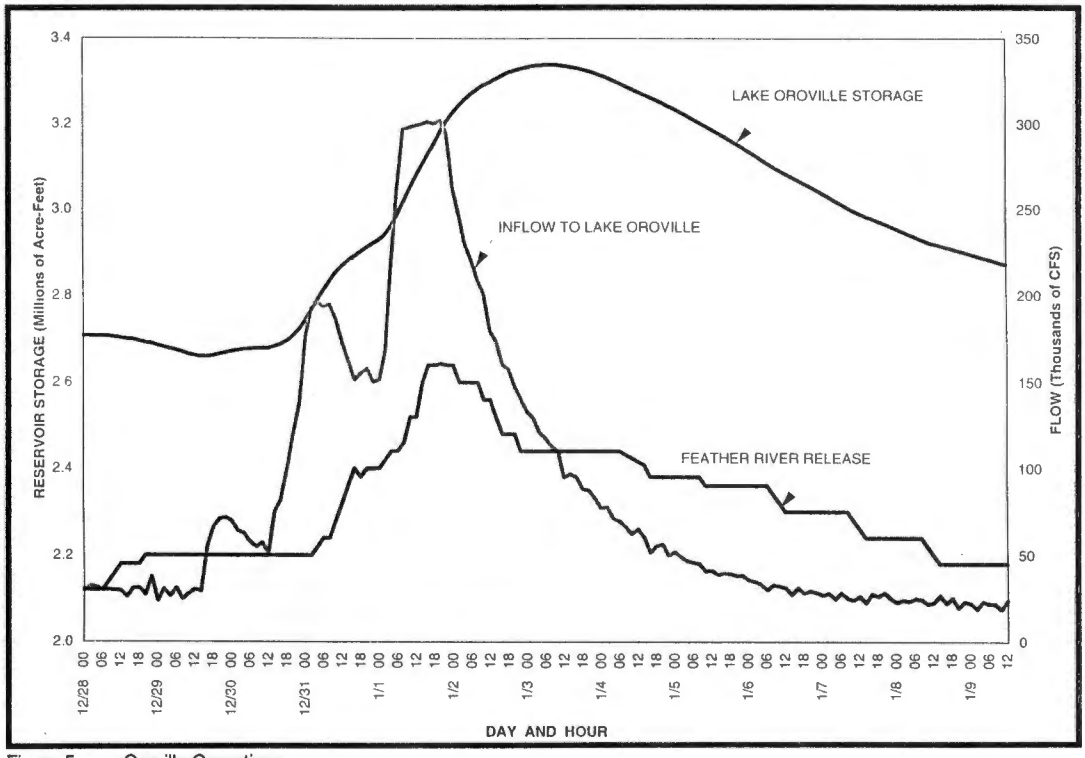

Figure 5 Oroville Operations

Comparison with Other Floods

I'd like to compare this flood to other floods this century using three Sacramento basin rivers. First, let's look at the 1-day estimated peak annual flows of the American River near Sacramento (Figure 6). Flood control on this stream has been the subject of controversy since the 1986 flood. Auburn Dam has been proposed to provide badly needed flood protection for the downstream urban area, but the proposal has been bogged down in environmental and cost controversy.

The existing major flood control dam, Folsom Dam, was designed just prior to 1950 and built in 1955, presumably to contain the standard project flood, with the record on hand. But look what has happened since. It seems there is a trend for bigger and bigger floods. Now, the original design probably doesn't provide over a 1 in 70-year protection. In spite of high levees, the consequences of a failure would be disastrous.

Where there are large flood control reservoirs, a better measure of comparison is the 3-day volume — which more nearly corresponds to the need for flood space (Figure 7). The 3-day chart on the American River (Figure 8) shows 1997 as essentially the same as 1986. Comparatively on the American River, the 1997 flood was a somewhat smaller flood than in river basins north and south of the American.

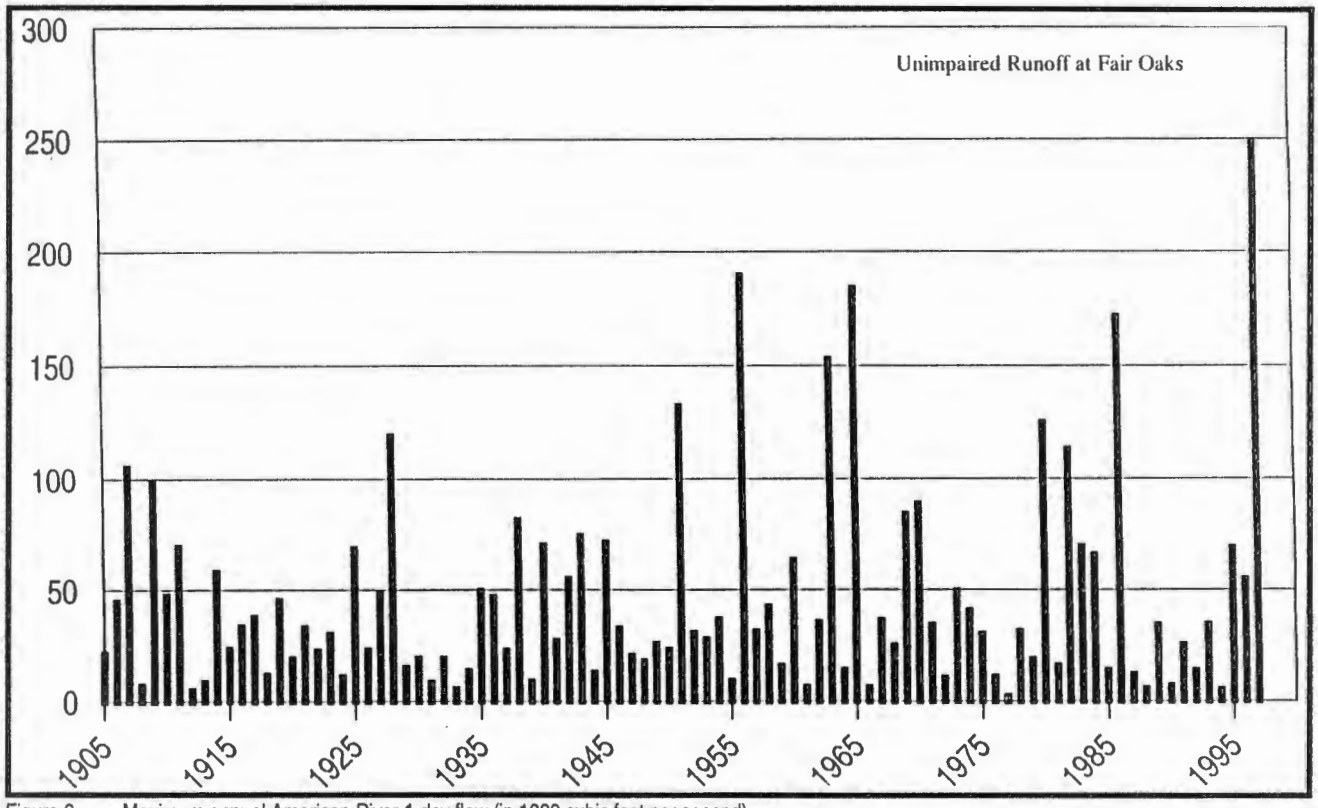

Figure 6 Maximum annual American River 1-day flow (in 1000 cubic feet per second)

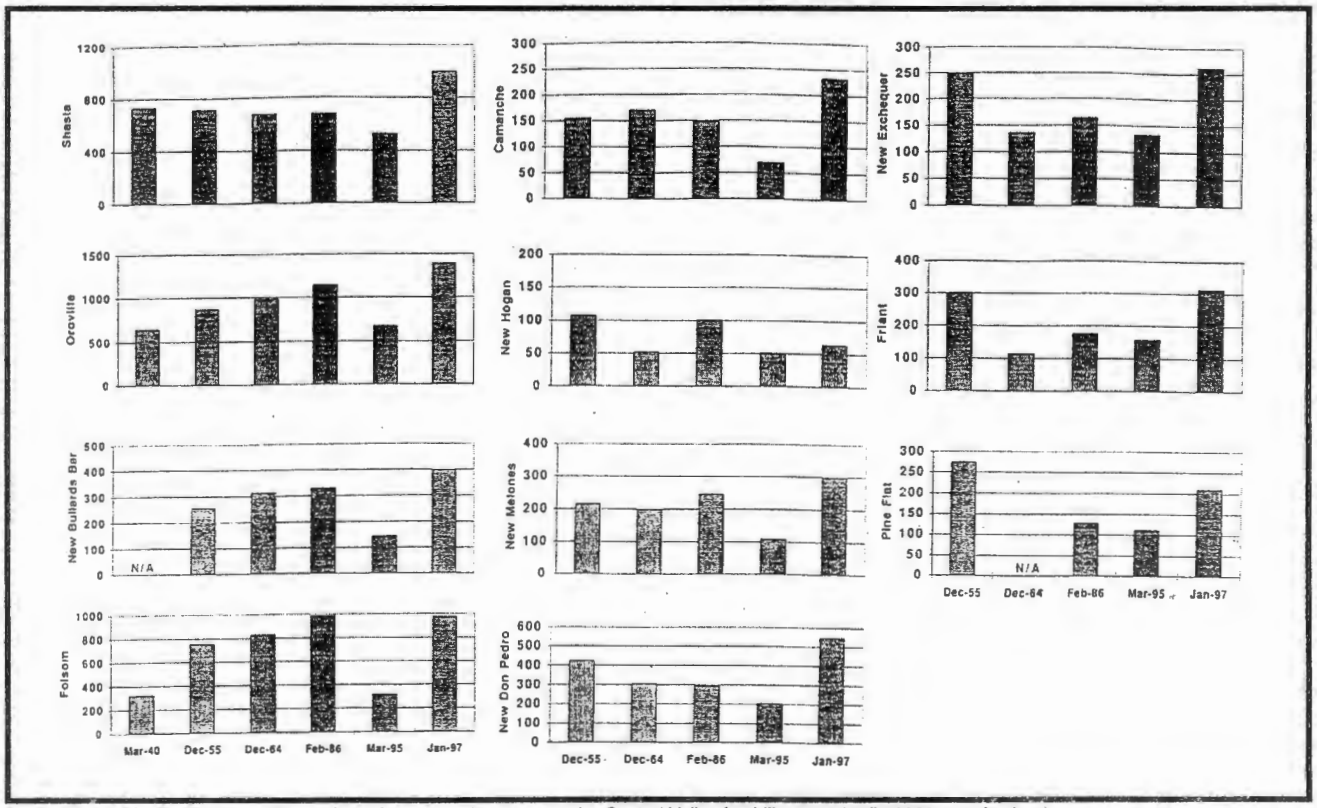

Figure 7 Maximum 3-day inflow volume for selected events—major Central Valley foothill reservoirs (in 1000 acre-feet)

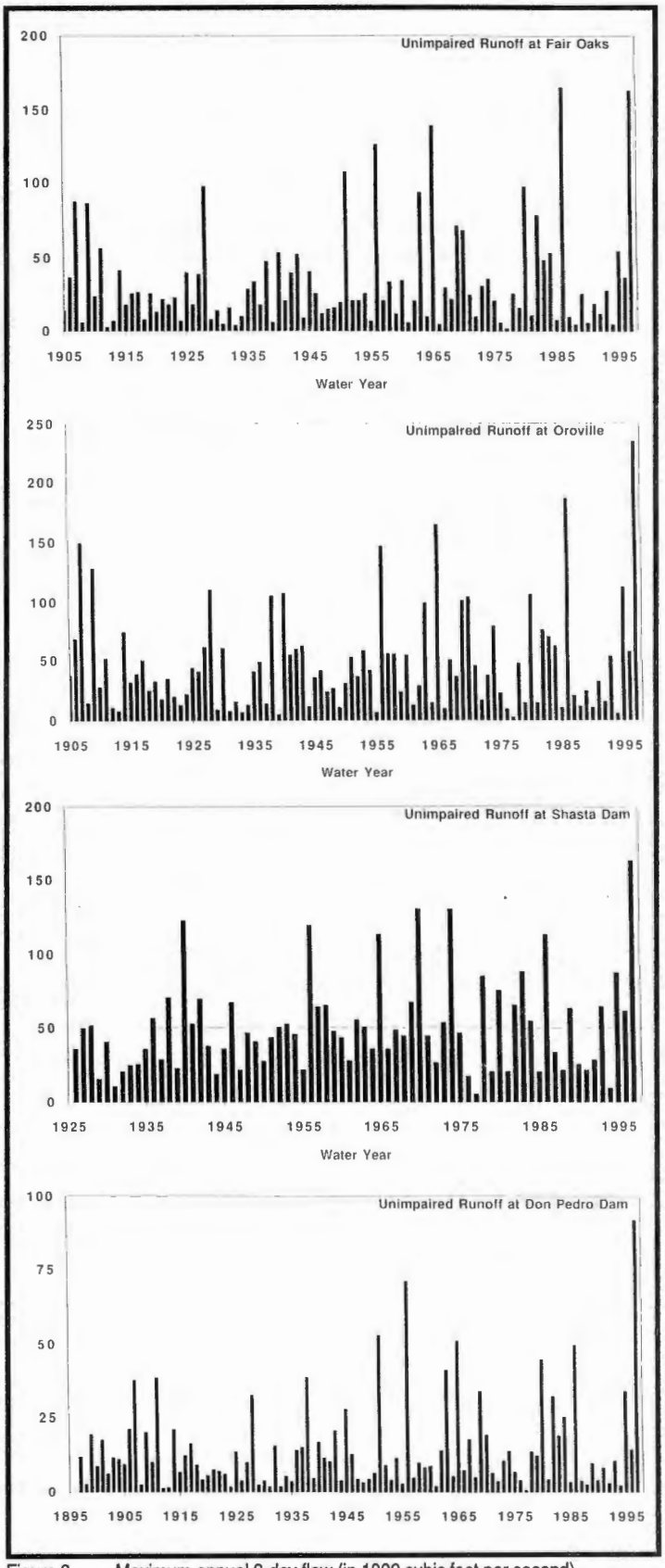

Figure 8 Maximum annual 3-day flow (in 1000 cubic feet per second)

The Feather River chart (Figure 8) shows the comparison for Oroville Dam. This one was perhaps 25 percent bigger than in 1986, which itself was the biggest to that time, although not too much more than a 1907 flood. Also, the increasing trend with time is not as obvious as on the American River, unless one looks at the last 1997 event.

Again, 1997 really stands out in the chart for the upper Sacramento River at Shasta Dam (Figure 8).

The Tuolumne River has 100 years of measured record, one of the longest in California. The 1997 flood was by far the biggest in the record (Figure 8). The only other near comparison was the December 1955 flood.

Figure 9 shows 3-day flood flows on the three Sacramento basin rivers, expressed as a ratio of the median flood. The historical medians are 44,300 cfs for the Sacramento River at Shasta Dam, 35,300 cfs for the Feather River at Oroville, and 22,400 cfs for the American River at Folsom. I've shown the 11 largest floods this century. Notice that the range (the ratio) becomes larger as one goes south to the American River. Also, the apparent increasing size trend is more

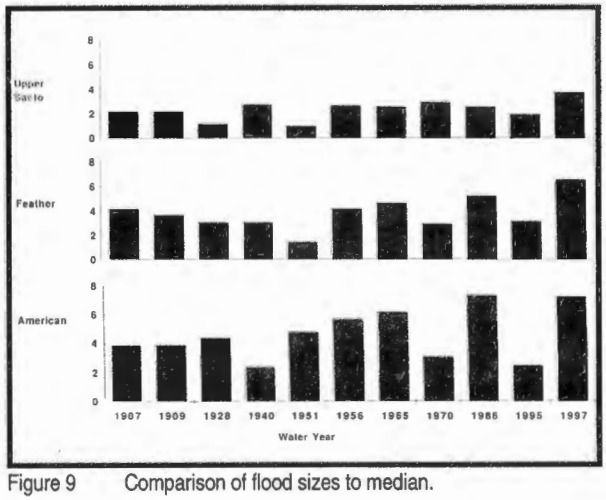

Figure 9 Comparison of flood sizes to median.

dominant in the American River. I'm not sure why. Could there be a possible influence from upwind urban areas?

Flood Frequencies

The recent flood again set many new records on major Sierra rivers. When these are plugged into a frequency determination, the amounts at a given frequency or the risk at given design levels will go up. We'll introduce a new round of charts and probably a bunch of determinations that the existing 100-year levels are not that anymore, but less, and a new round of project work will be needed to provide revised 100-year flood protection, some in areas that have just done a lot of work. This is one of the problems with working on statistics based on relatively short record. For major projects, perhaps we should go back to the old standard project flood idea or justify to some level of historical storm. People are being misled by all these numbers and risks, not realizing how tentative they are and the rather large uncertainty involved.

Conclusion

I'm sure there are a lot of other questions. But the great flood of 1997 is going to keep a lot of us busy for a while, evaluating its impact on how we provide flood protection for people and property and what the appropriate level of risk is. Looking back, it seems that we have often thought too small. Are we overreacting to an unusual event, or are things changing to the point when the past is not a reliable guide to the future?

The final report of the Governor's Flood Emergency Action Team, published in May 1997, recommends more than 50 long-term actions, which are now the basis for California's flood policy. Hopefully, as these are implemented, they will help protect the state from future flood disasters.

Teleconnections from Asia to the Canadian Prairies: Implications for Long-Range Weather and Crop Forecasting

E. Ray Garnett, Madhav L. Khandekar, and Jeff C. Babb

Abstract: The influence of the Indian/Asia monsoon on the El Niño/Southern Oscillation (ENSO) phenomenon and consequently on global climate is being increasingly recognized in recent years. Large-scale atmospheric circulations and features like Eurasian winter snow cover, the equatorial stratospheric quasi-biennial wind oscillation (commonly known as the stratospheric QBO) and the ENSO phenomenon are now identified as the large-scale controls of the Indian Monsoon. These macro scale features appear to provide teleconnective links to the Canadian prairie provinces through modulation of the Pacific North American atmospheric flow patterns.

The present study investigates the teleconnective link between large-scale features of Asia and the Indo-Pacific basin and the summer (June-July) weather patterns over the Canadian prairies. Associated with the modulation of the PNA atmospheric flow pattern is a sea surface temperature gradient in the North Pacific that appears related to Canadian prairie dry spells. Also the Pacific High, as measured by sea level pressure near Portland, is being examined as a possible precursor of climatic extremes over the Canadian prairies. Simple empirical analysis as well as statistical regression techniques are used to investigate this teleconnective link. Regression equations are being developed that include a suite of physically sound variables for explaining a large portion of Canadian prairie precipitation and temperature variation and ultimately for developing estimates of Western Canadian spring wheat yield with a lead time of 3 to 6 months.

Introduction

The Indian (Asian) monsoon is a vigorous atmospheric system that forms an important component of the atmospheric general circulation. The monsoon manifests itself during the Northern Hemisphere summer and provides rainfall of varying amounts over a large area of tropical and extratropical regions extending from east Africa to Japan. Several recent studies (Khandekar 1991, 1996; Khandekar and Neralla 1984; Garnett and Khandekar 1992; Bhalme, Rahalkar, and Sikdar 1987; Mooley and Parthasarathy 1984) have shown the Indian (and to some extent the Asian) monsoon to be intimately linked to some of the large-scale atmospheric features, namely El Niño/Southern Oscillation (ENSO), Quasi-Biennial Wind Oscillation (QBO), and Eurasian snow cover (ESC). More specifically, as set out by Khandekar (1996), these are the three main forcing functions for the Indian Monsoon.

The ENSO-monsoon connection has been hypothesized in a couple of recent papers (Khandekar 1991; Webster and S. Yang 1992). These and other related papers have hypothesized that the strength of the Indian/Asian monsoon may trigger an El Niño/La Niña event in the equatorial eastern Pacific. In a related paper, Yasunari (1990) has examined lag

In: R.C. Wilson and V.L. Tharp, Editors. 1998. *Proceedings of the Fourteenth Annual Pacific Climate (PACLIM) Workshop, April 6-9, 1997.* Interagency Ecological Program, Technical Report 57. California Department of Water Resources.

correlations between the Indian monsoon and sea surface temperatures at two selected locations (western and eastern Pacific) and has found interesting variation in the correlations, as shown in Figure 1. This figure shows how the Asian monsoon intensity can trigger variation in sea surface temperatures in the equatorial eastern and western Pacific. Another recent paper (Wainer and Webster 1996) suggests that inter-annual variability in the Pacific Ocean is produced by a combination of the monsoon variability and the internal dynamics of the coupled ocean-atmosphere system. Simply put, the Indian monsoon plays an active rather than a passive role in the global climate system.

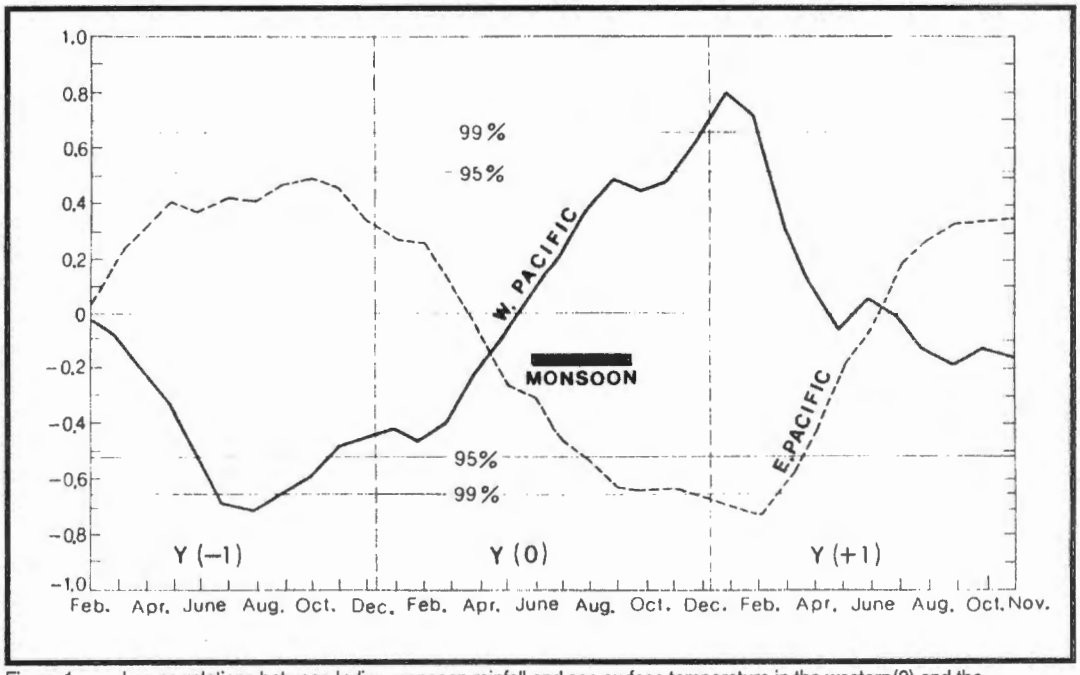

Figure 1 Lag correlations between Indian monsoon rainfall and sea surface temperature in the western(0) and the eastern Pacific. The reference monsoon season is shown with thick black bar. Y(0) denotes the year of reference monsoon and Y(-1) (Y(+1)) denotes the year before(after) the reference monsoon year.

Geographical Regions of Primary Concern

The two main geographical areas of interest in our research in Canada are the spring wheat growing region of the Canadian prairies, which produces on average about 25 mL tonnes of spring wheat annually and the United States corn crop, which constitutes 12% of world grain production based on U.S. Department of Agriculture statistics for 1985-1990 (Garnett and Khandekar 1992; Garnett, Khandekar, and Babb 1997).

Hypothesis

Khandekar (1991) hypothesized that a lighter (heavier) than normal Eurasian snow cover followed by a surplus (deficit) monsoon season over India and vicinity could induce a perturbation that would trigger an El Niño (La Niña) event in the eastern equatorial Pacific about 12-15 months following the surplus (deficit) monsoon season.

Forecasting the Indian Monsoon

Figure 1, taken from Yasunari (1990), shows the lag correlations between the Indian summer monsoon rainfall and the sea surface temperatures for wider areas in the equatorial western and eastern Pacific. It is noteworthy that the correlations of sea surface temperatures to Indian summer monsoon rainfall gradually increase from the summer of year(0) to the following winter, and reach the maximum (minimum) in January or February of year(+1) in the western (eastern) Pacific. Particularly in the western Pacific, the maximum value of the correlation coefficient reaches +0.79, which is far above the 99% confidence level. Relatively high correlations with sign opposite are found in the summer and fall months (June to November) of the year before year(-1), though these values are not as significant as those of the year(0)/year(+1) winter. Thus, sea surface temperature anomalies in the tropical Pacific, particularly in the western part, are closely associated with Indian monsoon activities in such a manner that sea surface temperatures follow as well as precede the monsoon with a lag of one to two seasons.

Other leading indicators helpful in forecasting the Indian monsoon are Eurasian snow cover in the winter months, and the 500 mb ridge position in April, which tends to be related to Eurasian snow cover (Table 1) (Garnett and Khandekar 1992). A greater than usual amount of snow cover usually means the 500-mb ridge position in April is displaced farther south than usual, prohibiting performance of the Indian monsoon. During the June-July period, concurrent correlations of +0.5 exist with Niño-3 sea surface temperatures and the QBO. The Niño-3 region is defined as the monthly SST anomalies over the Niño-3 region (5°N 5°S; 90°W-150°W) (Kousky 1989). During this period, El Niño conditions prohibit performance of the Indian monsoon while a westerly phase of the QBO favors performance of the Indian monsoon. The opposite influence exists with La Niña and the easterly phase of the QBO. Our research suggests that the QBO is of equal importance to El Niño in forcing the performance of the Indian monsoon during the June-September period.

Table 1
CORRELATION COEFFICIENTS BETWEEN
INDIAN MONSOON RAINFALL AND SEASONAL VALUES OF VARIOUS PARAMETERS

Seasonal Parameter	DJF Lag -2	MAM Lag -1	JJA Lag 0	SON Lag +1	DJF Lag +2
Sea Surface Temperature	0.33	–0.13	–0.51**	–0.72***	–0.69***
Southern Oscillation	–0.32	0.21	0.48*	0.62**	0.62**
April Ridge Location at 500 MB		0.53**			
Eurasian Snow Cover	–0.44*	–0.23	–0.13	–0.21	0.05
Stratospheric Winds:					
50 MB	–0.26	–0.09	0.51**	0.35	0.3
30 MB	0.09	0.28	0.40*	0.23	–0.03

* Significant at the 5% level.
** Significant at the 1% level.
*** Significant at the 0.1% level.

Importance of the Asian Monsoon and El Niño/Southern Oscillation

The Asian monsoon and ENSO phenomenon constitute the largest single source of interannual climatic variability on a global scale, and because their effects are wide ranging and often severe, it has attracted the attention of many scientists worldwide (Diaz and Markgraf 1992; Khandekar, personal communication, 1996). Recent research indicates that the ENSO phenomenon is generally a friend to the Canadian prairies during the summer (Garnett and Khandekar 1992). In 1997, Babb discovered a correlation of +0.6 between Niño-3 sea surface temperatures in April with July precipitation over the Canadian prairies, representing a leading lag of four months (Garnett, Khandekar, and Babb 1997). The Niño-1, Niño-2, Niño-3, and Niño 4 region of the world extend more than one quarter of the way around the planet and constitute an area greater than half the size of Canada. Large fluctuations in sea surface temperature anomalies in this region represent a huge source of energy.

Greatest Droughts in Recent History

Greatest droughts on the Canadian prairies in the past 50 years, 1961 and 1988, have occurred concurrently with a flood monsoon in India. Greatest global droughts since 1975 have also occurred a year after a monsoon failure (post El Niño). These years were 1975 in the former Soviet Union and 1983 and 1988 in the United States corn belt. These droughts came a year after a monsoon failure with an Indian flood monsoon the following year. The Indian monsoon is considered to be a flood monsoon when the percent of normal monsoon rainfall index for all India is greater than 110% of normal June-September and a drought monsoon when the index is less than 90% of the normal for June-September. Hence, highest risk situations for the Canadian prairies are those in which the monsoon is likely to flood or the years after a monsoon

failure when the monsoon floods. It is noteworthy that during the 1930s when dust bowl conditions prevailed on the Canadian prairies and in North America, there were no drought monsoons and three flood monsoons in India (Khandekar and Neralla 1984; John Knox, retired meteorologist Environment Canada, personal communication, 1992). Hence, the value in monitoring the main forcing functions that govern the performance of the Indian monsoon and knowing how the Indian monsoon performs each year. For example, a lack of Eurasian snow cover in the winter months; westerly stratospheric winds during June, July, and August; and La Niña conditions during June, July, and August would be somewhat ominous for the Canadian prairies and North America in general. About 80% of the time, La Niña conditions have had a major negative impact on North American weather (Dr. Gerald Bell, Climate Prediction Center, personal communication, 1996).

Pacific North American Teleconnection Index

A reflection of the El Niño/Southern Oscillation phenomenon is the Pacific North American teleconnection index, which was discovered by Wallace and Gutzler in 1981. The original four-point index is a measure of the 700-mb flow pattern over the eastern Pacific and North America. When the flow is zonal (*ie*, west to east) the index values are negative and when the flow is north-south or meridional, the index values are positive. The atmospheric flow over this very large region at 700-mb tends to be zonal during El Niño conditions and meridional during La Niña. As shown in Figure 2, the PNA index accumulates negatively during El Niño and positively during La Niña If a ridge is being thrown over North America, the PNA values will be positive beginning in September and will accumulate positively. In 1988, the hottest June-July on the Canadian prairies

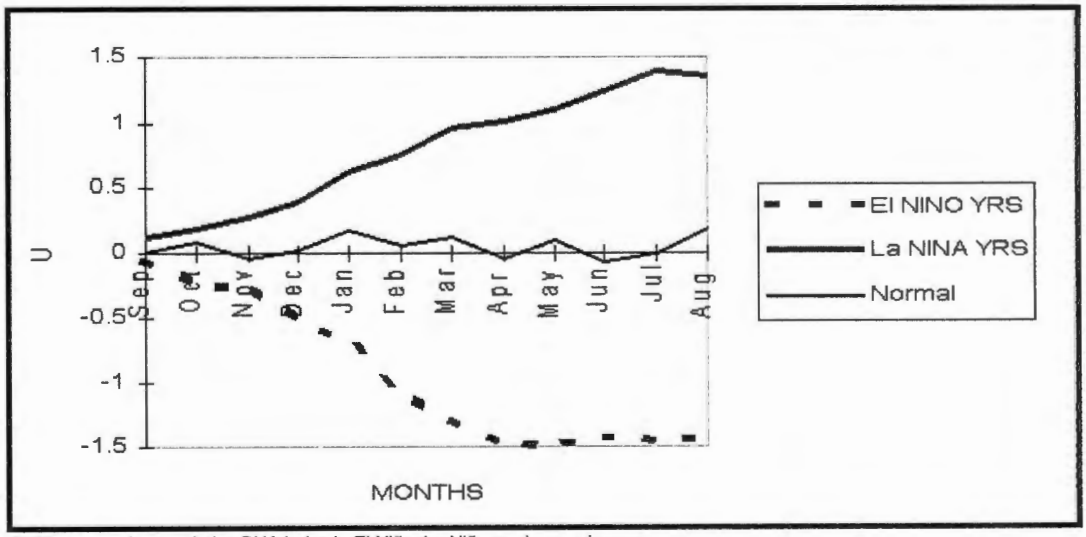

Figure 2 Accumulative PNA index in El Niño, La Niña, and normal years.
El Niño years (64/65, 71/72, 75,76, 81/82, 85/86)
La Niña years (69/70, 74/75, 82/83, 84/85, 87/88)
Normal years (66/67, 77/78, 78/79, 80/81, 89/90)

since 1964, and in 1993, the coldest June-July period since 1964, the four-point PNA index accumulated in a contrastingly different fashion (Garnett and Khandekar 1995). When the PNA index accumulates in a positive fashion, it has been termed as PNA blocking. There are many factors that may contribute to this blocking pattern, namely El Niño/La Niña, the Pacific High, and North Pacific sea surface gradient.

Influence of North Pacific Sea Surface Temperatures

In a Master's thesis done by Bonsal in 1991 at the University of Saskatchewan Geography Department, a gradient in North Pacific sea surface temperatures was investigated in relation to possible teleconnections to the Canadian prairies. Cold water in the southeastern Pacific combined with anomalously warm water off the coast of British Columbia has been associated with anomalous 500-mb heights over the Canadian prairies. When this positive anomaly persists at least 9 months, the probability of a major prairie dry spell was 100%. Dr. Bonsal hypothesizes that there is a feedback mechanism between the Aleutian Low and the gradient regions that he defined in his thesis. The Aleutian Low tends to be strong during an El Niño winter.

Statistical Findings

Using multiple regression analysis, it was found that up to 70% of the June-July temperature variation can be explained using a suite of predictors that includes Niño-3 sea surface temperatures in April and May prior to the growing season and the Pacific North American teleconnection index during September, October, November, and December prior to the critical growing period of June-July (Garnett, Khandekar, and Babb 1997).

It was found that up to 40% of the June-July precipitation prairie-wide can be explained using Niño-3 sea surface temperatures in March and April and the Pacific North American teleconnection index in September prior to the growing season and April Pacific North American index values prior to the growing season. A correlation of +0.59 has been discovered between Niño-3 sea surface temperatures in April and July rainfall on the prairies, a leading lag of 4 months establishing that El Niño conditions in the spring are favorable for the Canadian spring wheat crop. Concurrent correlations between Niño-3 sea surface temperatures and July precipitation are of the magnitude of +0.45. July precipitation is the most critical variable determining spring wheat yield on the Canadian Prairies (Garnett, Khandekar, and Babb 1997).

Wallace, J.M., and D.S. Gutzler. 1981. Teleconnections in the geopotential height field during the Northern Hemisphere winter. *Monthly Weather Review*, 109:784-812.

Webster, P.J., and S. Yang. 1992. Monsoon and ENSO selectively interactive systems. *Quarterly Journal Royal Meteorological Society*, 118:877-895.

Yasunari, T. 1990. Impact of Indian Monsoon on a Coupled Atmosphere/Ocean System in the Tropical Pacific. *Meterology and Atmospheric Physics*, 44:29-41.

Late Quaternary Paleoenvironmental Conditions Indicated by Marine and Terrestrial Molecular Biomarkers in Sediments from the Santa Barbara Basin

K.-U. Hinrichs, J. Rinna, and J. Rullkötter

Abstract: We investigated the relative distributions of selected extractable free lipids in sediments from the Santa Barbara basin, spanning the last 160 ka, to reconstruct paleoenvironmental conditions at the time of sediment deposition. The sediments were collected in 1992 during Ocean Drilling Program Leg 146. Climatic oscillations, affecting the Northeastern Pacific region and partly the Northern Hemisphere, are documented in sediment texture by a succession of laminated and homogeneous sediments, reflecting variations in bottom water oxygen content. Two major climatic features are documented in the 156 ka biomarker record from the Santa Barbara Basin:

Alkenone paleo-sea surface temperatures and terrestrial wax alkane chain length distributions indicate an outstanding character of the Eemian interglacial in the Late Quaternary regional history. We present evidence that the last interglacial climate in Southern California was warmer than that of the present interglacial and thus displayed typical characteristics of an El Niño-type situation.

Systematic variations of terrestrial *n*-alkane chain length distributions with bottom water oxygen-modulated sediment texture (laminated *vs* homogeneous sediments) reflect a sensitive coupling of oceanic and terrestrial paleoenvironmental conditions.

Introduction

The investigation of lipid biomarkers in continental margin sediments can provide valuable information on the paleoenvironmental history of marine and terrestrial environments (Brassell *et al* 1986, 1987; Prahl and Muehlhausen 1989). The determination of alkenone-derived paleo-sea surface temperatures (Brassell *et al* 1986; Prahl and Wakeham 1987) is an important established tool in paleoceanographic sciences. Marine sedimentary records of terrestrial organic matter were also shown to yield information on climatic variations in the corresponding source regions (Poynter 1989) or on periodic events of ice-rafted debris transport (Madueira *et al* 1997).

The sediments in the Santa Barbara basin are an excellent archive of paleoenvironmental information on both the marine and the nearby terrestrial environment. High sediment accumulation rates in the order of 1 m/ka allow for an excellent stratigraphic resolution of the entire sediment section (Ingram and Kennett 1995; Kennett 1995). The sedimentary organic matter is a mixture from marine and terrestrial sources (Hinrichs *et al* 1995; Stein and Rack 1995). Changing levels of bottom

In: R.C. Wilson and V.L. Tharp, Editors. 1998. *Proceedings of the Fourteenth Annual Pacific Climate (PACLIM) Workshop, April 6-9, 1997.* Interagency Ecological Program, Technical Report 57. California Department of Water Resources.

water oxygenation in response to Northern Hemisphere climatic oscillations led to an alternation of laminated and homogeneous sediments (Behl and Kennett 1996). Sedimentary pollen assemblages in homogeneous intervals deposited during glacials are generally consistent with a colder and more humid climate, whereas those in laminated glacial sediments correspond to warm and arid conditions (Heusser 1995). However, pollens fail to provide a consistent picture for terrestrial vegetation changes during periods of short-term fluctuations of climate and redox conditions at the sediment surface.

In this paper, we present paleoclimatic information derived from marine and terrestrial lipid biomarker profiles and emphasize the interrelationship of both environments.

Experimental Methods

A detailed summary of analytical conditions was presented by Hinrichs *et al* (1995). The sediments were recovered from Hole 893A drilled on Ocean Drilling Program (ODP) Leg 146 in December 1992. Sample aliquots of 10 to 15 g were extracted in a Soxhlet apparatus with a mixture of CH_2Cl_2 and MeOH (99/1, v/v). The resulting extracts were dissolved in a defined amount of *n*-hexane to precipitate the hexane-insoluble material. The hexane-soluble fraction was then separated by liquid chromatography into fractions of different polarity. The compounds of interest were analyzed by gas chromatography and combined gas chromatography-mass spectrometry. The average chain-length (ACL) values of major terrestrial higher plant-derived wax alkanes (C_{27}, C_{29}, C_{31}, C_{33}) were calculated after Poynter (1989, equation 1). The standard deviation in the determination of ACL values in replicate GC analyses was ±0.05.

$$ACL_{27-33} = \frac{27[n=C_{27}H_{56}]+29[n-C_{29}H_{60}]+31[n-C_{31}H_{64}]+33[n-C_{33}H_{68}]}{[n-C_{27}H_{56}]+[n-C_{29}H_{60}]+[n-C_{31}H_{64}]+[n-C_{33}H_{68}]}$$

(Equation 1)

The sea surface temperatures from unsaturation ratios of C_{37} long-chain alkenones ($U^{K'}_{37}$; Brassell *et al* 1987; Prahl and Wakeham 1987) were calculated according to the calibration of Prahl *et al* (1988). The error in the determination of alkenone concentrations due to uncertainties in peak integration led to an error of the $U^{K'}_{37}$ index of ±0.01, corresponding to an error in the SST values of ±0.3°C.

Evidence for an Outstanding Eemian Climate in Southern California

The Eemian climate is commonly regarded as an analog to that of the present interglacial. However, during the last decade a range of indications for significant differences of climatic patterns between the Holocene and Eemian interglacials were presented (*eg*, climatic instability during the Eemian [GRIP Members 1993; Fronval and Jansen 1996]; warmer paleo-sea surface temperatures in the tropical and southern Atlantic Ocean [Schneider *et al* 1995, 1996]). This tendency of higher water temperatures during the Eemian is particularly amplified in the Santa Barbara basin with a positive SST anomaly of 5-6°C (Hinrichs *et al* 1997; Herbert *et al* 1995), but is also evident, although less pronounced (about 3°C) in alkenone-SST time series from nearby oceanic sites to the north (R. Stax *et al* unpubl. data from ODP Leg 167).

The SST record from the Santa Barbara basin is presented in Figure 1a (modified from Hinrichs *et al* 1997). Alkenone-derived SST values in the 156-kyr record vary from 9°C to 19°C, with maximum temperatures in sediments from the Eemian climate optimum (about128-121 ka bp).

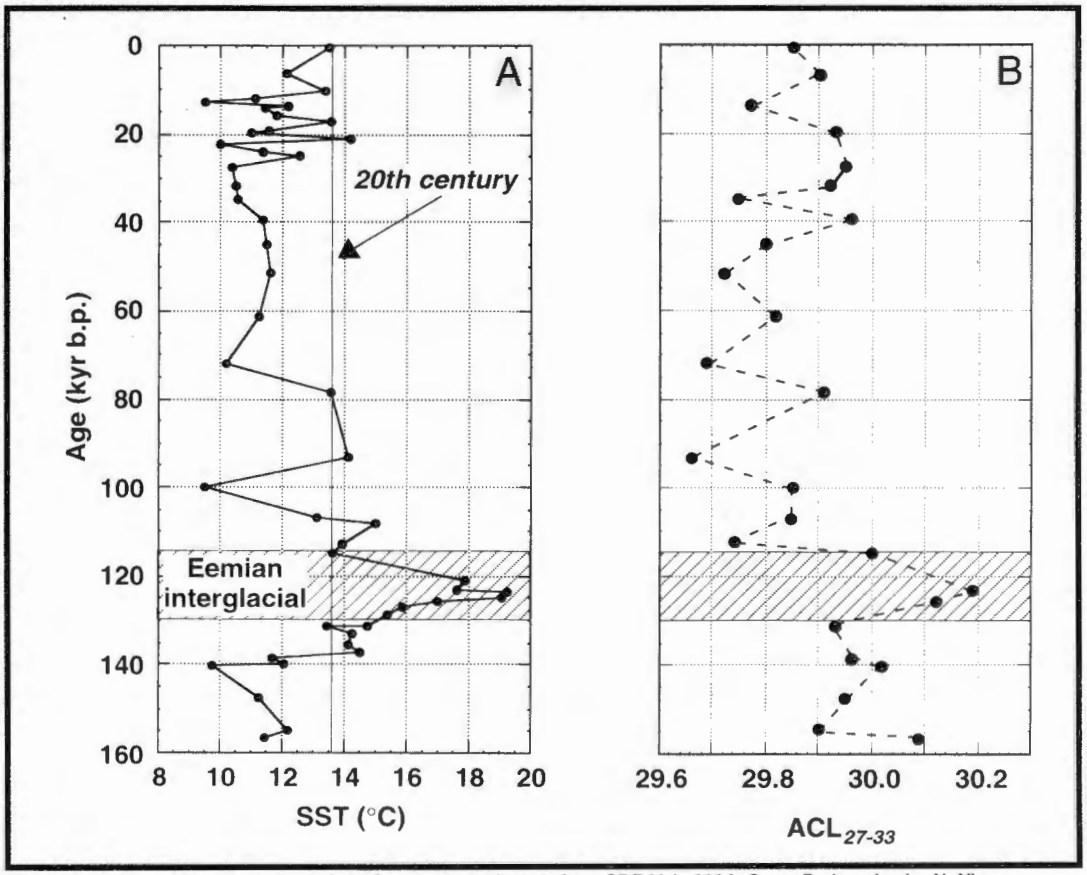

Figure 1 Biomarker time series in Late Quaternary sediments from ODP Hole 893A, Santa Barbara basin: A) Alkenone-derived SST data (from Hinrichs *et al* 1997). Given for comparation are mean annual SST values measured in 17 years during the second half of this century (cited by Kennedy and Brassell, 1992b). B) Average chain length (ACL) data of terrestrial higher plant-derived *n*-alkanes.

For comparison, representative mean temperatures from this century, measured in Santa Barbara basin surface waters, average at 13.6°C (data adopted from Kennedy and Brassell 1992). Assuming that the Eemian SST data also largely represent mean annual SST, as is the case in varves of the modern Santa Barbara basin (Kennedy and Brassell 1992a, b), the regional climatic situation significantly distinguishes the last and the present interglacials. In the present Santa Barbara basin, SST values as high as those in the Eemian sediments are only observed during El Niño years, when upwelling intensity and the influence of the California Current are drastically reduced. Therefore, we suggest a regional climatic regime for the California Borderland in the Eemian that displays major characteristics typical of an El Niño situation. Our interpretation of a prolonged El Niño-type climate in the Eemian is supported by model calculations, which predict the presence of an El Niño-type climate in response to an increase of the atmospheric CO_2 concentration above a certain threshold level (Meehl and Washington 1996).

Further evidence for the outstanding climatic situation of the Eemian interglacial is derived from the record of average chain length (ACL) distributions of terrestrial *n*-alkanes (Figure 1b). These compounds are constituents of the protective wax coatings of higher land plant leaves (*eg*, Eglinton and Hamilton 1967). In general, higher land plants biosynthesize waxes with higher relative abundances of long-chain compounds with decreasing latitude (Gagosian *et al* 1981, 1987; Simoneit *et al* 1981). In addition, waxes of tree leaves have compound distributions different from those of grasses with mostly the C_{29} *n*-alkane maximizing in trees and the C_{31} *n*-alkane in grasses (Cranwell 1973). The sensitivity of sedimentary *n*-alkane ACL values to past climatic changes was previously demonstrated by Poynter (1989).

The ACL values in the Late Quaternary record from the Santa Barbara basin vary between 29.66 and 31.19. Maximum values in this record were measured in sediments deposited during the climatic optimum of the Eemian interglacial. This observation strongly supports the presence of extraordinary climatic conditions in Southern California during the Eemian. In accordance with maximum SST values, we propose that the positive ACL anomaly reflects a warmer terrestrial climate. This climatic pattern may also explain the poorly understood elevated bottom water oxygen concentrations during the Eemian, which led to the deposition of homogeneous and bioturbated sediments in the central Santa Barbara basin (Kennett *et al* 1994).

Evidence for Coupling of Oceanic Conditions and Humidity Changes in Southern California

In addition to the Eemian anomaly, the ACL data reveal further information on paleoenvironmental variations on the continent (Figure 2). The lower-amplitude variations in this record are mostly related to alternating bottom water oxygen concentrations reflected by the presence or absence of laminae in the sediments. Although mostly taken from laminated intervals representing only a relatively short time span, the ACL values from laminated sediment samples tend to be remarkably lower than those from homogeneous samples. This implies that short-term oceanographic changes, associated with variations in bottom water oxygen concentration, were accompanied by concurrent environmental changes on the continent. In contrast to the Eemian positive temperature anomaly, these systematic ACL differences between the two sedimentary facies appear to be related to controls other than temperature changes.

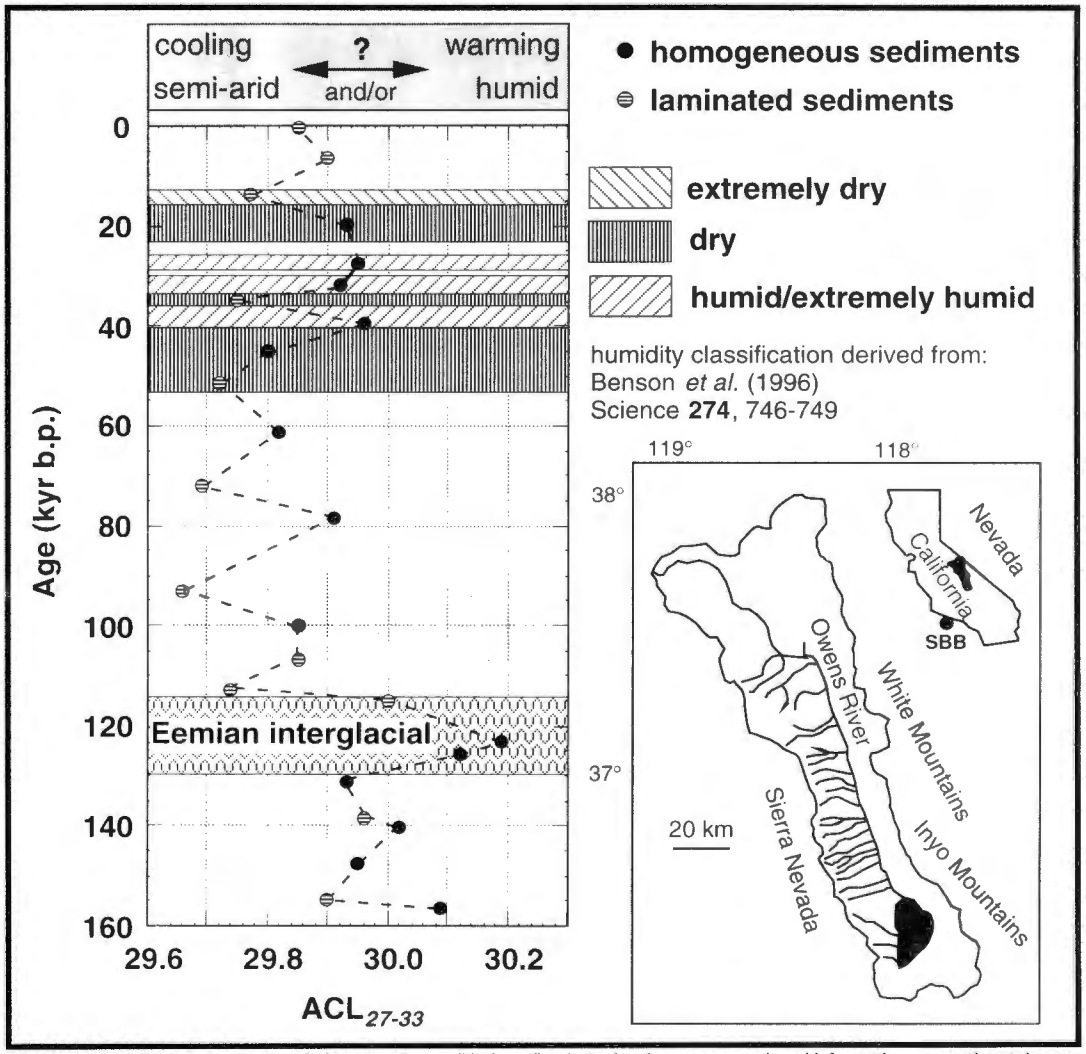

Figure 2 ACL times series in relation to sediment lithology (laminated vs homogeneous) and information on continental humidity from a study of a sediment core in the Owens Lake basin by Benson *et al* (1996).

This is indicated by relatively low ACL values in sediments deposited during the warm and semi-arid Holocene contrasting elevated values in sediments from the cold last glacial maximum.

Integrated information on continental humidity variations derived from a high-resolution study of Owens Lake basin sediments (Benson *et al* 1996; Figure 2) provides evidence of the factors controlling the sedimentary ACL variations, which occurred simultaneous to changes of oxygen concentration in bottom waters. ACL values higher than 29.9 in homogeneous sediments younger than 52 ky bp mostly correspond to humid or extremely humid conditions in the hinterland, whereas minimum values in the same interval coincide with periods of low precipitation. Furthermore, relatively low values occur in laminated sediments deposited during the semi-arid Holocene, whereas maximum values higher than 30.1 were recorded during the Eemian climatic optimum. Considering an El Niño-type climate for this period, these maximum values may also be related to more humid conditions.

We suggest that these signals preserved in *n*-alkane chain length distributions reflect systematic changes of paleoenvironmental conditions in Californian source regions of terrestrial detritus supplied to the Santa Barbara basin. Changing degrees of humidity were closely associated with oceanographic conditions through atmospheric/oceanic interactions. Our results complement those of Behl and Kennett (1996) who demonstrated the response of sediment surface redox conditions in the Santa Barbara basin to Northern Hemisphere climatic oscillations recorded in Greenland ice cores, and also those of Benson and coworkers (1996), who showed that the hydrography in the Owens Lake basin (California) was closely coupled to Northern Hemisphere climate.

Sedimentary ACL variations most probably recorded these climatic changes for the following two reasons:

- Vegetational patterns on the continent responded rapidly to short-term climatic oscillations, which were often characterized by drastic changes of temperature and precipitation. During relatively warm and dry Dansgaard-Oeschger interstadials when mainly laminated sediments were accumulated in the basin, smaller proportions of grass-derived biomass may have contributed to the sedimentary organic matter in the basin.
- Changes in continental precipitation patterns significantly affected the degree of erosion and the transport of terrigenous detritus to the ocean, enhancing the proportion of biomass from other source areas (probably over longer distances from higher altitudes). The latter hypothesis is considered to explain best the almost parallel and abrupt changes of oceanic conditions and terrestrial signals recorded in the sediments.

Conclusions

Lipid biomarker distributions in Late Quaternary sediments from the Santa Barbara basin reveal new information on the regional climate during the Eemian interglacial and on sensitive ocean/atmosphere interactions, respectively.

Both sedimentary alkenone-derived SST data and chain-length distributions of higher land plant-derived *n*-alkanes display positive excursions during the last interglacial, indicating a warmer and potentially more humid climate. Such a scenario can be explained as an analogy to a prolonged El Niño situation and provides an explanation for oxygenated bottom waters in the basin at that time.

Furthermore, the chain-length distributions of terrigenous *n*-alkanes indicate that the land climate has systematically changed concurrent to oceanic variations that affected the redox conditions at the sediment surface. Comparison to Recent lake records from the Californian hinterland (Benson *et al* 1996) provides evidence for continental humidity variations playing a major role in controlling the sedimentary *n*-alkane chain length distribution in Santa Barbara basin sediments. Apparently, precipitation patterns were most sensitively influenced by oceanic circulation changes. We suggest that during the formation of laminated sediments mainly a semi-arid to arid climate prevailed in the California Borderland area, whereas the periods of deposition of homogeneous sediments were accompanied by higher rates of precipitation.

References

Behl, R.J., and J.P. Kennett. 1996. Brief interstadial events in the Santa Barbara basin, NE Pacific, during the past 60 kyr. *Nature* 379:243-246.

Benson, L.V., J.W. Burdett, M. Kashgarian, S.P. Lund, F.M. Phillips, and R.O. Rye. 1996. Climatic and hydrologic oscillations in the Owens Lake Basin and adjacent Sierra Nevada, California. *Science* 274:746-749.

Brassell, S.C., G. Eglinton, I.T. Marlowe, U. Pflaumann, and M. Sarnthein. 1986. Molecular stratigraphy: a new tool for climatic assessment. *Nature* 320:129-133.

Brassell, S.C., G. Eglinton, and V.J. Howell. 1987. Palaeoenvironmental assessment of marine organic-rich sediments using molecular organic geochemistry. Pages 79-98 in *Marine Petroleum Source Rocks.* J. Brooks and A. J. Fleet, editors. Geological Society Special Publication 26, Blackwell, Oxford.

Cranwell, P.A. 1973. Chain-length distribution of *n*-alkanes from lake sediments in relation to postglacial environments. *Freshwater Biology* 3:259-265.

Eglinton, G., and R.J. Hamilton. 1967. Leaf epicuticular waxes. *Science* 156:1322-1335.

Fronval, T., and E. Jansen. 1996. Rapid changes in ocean circulation and heat flux in the Nordic seas during the last interglacial period. *Nature* 383:806-810.

Gagosian, R.B., E.T. Peltzer, and O.C. Zafiriou. 1981. Atmospheric transport of continentally derived lipids to the tropical North Pacific. *Nature* 291:312-314.

Gagosian, R.B., E.T. Peltzer, and J.T. Merrill. 1987. Long-range transport of terrestrially derived lipids in aerosols from the South Pacific. *Nature* 325:800-803.

GRIP-Members. 1993. Climate instability during the last interglacial period recorded in the GRIP ice core. *Nature* 364:203-207.

Herbert, T.D., M. Yasuda, and C. Burnett. 1995. Glacial-interglacial sea-surface temperature record inferred from alkenone unsaturation indices, Site 893, Santa Barbara Basin. Pages 257-264 in *Proceedings of the Ocean Drilling Program, Scientific Results, 146, Pt. 2.* J.P. Kennett, J. Baldauf, and M. Lyle, editors. Ocean Drilling Program, College Station, TX.

Heusser, L.E. 1995. Pollen stratigraphy and paleoecologic interpretation of the 160-k.y. record from Santa Barbara Basin, Hole 893A. Pages 265-279 in *Proceedings of the Ocean Drilling Program, Scientific Results, 146, Pt. 2.* J. P. Kennett, J. Baldauf, and M. Lyle, editors. Ocean Drilling Program, College Station, TX.

Hinrichs, K.-U., J. Rullkötter, and R. Stein. 1995. Preliminary assessment of organic geochemical signals in sediments from Hole 893A, Santa Barbara Basin, offshore California. Pages 201-211 in *Proceedings of the Ocean Drilling Program, Scientific Results., 146, Pt. 2.* J. P. Kennett, J. Baldauf, and M. Lyle, editors. Ocean Drilling Program, College Station, TX.

Hinrichs, K.-U., J. Rinna, J. Rullkötter, and R. Stein. 1997. A 160 kyr record of alkenone-derived sea-surface temperatures from Santa Barbara Basin sediments. *Naturwissenschaften* 843:126-128.

Ingram, B.L., and J.P. Kennett. 1995. Radiocarbon chronology and planktonic-benthic foraminiferal ^{14}C age differences in Santa Barbara Basin sediments, Hole 893A. Pages 19-27 in *Proceedings of the Ocean Drilling Program, Scientific Results., 146, Pt. 2.* J.P. Kennett, J. Baldauf, and M. Lyle, editors. Ocean Drilling Program, College Station, TX.

Kennedy, J.A., and S.C. Brassell. 1992a. Molecular records of twentieth-century El Niño events in laminated sediments from the Santa Barbara basin. *Nature* 357:62-64.

Kennedy, J.A., and S.C. Brassell. 1992b. Molecular stratigraphy of the Santa Barbara basin: comparison with historical records of annual climate change. *Organic Geochemistry* 19:235-244.

Kennett, J.P. 1995. Latest Quaternary benthic oxygen and carbon isotope stratigraphy: Hole 893A, Santa Barbara Basin, California. Pages 3-18 in *Proceedings of the Ocean Drilling Program, Scientific Results, 146, Pt. 2.* J.P. Kennett, J. Baldauf, and M. Lyle, editors. Ocean Drilling Program, College Station, TX.

Kennett, J.P., J. Baldauf, and M. Lyle. 1994. *Proceedings of the Ocean Drilling Program, Initial Results., 146, Pt. 2.* Ocean Drilling Program, College Station, TX.

Madueira, L.A.S., S.A. van Kreveld, G. Eglinton, M.H. Conte, G. Ganssen, J.E. van Hinte, and J.J. Ottens. 1997. Late Quaternary high-resolution biomarker and other sedimentary climate proxies in a northeast Atlantic core. *Paleoceanography* 11:255-269.

Meehl, G.A., and W.M. Washington. 1996. El Niño-like climate change in a model with increased atmospheric CO_2 concentrations. *Nature* 382:56-60.

Poynter, J.G. 1989. *Molecular Stratigraphy: the Recognition of Palaeoclimatic Signals in Organic Geochemical Data.* University of Bristol, Bristol, 324 pages.

Prahl, F.G., and L.A. Muehlhausen. 1989. Lipid biomarkers as geochemical tools for paleoceanographic study. Pages 271-288 in *Productivity of the Ocean: Present and Past.* W.H. Berger, V.S. Smetacek, and G. Wefer. John Wiley and Sons Ltd., New York.

Prahl, F.G., and S.G. Wakeham. 1987. Calibration of unsaturation patterns in long-chain ketone compositions for paleotemperature assessment. *Nature* 330:367-369.

Prahl, F.G., L.A. Muehlhausen, and D.A. Zahnle. 1988. Further evaluation of long-chain alkenones as indicators of paleoceanographic conditions. *Geochimica et Cosmochimica Acta* 52:2303-2310.

Schneider, R.R., P.J. Müller, and G. Ruhland. 1995. Late Quaternary surface circulation in the east equatorial Atlantic: Evidence from alkenone sea surface temperatures. *Paleoceanography* 10:197-219.

Schneider, R.R., P.J. Müller, G. Ruhland, G. Meinecke, H., Schmidt, and G. Wefer. 1996. Late Quaternary surface temperatures and productivity in the east-equatorial South Atlantic: Response to changes in trade/monsoon wind forcing and surface water advection. Pages 527-551 in *The South Atlantic: Present and Past Circulation.* G. Wefer, W.H. Berger, G. Siedler, and D.J. Webb, editors. Springer-Verlag, Berlin.

Simoneit, B.R.T., R. Chester, and G. Eglinton. 1977. Biogenic lipids in particulates from the lower atmosphere over the eastern Atlantic. *Nature* 267:682-685.

Stein, R., and F. Rack. 1995. A 160,000-year high-resolution record of quantity and composition of organic carbon in the Santa Barbara Basin (Site 893). Pages 125-138 in *Proceedings of the Ocean Drilling Program, Scientific Results, 146, Pt. 2.* J.P. Kennett, J. Baldauf, and M. Lyle, editors. Ocean Drilling Program, College Station, TX.

Abstracts 1997

Listed Alphabetically by First Author

Oral Presentations

Searching for Links Between the Patterns of Interdecadal to Centennial Variability in the California and Peru-Chile Current Systems

Tim R. Baumgartner, Andy Soutar, and Vicente Ferreira
CICESE, Ensenada, B.C., Mexico
Scripps Institution of Oceanography, University of California-San Diego

Recent work has shown that regional dynamics of the California Current is linked to larger-scale, basin-wide circulation driven by ocean and atmosphere coupling over interdecadal periods. Whether this is true for the Peru-Chile Current system—and whether there is some dynamic linkage across the tropics which may synchronize variability in the two Pacific Eastern Boundary Currents is an open question. Investigating the character of this interdecadal and longer period variability is hampered by the short length of instrumental records and the limited extent of records in the southern hemisphere. We are now working to develop natural archives from a number of depositional sites with anoxic, non-bioturbated conditions in both systems that will provide sufficient temporal resolution plus the spatial coverage necessary for comparative studies of interdecadal to centennial variability in ecosystem structure and ocean climate. This is a report on the progress made so far to initiate these comparative studies.

One of the principle tools we are applying to this work is the use of accumulation rates of fish scales of small, schooling pelagic species like sardines and anchovies. Changes in basin-wide ocean climate result in the latitudinal expansion and contraction of suitable habitat (with increase/decrease in overall abundance of the populations) for these species within the current systems. This appears to be particularly true for the sardine which is somewhat more sensitive to changes in temperature than is the anchovy (at least in the California system).

The best known record of these populations in the northern hemisphere is the 1600-year history from the Santa Barbara Basin off southern California (representing variability in the central region of the California Current). Two other sites are located at the southern and northern extremes of the California Current system. These are the Soledad Basin off southern Baja California, Mexico (with a 200-year record so far) and a small fjord on the west coast of Vancouver Island (Effingham Inlet, discovered in December 1995, studies are just beginning).

There are two sites in the Peru-Chile system known so far to have continuous, high-resolution fish-scale deposition records for the past 100 to 150 years. Both of these are off Peru, one off Callao at 12°S (record

from 1885-1975), the other off Pisco, just north of 15°S (record from 1825-1975). These two sites are ideally located to track equatorward expansion of sardine habitat from the population center off northern Chile. The Peruvian chronology is based on ^{210}Pb and is reliable at least to the base of the core off Callao.

Comparison of the California and Peru fisheries records, in combination with the paleo fish-scale record back to the 1880s suggest that inter-decadal change was generally synchronous, exhibiting two periods of coastal warming (and expansion of sardine habitat) from approximately 1910 into the 1940s, and form the 1970s into the 1980s for Peru and into the 1990s in the California system.

Sunspot Cycles and Santa Barbara Basin Sediments

Wolfgang H. Berger and Carina B. Lange
Scripps Institution of Oceanography, University of California-San Diego

Whether sunspot cycles affect the weather has been a topic of discussion for some time. To check for relationships between sunspot activity and climate, we studied the deposition of yearly sediment layers ("varves") in the center of Santa Barbara Basin, off California. The thickness of these varves depends on supply of mud through runoff, which in turn is tied to precipitation in the catchment region. An adequate sunspot record is available for the time since AD 1700. Thus, our varve record (detrended for compaction) can be compared with sunspot activity over this time span. A visual comparison shows no obvious relationship between the two records. Fourier expansion of an autocorrelation record (regression of 100-year section sliding past the entire record, from 0 lag to 200 yr) yields spectral characteristics for the two series. The sunspot spectrum is characterized by cycles with periods between 9.2 and 12.1, with peaks at 9.9 yr, 10.5 yr, and 11.2 yr. Among the longer periods, there is a strong peak near 95 yr, and a broad one near 50 yr. The intermediate range is occupied by a modest peak at 21.3 yr. The spectrum of varve thicknesses is distinctly different from that of the sunspots. The dominant period is at 24 yr, in a region with little or no sunspot power. Other important peaks are at 84 yr and 52.5 yr. In the vicinity of major sunspot variation (9.2 to 12.1 yr) there is but one period in the varve data, near 11.8 yr. Also, there are cycles near 15.5 yr, 7.2 yr, and 6.6 yr.

Our data suggests that there is little or no direct relationship between sunspots and the weather around Santa Barbara, California (a region influenced both by El Niño and changes in the strength of the Aleutian Low). Any apparent correlation, within the band of maximum activity, apparently is due to coincidental alignment with the periods at 11.8 yr, 15.5 yr, and 24 yr. These alignments change through time, so that conclusions drawn from a 80-year study in AD 1900 would be diametri-

cally opposed to those drawn from similar study done in 1800 AD. We note that a beating of the major sunspot period at 9.9 yr with those at 11.2 yr and 12.1 yr should yield difference tones of 85 yr and 54 yr, respectively. Also, a beat of 11.2 yr with 21.3 yr produces a difference tone at 23.6 yr, which might conceivably resonate with the dominant period in the system producing our record. Thus, we cannot exclude subtle effects of sunspot cycles on climate at the longer periods, and perhaps even at the dominant varve cycle. However, the period near 11.8 yr seems unrelated to sunspots. We note that this period (11.84, as found by detailed Fourier expansion) is very close to the Jupiter period of 11.86 yr. In fact, if we assume that we missed one year, in an interval of disturbed varves between AD 1835 and AD 1840, the variation in varve thickness at the ~12-yr period is then exactly in phase with Jupiter-Sun conjunction late in November, over the last 300 years.

Decadal Variability of Snow in the Western United States

Dan Cayan and Larry Riddle
Scipps Institution of Oceanography, University of California-San Diego
U.S. Geological Society

Much of the water supply in the western United States is derived from snowmelt runoff. For example, it is estimated that 75 percent of the annual discharge of most of the major streams in the western U.S. is from melting mountain snowpack (Palmer 1988). Topography plays a strong role—the heaviest snow accumulations are at middle-to-high elevation mountain sites usually with exposures to the west or southwest. In the Sierra Nevada, the primary water-bearing region for California, most snowmelt is derived from snowpack accumulated during winter storms at elevations above 1,300 meters. Regional precipitation is very seasonal; most locations west of the Rocky Mountains have a winter maximum and a summer minimum. Combined with the annual temperature cycle, this seasonality produces a spring maximum in snow accumulation, so that most snow courses attain their climatological maximum snow water equivalent (SWE) at about the beginning of April. Snow course observations are generally collected on or about the first of the month during the winter and spring. The greatest frequency of sampling over the historical period is for April 1.

How much variability occurs in the snow accumulation? A survey of historical snow course records over the western states indicates the coefficient of variation (CV) of April 1 SWE ranges from 20 percent to well over 100 percent. For the 200 snow courses used in this study, 45 had a CV $\geq$50 percent, while only 23 had a CV $\leq$25 percent. This level of variability is comparable to that of seasonal precipitation over this region (Granger 1977; Chanagnon *et al* 1991). Snowpack accumulations are coherent over scales of at least a few hundred kilometers; Aguado (1990)

showed in California that for 28 snow courses across the Sierra Nevada, over 80 percent of the variance of SWE was accounted for by a single principal component.

Although mountain snow accumulations have been routinely monitored for several years to gage water supplies, these measurements have not been fully exploited as a climate data set. A comprehensive study of short period climate variability of snow pack in the West has not been undertaken, but there are noteworthy regional examples. In examining snow course records in the Rocky Mountains, Chanagnon *et al* (1991) demonstrated that spring snow accumulation serves as a regional climatic indicator; Chanagnon *et al* (1993) derived effects of synoptic atmospheric circulation patterns and a tendency for out-of-phase multi-year shifts in snow accumulation and associated circulation patterns over the central part of the northern and southern Rocky Mountains. Concerning El Niño, Redmond and Koch (1991) demonstrated that snowfall in Oregon is significantly biased with a low in years with a low Southern Oscillation Index (SOI) relative to those with a high SOI; and Cayan and Webb (1992) derived the pattern of SWE over the western United States in conjunction with the SOI.

Both precipitation and temperature affect snowpack, but their aggregate impacts are not entirely clear. There does not appear to be a strong temperature-snow relation over the entire region (Walsh *et al* 1982; Leathers and Robinson 1993; Karl *et al* 1993). However, anomalous temperature impacts are evident in Sierra Nevada spring runoff variations (Aguado *et al* 1992; Cayan *et al* 1993). Also, winter temperature trends appear to be involved in a decades-long change in the fraction of runoff occurring in late spring and summer runoff found in the Sierra Nevada and many other snowmelt-driven streams over the western United States (Roos 1987, 1991; Wahl 1992; Aguado *et al* 1992; Dettinger and Cayan 1995). Its dependence on temperature makes snow a key diagnostic in climate change scenarios (e.g., Gleick 1987; Roos 1989; Lettenmaier and Gan 1990; Dettinger and Jeton–in press). Temperature and precipitation are not well correlated during the cool seasons in the West (Zhao and Khalil 1993; Cayan and Peterson 1993), so their individual influences on snowpack should be separable.

A Mid-to Late-Holocene Stratigraphic Record from Los Penasquitos Lagoon, Southern California

Kenneth L. Cole and Eugene R. Wahl
Department of Forest Resources, University of Minnesota
Department of Ecology, Evolution, and Behavior, University of Minnesota

Several sediment cores from Penasquitos Lagoon, within the Torrey Pines State Reserve, California, reveal the sedimentological and vegetational changes occurring over the last 4,000 years. Fossil pollen, charcoal, chemistry, magnetic susceptibility, and particle size were analyzed in order to characterize late-Holocene environments in and near the estuary. The sediment cores were dated using radiocarbon dates and pollen stratigraphy of recently introduced exotic species. The pollen analysis suggests a major expansion of grasslands around 2700 year B.P. followed by a contraction around 1800 year B.P. Post-settlement sediments in the top 60 cm of the core are indicated by a rise in the magnetic susceptibility of the sediments and increases in exotic pollen taxa such as storksbill (*Erodium* sp.). These data were used to reconstruct the population and fire history of the nearby stand of Torrey Pine (*Pinus torreyana*). The Torrey Pine stand, one of only two native stands, has been present at the site throughout the 4,000 year record recovered thus far. Past levels of microscopic charcoal are moderately high throughout the record, especially during the last 2,000 years. The increase in charcoal around 2000 year B.P. could be due to changing climates, changing cultural practices by native Californians, or both. Charcoal values increase further around AD 1800, possibly due to burning to increase cattle forage as early ranching began in the area. By the mid-1800s charcoal values decrease and stay at low levels until the late 1900s.

High-Resolution Palaeoclimatic Reconstructions from Annually-Laminated Sediment, Saanich Inlet, British Columbia

Arlene D. Collins
Department of Earth and Atmospheric Sciences, University of Alberta
Edmonton, Alberta, Canada

Analyses of a continuous sequence of seasonal-scale sediment laminations from two cores from Saanich Inlet provide the first high-resolution geochemical record for palaeoclimate reconstruction for the west coast of Canada. This record (spanning 1860-1993; collected in 1994) completes the Holocene sedimentary record that the later ODP cores (collected in 1996) could not recover from the same selected site. My results offer insights into climatic controls during the years 1900-1985. The objectives were to reconstruct climatic parameters at seasonal-scale resolution using sediment characteristics. The characteristics for total sediment, lithics, opal, total carbon, carbonate carbon, organic carbon, nitrogen,

$CaCO_3$, porosity, and lamina thickness indicate that temperatures are warming since 1990, especially during the last decade.

Rhythmites are annual (varves) as determined from:

(1) wood chips located only in varve years 1864-1879. A lumber mill operation (1863-1878) located at a creek mouth on the inlet shore deposited chips into the basin during winter discharge initiated by coastal winter precipitation;

(2) pronounced Cesium137 peak at varve year 1964 (produced from atomic testing); and

(3) elevated $CaCO_3$ (%) values that reflect the yearly timing and activity of a cement plant operation (1913-1980) located on the inlet shore. Varves are comprised mainly of lithics and opal. Lithics arrive mainly from the nearby Cowichan River throughout the winter and predominate in both dark and light layers with average values of 74 percent and 66 percent, respectively. Opal, the secondary component, reflects diatom production and increases on average from dark to light layers from 20 percent to 28 percent.

The seasonal and annual accumulation of total sediment during 1864-1993 show an increase from 1863 to the early 1920s, then decrease to the 1940s, then a more recent increase during the last decade. This pattern is reflected in extreme high, low, then high accumulation rates of 0.53gxcm-2xy-1 during 1888, 0.15 gxcm-2xy-1 during 1947, and 0.61 gxcm-2xy-1 during 1987.

A climate signal is recorded in the sediment at seasonal resolution as shown from stepwise multiple regression tests upon instrumental climate data and sediment characteristics. Climatic parameters occurring outside the basin are linked to the sedimentary processes within the inlet. Since 1900, Cowichan River discharge (an indicator of precipitation) is decreasing and sea surface temperature has increased on average by 0.5°C; this indicates a warming trend.

Spatially Variable Hydrologic Patterns in Lakes of the Northern Great Plains during the Last 2K

Sherilyn C. Fritz, Katherine R. Laird, Emi Ito, and Dan Engstrom
Department of Earth & Environmental Sciences, Lehigh University, Bethlehem, PA
Department of Biology, Queens University, Kingston, Ontario, Canada
Department of Geology & Geophysics, University of Minnesota
St. Croix Watershed Research Station, Marine-on-St. Croix, Minnesota

Closed-basin lakes often show shifts in lake level and ionic concentration (salinity) and ionic composition in response to interannual shifts in the balance between precipitation and evaporation. These hydrochemical shifts in turn affect the distribution of organisms sensitive to salinity, as well as the precipitation of minerals from solution. This simplified model is commonly used by paleolimnologists as a foundation for the interpretation of shifts in effective moisture from the stratigraphic record of closed-basin lakes. However, the magnitude of lake response to fluctuations in P-E depends on the relative contribution of groundwater inflow and outflow to both the water and salt budgets of a lake, and thus in some systems groundwater influences may dominate the hydrochemical response of a lake to climatic shifts.

We have used the stratigraphic record of diatoms and the isotopic and trace element chemistry of ostracodes to reconstruct the hydrochemical history of lake systems in the northern Great Plains and to infer Holocene patterns of drought. Recently completed salinity reconstructions from two closely spaced sites in southeastern North Dakota (within 200 km of each other) show different patterns of decadal-scale salinity fluctuations over the past 2,000 years. At Moon Lake, high salinity episodes of greater severity and duration than those characteristic of the Dust Bowl droughts of the 1930s were more frequent from ca. 2,300 to 750 years ago, an interval that includes the Medieval Warm Period. The period from 750 years B.P. onward, which includes the Little Ice Age, shows a higher frequency of freshwater periods and includes intervals fresher than any since the early Holocene.

A second record from Coldwater Lake also shows a major shift in lake hydrochemistry about 750 years ago. However, in this case the lake shifts to more frequent high-salinity episodes in comparison to the previous 1,200 years. It is unclear whether the differences in lake behavior reflect different hydrologic responses to the same climatic forcing or alternatively whether the lakes were experiencing different climate. Relatively small-scale spatial variability in effective moisture has characterized the Great Plains region during the 20th century, so the latter possibility is not unreasonable.

Clearly additional sites are needed to discern whether or nor there is some spatially coherent pattern of lake response that might indicate sharp moisture gradients over relatively small spatial scales within the

past 2,000 years or whether differences in lake hydrology are the more reasonable explanation for temporal patterns of salinity change over decadal time scales.

Late-Glacial Variations in Vegetation and Climate in Western Oregon: Evidence of a Younger Dryas Cooling?

Laurie D. Grigg and Cathy Whitlock
Department of Geography, University of Oregon

Pollen data from two sites in western Oregon provide information on vegetation and climatic variability during the transition form glacial to Holocene conditions. During full-glacial time, Little Lake in the central Coast Range supported an open forest of *Picea*, *Abies*, *Pinus*, *Tsuga mertensiana* and *T. heterophylla* during a period of cool dry conditions. A brief warm period between 14,850 and 14,500 calendar year B.P. is evidenced by an increase in temperate taxa, including *Pseudotsuga* and *Alnus rubra*. This period has not been described at other sites, which have generally been sampled at wide stratigraphic intervals. Corresponding increases in sedimentary charcoal suggest that the vegetation change at Little Lake may have been triggered by a change in fire frequency. Montane forests of *Picea* and *T. mertensiana* were reestablished at 14,500 calendar year B.P. indicating a return to cool conditions. After 14,250 year B.P., increased summer insolation fostered warmer summers that led to the establishment of *Pseudotsuga*, *Alnus rubra*, *Pinus*, *Abies*, and *T. heterophylla*. This warming trend was offset between 12,400 and 11,000 calendar year B.P. by a cool period that allowed an expansion of *Pinus monticola*. After 11,000 calendar year B.P. *Pseudotsuga*, *A. rubra*, and *Corylus* increased in number as conditions became warmer and drier than at present in the early Holocene.

Gordon Lake in the western Cascades supported open *Picea-Pinus* subalpine forest following deglaciation at ca. 15,500 calendar year B.P. The establishment of *T. mertensiana*, *T. heterophylla*, and *Abies* after 14,500 calendar year B.P. is consistent with warmer summers as a result of increased summer insolation. As at Little Lake, Gordon Lake shows an expansion of *Pinus* between ca. 12,600 and 11,000 calendar year B.P. that may be evidence of a climatic reversal. Similar increases in *Pinus* pollen occurred at other sites in the PNW between 12,600 and 11,000 calendar year B.P. and suggest a shift towards greater seasonality. This interval may be a response to (1) submillennial climate changes associated with the Younger Dryas (YD) paleoclimatic oscillation (12,900-11,600 calendar year B.P.) or (2) millennial-scale climatic variations related to changes in the seasonal cycle of insolation. The pattern of vegetation changes during this period suggests that climate shifts were driven by decreases in sea-surface temperatures and that cooling in the PNW is not synchronous with the YD oscillation in the North Atlantic.

Recent Changes in Pacific Hemisphere Teleconnections

Steven M. Hodge
U.S. Geological Survey, Anchorage, Alaska

The seasonal mass balances, winter and summer, of two maritime-regime glaciers in western North America, South Cascade Glacier in the Pacific Northwest and Wolverine Glacier in Alaska, correlate well with many Pacific climate indices. The strongest correlations are between the winter balance—a measure of the total winter snowpack of the region—and two North Pacific indices, PNA (Pacific/North American) and CNP (Central North Pacific). However, remarkably strong correlations also occur between the winter balance and more distant tropical indices, SOI (Southern Oscillation Index) and SST (sea surface temperature). The correlations are strongest when a phase lag is introduced between the index (the forcing) and the balance (the response); in most cases, the lags are substantial, often to climate conditions that existed before the balance season commenced. One of these teleconnections has changed drastically in recent years: the most recent 15-20 years of data do not show *any* significant correlation between SOI and the winter balance of South Cascade Glacier, even though this correlation reaches values almost as high as 0.7 in prior years. This "breakdown" of a Pacific Northwest-SOI teleconnection started in 1989, the same year that both glaciers, and a third, continental-regime glacier (Gulkana Glacier in the interior of Alaska), started losing mass at the highest rate in the entire 30- and 37-year data records. This was also the first time that all three glaciers started showing the *same* multiyear trend, that is, mass loss on all three glaciers. Hence, the average atmospheric/oceanic circulation patterns in the Pacific basin may have shifted in 1989 to a new set of quasi-stable centers of activity, over new geographic regions.

This change in teleconnection is evident in the other glacier balance/climate index correlations as well. The teleconnections between conditions in the tropics (SOI and SST) and the winter snowpack of both the Pacific Northwest and coastal Alaska all decreased in strength dramatically in the late 1980s/early 1990s. The corresponding teleconnection with PNA, however, shows a less dramatic decrease, and with CNP, almost no change. This suggests that this change is primarily one involving the less dominant *tropical* teleconnections, not the more dominate North Pacific ones. The PNA change is possibly intermediate between the two because it is a combination of North Pacific and more tropical (Hawaii and Gulf of Mexico) conditions. The results suggest that a change took place in the late 1980s/early 1990s in the teleconnection links between the atmospheric/oceanic circulation patterns of the tropical and northern Pacific, independently of the links to snowpack in western North America.

Correlations with the *summer* balance are much weaker, and only the correlation between the summer balance of the South Cascade Glacier

and CNP has a strength approaching that of the winter balance correlations. A similar analysis of this teleconnection shows that it too has changed, but in a different way. During the *mid*-1980s, the correlation lost all statistical significance for a period of several years, but *starting* in the late 1980s/early 1990s, it has recovered to almost its original pre-1980 strength.

Finally, the results suggest that in the last 2 or 3 years, these teleconnetions may be starting to return to their long-term, "normal" condition. The late 1980s/early 1990s may have been a period of "anomalous" teleconnection patterns superimposed on more consistent, longer-term ones.

Diagnosing the Sensitivity of Western U.S. Climate to Tropical Pacific Forcing

Martin P. Hoerling, Arun Kumar, Taiyi Xu, and Min Zhong
CIRES, University of Colorado-Boulder
NOAA/NCEP/EMC

Susceptibility of North America to anomalous tropical Pacific sea surface temperatures (SSTs) is greatest during winter/spring, at which time circulation anomalies having deep tropical roots can significantly alter surface climate conditions. Not all regions of the continent are equally affected, and indeed large year-to-year climate variations occur in midlatitudes without anomalous tropical forcing. The impact of tropical forcing on midlatitudes can thus be viewed best as altering the probability of occurrence of certain climate events, such as floods and droughts, though not solely regulating the outcome of the seasonal climate. It is with great scientific and practical interest that we pursue the influence of tropical SSTs on the western U.S. (West of about 115°W) since that region's "rainy season" matches the period of large tropical impact on North America as a whole.

Observational evidence for hydrologic variability over the western U.S. related to El Niño/Southern Oscillation (ENSO) paints a confused picture, however, and the precise influence on the West remains an open question. On the one hand, diagnosis of historical rainfall data reveals no significant ENSO link over the Pacific West Coast during the rainy season (Ropelewski and Halpert 1987; Kiladis and Diaz 1989). On the other hand, analysis of streamflow data does show an ENSO in the Pacific Northwest and the far southwest U.S. (Cayan and Webb 1992). Analyses of both variables are consistent, however, in demonstrating that no reliable ENSO impact exists between 35°N-45°N in the western U.S., a region including much of California and Oregon. Yet even here one encounters some important exceptions, most notably the extensive flooding that plagued much of the Pacific West Coast during the extreme tropical warm event of 1982/83. During some other El Niño events, opposite hydrologic extremes have occurred in these regions (e.g., 1976-

78), and this seemingly erratic behavior continues to spawn active debate on the nature of ENSO's effect on the western U.S.

In order to explore the sensitivity of the western U.S. climate to low frequency tropical forcing, results from a suite of atmospheric general circulation model (AGCM) simulations and dynamical model experiments are studied. One set of nine AGCM experiments is forced with the observed monthly evolving tropical Pacific SST variations for 1950-95. The analysis focuses on the model's composite ENSO signal, the seasonality of that signal during the course of the Pacific West Coast's rainy season, and the variation of the signal from one El Niño event to another. A second set of runs uses a fixed positive tropical Pacific SST anomaly in a 40-year seasonal cycle integration. These runs seek to elucidate the relationship between the atmosphere/ocean system's annual cycle and the seasonally varying response to El Niño. A third series of experiments uses a perpetual winter version of the AGCM. Positive tropical Pacific SST anomalies are shifted systematically westward across the Pacific basin, and the sensitivity of the North American response to different positions of the tropical forcing is examined. Finally, in order to test the realism of the AGCM simulations, diagnostic modeling of the circulation response over North America to tropical convective forcing is performed. Using prescribed tropical heating anomalies, these experiments further study the sensitivity of the North American response to the observed monthly changes in climatological circulation, and to the observed monthly changes in tropical rainfall patterns that frequently occur during El Niño.

Decade to Century-Scale Climate Variation in Western North America Over the Last 1,000 Years, in a Global Context

Malcom K. Hughes
Laboratory of Tree Ring Research, University of Arizona

Aspects of precipitation (mainly winter) and summer temperatures have been reconstructed from tree rings for much of the interior West for 1,000 years or more. The extent to which these records accurately represent decade to century-scale variability will be examined, and comparisons made with other types of records from this and neighboring regions. Preliminary examination suggests that natural records of precipitation from western North America, the Great Plains, the Peruvian Andes, the Tibetan Plateau and other regions evidence greater incidence of drought in the centuries before AD 1600 than after that date. Is this so? What does it mean?

Index of OSCURS Model Winter Drift Trajectories from Ocean Station PAPA (1901-1997) Indicates the Fourth Decadal Oscillation During the 20th Century Is Ending; PNA, PNI, Precipitation, Salmon, Oysters, and Tree Ring Data Covary

W. James Ingraham, Jr., Curtis C. Ebbesmeyer, and Richard A. Hinrichsen
Alaska Fisheries Science Center/NMFS/NOAA
Evans-Hamilton, Inc., Western Region
Columbia Basin Research, University of Washington

New information on interannual and decadal variability of surface currents in the northeast Pacific Ocean and Bering Sea was derived from a time series of drifter tracks (1901-97) simulated with the OSCURS (Ocean Surface Current Simulations) model. Development of OSCURS was motivated by the need in fisheries research for indices that describe variability in ocean surface currents. These synthetic data, derived through empirical modeling and calibration, provide insight which far exceeds their accuracy limitations. OSCURS daily surface current vector fields are computed using empirical functions on a 90 km ocean-wide grid based on monthly mean sea level pressures (1900-1945) and daily sea level pressures (1946-1997); long-term mean geostraophic currents (0/2000 db) were added.

The model was tuned to reproduce trajectories of satellite-tracked drifters (drouged at 20 m) in the Gulf of Alaska. The starting location for simulated drifters was chosen at Ocean Station PAPA (50°N, 145°W), where the 3-month winter trajectories (December, January, February) proceeded northeastward into the Gulf of Alaska, but year-by-year the latitudes of the trajectory end points varied by 1,700 km (45°N-60°N) in their north-south distribution. Recently, the 5-year running mean plot has returned from the northward mode to its mean latitude of 54.4°N, anticipating the next oscillation (southward mode).

This latitude index of surface flow covaried with the Pacific North American (PNA) atmospheric index, the Pacific Northwest Index (PNI), the monthly precipitation at Astoria, the Northern Diversion Rate (NDR) for sockeye salmon (*Oncorhynchus nerka*), and the Washington State Oyster (*Crassostrea gigas*) Condition Index (OCI). Furthermore, eight western juniper (*Juniperus scopulorum*) trees located in Eastern Oregon showed ring widths varying at decadal frequencies which aligned approximately with the PNI in this century. Two of the covariates, the tree rings and Astoria precipitation, contained data prior to this century. Astoria precipitation data may be the longest continuous instrumental time-series for the northwest coast, showing eight 17-year period oscillations from 1851 to present. Using the juniper trees, which showed decadal oscillations of 18 years extending back to the 15th century, we may be able to derive a composite decadal index back to 1447 with 30+ cycles. Decadal cycling apparently represents a physical process that has operated continuously since at least 1447 AD.

Evidence of Increased Growth of Vegetation in Northern North America and Eurasia from AVHRR Global Vegetative Index and Atmospheric Carbon Dioxide Data

@ABSTRACT AUTHOR = Charles D. Keeling, Stephen C. Piper, and Timothy Whorf
Scripps Institution of Oceanography, University of California-San Diego

Increases in the amplitude of the seasonal cycle of atmospheric carbon dioxide are seen at stations from Hawaii to Alaska. Evidence that these increases are related to widespread increases in plant growth come from gridded time series data of the normalized difference vegetative index (NDVI) derived from AVHRR radiometers mounted on NOAA satellites.

A likely cause of vegetative changes were pulses of warming over most of the Northern Hemisphere, but especially in the interiors of the continents of Eurasia and North America. This warming appears to be related to decadal variability in global temperature, in which the Quasi-Biennial Oscillation (QBO) may have played a role, because, as we discussed at the PACLIM meeting in 1995, much of the warming occurred during the westerly phase of the QBO.

Teleconnection Between ENSO and ITCZ Position: Decadal Variations of Regional Precipitation in Southwestern South America

Hong-Chun Li and The-Lung Ku
Department of Earth Sciences, University of Southern California

Seven weather stations in the southwestern South America have been selected for historical precipitation analysis. The study area can be divided into two climate regions: Region I with dry summer subtropical climate and Region II of subtropical desert and steppe. Region I is represented by three stations in central Chile within 29.9 to 33.5°S and 71.3 to 78.9°W, where precipitation occurs predominantly in the cold season (April to September). In the summer (January), although the intertropical convergence zone (ITCZ) is closer to the region, little precipitation occurs because the region is dominated by the stable eastern side of the oceanic subtropical highs. In the winter (July), as the wind and pressure systems follow the sun equatorward, the region is within the range of cyclonic storms of the polar front. Therefore, the climatic regime in Region I is not controlled by shift of the ITCZ position. Region II is covered by four stations in northwest Argentina within 26.8 to 32.9°S and 65.2 to 68.9°W. It receives precipitation predominantly during warm seasons. Although rainfall in the region is somewhat too poleward to be controlled by the ITCZ low, it has marked patterns—wet summers followed by dry winters. In summertime (January), the rainy season commences with the advance of the ITCZ toward the region. With the retreat of the ITCZ in winter (July), the subtropical high moves into the

region and intensifies drought conditions. In general, the length of the rainy season in Region I depends on the region's distance from the polar front, whereas in Region II it depends on the distance from the ITCZ.

By comparing instrumental precipitation records of the two regions with the Southern Oscillation Index (SOI) for the past 100 years, we have found strong correlations among them with an apparent decadal periodicity. This observation indicates that the prevailing mean position of ITCZ is influenced by ENSO variability. During a weak ENSO (in favor of El Niño events) period, the cold Peruvian current is replaced (or weakened) by the warm water from the equator. The warm surface waters cause air masses to uplift and weaken the subtropical high. The weakened subtropical high leads to further than normal movement of the polar front equatorward in winter (July) and further poleward shift of the ITCZ in summer (January). In addition, warmer conditions produce unstable rising air and low pressure system along the coastal region, creating more cyclonic storms of the polar front during wintertime. By contrast, the aridity of these regions during a strong ENSO period is intensified because the lower atmosphere is strongly chilled by cold offshore waters, which further stabilizes the subtropical high. Therefore, strong ENSO leads to equatorward shift of the ITCZ and vice versa. While the forcing mechanism of the decadal variability of ENSO is still being investigated, the results thus far obtained may contribute to the understanding of the coupled ocean-atmospheric circulation on climate dynamics.

Climate Teleconnection During the Late-Glacial Period in Southern South America

Vera Markgraf, R. Figge, R. Kenny, and J.C.W. White
INSTAAR, University of Colorado-Boulder

An interdisciplinary study of a peat core from Harberton bog in the eastern Beagle Channel, Tierra del Fuego (54°53'S lat., 67°10'W long.) for pollen, carbon and hydrogen stable isotopes, revealed repeated high amplitude excursions during the interval between 14,000 and 10,000 B.P. The δD record, interpreted to reflect temperature, and pollen show simultaneous changes, with arid heath taxa increasing when δD increased and mesic grassland increasing when δD decreased. This suggests that during that time when moisture levels in the high latitudes were overall low, because the westerlies were still focused farther equatorwards, temperature changes greatly influenced vegetation patterns.

Timing, rate, and amplitude of the δD excursions in the peat record are comparable to the Greenland $\delta^{18}O$ or δD ice core records. This suggests an interhemispheric teleconnection of heat transport, thought to relate to changes in intensity of the thermohaline circulation. High resolution

late-glacial marine records from the North Atlantic document rapid changes in intensity of thermohaline circulation, which are apparently synchronous to the δD excursions in both ice core and peat record. Supporting evidence for the interhemispheric effects of the intensity changes in the thermohaline circulation comes also from the $\delta^{13}C$ record from the Haberton peat core, interpreted to reflect pCO_2 variability. Peaks of pCO_2 at 12,700 B.P., 11,000 B.P., and 10,000 B.P., interpreted to represent ocean degassing events, occur at the same time as intensity changes in the thermohaline circulation.

A Pacific Interdecadal Climate Oscillation with Impacts on Salmon Production

Nathan J. Mantua, Steven R. Hare, Yuan Zhang, John M. Wallace, and Robert C. Francis
Joint Institute for the Study of the Atmosphere and Oceans (JISAO), University of Washington
International Pacific Halibut Commission, University of Washington
Fisheries Research Institute, University of Washington

Evidence gleaned from the instrumental record of climate data identifies a robust, recurring pattern of ocean-atmosphere-climate variability centered over the mid-latitude Pacific basin. Over the past century, the amplitude of this climate pattern has varied irregularly at interannual-to-interdecadal time scales. There is evidence of reversals in the prevailing polarity of the oscillation occurring around 1925, 1947, and 1977; the last two reversals correspond with dramatic shifts in salmon production regimes in the North Pacific Ocean. This climate pattern also affects coastal sea and continental surface air temperatures, as well as streamflow in major west coast river systems, from Alaska to California.

Long-Range Streamflow Forecasting in the Columbia River Basin and the El Niño-Southern Oscillation

Thomas C. Piechota and John A. Dracup
Civil and Environmental Engineering Department
University of California-Los Angeles

Long-range forecasting of streamflow is important to hydrologists and water resource planners for the maintenance of a diverse ecosystem and for optimal operation of water resource systems. In the western U.S., there is a significant relationship between streamflow and the El Niño-Southern Oscillation (ENSO). The Southern Oscillation Index (SOI) and the Wright Sea Surface Temperatures (SST_w) are used here to study the lag relationship between western U.S. streamflow and ENSO indices. Preliminary research has shown that the North (Montana, northern Idaho, eastern Washington) experiences below normal spring-summer runoff during ENSO events while the South (New Mexico, Arizona, southern California) experiences above normal spring-summer runoff. In both of these regions, the spring-summer runoff is significantly correlated with the prior summer and autumn SOI and SST_w values. These 6-

to 9-month lag correlations are important in making long-range streamflow forecasts.

A long-range seasonal streamflow forecasting model is developed and tested on the Columbia River Basin, Washington State. A probabilistic streamflow forecast is made from an optimal linear combination of SOI Phase, SST_w Phase, and SOI Linear Discriminant Analysis (LDA), and SST_wLDA forecasts. The forecast takes the form of a probability of the streamflow occurring in specified categories (i.e., below normal, normal, and above normal). The optimal linear combination of the four models is the forecast that minimizes the mean square error (Half-Brier score) and is the forecast with the best overall skill. This final combination forecast is referred to as a "consensus forecast."

This consensus model is used on seven Columbia River basin streamflow stations that cover the period 1933-1992. It was found that the best predictor period for spring-summer runoff, based on SOI and SST_w data, was the previous year's summer (6-month lead time), and the SOI is generally a better predictor of spring-summer runoff than SST_w. This work demonstrates the potential of using ENSO indicators for long-range streamflow forecasting in the Columbia River basin.

Seasonal Variation in Living (Stained) Deep-Sea Benthic Foraminiferal Assemblages and Stable Isotopes from the California Current System

Anthony E. Rathburn and Kyger C. Lohmann
Scripps Institution of Oceanography,University of California-San Diego
Department of Geological Sciences, University of Michigan

Faunal and preliminary stable isotope analyses of living (Rose Bengal stained) deep-sea benthic foraminifera in surficial samples (0-1 cm) from two sites on the Southern California margin reveal temporal changes in foraminiferal assemblages. Replicated multicorer samples were collected from two sites during CalCOFI cruises in October 1995, and February, May, August, and October 1996. One site (located near CalCOFI site 83-55, west of the Santa Barbara Basin at a water depth of 1,000 m) has bottom-water oxygen values ranging from 0.41 to 0.47 ml/l, and bottom-water temperatures of about 4°C. *Uvigerina peregrina*, *Bolivina spissa*, and *Hoeglundina elegans* are present in significant densities in the 0-1 cm interval of each sampling. *Epistominella smithi* is present in significant, but variable, numbers in all sampling times except August, whereas *Nonionella fragilis* appears in significant densities in surficial samples only in May and October 1996. Changes in the abundances of these taxa correspond to changes in inferred phytodetrital flux. Preliminary $\delta^{13}C$ and $\delta^{18}O$ results from October 1995 through August 1996 indicate expected differences between species. Isotope analyses of *U. peregrina* show that May has the most negative $\delta^{13}C$ value and August the more positive value (difference of about 0.36 ‰) as would be expected if there

was a direct or indirect phytodetrital influence of stable isotopic composition in this species. The southern site (located west of the California-Mexico border at a water depth of 1,300 m) has bottom-water oxygen levels of about 0.86 to 0.96 ml/l and bottom-water temperatures of about 3°C. *Uvigerina proboscidea*, *U. peregrina*, *Cibicidoides* species, and *H. elegans* dominate the 0-1 cm samples from this site. Analyses of the isotopic composition of *U. peregrina* at this site show little variation between sampling times (within 0.10 ‰), suggesting less seasonality at this site. Comparisons of these results with concurrent water column productivity data and previous foraminiferal studies suggest that the faunal differences between sites and temporal assemblage changes observed in this study result from spatial and temporal differences in the availability of organic flux. These results suggest that selected benthic foraminiferal faunal and stable isotope data may be useful to assess short-term paleoceanographic and paleoclimatic variability in the eastern Pacific.

The Western Winter of 1996-97 and Possible Teleconnections

Kelly T. Redmond
Western Regional Climate Center
Reno, Nevada

The hyperactive winter of 1996-97 in western North America began in earnest in October, and brought a wide variety of significant weather throughout the region. Heavy precipitation and snowfall, high winds, severe cold outbreaks, and extensive flooding affected the area. By late winter, an extensive and much deeper than average snowpack had accumulated in nearly every major mountain range. Of approximately 70 basins, only the Verde, Mimbres, and central Mogollon Rim drainages were reporting below normal (although nearly so at 90-95 percent) winter precipitation. The potential for spring snowmelt floods was very high.

It is relatively unusual for almost all of the western U.S. to experience a seasonal precipitation anomaly of the same sign. The northern and central West were relatively much wetter than the southern West. From Washington across to Montana, temperatures averaged below normal, with most of the remainder near to above average. This pattern is reminiscent of other winters with a positve antecedent Southern Oscillation Index, especially in the Pacific Northwest and the far southwest, where the relationship has been most consistent over the past 63 years. Upper air patterns show similar consistencies.

Madden-Julian intraseasonal oscillations over Indonesia and their lagged teleconnections to North America appear to be related to several of the more dramatic events, including the record flooding around New Years Day. After 10 consecutive low years, the Columbia River will flow well above average for the second year in a row. In the past 11 years, Lake

Tahoe has traversed a range from its highest level in 80 years to its lowest level on record and back to the same high level. Large positive and negative impacts from temperature, snowpack, and precipitation are expected for fish and wildlife populations all around the region. The record flooding in California and other places is hastening a re-examination of the relative roles of structural versus behavioral approaches to dealing with the effects of environmental variability.

Large-Scale Weather Regimes and Local Climate Over the Western United States

Andrew W. Robertson
Department of Atmopsheric Sciences
University of California-Los Angeles

Teleconnection patterns (recurrent, geographically fixed, persistent large-scale weather regimes) are constructed from winter daily 700-mb heights (1949-94) over the north Pacific sector using cluster analysis. Six teleconnection patterns, or weather regimes, are identified, including the PNA, reverse-PNA, and omega Pacific block.

Firstly, we examine to what extent these large-scale regimes condition the local daily distributions of precipitation and temperature in eight local districts within the western United States. Most of the regimes do have a statistically significant effect on the frequency of daily precipitation and median temperature. Local daily extremes are less well classified.

Secondly, we investigate how far ENSO modulates the probability of occurrence of each of the six weather regimes. El Niño winters are clearly associated with increased prevalence of a PNA-like regime, in which negative height anomalies exhibit a northwest-southeast tilt over the North Pacific. The PNA regime itself exhibits only a weak link with El Niño. Changes in regime frequency are less marked during La Niña winters, but the reverse-PNA, and a ridge over southwestern North America both become more prevalent.

The Continuing Decline of Primary Productivity in the Bering Sea: Implications for Marine Mammal Populations

Donald M. Schell
Water and Environmental Research Center
University of Alaska-Fairbanks

Recent findings in both laboratory and natural environments indicate that carbon isotope ratios of phytoplankton are closely linked to cell growth rates where other floristic and environmental conditions are similar. Once incorporated into phytoplankton, the isotope ratios are conservatively transferred into the food web supporting consumer organisms. Bowhead whale (*Balaena mysticetus*) baleen grown while the

whales were feeding in the Bering-Chukchi seas provides a multi-year temporal record of isotope ratios in their zooplankton prey and by proxy, the phytoplankton supporting the consumer food webs. By using baleen plates from 26 whales archived at the Los Angeles County Museum and recently taken by native hunters, we have assembled a record that extends from 1947 to 1995. From this, we infer that primary productivity in the Bering Sea was at a higher rate over the period 1947 - 1966 and then underwent a general decline that continues to the most recent samples (1995). Assuming a close correlation to the laboratory relationships established between primary productivity and carbon isotope ratios, the decline in the Bering Sea isotope ratios suggests a loss of up to 40 percent of the carrying capacity that existed 30 years ago. This drastic decline is evident in recent zooplankton biomass estimates and is very likely implicated in the continuing decline of marine mammal populations in the western Gulf of Alaska and Bering Sea.

Upstream-Downstream—Its All About Time—and Space

Gary D. Sharp and Kathleen Dorsey

The sequence of processes that effect ecological systems is continuous, with many upstream processes commingled at any site. These process interactions define such local concepts as microclimates, niche space, and lebensraum for living individuals, communities, and ecotomes. The fact that all of these local processes and interactions are embedded in the several scales and time frames above the local scale, and it is often interesting to explore the response patterns for their information content about large scale systems. The most interesting responses come from critters that migrate, and shift their ranges to meet their optima, where they can find them. The less obvious situations are when migratory species simply stop coming back to historical habitats, because this can set off alarms, when they may not be warranted. The trick is to know the difference between a natural pattern of changes, and one induced by human interventions.

This is the dilemma of sustainability versus manipulability that has dogged science and human nature's irrepressible urge to "engineer" short-term solutions. These usually end up creating more problems than they resolve, as the downstream consequences emerge. Examples will be given.

The Effect of Atmospheric pCO_2 on $^{13}CO_2$ Discrimination in Wood C_3 Plants: Implications for Estimating Paleo-Atmospheric pCO_2

A. Sinha and L.D. Stott
Department of Earth Sciences
University of Southern California

It has been suggested that the ratio of intercellular CO_2 to ambient CO_2 concentrations (Ci/Ca) tends to remain constant at vary atmospheric CO_2 concentrations in terrestrial C_3 plants. The inferred "constancy" of the Ci/Ca ratio has been primarily attributed to C_3 plants' ability to regulate their stomatal density (and presumably stomatal conductance) in order to maintain a balance between the CO_2 uptake and water loss. Utilizing a long-term tree growth experiment in a CO_2 enriched environment, we have demonstrated that $^{13}CO_2$ isotopic discrimination (Δ) of woody C_3 plants increases as pCO_2 increases; and infer that Ci/Ca ratio must increase with increasing atmospheric CO_2. A review of the available $\delta^{13}C$ data for C_3 vegetation suggests a decrease (3-4 per mil) in the $\delta\ ^{13}C$ of C_3 plants with rising atmospheric CO_2 concentrations since the last glacial time and an increase in the Ci/Ca ratio of "woody" vegetation. The $\delta^{13}C$ of atmospheric CO_2 over the corresponding time interval has also decreased (~0.8 per mil) but fails to account for all of the $\delta^{13}C$ decline in C_3 woody vegetation. Although several environmental factors must have played a role in contributing to the observed variation in $\delta^{13}C$ of C_3 vegetation since the last glacial, the presence of a long-term trend in $\delta^{13}C$ of trees on a hemispheric as well as on a regional scale clearly indicates that a larger mechanism is responsible for $\delta^{13}C$ change. The best explanation for these observations is that there is a systematic relationship between ^{13}C discrimination (and in Ci/Ca) of C_3 plants to increasing atmospheric CO_2 concentrations. We propose a preliminary calibration of Δ ($\delta^{13}Catm$-$\delta^{13}Cplant$) as a function of atmospheric CO_2 concentration and illustrate how this relationship might be used to estimate CO_2 concentrations for ancient atmospheres. Because plant fossils are abundantly preserved in the geologic record, a validation of this technique would provide the opportunity to resolve paleo-CO_2 concentrations on a much longer time scale than is possible with ice cores.

Mapping of the Pacific Interdecadal Variability Using Complex EOF Methodology

Yves M. Tourre, Yohanan Kushnir, and Warren B. White
Lamont-Doherty Earth Observatory
Scripps Institution of Oceanography

The characteristics of the interdecadal variability in the north Pacific Ocean regions are explored. To that purpose, a Complex EOF (CEOF) methodology is applied to seasonal and annual winter values of surface atmospheric parameters (sea-level pressure, wind-stress, sensible and latent heat fluxes) and of surface and subsurface oceanic parameters (sea

surface temperature, temperature at standard depths and heat storage in the first 400 m). The analyzed period is from 1901 until 1994 for surface parameters and from 1970 until 1994 for the subsurface. While the first CEOF modes display variability on ENSO time scales, the second modes have interdecadal time scales properties (approximately 20 years for the full cycle) with maximum spatial amplitudes associated with the north Pacific baroclinic subtropical gyre. The space and time evolution of the interdecadal variability of the heat storage (HS) is consequently reconstructed through yearly mapping. Insights into the surface physical mechanisms involved are deduced from regressing each parameters against HS second mode. Animation of the second HS mode is available at:

http://cyberia.ucsd.edu/TOURRE

In the 30-40 N zonal band the anomalies are all in-phase all the way down to 400 m. East and south there is evidence of slow anticyclonic propagation along the mean circulation of the gyre associated with subduction processes in the 140°W - 160°W meridional band.

Forecasting the Inflows to the Howard Hanson Reservoir, Green River, Washington, for the Fall-Transition Season

John J. Vaccaro
U.S. Geological Survey, Tacoma, Washington

A method for forecasting inflows with long-lead times for the fall-transition season was formulated, analyzed, tested, and applied. The inflows forecasted are for the Howard A. Hanson Reservoir, Green River, Washington, and long-lead times are considered to be on the order of 2 years to 4 months prior to the beginning of the season (September-November). The method uses multiple linear-regression to estimate the monthly-mean streamflow for the combined months of September and October (a low-flow period), October (initial fall-transition), and November (onset of the fall-precipitation season). The predictors in the equations are monthly and 3-month sums or averages of hemispheric-to-regional indices calculated using atmospheric and sea-surface-temperature data, hydrometeorological data, and, in one case, sunspot number. The period of record for the analyses is water years 1950-95.

Initially, five equations for five different periods of record were calibrated for two different lead times for the combined September-October inflows. These 10 equations were then tested, and the results of the testing were analyzed to assess their stability and reliability. Next, two equations were calibrated and tested for September-October inflows (17-month lead times); two equations were calibrated and tested for October inflows (11-and 5-month lead times); and one equation was calibrated and tested for November inflows (11-month lead time).

The final equations were calibrated using 27 years of data, tested using the remaining 17 years of record, and further tested for the inflows for water years 1996-97. The calibration years were chosen randomly from each tercile of the September-October inflows, while at the same time reserving data for 1992-95 for testing. The results of the testing indicated that the equation for November had the largest r-squared value (0.67), and the equations for the other months had values that ranged from 0.41 to 0.56. For all equations, the standard error for the testing period was less than the standard deviation of the observed values, and the highest significance level was 0.006.

The equations should provide an additional tool for the management of reservoir outflows, especially in helping to guide existing management decisions, such as releasing water in the spring for flushing salmon smolt and at the same time storing water for fall-releases for steelhead migration and spawning. The ability to estimate fall-transition inflows well before the beginning of the fall runoff may decrease some of the uncertainty in the task of regulation decisions.

$\delta^{13}C$ Variability in Modern *Atriplex* Communities; Implication for Reconstructing $\delta^{13}C$ of Past Atmospheres

Peter K. Van de Water, Steve Leavitt, Julio Betancourt, and Lisa Pedecino
Laboratory of Tree Ring Research, University of Arizona-Tucson
U.S. Geological Survey, Tucson, Arizona

Carbon isotopes from C_4 plants have been tendered as one proxy for past atmospheric $\delta^{13}C$, permitting calculation of past plant physiological parameters, as well as isotopic values necessary for terrestrial and oceanic modeling efforts, including reconstructions of past teleconnections. Packrat middens provide a rich source of C_4 plant material from the late Quaternary, a time when ice core records imply large swings in atmospheric CO_2 and purported plant physiology changes. The key assumption in using C_4 plants to reconstruct $\delta^{13}C_{air}$ both in modern and fossil plant material, is that a constant $\delta^{13}C_{plant}$-$\delta^{13}C_{air}$ offset exists. Therefore, plants of the same age must have effectively the same isotopic composition. We compared $\delta^{13}C$ of holocellulose from leaves from modern *Atriplex canescens* and *A. confertifolia*, two C_4 shrubs commonly represented in packrat middens, growing on north versus south-facing slopes along elevational transects in southeastern Utah and southern New Mexico, localities with particularly rich midden records. Intraplant variability is well constrained with values ranging from ±0.24‰ to ±0.33‰(n=20, *A. canescens* only). Interplant variability, at a given site, is less constrained with standard deviations ranging from ±0.38‰ to ±1.58‰ (n=7 sites, *A. canescens* in New Mexico), ±0.71‰ to 1.12‰ (n=4 sites, *A. canescens* in Utah), and ±0.57‰ to ±2.4‰ (n=9 sites, *A. confertifolia* in Utah). No apparent trend in $\delta^{13}C$ with slope aspect or

elevation is evident. Analysis of material from herbarium sheets collected over the last 100 years reveals a similar range of $\delta^{13}C$ values indicating long standing landscape scale variability. Because the Late Pleistocene to Holocene shift of atmospheric $\delta^{13}C$ has been estimated at ~0.5 to 1.0‰, variability within and between populations may swamp any atmospheric $\delta^{13}C$ signal present in plant tissue. Our results demonstrate the need for great caution in attempting to reconstruct $\delta^{13}C$ of past atmospheres from fossil leaves of these two C_4 species.

The Slow Eastward Propagation of ENSO-Scale Signals Over the Global Ocean

Warren White, Ray Peterson, Shyh-Chin Chen, Dan Cayan, Yves Tourre
Scripps Institution of Oceanography, University of California-San Diego

White and Peterson (1996) have established a slow eastward propagation of ENSO-scale signals in SST, SLP, meridional surface wind (MSW), and sea ice extent (SIE) in the Southern Ocean, called the Antarctic Circumpolar Wave (ACW). The ACW takes approximately 8 years and 2 wavelengths to propagate around the Southern Ocean. SST anomalies are apparently advected by the background mean flow of the Antarctic Circumpolar Current, but this alone is insufficient to explain the observed propagation speed around the Southern Ocean. White and Chen (1997) have demonstrated that the observed coincidence between warm SST and poleward MSW anomalies in the ACW is consistent with a quasi-stationary potential vorticity model for the troposphere, where SST anomalies instigate mid-level diabatic heating anomalies on interannual time scales. This atmospheric vorticity response to SST anomalies allows us to construct a simple coupled model for the ACW, where feedback from the atmosphere to the ocean occurs through meridional Ekman advection. This simple coupled model yields the correct eastward speed of the ACW and maintains its amplitude against dissipation. Moreover, this coupled mechanism may be able to explain much of slow eastward and poleward propagation of ENSO-scale signals observed over the rest of the global ocean (White and Cayan 1997; Tourre and White 1997).

Response of Vegetation in the Pacific Northwest to Millennial-Scale Climatic Changes During the Last 125 kyr

Cathy Whitlock and Patrick J. Bartlein
Department of Geography, University of Oregon-Eugene

Paleovegetation records spanning the last 21 kyr from the western U.S. display coherent spatial patterns of change that reflect the influence of variations in the large-scale controls of climate. Among these controls are millennial variations in the seasonal cycle of insolation and the size of the ice-sheet, which affect regional climates directly through changes in temperature and effective moisture and indirectly by shifting the position

of storm tracks, the intensity of onshore flow, and the strength of the subtropical high pressure system. Longer records provide an opportunity to examine the regional response to different combinations of these large-scale controls, but such records are rare in North America. A record of vegetation and climate change from Carp Lake at the lower forest/steppe border of the eastern Cascade Range discloses alternations of forest and steppe for the last 125 kyr.

The similarities between the pollen record and variations in summer insolation and global ice volume confirm that climate variations are the primary cause of regional vegetation change on millennial time scales; nonclimatic control, such as delayed migration, are secondary. The previous interglacial (Stage 5e) supported temperate xerothermic forests of pine and oak and a southward and westward expansion of steppe and juniper woodland. The period from 85-117 ka contains intervals of pine forest and parkland alternating with pine-spruce forest, suggesting shifts from cold humid to cool temperate conditions. Between 72 and 85 ka, a forest of oak, hemlock, Douglas-fir, and fir developed that has no modern analogue and suggests a period of warm wet summers and cool wet winters. Cool humid conditions during the mid-Wisconsin interval supported mixed conifer forest with Douglas-fir and spruce. The glacial interval featured cold dry steppe, with an expansion of spruce in the late-glacial. Xerothermic communities prevailed in the early Holocene, when temperate steppe was widespread and the lake dried intermittently. The middle Holocene was characterized by ponderosa pine forest, and modern vegetation was established in the last 3,900 years, when ponderosa pine, Douglas-fir, fir, and oak were part of the local vegetation.

The Square-Root Normal Distribution of Daily Rainfall Along the U.S. Pacific Coast—Further Studies

Raymond C. Wilson
U.S. Geological Survey, Menlo Park, California

As reported at PACLIM '96, an examination of data from Pacific coastal rain gages from San Diego to Cape Flattery disclosed that the square root of the daily rainfall closely approximates a normal distribution function. The square-root-normal distribution, SQRND, provides a precise tool for analyzing spatial variations in precipitation. In comparing the square-root of daily rainfall between coastal and inland stations, orographic enhancement produces a constant multiplication; a rain shadow produces a constant decrement. The SQRND also allows precise, robust estimation of the precipitation frequency, expressed as the number of rain days per year (#RDs). The #RDs appears to be strongly correlated with latitude, increasing northward from southern California (~50 days per year) to the Pacific Northwest (~225 days per year). The physical

mechanisms underlying the square-root normal distribution remain unknown, unfortunately.

Subsequent work has explored several topics: (1) The coastal rainfall data base was used to compare the SQRND to the cube-root normal distribution, proposed by C.K. Stidd some years ago. For equivalent values of mean annual precipitation (MAP), the cube-root model predicts higher frequencies of "trace" amounts of precipitation and higher daily rainfall amounts for very long return periods. For Pacific coastal records, however, the SQRND provides better fits to the data. (2) The correlation of the #RDs with latitude appears to be related to the midlatitude storm track across the North Pacific. Nearshore sea surface temperatures, however, appear to exert an additional influence on the MAP. (3) The SQRND model has also been used to estimate normalized rainfall thresholds for debris-flow initiation in regions with different precipitation climates. Using data from several storms that triggered significant debris-flow activity in southern California, San Francisco Bay, and the Pacific Northwest, peak 24-hour rainfalls were plotted against the rainy-day normal, RDN=MAP/#RDs, displaying a linear relationship with a lower bound at about 14 times the RDN. This may provide a broad-scale regional threshold for debris-flow activity along the whole Pacific coast.

Poster Presentations

Quaternary Record of Paleolacustrine Environments in the Laguna Chapala Basin Area of Northern Baja California

Loren G. Davis
Department of Anthropology, University of Alberta, Edmonton, Canada

Archaeological investigations will be carried out to determine the record of prehistoric human adaptation to changing Late Quaternary lacustrine environments in the Laguna Chapala basin area of Northern Baja California's Central Desert Region. A basic stratigraphy and sedimentation model will be constructed in order to elucidate lake evolution, environment, and climate. Digital elevation modeling will provide a basis for reconstructing paleobathymetry and interbasin drainage networks. Datable materials form archaeological sites and packrat middens will provide limiting dates on lake elevations as well as providing additional information on environmental conditions. Comparisons made between the Laguna Chapala palolacustrine record and eastern Pacific marine cores are expected to generate a better understanding of Late Quaternary climate systems of the California Borderlands regions.

Forecasting the Frequencies of U.S. Intraseasonal Extremes

Alexander Gershunov
Scripps Institution of Oceanography, University of California-San Diego

ENSO predictability of daily occurrence frequencies of wintertime heavy and extreme precipitation and extreme temperatures is investigated. This is done empirically using six decades of daily data at 168 stations distributed over the contiguous U.S. ENSO sensitivity in the extreme ranges of intraseasonal precipitation and temperature probability density functions (PDFs) is demonstrated with regional PDFs composited by ENSO phase. Predictability of extremes is then investigated with simple ENSO-based statistical models. It is found that the simplest possible model which takes ENSO phase as the only predictor is generally more skillful and stable then models which attempt to exploit ENSO intensity as well. In an attempt to improve the performance and practicality of the ENSO phase model, a categorical forecasting approach is considered. A three-level categorical ENSO phase-based forecasting model is defined and tested. Its accuracy and practicality is assessed in a geographic context. Useful predictive skill is found in many coherent regions of the U.S. for various combinations of frequency variable and ENSO phase.

Searching for Interdecadal Cycles in Western Oregon Precipitation

David Greenland
Department of Geography, University of Oregon-Eugene

Central North Pacific index values and precipitation values for the Northern Cascades and Willamette Valley climate divisions and for the H. J. Andrews Experimental Forest are investigated using the winter water year (October through April) as the basic unit. Power spectral analysis (PSA) is applied to standardized, detrended data sets which are referred to here as "raw" data. No significant cycles are found in the raw data although there are suggestions of the presence of cycles.

The difficulty of interpreting PSA of 'real' climatological data sets is demonstrated by applying such analysis to synthetic time series data sets which contain known modal changes (interdecadal type) and regular episodic (ENSO type) occurrences. This part of the analysis sugggests that it is unlikely that PSA would identify interdecadal cycles in a real data set which also includes ENSO signals and expected noise. Filtering of the raw data sets with filters varying form 2 to 5 year moving averages of equally weighted terms provides new data sets from which PSA does begin to identify meaningful cyclic behavior at the interdecadal scale. When 5 year filters are used the CNP record shows statistically significant power at a period of 18.0 years and the Andrews record shows cycles at 36.0 and 10.3 years. The cycles for the CNP data are significant at the 95 percent confidence level, while those at the Andrews are almost but not

quite significant at that level. This analysis would benefit from having longer than about 100 year records—possibly by using dendrochronological data. If these cycles are real, there remains the difficulty of explaining how real this "statistical reality" is to ecosystem managers who are concerned with making decisions on decadal time scales.

Prediction of Drought Persistence in California

Henry Gu and John Dracup
Civil and Environmental Engineering
University of California-Los Angeles

Using National Climatic Data Center (NCDC) precipitation data, seven severe-sustained California water-year droughts (1917-1920, 1928-1934, 1944-50, 1953-55, 1959-1961, 1975-1977, 1987-1992) of this century have been identified. Factors causing the initiation, persistence, and termination of these California droughts are being investigated.

Studies suggest that California droughts are highly influenced by the interaction between the atmosphere, the sea surface temperatures of the Pacific Ocean, and by the middle-latitude jet-stream over the North American continent. Once a California drought is well established: (1) there is little chance for the warm, wet Pacific air to flow across the western United States; (2) the frequency for the storm-belt invading Northern California is greatly reduced; and (3) the western U.S. is mostly dominated by a quasi-steady high pressure system. This drought situation will be maintained unless the channel for the Pacific air flow to the western U.S. is again "switched-on."

Among those factors associated with California drought persistence, 700mb height anomaly, as suggested by correlation technique, is the most significant factor. As a preliminarily study, this paper is focused on exploring the role of the 700mb height anomaly on drought persistence. A regression model has been formed using the following steps: (1) a modeled region is chosen (20°N northward to 80°N, 0° westward to 200°W (or 160°E)); (2) Scripps' $5^0 \times 5^0$ diamond grid 700mb height data are analyzed since they are the longest available high-level pressure data (December 1946 through December 1995); (3) Principal Component Analysis (PCA) has been performed on the 700mb height anomalies; and (4) a regression model has been formed using the leading-modes as independent variables.

Results show that the 20 leading eigen-modes capture only 92 percent of total system variance, while the first three leading modes extract more than 50 percent. This strongly indicates the need for the rotation of these eigen-modes before regressing California precipitation on these eigen-modes. Therefore, Varimax rotation has been performed to obtain a "simpler structure" of the eigen-modes and to more easily attach a

physical explanation on these rotated eigen-modes. The regression of the California precipitation on the rotated eigen-modes has been performed and the effectiveness of this regression model was judged by an index ROT, which is defined as the accumulative relative error between the observed and the model-predicted precipitation in California.

ROT seems to show that California droughts cannot perfectly be predicted by 700mb height field. This suggests the necessity of forming a more comprehensive regression model on 700mb height anomaly, SST anomaly, sea-level pressure anomaly, and circulation patterns.

High Altitude Ice Core Data and Teleconnections

G. Holdsworth
Arctic Institute of North America
University of Calgary, Alberta, Canada

A continuous time series of net annual snow accumulation spanning the last three centuries was derived from ice core data on Mt. Logan, Yukon (Holdsworth 1990). At the site latitude of 60.5°N and altitude of 5,340 m, these data apply approximately at the mean annual (but more closely the winter) 500 mbar level. The first 100 years of this series has been cross-correlated with northern hemisphere station data (Holdsworth 1992). The highest cross-correlation coefficients are obtained with data from stations in Japan (Pearson product moment coefficients ≥ 0.5). Most of these stations are close to sea level (10 to 47 m asl) and have a spread of latitude from about 33°N to 43°N. Data spans 1883-1987. This long distance atmospheric association qualifies as a teleconnection (Glantz 1991).

In contrast to this result, cross-correlation coefficients obtained between Mt. Logan and coastal Alaskan sites near sea level, using data from 1899 to 1984, have no significance at the 95 percent level, except when the series are partitioned. A significant positive correlation between these data is obtained only from about 1950 to 1984. Yamamoto *et al* (1987) refer to "climatic jumps" associated with changes in regime of the long planetary waves. One of the two "climatic jumps" identified in Japanese climate data was in 1950. Thus it is possible that coherence between the Mt. Logan data and the Alaskan coastal data after 1950 was related to a major change in atmospheric circulation of the north Pacific region at that time. This implies that there are (decadal scale) periods of weaker and stronger coupling between low altitude and high altitude air masses in the region of the St. Elias Mountains. Spectral analyses (Holdsworth 1990) indicated modulation of the Mt. Logan net snow precipitation time series by ENSO related processes.

Relevant to the problem of the vertical variation of precipitation, it has been found (Holdsworth *et al* 1991) that the mean annual value of $\delta^{18}O$

and δD for snow between 1,800 m and 5,930 m on Mt. Logan and elsewhere in the St. Elias Mountains, defines a three-layered atmospheric structure in that region. The lowest layer, about 1,500 m thick, corresponding to the planetary boundary layer, is separated from the upper "geostrophic flow" region by a mixed 'layer' or transition zone. The Mt. Logan ice core site is located at the lower edge of the 'geostrophic flow' region, but may sometimes lie in the mixed layer (due to stronger air flows). The δ profile indicates that the ice core site is generally supplied with moisture from lower (warmer) latitudes than the lower altitude sites (between 1,800 m and 3,300 m). Moisture path length is also involved, but this has not been quantified.

The results also have implications in terms of explaining the physics of the claimed teleconnection. The structure of cyclonic storms in the Gulf of Alaska region (McBean and Stewart 1991) is such that at the 500 mbar level on Mt. Logan, the bulk of the moisture could easily be derived from south of latitude 50°N. This provides a connection with the subarctic current which flows ENE from Japan at about latitudes 35 to 43°N. The Alaska current is one extension of this major trans-Pacific Ocean current (Tabata 1975). This current follows the same general direction as the polar jet stream. Thus, there is expected to be strong coupling between the atmosphere and the ocean between Japan and the northeastern Pacific Ocean regions north of 50°N. Moisture arriving at high altitude on Mt. Logan would thus be the integrated sum over a much longer path length than for the lower altitude sites. The stable isotope-altitude model of Fisher (1990) is consistent with this concept.

References

Fisher, D.A., 1990. "A zonally-averaged stable-isotope model coupled to a regional variable-elevation stable-isotope model." *Annals of Glaciology* v. 14, pp. 65-71.

Glantz, M.H., 1991. Introduction in *Teleconnections Linking Worldwide Climate Anomalies*. M.H. Glantz, R.W. Katz, and N. Nicholls, editors. Cambridge University Press, N.Y., pp. 1-12.

Holdsworth, G., 1990. "Changes in mid-troposphere snow accumulation on Mt. Logan, Yukon, over the last three centuries," in *Proceedings of the Sixth Annual Pacific Climate Workshop*, March 5-8, 1989. J.L. Bentancourt and A.M. Mackay, editors. California Department of Water Resources, Interagency Ecological Studies Program Technical Report 23, pp.145-147.

———. 1992. "Ice cores as a source of long-term net precipitation data: a North American perspective," in *Using Hydrometic Data to Detect and Monitor Climatic Change*. G. W. Kite and K.D. Harvey, editors. Proceedings of National Hydrology Research Institute Symposium No. 8, April 1991, Saskatoon, Canada, pp. 107-120.

Holdsworth, G., S. Fogarasi, H.R. Krouse, 1991. "Variation of the stable isotopes of water with altitude in the Saint Elias Mountains of Canada." *Journal of Geophysical Research* v. 96 (D4), pp. 7483-7494.

McBean, G.A., and R.E. Stewart, 1991. "Structure of a frontal system over the Northeast Pacific Ocean." *Monthly Weather Review* v. 119, pp. 997-1013.

Tabata, S., 1975. "The general circulation of the Pacific Ocean and a brief account of the oceanographic structure of the North Pacific Ocean." *Atmosphere* v. 13 (4), pp. 133-168.

Yamamoto, R., T. Iwashima, and M. Hoshiai, 1987. "Climatic jump in the polar region (I)." *Proceedings of the National Institute of Polar Research Symposium on Polar Meteorology and Glaciology* v. 1, pp. 91-102.

Holocene Paleoceanographic Changes in Santa Barbara Basin: Radiocarbon Records

B. Lynn Ingram, Douglas Kennett, James Kennett, Brendan Roark, and Jon Erlandson
Department of Geography, University of California-Berkeley
Department of Anthropology, University of California-Santa Barbara
Marine Science Institute, University of California-Santa Barbara
Department of Anthropology, University of Oregon-Eugene

Radiocarbon measurements of coexisting planktonic and benthic foraminifera from marine sediments and of shell-wood pairs from stratified archaeological deposits from Santa Barbara Basin were made to evaluate changes in the relative ^{14}C content of surface waters relative to the atmosphere and bottom water to surface waters during the Holocene. The radiocarbon content of surface and bottom waters along coastal California reflect both regional wind-driven upwelling and global thermohaline circulation. Regional deviations (ΔR) from the average reservoir age of surface waters of 400 years along coastal California vary between 220 years in southern California to 290 years in northern California, based on ^{14}C measurements of shells collected prior to nuclear testing. Mussel shells from the Santa Barbara channel have an average ΔR value of 233 years. Temporal changes in the ^{14}C age of surface waters relative to the atmosphere, and deep waters relative to surface waters, may occur on a variety of time scales, due to changes in thermohaline circulation and/or regional oceanographic changes such as upwelling intensity. Past values of ΔR can be determined with ^{14}C measurements of contemporaneous shell (reflecting surface water ^{14}C) and organic carbon (reflecting atmospheric ^{14}C) separated from sediments or stratified archaeological deposits.

Shell and charcoal samples were collected from Early to Middle Holocene shell mounds SMI-261 (Daisy Cave) and Cave of the Chimneys, from the northeastern coast of San Miguel Island. Planktonic and benthic foraminifers were separated from marine sediments from ODP Hole 893A in Santa Barbara Channel for comparison. The shell/charcoal pairs indicate a general decrease in the reservoir age of surface waters in the Santa Barbara Basin from 8,250 years to the present, whereas the

foraminiferal record indicates a gradual increase in ^{14}C content over the past 9,200 years, suggesting that coastal upwelling may have been decreasing between the early Holocene and the present. Both records exhibit their lowest values during the early Holocene (8,900 to 9,300 years BP), possibly due to variations in thermohaline circulation, decreasing the age of Pacific intermediate water entering Santa Barbara Basin.

The Influence of Water Column Dynamics on Foraminiferal Flux Patterns

Eileen Kincaid, Robert C. Thunell, and Jianning Le
Department of Geological Sciences, University of South Carolina-Columbia

We are now in the third year of a sediment trap experiment in the Santa Barbara Basin. Results of this experiment suggest linkages between water column dynamics and variations in biogenic fluxes, foraminiferal species succession and the stable isotopic composition of planktonic foraminifera.

Annual hydrographic conditions are influenced by seasonality and source water variation. Sea surface temperature (SST) minima occur in early spring as water upwelled off Point Conception advect into the basin. As solar insolation increases, surface waters warm and a strong seasonal themocline develops. SST maxima occur from August through early November when a strong seasonal thermocline is present and the water column is highly stratified. In winter the upper water column becomes well mixed and cools to nearly isothermal conditions. The siliceous biogenic flux (predominately diatoms) increases rapidly at the onset of upwelling. The foraminiferal flux increases significantly approximately one month following the diatom bloom, probably due to utilization of diatoms as a food source. Maximal foraminiferal fluxes occur during later stages of upwelling and from the late summer to early fall when SSTs are warmest. Foraminiferal populations are significantly reduced during El Niño events with slow recovery to previous levels following the breakdown of the El Niño.

Temperatures calculated from oxygen isotope values of planktonic foraminifera are well correlated with measured SSTs from the spring through the fall. However, this relationship breaks down during the winter. The identification of flood events by Hendershott and Winant (1996) may explain the source of anomalous mid- and late-winter stable isotope values at this time.

Temporal Sedimentation Patterns of Siliceous Microorganisms in Santa Barbara Basin, California: Results from Sediment Traps

Carina B. Lange, Amy L. Weinheimer, Freda M. H. Reid, and Robert C. Thunell
Scripps Institution of Oceanography, University of California-San Diego
Department of Geological Sciences, University of South Carolina-Columbia

We report on fluxes of siliceous microorganisms (diatoms, radiolarians, and silicoflagellates), organic carbon, calcium carbonate, biogenic silica and lithogenic particles in the Santa Barbara Basin (34°14'N, 129°02'W), offshore California, within a sediment trap set at 540 m water depth, from August 1993 to November 1994. Although total mass flux was dominated by lithogenic components throughout the sampling period, we believe that overall flux variations at 540 m were closely coupled with oceanographic conditions at the surface. Organic carbon and biogenic silica fluxes show distinct variations with maxima during the upwelling period, from May to July 1994, and low fluxes from September to March. Diatoms were the main contributor to the biogenic silica fraction (mean daily flux = 3.98×10^5 valves m^{-2} d^{-1}), followed by radiolarians (mean = 7.05×10^3 tests m^{-2} d^{-1}) and silicoflagellates (mean = 1.48×10^3 skeletons m^{-2} d^{-1}).

Each group showed a distinct pattern, with marked production maxima at different times of the year: radiolarians in late summer and fall, silicoflagellates in winter, and diatoms in spring. In total, 150 diatom and 165 radiolarian taxa were identified. Species composition associated with flux peaks differed, reflecting seasonal changes in circulation patterns and water mass sources in the basin. Spring upwelling is reflected by the co-occurrence of deep-living intermediate radiolarian fauna (mainly *Lithomelissa setosa*) and diatom resting spores (mainly *Chaetoceros radicans*).

Non-updwelling conditions, summer through winter, with water entering the basin from the west or the east, are represented by a warm water, surface-dwelling radiolarian fauna and diatoms which are typically found in temperate and temperate-warm offshore waters. The intra-annual sequence of events, each characterized by a distinct diatom assemblage can be identified in the laminated sediments of the Santa Barbara Basin. *Chaetoceros* resting spores, which is the diatom representative in the trap of the productive spring season, dominates the sedimentary imprint, and thus the effect of preservation in the sedimentary record does not seem to remove information from the most productive season, as is the case in most other areas of the world. Since species in the plankton and in the trap occur simultaneously and are observed within the surface sediment layer in pristine conditions, we assume that dissolution is minimized by rapid descent through the water column. Dissolution seems to take place immediately below the sediment/water interface and weakly silicifed species are removed from the sedimentary record.

Linking Atmospheric and Paleoclimatic Records, Lake Estancia, NM

Kirsten M. Menking, Bruce D. Allen, Roger Y. Anderson, and Thomas A. Loveland
Department of Earth and Planetary Sciences, University of New Mexico-Albuquerque
New Mexico Bureau of Mines, Albuquerque, NM

The 5,000 km^2 Estancia Basin in central New Mexico holds a remarkably complete lacustrine record of late Pleistocene and Holocene climate change. We plan to establish quantitative linkages between past hydrologic changes in the basin, as measured by an assemblage of climate proxies, and associated changes in the atmosphere.

Today, Estancia Basin contains more than 80 ephemerally wet playas which are maintained largely by groundwater discharge from adjacent mountains to the west. Lakes within the basin expanded and contracted many times during the Holocene and late Pleistocene in response to changes in groundwater discharge, surface runoff, and evaporation. Fluctuations in lake level are recorded in geomorphic features, changes in ostracode abundances and species assemblages, and mineralogical and geochemical changes in lake sediments. Previous work involving correlation of distinctive ostracode species between basin center and marginal sediments has allowed the construction of a quantitative lake level history for the last 24,000 years. This history, combined with modern climatic and lake level data and output of regional climate models (RCMs), will be used to constrain past changes in meteorological variables.

In the initial phase of the study, Bowen ratio stations and nests of piezometers are being used to calibrate a coupled landscape-scale energy balance and hydrologic balance model of the basin. Bowen ratio stations include a net radiometer, temperature and relative humidity probes arranged in a vertical profile, a tipping bucket rain gage, an anemometer, and a wind vane. In addition, thermocouples have been inserted into the playa sediments to measure temperature gradients with depth, and a soil heat flux plate buried 10 cm below the surface measures solar heating of the playa surface. Evaporation rates calculated from Bowen ratio data will be compared to discharge of groundwater measured from hydraulic head differences in nested piezometers.

Once modern hydrologic and evaporative responses to changes in atmospheric conditions have been characterized, lake level history will be used to extrapolate changes in water balance over the last 24,000 years. Results will be compared to RCMs.

Seasonal Cycle of the Global Ocean Mixed Layer Depth Based on the Climatological Monthly Mean Hydrographic Data

Grigory Monterey and Sydney Levitus
PFEG/NMFS/NOAA, Pacific Grove, CA
NODC/NOAA, E/OC5, Silver Spring, MD

Amplitude of seasonal cycle of the mixed layer depth (MLD) is typically much larger than its interannual changes. Phase of seasonal cycle may indicate regime shifts on interannual time scale. Therefore, estimation and visualization of the climatological seasonal cycle of MLD is a prerequisite for study of its longer term variability. Global coverage is favorable for analysis of teleconnections. The forthcoming NOAA atlas by Grigory Monterey and Sydney Levitus presents maps of the climatological monthly mean MLD for the World Ocean as well as their deviations from the climatological annual mean. The MLD is computed by processing 1^0 x 1^0 averaged climatological monthly mean vertical profiles of potential temperature and potential density based on three different criteria: (1) the temperature change from the ocean surface of 0.5°C, (2) the density change from the ocean surface of 0.125 in sigma units, and (3) the variable density change from ocean surface corresponding to the temperature change of 0.5°C. The MLDs based on these criteria are about the same in mid-latitudes, but differ in some areas located in tropical and polar latitudes due to effects of salinity. In mid-latitudes MLD typically changes form ~25 m during warm season to ~100 m during cold season. MLD increases gradually over 5-6 months and decreases rapidly during 1-2 months. Shallower mixed layer during warm season is more spatially homogeneous than deeper mixed layer during cold season. Climatological monthly mean 1^0 x 1^0 MLD files computed based on three criteria indicated above are expected to be available by mid-1997 via the National Oceanographic Data Center/NOAA home page: http://www.nodc.noaa.gov

Simulation of Dispersal of Saguaro Cactus

Leila Shiozawa and Rachael Craig
Kent State University, Ohio

We use a model of Saguaro survival, growth, dispersal, establishment and mortality that we have previously reported (Shiozawa and Craig 1996) to perform simulations extending year-by-year for several thousand simulated years throughout an area that includes the entire Sonoran Desert. The inter-and intra-annual variability of climate (mean monthly maximum daily temperature and total monthly precipitation) is represented through a local climate model that calculates both the mean and variance of climate at each point of a grid whose cells are 15 km on a side. Monte Carlo methods are used to represent the natural climate variability at each grid cell. Improvement of calculation speed is achieved by a prob-

ability theory approach to determining if climates are suitable and this has allowed the longer simulations over larger areas. We have also removed the artificial limit on plant height that was present in our earlier model.

Our first experiments were confined to southern Arizona and included an evaluation of the spreading history of Saguaro in this area. Van Devender (1995) reported ^{14}C dates that suggested arrival of Saguaro at Organ Pipe National Monument approximately 2,000 years prior to its first occurrence at Picacho Peak, AZ (between Tucson and Phoenix). Our simulation suggests that under modern climate variability Saguaro could spread across this area in approximately 600 years. More recent AMS ^{14}C dates (van Devender 1996, written communication) from remains of Saguaro preserved in packrat middens now support a delay in arrival of approximately 600 years and are in agreement with our model results.

A second set of experiments included an area representing the entire Sonoran Desert in which the objective was to determine the amount of time required for Saguaro to spread throughout its entire known range from a single starting location (such as could have been the case at the end of the last ice age when Saguaro apparently were confined to only a few 'refugia'). Initial conditions for these experiments were a square group of nine cells occupied by post-seedling stage but pre-mature stage Saguaro. Three different refugia were examined as starting locations each having different climatic characteristics more or less favorable to establishment of Saguaro. Regardless of starting conditions, Saguaro spread throughout their known range; the required time varied significantly. Spread was fastest when starting from Organ Pipe National Monument in which case Saguaro covered its known range in 2,400 years. Spread from a starting point in southern Sonora was slowest and took about 3,100 years. In each case equilibration of range to modern climatic conditions was demonstrated by stochastic stability in the number of cells occupied for 500 years or longer.

Results of these experiments are evaluated through a set of statistical and graphical tools that allow us to extract useful information about the population structure and dynamics. For example, first arrival time in each cell is recorded and can be displayed as an image map showing the spread of the species. The number of years that the cell is occupied is not directly related to first arrival time since the mortality scenario included in the model can result in cells becoming unoccupied and later reoccupied by spread from adjacent cells. Average height of plants in the cell is an indicator of the climatic stress the plants encounter, and the number of mortality events experienced in each cell is a complex function of growth rates and re-establishment history.

Long-Range Streamflow/Drought Predictions Using Artificial Neural Networks

David Silverman and John Dracup
Department of Civil and Enviornmental Engineering
University of California-Los Angeles

Long-range streamflow/drought prediction is important to water-hungry California. As demands increase, reliable estimates of future water supply is necessary for efficient allocation of current supply and for planning.

Currently, research is being conducted on the role of interacting systems, or *teleconnections*, in explaining regional and global patterns of climatic variability. These patterns occur with enough frequency and with similar characteristics over a sufficient length of time that they offer opportunities to improve our long-range climate prediction. Systems that may affect California include El Niño/Southern Oscillation (ENSO), North Pacific SST, solar irradiance, and circulation patterns over North America and the north Pacific.

The relation between these systems and future streamflows is most likely nonlinear and not easily determined by statistical methods. Neural networks (NN) are especially useful for classification and function approximation/mapping problems which are tolerant of some imprecision, but to which hard and fast rules (such as those that might be used in an expert system) cannot easily be applied. NN's are good when data are "fuzzy" (opinions, ill-defined, large errors), subtle or deeply hidden patterns exist, significant unpredictable nonlinearity exit (ARIMA and Kalman filters would fail), or data is chaotic. After a NN is trained, examination of the network can show what parameters the network considers important, leading to a greater insight into the connection between the various parameters.

A NN was trained to predict from ENSO information the streamflow for the following year. Only 20 percent of the years of data (randomly chosen) were used in the training. The trained network was then tested against the full data set to determine the effectiveness of the network, and ~75 percent accuracy was observed.

Modeling the Natural Variability of Streamflow in the Sierra Nevada

Marina Timofeyeva and Rachael Craig
Department of Geology, Kent State University, Ohio

We report here an extension of the methods of Timofeyeva and Craig (1996) that greatly improves the quality of calculations of temperature, precipitation and streamflow for any selected location in the western United States. These calculations use Monte Carlo techniques to estimate the month-by-month variability of temperature and precipitation for

drainage basins represented by a digital elevation model at a spatial resolution of 1 km. Temperature and precipitation form the input to hydrologic calculations that solve runoff at the same grid spacing and route the runoff to estimate discharge at selected points such as gauging stations.

Improvements to the model include a new algorithm for estimating the variance of temperature and of precipitation at the same monthly time scale and 1 km spatial scale. Because precipitation is represented as a log-normal variate in which the variance is proportional to the mean and therefore the two distribution parameters are not independent of one another, it is necessary to have unbiased estimates of both mean and variance (of the log values) to estimate the parameters of the original distribution. We have achieved these estimates. Interestingly, we find that the variance of temperature (a mean monthly value) is appropriately modeled as the standard error of the *regression* from our canonical regression equation. In the case of precipitation (a sum of daily values) the variance is appropriately modeled as the standard error of the *prediction*. This distinction is important in achieving unbiased estimators, a point not previously recognized.

We have tested the climate solutions (both means and variances) at four stations proximal to the Upper San Joaquin drainage basin. Our assessment of natural variability is based on sets of averages of five sequential years chosen at random from the observational records. We examine the ratio of observed precipitation and the difference in temperature from one period to another and find that model means and variances are unbiased estimators of the stations means and variances regardless of station elevation. Using those climate estimators we calculate a series of Monte Carlo estimates of climate and the resulting runoff and streamflow and this streamflow time series is compared to the recalculated unimpeded flow of the San Joaquin River upstream of Millerton Lake. Comparison of model and observed is based on sets of 10 sequential years of streamflow chosen at random from the observational record. We find the simulated record is unbiased and represents the natural variability of the long-term (93 year) record closely for most of the year, but does tend to underestimate flow in the highest runoff period (April through June) although the modeled flows are still within the natural range of variability of flows for these months.

Appendix A
Agenda

Fourteenth Annual Pacific Climate (PACLIM) Workshop
Wrigley Institute for Environmental Studies (WIES)
Two Harbors, Santa Catalina Island, California
April 6-9, 1997

PACLIM is a multidisciplinary workshop broadly focused on climate phenomena occurring in the eastern Pacific and western Americas. Its purpose is to understand the climate effects in this region by bringing together specialists from diverse fields including both physical and biological sciences. Time scales range from weather to paleoclimate.

Our theme session, convened throughout the day on Monday, April 7, deals with aspects of teleconnections. This session is in remembrance of Jerome Namias (1910-1997), a pioneer in climate research and extended range prediction, and an active PACLIM attendee throughout the first several years of the Workshop.

This year, we are meeting for the first time at the Wrigley Institute for Environmental Studies Conference Center (WIES) on Santa Catalina Island. The atmosphere of the Workshop is intentionally informal, and room and board are provided for the participants. The Workshop is organized by a committee of representatives from several organizations, but historically it has been spearheaded by U.S. Geological Survey scientists. Held annually, the Workshop has benefited from funding and other forms of support from several agencies, public and private (see Sponsors, page iii).

Agenda

Fourteenth Annual Pacific Climate (PACLIM) Workshop
Wrigley Institute for Environmental Studies (WIES)
Two Harbors, Santa Catalina Island, California
April 6-9, 1997

WIES Meal Schedule
Breakfast 7:30-8:30 a.m.
Lunch 12:00-1:00 p.m.
Dinner 6:00-7:00 p.m.

Sunday Evening **April 6, 1997**

Moderator: Lowell Stott

7:00-7:05	Welcome and Announcements
7:05-7:25	The Western Winter of 1996-97 and Possible Teleconnections Kelly T. Redmond WRCC, Desert Research Institute, Reno
7:25-7:45	The Great New Year's Flood of 1997 in Northern California Maurice Roos, Department of Water Resources, Sacramento, California
7:45-8:05	Upstream-Downstream—It's All About Time—and Space Gary D. Sharp and Kathleen Dorsey Center for Climate/Ocean Resource Study California State University, Monterey Bay
8:05	Social Gathering

Monday Morning **Teleconnections Session** **April 7, 1997**

This year's theme session on Teleconnections is dedicated to Jerome Namias, 1910-1997.

Moderator: Dan Cayan

8:30-9:00	Large-Scale Weather Regimes and Local Climate over the Western U.S. Andrew W. Robertson Department of Atmospheric Sciences, UCLA
9:00-9:30	A Pacific Interdecadal Climate Oscillation with Impacts on Salmon Production Nathan Mantua, Steven R. Hare, Yuan Zhang, John M. Wallace, and Robert C. Francis JISAO, Atmospheric Sciences, University of Washington
9:30-10:00	Climate Teleconnection During the Late-Glacial Period in Southern South America Vera Markgraf, R. Figge, R. Kenny, and J.C.W. White INSTAAR, University of Colorado, Boulder
10:00-10:15	Break
10:15-10:45	Diagnosing the Sensitivity of Western U.S. Climate to Tropical Pacific Forcing Martin P. Hoerling, Arun Kumar, Taiyi Xu, and Min Zhong CIRES, University of Colorado, Boulder

10:45-11:15 Searching for Links Between the Patterns of Interdecadal to Centennial Variability in the California and Peru-Chile Current Systems
Tim R. Baumgartner, Andy Soutar, and Vicente Ferreira
CICESE, Scripps Institution of Oceanography

11:15-11:55 Influence of the North American Monsoon System on the United States Summer Precipitation Regime
R.Wayne Higgins, Y.Yao, E.L. Wang, and K.C. Mo
Climate Prediction Center, NOAA/NWS/NCEP, Washington, D.C.

12:00-1:30 Lunch

Monday Afternoon **Teleconnections Session** **April 7, 1997**

Moderator: Malcom Hughes

1:30-2:15 Spatially Variable Hydrologic Patterns in Lakes of the Northern Great Plains During the Last 2 k
Sherilyn C. Fritz, Katherine R. Laird, Emi Ito, and Dan Engstrom
Earth and Environmental Sciences, Lehigh University, Bethlehem, PA

2:15-2:45 Recent Changes in Pacific Hemisphere Teleconnections
Steven M. Hodge
U.S. Geological Survey, Anchorage, Alaska

2:45-3:15 "The Continuing Decline of Primary Productivity in the Bering Sea: Implications for Marine Mammal Populations"
Donald M. Schell
Institute of Marine Science, University of Alaska, Fairbanks

3:15-3:30 Poster Introductions

3:30-4:00 Break

4:00-5:30 Posters

5:30-7:00 Dinner

Monday Evening **Teleconnections Session** **April 7, 1997**

7:30-8:15 The Slow Eastward Propagation of ENSO-Scale Signals over the Global Ocean
Warren B. White, Ray Peterson, Shyh-Chin Chen, Dan Cayan, and Yves Tourre
Climate Research Division, Scripps Institution of Oceanography

Moderator: Ray Wilson

8:30-8:50	Index of OSCURS Model Winter Drift Trajectories from Ocean Station PAPA (1901-1979) Indicates the Fourth Decadal Oscillation During the 20th Century is Ending; PNA, PNI, Precipitation, Salmon, Oysters, and Tree Ring Data Covary W. James Ingraham Jr., Curtis C. Ebbesmeyer, and Richard A. Hinrichsen Alaska Fisheries Science Center, NOAA, Seattle
8:50-9:10	A 160 kyr Record of Alkenone-Derived Sea Surface Temperatures and Other Molecular Climate Indicators in Santa Barbara Basin Sediments Jürgen Rullkötter, Kai-Uwe Hinrichs, and Joachim Rinna ICBM, University of Oldenburg, Germany
9:10-9:30	Late-Glacial Variations in Vegetation and Climate in Western Oregon: Evidence of a Younger Dryas Cooling? Laurie D. Grigg and Cathy Whitlock Geography, University of Oregon, Eugene
9:30-9:50	Sunspot Cycles and Santa Barbara Basin Sediments Wolfgang H. Berger and Carina B. Lange Geosciences Research Division, Scripps Institution of Oceanography
9:50-10:20	Break
10:20-10:40	Mapping of the Pacific Interdecadal Variability Using Complex EOF Methodology Yves Tourre, Yohanan Kushnir, and Warren B. White Lamont-Doherty Earth Observatory, Columbia University
10:40-11:00	A Mid-to-Late Halocene Stratigraphic Record from Los Penasquitos Lagoon, Southern California Kenneth L. Cole and Eugene R. Wahl U.S. Geological Survey, University of Minnesota, St. Paul
11:00-11:20.	Response of Vegetation in the Pacific Northwest to Millennial-Scale Climatic Changes During the Last 125 kyr Cathy Whitlock and Patrick J. Bartlein Department of Geography, University of Oregon, Eugene
11:20-11:40	The Square-Root Normal Distribution of Daily Rainfall Along the U.S. Pacific Coast—Further Studies Raymond C. Wilson U.S. Geological Survey, Menlo Park, California
11:40-12:00	Decade-to-Century-Scale Climate Variation in Western North America Over the Last 1000 Years, in a Global Context Malcom K. Hughes Laboratory of Tree Ring Research, University of Arizona, Tucson
12:00-1:30 p.m.	Lunch

Tuesday Afternoon **April 8, 1997**

Moderator: Caroline Issacs

1:30-1:50 Evidence of Increased Growth of Vegetation in Northern North America and Eurasia from AVHRR Global Vegetative Index and Atmospheric Carbon Dioxide Data
Charles D. Keeling, Stephen C. Piper, and Timothy Whorf
Geosciences Research Division, Scripps Institution of Oceanography

1:50-2:10 $\delta^{13}C$ Variability in Modern Atriplex Communities; Implication for Reconstructing $\delta^{13}C$ of Past Atmospheres
Peter K. Van de Water, Steve Leavitt, Julio Betancourt, and Lisa Pedecino
Laboratory of Tree Ring Research, University of Arizona, Tucson

2:10-2:30 High Resolution Palaeoclimatic Reconstructions from Annually-Laminated Sediment, Saanich Inlet, B.C.
Arlene Collins
Department of Earth and Atmosphere, University of Alberta, Canada

2:30-2:50 The Effect of Atmospheric pCO_2 on $^{13}CO_2$ Discrimination in Wood C_3 Plants: Implications for Estimating Paleo-Atmospheric pCO_2
A. Sinha and L.D. Stott
Department of Fish Sciences, University of California, Los Angeles

Tuesday Evening **April 8, 1997**

7:30-8:15 Climate Science and Insurance Risk
Anthony Michaels
Director, Wrigley Institute for Environmental Sciences and Department of Biological Sciences, University of Southern California

Wednesday Morning **April 9, 1997**

Moderator: Kelly Redmond

8:30-8:50 ENSO Signal in $\delta^{13}C$ of Pre-and Post-False Latewood of Ponderosa Pine Tree Rings in Southeastern Arizona
Steven Leavitt, William E. Wright, and Austin Long
Laboratory of Tree Ring Research, University of Arizona, Tucson

8:50-9:10 Teleconnections from Asia to the Canadian Prairies—Implications for Long Range Weather and Crop Forecasting
E. Ray Garnett and M.L. Khandekar
Canadian Wheat Board, Manitoba, Canada

9:10-9:30 Long-Range Streamflow Forecasting in the Columbia River Basin and the El Niño-Southern Oscillation
Thomas C. Piechota and John A. Dracup
Civil and Environmental Engineering, UCLA

9:30-10:00 Break

10:00-10:20 Forecasting the Inflows to the Howard Hanson Reservoir, Green River, Washington for the Fall-Transition Season
John J. Vaccaro
U.S. Geological Survey, Tacoma, Washington

10:20-10:40	Teleconnection Between ENSO and ITCZ Position: Decadal Variations of Regional Precipitation in Southwestern South America Hong-Chun Li and Teh-Lung Ku Department of Earth Sciences, University of California, Los Angeles
10:40-11:00	Winter Atmospheric Circulation and Tree Growth in the Sierra Nevada Gregg M. Garfin Laboratory of Tree Ring Research, University of Arizona, Tucson
11:00-11:20	Seasonal Variation in Living (Stained) Deep-Sea Benthic Foraminiferal Assemblages and Stable Isotopes from the California Current System Anthony E. Rathburn and Kyger C. Lohmann
11:20-11:40	Decadal Variability of Snow in the Western U.S. Dan Cayan and Larry Riddle Climate Research Division, Scripps Institution of Oceanography and the U.S. Geological Survey
12:00-1:30	Lunch

Appendix B
Poster Presentations

Fourteenth Annual Pacific Climate (PACLIM) Workshop
Wrigley Institute for Environmental Studies (WIES)
Two Harbors, Santa Catalina Island, California
April 6-9, 1997

Appendix B
Poster Presentations

Fourteenth Annual Pacific Climate (PACLIM) Workshop
Wrigley Institute for Environmental Studies (WIES)
Two Harbors, Santa Catalina Island, California
April 6-9, 1997

Quaternary Record of Paleolacustrine Environment in the Laguna Chapala Basin Area of Northern Baja California
Loren G. Davis, University of Alberta, Alberta, Canada

Forecasting the Frequencies of U.S. Intraseasonal Extremes
Alex Gershunov, Climate Research Division, Scripps Institution of Oceanography

Searching for Interdecadal Cycles in Western Oregon Precipitation
David Greenland, Department of Geography, University of Oregon, Eugene, Oregon

Prediction of Drought Persistence in California
Henry Gu and John Dracup, Civil and Environmental Engineering,
UCLA, Los Angeles, California

High Altitude Ice Core Data and Teleconnections (abstract only)
Gerald Holdsworth, Department of Earth and Atmosphere,
University of Alberta, Alberta, Canada

Holocene Paleoceanographic Changes in Santa Barbara Basin: Radiocarbon Records
B.Lynn Ingram, Department of Geography, University of California, Berkeley, California

Addendum II: The Solar Isolation/Tidal Resonance Climate Model: 'Teleconnections' in a Broad Spectrum of Types and Time Scales
Thor Karlstrom, U.S. Geological Survey, Seattle, Washington

The Influence of Water Column Dynamics on Foraminiferal Flux Patterns
Eileen Kincaid, Department of Geological Sciences,
University of South Carolina, Columbia, South Carolina

Decadal Climatic Reconstruction from Stable Isotope Records of Speleothem in Shihua Cave China: A Summer Monsoon Domain
Teh-Liang Ku, Hong-Chun Li, and Lowell D. Stott, Department of Earth Sciences,
University of Southern California, Los Angeles, California

Sedimentation Patterns of Siliceous Microorganisms in Santa Barbara Basin
Carina B. Lange, Amy L. Weinheimer, Freda M.H. Reid, and Robert C. Thunell,
Geosciences Research Division, Scripps Institution of Oceanography,
La Jolla, California

Relationship Between Atmospheric Turbidity of the Southwest U.S. and High Elevation Surface Temperatures of the Central Mountain Region
Mark Losleben, University of Colorado, Mountain Research Station,
Nederland, Colorado

Linking Atmospheric and Paleoclimatic Records, Lake Estancia, NM
Kirsten M. Menking, Bruce D. Allen, Roger Y. Anderson, and Thomas A. Loveland, Earth and Planetary Sciences, University of New Mexico, Albuquerque, New Mexico

Seasonal Cycle of the Global Ocean Mixed Layer Depth Based on the Climatological Monthly Mean Hydrographic Data
Grigory Monterey and Sydney Levitus, PFEG/NMFS/NOAA, Pacific Grove, California

Simulation of Dispersal of Saguaro Cactus
Leila Shiozawa and Rachael Craig, Kent State University, Kent, Ohio

Long-Range Streamflow/Dought Predictions Using Artificial Neural Networks
David Silverman and John Dracup, Civil and Environmental Engineering, Univereisty of California–Los Angeles, Los Angeles

Modeling the Natural Variability of Streamflow in the Sierra Nevada
Marina Timofeyeva and Rachael Craig, Department of Geology, Kent State University, Kent, Ohio

A Full Glacial Pollen Biozone for Central California
G.James West, U.S. Bureau of Reclamation, Sacramento, California

The Response of Desert Vegetation to Climate Change During the Past 150,000 Years in the Southern Owens Valley Region, California
Wallace B. Woolfenden, Inyo National Forest, Lee Vining, California

Appendix C
Attendees

Fourteenth Annual Pacific Climate (PACLIM) Workshop
Wrigley Institute for Environmental Studies (WIES)
Two Harbors, Santa Catalina Island, California
April 6-9, 1997

Appendix C
Attendees

Fourteenth Annual Pacific Climate (PACLIM) Workshop
Wrigley Institute for Environmental Studies (WIES)
Two Harbors, Santa Catalina Island, California
April 6-9, 1997

Roger Anderson
University of New Mexico
Earth and Planetary Sciences
Albuquerque, NM 87161
(P) (505) 227-1639
(F) (505) 227-8843
ryand@unm.edu

Wolf Berger
Scripps Institution of Oceanography
9500 Gilman Drive
La Jolla, CA 92093-0215
(P) (619) 534-2826
(F) (619) 453-0167
wberger@ucsd.edu

Greg Bohr
San Diego State University, Geography
5840 Lindo Paseo #20
San Diego, CA 92115
(P) (619) 583-8544
bohr@orhan.sdsu.edu

J. Platt Bradbury
U.S. Geological Survey
Box 25064, MS 980
Federal Center
Denver, CO 80225
(P) (303) 236-5666
(F) (303) 236-5349
jbradbur@usgs.gov

Annette Casey
Ocean Research Institute
650 Loring Street
San Diego, CA 92109
(P) (619) 483-6507

Richard Casey
Ocean Research Institute
650 Loring Street
San Diego, CA 92109
(P) (619) 483-6507

Dan Cayan
Climate Research Division 0224
Scripps Institution of Oceanography
9500 Gilman Drive
La Jolla, CA 92093-0224
(P) (619) 534-4507
(F) (619) 534-8561
dcayan@ucsd.edu

Kenneth Cole
U.S. Geological Survey
University of Minnesota
Forest Resources
St. Paul, MN 55108
(P) (612) 624-4296
(F) (612) 625-5212
kcole@forestry.umn.edu

Arlene Collins
Department of Earth and Atmosphere
University of Alberta
Edmonton, Alberta, Canada T6G2E3
(P) (403) 492-1120
(F) (403) 492-2030
acollins@aofc.forestry.ca

Loren Davis
University of Alberta
Anthropology, 13-15 Tory
Edmonton, Alberta, Canada T6G2H4
(P) (403) 492-1120
(F) (403) 492-5273
lgdavis@gpu.srv.ualberta.ca

Diane DeRobertis
University of California, Berkeley
Geography
2100 Channing Way #414
Berkeley, CA 94704
(P) (510) 664-0792
dianamd@violet.berkeley.edu

Kathleen Dorsey
Kinnetic Laboratories
307 Washington Street
Santa Cruz, CA 95060
(P) (408) 457-3950
(F) (408) 426-0405
kinnetic@cruzio.com

John Dracup
University of California, Los Angeles
Atmospheric Sciences
5732 Boelter Hall
Los Angeles, CA 90095-1595
(P) (310) 825-2176
(F) (310) 206-7245
dracup@seas.ucla.edu

Richard Forester
U.S. Geological Survey
MS980 DFG
Denver, CO 80225
(P) (303) 236-5656
(F) (303) 236-5349
forster@usgs.gov

Sheri Fritz
Leheigh University
31 Williams Drive
Bethlehem, PA 18015
(P) (610) 758-6580
(F) (610) 758-3677
scfa@lehigh.edu

Gregg Garfin
Laboratory of Tree Ring Research
University of Arizona
Building 58, Room 105 D2
Tucson, AZ 85721
(P) (520) 626-3142
(F) (520) 621-8229
g@ltrr.arizona.edu

David Greenland
Geography
University of Oregon
Eugene, OR 97403-5351
(P) (541) 346-4561
(F) (541) 346-2067
greenland@oregon.uoregon.edu

Laurie Grigg
University of Oregon
Geography
Eugene, OR 97403
(P) (541) 346-2698
(F) (541) 346-2067
lgrigg@darkwing.uoregon.edu

Henry Gu
University of California, Los Angeles
3066 Engineer I
Civil and Environmental Engineering
Los Angeles, CA 90095-1593
(P) (310) 206-8612
(F) (310) 206-7245
henryg@seas.ucla.edu

Felipe Gutierrez
University of California, Los Angeles
3181 Sepulveda Blvd. 107
Los Angeles, CA 90034
(P) (310) 398-1672
(F) (310) 398-1672
fgutierr@ucla.edu

Steven R. Hare
International Pacific Halibut Commission
P.O. Box 95009
Seattle, WA 98145
(P) (206) 634-1838x230
(F) (206) 632-2938
hare@iphc.washington.edu

Hugo Hidalgo
62248 Metz Street
Long Beach, CA 90808
(P) (310) 425-1331
hhidalgo@ucla.edu

Wayne Higgins
Climate Prediction Center
NCEP/NWS/NOAA
5200 Auth Road, Room 605
Camp Springs, MD 20746
(P) (301) 763-8227x7547
(F) (301) 763-8395

Steven Hodge
U.S. Geological Survey
University of Puget Sound
Tacoma, WA 98416
(P) (206) 593-6516
(F) (206) 383-7967
smhoge@usgs.gov

Martin Hoerling
CIRES
University of Colorado at Boulder
Campus Box 449
Boulder, CO 80309
(P) (303) 492-1114
(F) (303) 497-7013
mph@cdc.noaa.gov

Malcom Hughes
Laboratory of Tree Ring Research
University of Arizona
Tucson, AZ 85721
(P) (520) 621-6670
(F) (520) 621-8229
mhughes@ltrr.arizona.edu

B. Lynn Ingram
Univerity of California, Berkeley
Geography Department
Berkeley, CA 94720
(P) (510) 643-1473
(F) (510) 642-3370
ingram@socrates.berkeley.edu

W. James Ingraham, Jr.
NOAA-NMFS-Alaska Fisheries Science Center
7600 Sand Point Way, NE, BIN C15700

Seattle, WA 98115-0070
(P) (206) 526-4241
(F) (206) 526-6723
jingram@afsc.noaa.gov

Brenda Johnson
University of California, Davis
DES
Center Ecological Health Research
Davis, CA 95616
(P) (916) 756-7069
(F) (916) 752-3350
bjohnson@mother.com

Thor and Carol Karlstrom
4811 SW Brace Point Drive
Seattle, CA 98136
(P) (206) 935-7087

Charles D. Keeling
Scripps Institution of Oceanography, 0220
La Jolla, CA 92093-0220
(P) (619) 534-4230
(F) (619) 534-8814
cdkeeling@ucsd.edu

Eileen Kincaid
University of South Carolina
Department of Geological Sciences
Columbia, South Carolina 29208
(P) (803) 777-4526
(F) (803) 777-6610
kincaid@geol.sc.edu

Teh-Liang Ku
USC, Department of Earth Sciences
Los Angeles, CA 90089-0740
(P) (213) 740-5826
(F) (213) 740-8801
rku@earth.usc.edu

Carina Lange
Scripps Institution of Oceanography
9500 Gilman Drive
La Jolla, CA 92093-0215
(P) (619) 534-4605
(F) (619) 534-0784
clange@ucsd.edu

Steve Leavitt
Laboratory of Tree Ring Research
105 W. Stadium
University of Arizona
Tucson, AZ 85721
(P) (520) 621-6468
(F) (520) 621-8229
sleavitt@ltrr.arizona.edu

Peggy Lehman
California Department of Water Resources
3251 S Street
Sacramento, CA 95816
(P) (916) 227-7551
(F) (916) 227-7554
plehman@water.ca.gov

Hong-Chun Li
University of Southern California
Earth Sciences
Los Angeles, CA 90089-0740
(P) (213) 740-6736
(F) (213) 740-8801
hli@earth.usc.edu

Mark Losleben
University of Colorado
Mountain Research Station
838 County Road 116
Nederland, CO 80466
(P) (303) 492-8841
(F) (303) 492-8841
markl@culter.colorado.edu

Nathan Mantua
University of Washington, JISAO
Box 354235
Seattle, WA 98195-4235
(P) (206) 616-5347
(F) (206) 616-5775
mantua@atmos.washington.edu

Vera Markgraf
INSTAAR
University of Colorado
Boulder, CO 80309-0450
(P) (303) 492-5157
(F) (303) 492-6388
markgraf@spot.colorado.edu

Kirsten Menking
Earth and Planetary Sciences
University of New Mexico
Northrup Hall
Albuquerque, NM 87151
(P) (505) 227-1639
(F) (505) 227-8843
menking@unm.edu

Art Miller
Scripps Institution of Oceanography, 0224
University of California, San Diego
La Jolla, CA 92093-0224
(P) (619) 534-8033
(F) (619) 534-8561
ajmiller@ucsd.edu

Monika Olsen
1216 Babel
Concord, CA 94518
(P) (510) 676-2228

Grigory Monterey
JIMAR
University of Hawaii

Tom Piechota
University of California, Los Angeles
Civil and Environmental Engineering
3066 Engineering I
Los Angeles, CA 90095-1593
(P) (310) 206-8612
(F) (310) 206-7245
piechota@seas.ucla.edu

Anthony Rathburn
MLRG-0218
Scripps Institution of Oceanography
9500 Gilman Drive
La Jolla, CA 92093-0218
(P) (619) 534-1864
(F) (619) 534-6500
rathburn@coast.ucsd.edu

Andrew Robertson
Atmospheric Sciences
Univeristy of California, Los Angeles
405 Hilgard Avenue
Los Angeles, CA 90095-1565
(P) (310) 825-1038
(F) (310) 206- 5219
andy@atmos.ucla.edu

Christine Roensch
Pacific Gas and Electric
77 Beale Street, Room 1654
San Francisco, CA 94179
(P) (415) 973-3560
(F) (415) 993-1521
cmra@pge.com

Kelly T. Redmond
Western Regional Climate Center
Desert Research Institute
P.O. Box 60220
Reno, NV 895006-0220
(P) (702) 677-3139
(F) (702) 677-3243/3157
krwrcc@sage.dri.edu

Brendan Roark
University of California, Berkeley
Geography Department
Room 501 McCone
Berkeley, CA 94720
(P) (510) 643-1816
(F) (510) 642-3370
ebbroark@violet.berkeley.edu

Maurice Roos
California Department of Water Resources
3310 El Camino Avenue, Room 200
P.O. Box 219000
Sacramento, CA 95821-9000
(P) (916) 574-2625
(F) (916) 574-2767
mroos@water.ca.gov

Jürgen Rollkötter
University of Oldenburg
P.O. Box 2503
D-26111
Oldenburg, Germany
(P) 49 411 970-6359
(F) 49 411 798-3404
jrullkoetter@ogc.icbm.uni-oldenburg.de

Donald M. Schell
Institute of Marine Science
University of Alaska, Fairbanks
Fairbanks, Alaska 99775
(P) (907) 474-7978
(F) (907) 474-5863
schell@ims.alaska.edu

Gary D. Sharp
Center for Climate/Ocean Resources Study
780 Harrison Road
Salinas, CA 93907
(P) (408) 449-9212
(F) (408) 582-3656
gary_sharp@monterey.edu

David Silverman
University of California, Los Angeles
1128 W. 30th Street
Los Angeles, CA 90007
(P) (213) 748-3043
(F) (818) 222-3700
dsilverm@ucla.edu

Tom Suchanek
University of California, Davis
DES
Davis, CA 95616
(P) (916) 752-9035
(F) (916) 752-3350
thsuchanek@ucdavis.edu

Robert N. Swanson
Climatological Consulting Corp.
1216 Babel Lane
Concord, CA 94518
(P) (510) 676-2228
mswanson@woldnet.attt.net

Jancice Tomson
Long Beach City College
4901 E. Carson Street
Long Beach, Ca 90808
(P) (562) 938-4448

Yves Tourre
Lamont -Doherty Earth Observatory
Columbia University
tourre@ldeo.columbia.edu

John J. Vaccaro
U.S. Geological Survey
1201 Pacific, Suite 600
Tacoma, WA 98402
(P) (206) 593-6510
(F) (206) 593-6514

Pete Van de Water
Laboratory of Tree Ring Reserach
University of Arizona
2415 East First Street, #1
Tucson, AZ 85719
(P) (520) 881-7418
(F) (520) 881-7418
petevaw@hrp.arizona.edu

Eugene R. Wahl
Ecology, University of Minnesota
100 Ecology, Evolution & Behavior
1987 Upper Buford Circle
St. Paul, MN 55108
(P) (612) 624-6713
(F) (612) 624-6777
wahl0040@ggold.tc.unm.edu

G. James West
U. S. Bureau of Reclamation
3429 Oyster Bay
Davis, CA 95616
(P) (916) 979-2478
(F) (916) 979-2139
gjwest@prodigy.com

Warren B. White
Scripps Institution of Oceanography, PORD
8605 La Jolla Shores Drive
La Jolla, CA 92093-0230
(P) (619) 534-4826
(F) (619) 534-7452
wbwhite@ucsd.edu

Cathy Whitlock
University of Oregon
Geography Department
Eugene, OR 97403
(P) (541) 737-2940
(F) (541) 750-7329
whitlock@oregon.uoregon.edu

Ray Wilson
U.S. Geological Survey, MS-977
345 Middle Field Road
Menlo Park, CA 94025
(P) (415) 329-4892
rwilson@mojave.wr.usgs.gov

Michael Wittman
University Weather & Aviation
6201 W. Imperial Highway
Los Angeles, CA 90045
(P) (213) 776-8651
(F) (213) 776-9654
mikewitt@msn.com

Wally Woolfenden
U.S. Department of Agriculture, Forest Service
Mono Lake Ranger Station
Inyo National Forest
P.O. Box 429
Lee Vining, CA 93541
(P) (619) 647-3035
(F) (619) 647-3027